DOE/ER/01062--T9

TRIANGLE UNIVERSITIES NUCLEAR LABORATORY
PROGRESS REPORT — TUNL XXX

1 SEPTEMBER 1990 – 31 AUGUST 1991

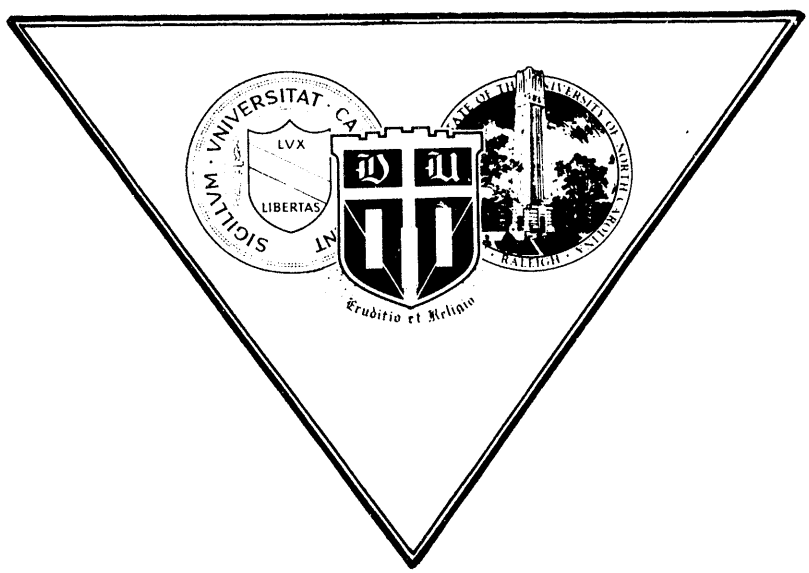

Duke University
University of North Carolina at Chapel Hill
North Carolina State University at Raleigh

DOE/ER/01067--T9

DE92 002539

PROGRESS REPORT – TUNL XXX

1 September 1990 – 31 August 1991

TRIANGLE UNIVERSITIES NUCLEAR LABORATORY

Duke University
University of North Carolina at Chapel Hill
North Carolina State University at Raleigh

Duke Station, Durham, North Carolina 27706, USA

Work described in this Progress Report is supported by the United States Department of Energy, Office of High Energy and Nuclear Physics, under:

Contract No. DE-AC05-76ER01067 (Duke University),

Grant No. DE-FG05-88ER40442 (University of North Carolina),

and

Grant No. DE-FG05-88ER40441 (North Carolina State University).

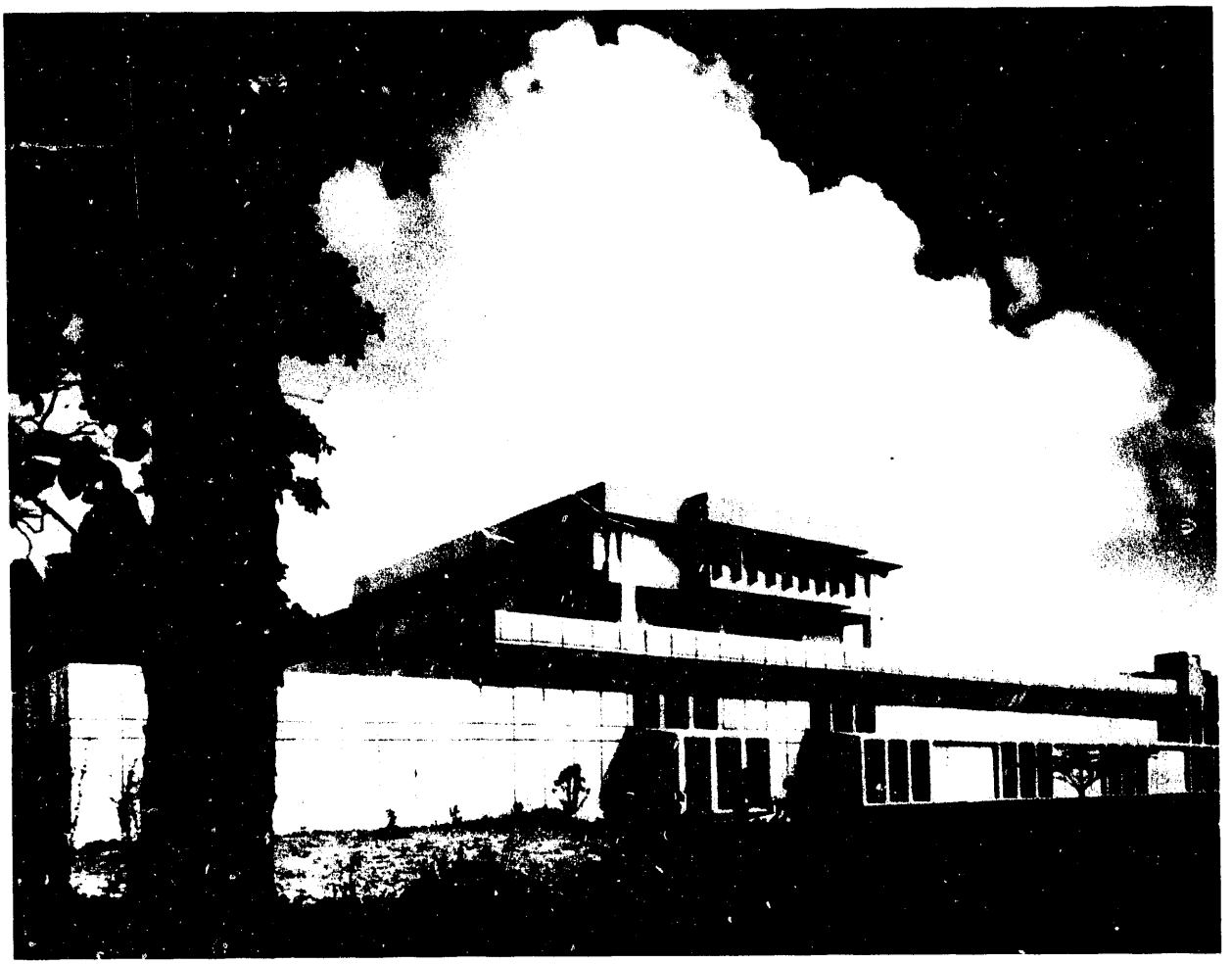

TRIANGLE UNIVERSITIES NUCLEAR LABORATORY

CONTENTS

APPENDICES

▽ ▽ ▽

INTRODUCTION

Triangle Universities Nuclear Laboratory (TUNL) has had a very successful year in 1990 – 91, with much progress being made in research, instrumentation development, and the training of nuclear physics students from the three collaborating universities – Duke, North Carolina State, and University of North Carolina.

In research, the TRIPLE collaboration at LAMPF is finding interesting and unexpected systematics in the parity-violating amplitudes for epithermal-neutron scattering. The collaboration is beginning experiments to significantly decrease the limits on time-reversal-invariance violation in the strong interaction. The expertise of TUNL in the construction and characterization of cryogenic polarized targets of elements from hydrogen to holmium continues to be important in forefront nuclear physics research.

We have a broad-ranging program for probing the low- to medium-energy internucleon interactions, starting with *n-p* scattering and progressing to the three- and several-nucleon systems. Of particular interest are three-nucleon systems, both in elastic scattering and in three-body breakup. In the past year we have made rigorous calculations of these systems, using modern nuclear forces and the Cray Y-MP at North Carolina Supercomputer Center. Several experiments to test the predictions are underway at TUNL. Many of these require the intense beams of polarized deuterons provided by our new high-intensity atomic-beam source. Among the questions of fundamental interest are the nature of three-nucleon forces and the extent of charge-independence or charge-symmetry breaking in the two-nucleon interaction.

Other studies of the dynamics of very light nuclei that engaged our efforts include spin observables at very low energies (using our new low energy beam facility and the intense polarized-ion source), and D-state parameters for light nuclei studied by transfer and radiative-capture reactions.

Several facets of the nuclear many-body problem and nuclear structure have been elucidated through our research programs during 1990 – 91. Our program in nuclear astrophysics, which uses a wide variety of techniques to measure and interpret nuclear reactions that are of interest to astrophysics, has had a very successful first year. Experiments are underway at TUNL and Princeton University, and preliminary runs have been made to evaluate the feasibility of using radioactive beams at HHIRF (ORNL) for nuclear astrophysics measurements.

Nuclear scattering and nuclear excitation mechanisms are being studied through neutron,- proton-, and deuteron-induced reactions, as well as through radiative capture. The nuclear data evaluation project for A = 3 – 20 has been transferred from the University of Pennsylvania to TUNL during the past year, and it will continue to provide a service to the nuclear physics and applied sciences communities.

In nuclear instrumentation TUNL is maintaining and developing equipment for basic research that is also of a scale suitable for training graduate students. The staged upgrade of the TUNL FN tandem Van de Graaff was completed on schedule and on-cost during 1990 – 91 without significant disruption of our in-house research programs. The much-

improved performance of this machine is already of significant benefit to our research efforts. Several improvements were also made to the KN Van de Graaff accelerator at TUNL, including construction of a novel compact ECR ion source. The new intense polarized-ion source operated smoothly, and novel beam-diagnostic schemes and beam-polarization monitors were designed and tested.

Instrumentation projects that were supported by the DOE University Research Instrumentation program, such as installation and refurbishment of the Enge split-pole magnetic spectrometer, the development of a Compton-suppressed γ-ray spectrometer for (p,γ) reactions, and the Low Energy Beam Facility at TUNL, all made much progress during the year. TUNL expertise in instrumentation is beginning to benefit the development of the CEBAF instrumentation efforts, with two collaborations involving TUNL physicists (Hall-A spectrometer and Hall-B electron polarimeter) being underway during 1990 – 91. The nuclear physics computer workstation network at TUNL and the three universities was completed during the year. Its greatly increased power, convenience, and flexibility over the previous system are proving to be of great benefit to faculty and students.

The varied talents of 17 faculty members and of 33 graduate students from the three campuses are indispensable for the wide variety of TUNL research activities. We benefit from the extensive skills of the TUNL technical support staff, of temporary student helpers who are being introduced to nuclear physics, and of the large number of visitors and collaborators who broaden our research programs.

The TUNL Advisory Committee – Drs. David Balamuth (University of Pennsylvania), Gerald Garvey (LAMPF), Wick Haxton (University of Washington), Steve Vigdor (IUCF), and Dirk Walecka (CEBAF) – continues to provide sound advice for our research program. The U.S. Department of Energy, Division of Nuclear Physics, provides major support for the research programs of TUNL through grants to the three collaborating universities.

The research summaries presented in this progress report are preliminary. They should not be referenced in other publications. If you wish to know the current status of a research project, please contact the scientist whose name is underlined in the author list at the beginning of each article.

Triangle Universities Nuclear Laboratory

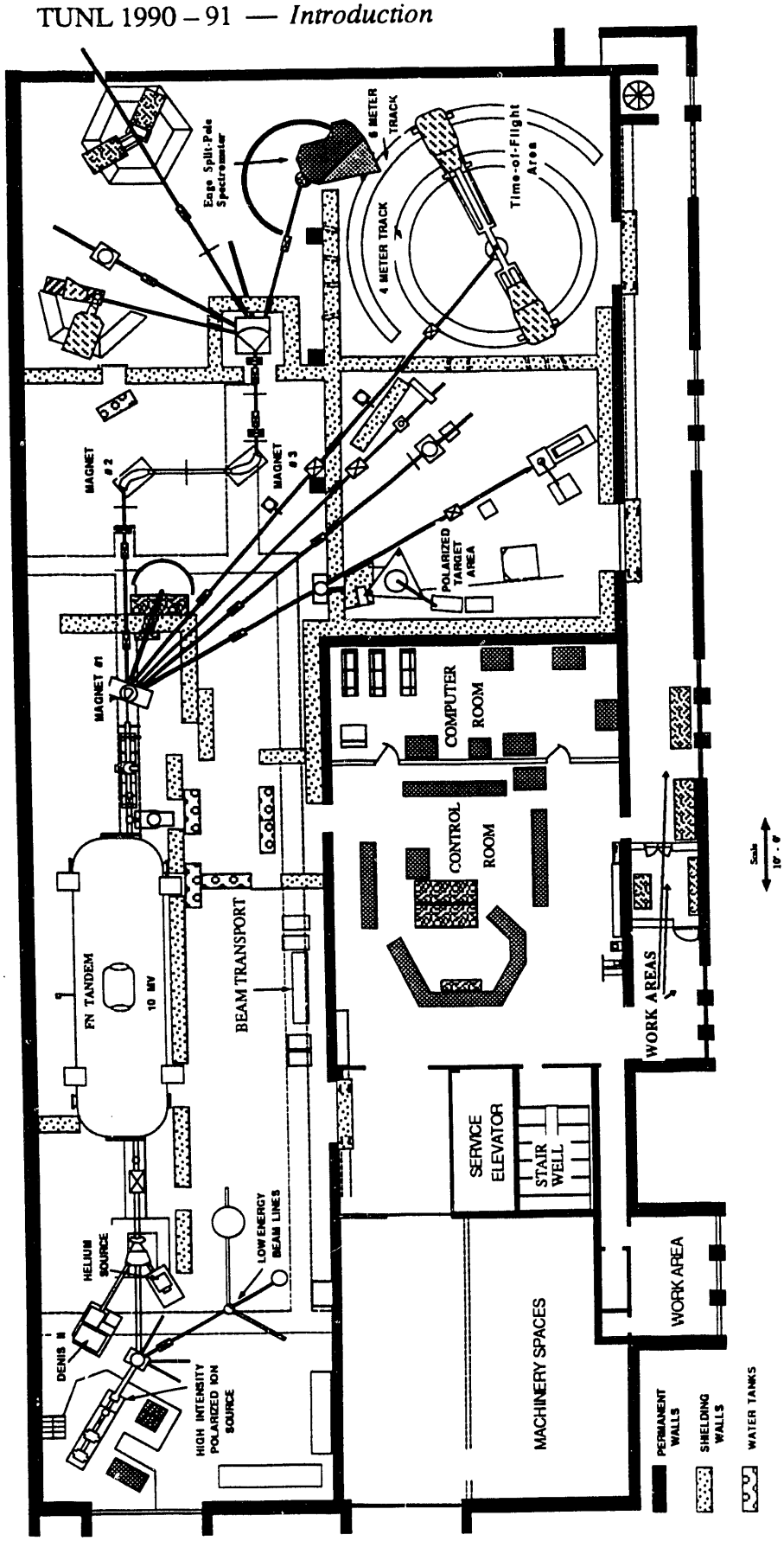

TRIANGLE UNIVERSITIES NUCLEAR LABORATORY

PERSONNEL

Department of Physics, Duke University, Durham, NC 27706

Department of Physics and Astronomy, University of North Carolina, Chapel Hill, NC 27599-3255

Department of Physics, Box 8202, North Carolina State University, Raleigh, NC 27695-8202

Faculty

Bilpuch, E. G. (director, professor)	Duke
Clegg, T. B. (professor)	UNC
Champagne, A.E. (associate professor)	UNC
Gould, C. R. (professor)	NCSU
Haase, D. G. (professor)	NCSU
Howell, C. R. (assistant professor)	Duke
Karwowski, H. (associate professor)	UNC
Lewis, H. W. (professor emeritus)	Duke
Ludwig, E. J. (professor)	UNC
Merzbacher, E. (professor)	UNC
Mitchell, G. E. (professor)	NCSU
Roberson, N. R. (deputy director, professor)	Duke
Seagondollar, L. W. (professor)	NCSU
Thompson, W. J. (professor)	UNC
Tilley, D. R. (professor)	NCSU
Tornow, W. (research associate professor)	Duke
Walter, R. L. (professor)	Duke
Weller, H. R. (professor)	Duke

Research Staff

Chasteler, B. (research associate)	Duke
Das, R. (research associate)	UNC
Koster, J. (research associate)	Duke
Hooke, W. M. (senior research scientist)	Duke
Westerfeldt, C. (research scientist)	Duke

Graduate Students

Adams, A.	NCSU
Al Ohali, M.	Duke
Balbes, M.	Duke
Black, T.	UNC
Blackman, J.	UNC
Braun, R.	Duke
Bybee, R.	NCSU
Crosson, E.	UNC
Dinge, D.	UNC
Drake, J.	NCSU
Fletcher, K.	UNC
Godwin, M.	Duke
Gonzalez, D.	Duke
Hennesey, D.	Duke
Hendrix, B.	UNC
Huffman, P.	Duke
Jackson, C.	NCSU
Keith, C.	NCSU
Kramer, L.	Duke
Lemieux, S.	UNC
Murphy, T.	NCSU
Nagadi, M.	Duke
Patterson, S.	NCSU
Philp, C.	UNC
Roper, C.	Duke
Salinas, F.	Duke
Schmid, G.	Duke
Setze, H. R.	Duke
Vavrina, G.	NCSU
Wallace, P.	Duke
Weisel, G.	Duke
Wilburn, S.	Duke
Williams, Z.	Duke

Technical Support Staff

Atkinson, P.	Editorial Assistant
Bailey, D.	Draftswoman
Carter, E. P.	Accelerator Supervisor
Dunham, J.	Accelerator Technician
Edwards, S. E.	Computer Maintenance Supervisor
Gibson, P. M.	TUNL Staff Assistant
Harris, E. P.	Instrument Maker
Hogan, R. G.	Instrument Maker
Huffman, R. G.	Staff Specialist
Lovette, A. W.	Shop Foreman, Instrument Maker
Dzubay, J. M.	TUNL Secretary
Mulkey, P.	Electronics Technician

TUNL Advisory Committee

Balamuth, David P.	University of Pennsylvania
Garvey, Gerald T.	Director, Los Alamos Meson Physics Facility
Haxton, Wick C.	University of Washington
Vigdor, Steven E.	Indiana University Cyclotron Facility
Walecka, J. Dirk	Scientific Director, Continuous Electron Beam Accelerator Facility

Visiting Scientists

Delaroche, J. P.	4/91-5/91	Bruyères-le-Châtel, France
Eiro, A.	4/91	University Lisboa, Portugal
Hayward, E.	10/90-1/91	NIST, Gaithersburg
Hofmann, H.	4/91	University of Erlangen, Germany
Koike, Y.	8/91	Hosei University, Japan
Lambert, J.	9/90-3/91	Georgetown University
Li, J.	9/88-10/90	Shanghai, PRC
Mao, Z. Q.	5/91	Drexel University, Philadelphia
Mertens, G.	3/91	University of Tübingen, Germany
Prior, R.	7/91-8/91	West Georgia State College
Riley, J.	3/91	University of South Carolina at Spartanburg
Slaus, I.	2/91-3/91	Zagreb, Yugoslavia
Shriner, J. F.	6/91-8/91	Tennessee Technological University
Tanifuji, M.	11/91	Hosei University, Japan
Thiel, A.	9/88-9/90	University of Frankfurt, Germany
Vanhoy, J.	7/91	U.S. Naval Academy
Vogelaar, R. B.	5/91	Princeton University
Unkelbach, M.	8/90	University of Erlangen, Germany
Vlahovic, B.	11/90	Zagreb, Yugoslavia
Witała, H.	7/91-8/91	Jagellonian University, Cracow, Poland
Zemin, C.	6/91	Beijing, People's Republic of China

Temporary Student Personnel

Bailey, J.	NCSU
Chang, R.	UNC
Law, C.	UNC
Mehan, S.	UNC
Moore, E.	Tennessee Tech
Slayton, T.	Tennessee Tech
Yuan, X.	UNC

1. FUNDAMENTAL SYMMETRIES IN THE NUCLEUS

During the past year we have begun to harvest the fruits from several years of developing techniques for measuring symmetry-breaking effects in nuclear interactions. These techniques are now being used to measure and interpret large parity-violation effects in polarized epithermal-neutron scattering from heavy nuclei, as well as to improve the upper limits for time-reversal-violating terms in scattering. Fluctuation properties of nuclear states are also being investigated in order to understand their role as signatures of quantum chaos.

In the following sections we summarize our recent progress in these areas of fundamental research.

1.1 Parity-Violation Measurements Using Neutrons

This year has seen great progress in the measurements of parity violation in neutron resonances and in their interpretation. Now that many parity-violating resonances have been measured, we see very strong evidence for a systematic sign for the parity-violating amplitudes, an unexpected result. The interpretation of this systematic behavior is of intense current interest.

The experiments are being performed at Los Alamos National Laboratory (LANL) in a collaboration of physicists from LANL, TUNL, the University of Delft, the Joint Institute for Nuclear Research (Dubna, USSR), and TRIUMF (Vancouver, Canada).

1.1.1 The TRIPLE Experiments with Epithermal Neutrons

J.D. Bowman[1], J. Bush, P.P.J. Delheij[2], C.M. Frankle, C.R. Gould, D.G. Haase, J. Knudson[1], J.E. Koster, G.E. Mitchell, S. Penttila[1], Yu.P. Popov[3], H. Postma[4], N.R. Roberson, S.J. Seestrom[1], E.I. Sharapov[3], J.J. Szymanski[1], S.A. Wender, V. Yuan[1], X. Zhu

The TRIPLE collaboration (Time Reversal Invariance and Parity at Low Energies) was formed to make tests of fundamental symmetries in strong-interaction physics in the compound-nucleus (CN) regime. The large parity-violating effects observed for the 0.73 eV p-wave resonance in ^{139}La [Alf83] and for the 38.2 and 64.5 eV p-wave resonances in ^{232}Th [Fra91] have demonstrated that for suitable observables symmetry violations in the effective nucleon-nucleon (NN) interaction are enhanced in the many-body system.

A single observation, while interesting, does not permit a quantitative connection between the symmetry violation and the effective NN interaction. Our goal is to carry out a series of transmission and radiative capture measurements of symmetry violations for many resonances in heavy nuclei and to extract the variance of the CN symmetry-violating matrix elements. The information about the symmetry-breaking interaction is contained in the square root of the variance, i.e., in the root-mean-square matrix element.

---

[1] Los Alamos National Laboratory
[2] TRIUMF, Vancouver, British Columbia, Canada V6T 2A3
[3] Joint Institute for Nuclear Research, Dubna, USSR
[4] University of Technology, Delft, The Netherlands

The TRIPLE collaboration is pursuing a multi-year program to carry out tests which will study the following terms in the neutron-nucleus forward scattering amplitude:

$\mathbf{s}\cdot\mathbf{k}$	P-odd, T-even	Helicity
$\mathbf{s}\cdot\mathbf{I} \times \mathbf{k}$	P-odd, T-odd	Three-fold correlation
$(\mathbf{s}\cdot\mathbf{I} \times \mathbf{k})\ (\mathbf{I}\cdot\mathbf{k})$	P-even, T-odd	Five-fold correlation

where the dynamical variables are neutron spin **s**, neutron momentum **k**, and target spin **I**. The helicity parity-violation test is carried out with a polarized beam and an unpolarized target. The helicity dependence of the p-wave resonance cross section is given by the analyzing power P,

$$P = (\sigma(+) - \sigma(-)) / (\sigma(+) - \sigma(-))$$

where $\sigma(+/-)$ = resonance cross section for $\mathbf{s}\cdot\mathbf{k} = +/-$. The analyzing power is determined from the difference in count rates in the two helicity states.

Our experiments make use of the intense epithermal neutron beams at the Los Alamos Neutron Scattering Center (LANSCE). A block diagram of the experimental apparatus for the helicity test is shown in fig. 1.1-1. A more detailed description was presented in an earlier progress report [TUN90], so only changes made for the 1991 run cycle will be noted. The 800-MeV H^- beam from the LAMPF accelerator is used to produce the neutrons by the spallation process. Pulses are delivered at a rate of 20 Hz and with an average current of about 60 μA. These pulses are sent into a proton storage ring where they are compressed to approximately the shape of an isosceles triangle having a FWHM of 125 μsec. After extraction, the beam is directed to a tungsten production target where 17 to 18 neutrons are produced for each incident proton. Modifications were made to the production target prior to the 1991 run cycle, which resulted in a drastic reduction (at least a factor of ten) of the gamma-flash which occurs at the beginning of the neutron burst.

The neutron beam is polarized by transmission through a polarized proton sample. Since the n-p spin-spin cross section is basically constant from 1 eV to 50 keV, this technique makes an ideal neutron spin filter. The polarized protons are dynamically polarized by microwave radiation while the proton containing material is cooled to near 1 K in a 2-Tesla magnetic field. Originally the protons were contained in the water of hydration of $(La, 0.5\%\ Nd)_2\ Mg_3\ (NO_3)_{12}\cdot 24H_20$ (LMN) crystals. The LMN crystals were very fragile, hygroscopic and subject to radiation damage. The proton polarization during 1989 was typically 37-38%, which produced a neutron polarization of about 40%. By the end of the 1990 run cycle, the proton polarization had fallen by a factor of approximately two. For the 1991 run, the LMN crystals were replaced with butanol in which ^{v}Cr-complexes are dissolved. Because of the smaller amount of additional atoms as compared with LMN, the flux of polarized neutrons is improved. Typical proton polarizations of from 30-35% were obtained with the butanol system. As mentioned in [TUN90], a new spin filter has been funded and a design has been completed by the TRIPLE cryogenic specialists and should be available for the 1992 run cycle.

In addition to our ^{6}Li-loaded glass and ^{10}B-loaded liquid scintillators which are used for neutron transmission measurements, we installed for the 1991 run cycle a prototype

capture-gamma-ray detector. This system, located 25 m from the neutron source, consisted of five pure CsI detectors, each 12" (long) x 4" x 4". The five detectors were arranged symmetrically about the beam pipe, with the long axis parallel to the beam. High current phototube bases, with transistor stabilization of the last 4 dynodes, were used to reduce gain shifts during, and to provide fast recovery following, the neutron and gamma-flash which occur at the beginning of each beam burst. Fast discriminators were used to determine the capture gamma-rays of interest and the pulses were counted individually with a multiscaler module connected to a summation memory. Substantial polyethelene shielding was located upstream from the detector. The detector itself was located in a lead-lined boron-loaded polyethelene housing. Neutrons scattered from the target were absorbed by 0.25" of boron-loaded rubber followed by 0.50" of ^{6}LiD. Part of a time-of-flight spectrum obtained with a ^{238}U target is shown in fig. 1.1-2 and covers the energy range from about 62 to 115 eV. The small peak near channel 2030 is due to the 63.5 eV p-wave resonance that we have previously studied in transmission [Bow90]. Analysis of these data is underway and we hope to improve the statistical significance of the previously studied [Bow90] p-wave resonances in ^{238}U. Experience gained with the CsI crystals will be used to help design a new gamma-ray detector for the 1992 run cycle.

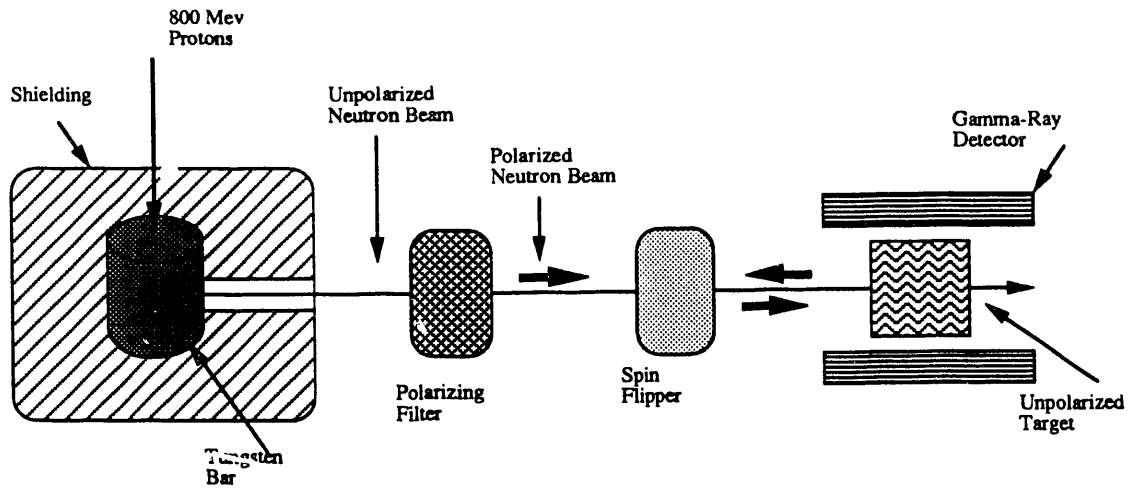

Fig. 1.1-1 Schematic of the LANSCE beam line used for measurements of P-violation with a polarized neutron beam.

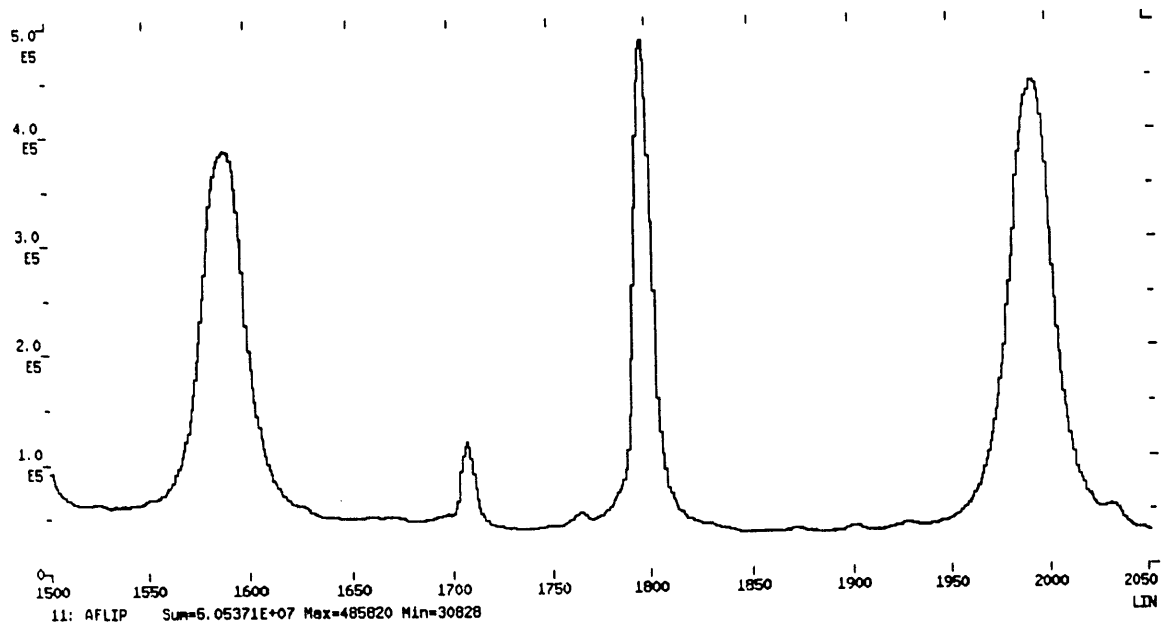

Fig. 1.1-2 Time-of-flight spectrum obtained for radiative capture with a ^{238}U target. The bin width is 1 μsec and the energy range is from approximately 62 to 115 eV.

[Alf83] V.P. Alfimenkov *et al.*, Nucl. Phys. **A398** (1983) 93
[Bow90] J.D. Bowman *et al.*, Phys. Rev. Lett. **65** (1990) 1192
[Fra91] C.M. Frankle *et al.*, Phys. Rev. Lett. **67** (1991) 564
[TUN90] TUNL Progress Report - TUNL XXIX (1990) 1

1.1.2 Sign Correlations and Parity Nonconservation for Neutron Resonances in ^{232}Th

C.M. Frankle, J.D. Bowman[1], J.E. Bush, P.P.J. Delheij[2], C.R. Gould, D.G. Haase, J.N. Knudson[1], G.E. Mitchell, S. Penttila[1], H. Postma[3], N.R. Roberson, S.J. Seestrom[1], J.J. Szymanski[1,4], S.H. Yoo[1], V.W. Yuan,[1] X. Zhu

Polarized neutron transmission experiments show remarkable sensitivity to the presence of small symmetry-violating forces in nuclear interactions. Parity-nonconserving (PNC) analyzing powers of order a percent or more have been observed [Alf83, Mas89, Bow90] for p-wave resonances in nuclei ranging from ^{81}Br to ^{238}U. The large enhancement over

---

[1] Los Alamos National Laboratory, Los Alamos, NM 87545
[2] TRIUMF, Vancouver, British Columbia, Canada V6T 2A3
[3] University of Technology, Delft, The Netherlands
[4] Present address: Indiana University, Bloomington, IN 47405

the 10^{-7} size of typical weak interaction effects has been explained by the assumption that the mixing occurs between wave functions of closely spaced compound nuclear (CN) levels of the same spin, J, but opposite parity, $\pm\pi$ [Sus82, Bun83]. The wave function admixture scales as the square root of the level density, and the PNC analyzing power is further enhanced by the favorable ratio of s-wave to p-wave decay amplitudes.

Previous results [Alf83, Mas89, Bow90] were generally consistent with these ideas. But because only five large effects had been observed, a number of questions about the mechanism of parity mixing remained. The statistical theory predicts that all pairs of $J^{\pm\pi}$ resonances should interfere and, at some level, show nonzero PNC analyzing powers. In addition, the signs of effects are expected to be random because the matrix elements, neutron decay amplitudes, and energy differences are themselves randomly distributed in sign.

The TRIPLE collaboration has recently studied 23 p-wave resonances in ^{232}Th and for the first time has verified that many p-wave resonances in a single nucleus show non-zero PNC effects. Two of the analyzing powers are as large as any previously observed. However, the results show significant sign correlations that are not consistent with the simple model of randomly distributed matrix elements and CN variables.

The measurements were carried out on the 56-m flight path at the Los Alamos Neutron Scattering Center (LANSCE). The experimental techniques were similar to those described in our earlier work [Bow90]. Resonances up to $E_n \sim 400$ eV were studied. The most recent ^{232}Th evaluation [Ols82] identifies 39 p-wave resonances in this energy range and 23 of these were strong enough to be analyzed reliably.

Two thirds of the ^{232}Th p-wave resonances are expected to have $J = 3/2$, and cannot exhibit s - p parity mixing. The $p_{3/2}$ resonances will be somewhat weaker than the $p_{1/2}$ resonances on average, but if we assume one-third of our data set is $p_{1/2}$, then we expect to see about eight PNC effects. In fact we see seven results at $> 2\sigma$ statistical significance (95% confidence). These correspond to the resonances at 8, 37, 38, 64, 128, 167, and 196 eV. Two of the effects (38 and 64 eV) are of order 10%, as large as any effect seen previously. The data thus show convincingly that parity violation is a general feature of all $p_{1/2}$ resonances in ^{232}Th.

In the statistical model of CN mixing, the longitudinal analyzing power P_i of the p-wave resonance at energy E_{pi} arises from admixtures of s-wave resonances at energies E_{sj}:

$$P_i = \sum_j A_{ij} V_{ij} \quad \text{with} \quad A_{ij} = \frac{2\gamma^n_{sj}/\gamma^n_{pi}}{E_{sj} - E_{pi}}$$

The partial neutron width amplitudes of the resonances γ^n_{pi} and γ^n_{sj}, and the PNC mixing matrix elements V_{ij} are expected to be independent Gaussian-distributed random variables with mean zero. In addition, the sign of the energy difference $E_{sj} - E_{pi}$ is expected to vary randomly, since close-lying s-wave resonances are as likely to be above in energy as below compared to the p-wave resonance.

Figure 1.1-3 shows the statistical significance, P_i/σ_{Pi}, and the signs of the analyzing powers. All seven results at $> 2\sigma$ are positive in sign. The chance of obtaining the same

sign for seven out of seven randomly distributed quantities is 1.6% (given by twice the binomial distribution factor $P(x,n,p) = \frac{n!}{x!(n-x)!}\, p^x\, (1-p)^{n-x}$).

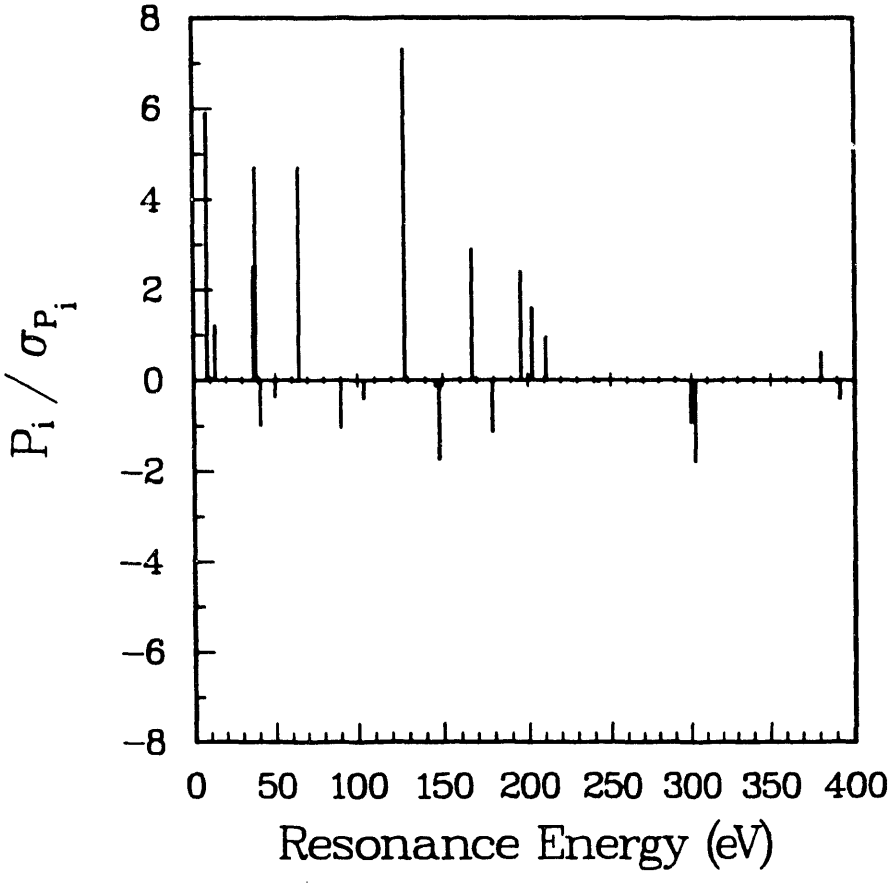

Fig. 1.1-3 Statistical significance, P_i/σ_{P_i}, of longitudinal analyzing powers for p-wave resonances in ^{232}Th. Note that all of the parity violations with statistical significance greater than 2σ have positive signs.

Six of eight results at $> 2\sigma$ for analyzing powers measured for other nuclei are also positive in sign. These are results from Alfimenkov *et al.* [Alf83] for ^{81}Br (0.88 eV), ^{111}Cd (4.53 eV), ^{117}Sn (1.33 eV), and ^{139}La (0.73 eV), and from our previous work [Bow90] for ^{238}U (57.9; 63.5, 83.7, and 89.2 eV). The sign of the ^{139}La (0.73 eV) effect has been confirmed by Masuda *et al.* [Mas89] and by us [Yua91]. We have also confirmed the sign of the ^{81}Br and ^{117}Sn effects. The only known negative values are a 7σ effect for the 4.53 eV resonance in ^{111}Cd and a $\sim 2\sigma$ effect for the 89.2 eV resonance in ^{238}U. The chance of obtaining the same sign for 13 of 15 randomly distributed quantities is 0.6%. We conclude, therefore, that the present data for ^{232}Th and data in the literature for other nuclei suggest an unexpected correlation in the signs of PNC analyzing powers for CN resonances.

The results have been published in Physical Review Letters. We are currently investigating valence model theories to determine if they are able to explain quantitatively the magnitudes of the effects.

[Alf83] V.P. Alfimenkov *et al.*, Nucl. Phys. **A398** (1983) 93
[Bow90] J.D. Bowman *et al.*, Phys. Rev. Lett. **65** (1990) 1192
[Bun83] V.E. Bunakov and V.P. Gudkov, Nucl. Phys. **A401** (1983) 93
[Mas89] Y. Masuda *et al.*, Nucl. Phys. **A504** (1989) 269
[Ols82] D.K. Olsen, ORNL / TM-8056 (1982)
[Sus82] O.P. Sushkov and V.V. Flambaum, Sov. Phys. Usp. **25** (1982) 1
[Yua91] V.W. Yuan *et al.* (to be published)

1.1.3 Acquired Polarization Effects in Parity-Violation Experiments

G.E. Mitchell, J.R. Vanhoy[1], P.A. Larson[1]

The recent emphasis on tests of fundamental symmetries has made clear the need for a detailed understanding of all aspects of the physical processes involved in these experiments. It is crucial to understand experimental errors (eg., beam or target polarization misalignments) which mimic symmetry violation or the combination of two symmetry conserving effects which together mimic symmetry violation. This is particularly true for the threefold correlation test of time reversal invariance.

The most direct approach is to include explicitly all angular momentum factors and to use experimental resonance parameters whenever possible. As a first step we have considered parity violation experiments of the type $\mathbf{I}\cdot\mathbf{k}$ – an unpolarized beam on a polarized target. Such experiments have been proposed [Haa88] and the analysis of such measurements discussed [Van89, Gou90].

In these proposed experiments an unpolarized beam is passed through a target polarized in the +z and –z directions and the experimental difference in transmission measured. The longitudinal asymmetry in the simplest case is ε = constant n P^Tt, where n is the target density, P^T is the z component of the target polarization, and t is the target thickness. However, while passing through the target the neutron acquires polarization due to the parity-conserving spin-spin interaction. This effect is well known; the issue is whether it is important for the parity-violation experiment. Intuitively one expects the parity violation due to this effect to be small relative to the standard term, or at most comparable. In fact the acquired polarization term can dominate by orders of magnitude.

We follow the approach of Postma [Pos62] for the analysis of acquired polarization for an unpolarized beam on a polarized target in the parity-conserving case. He considers the expressions for the number of neutrons ω_+ (ω_-) with spin parallel (antiparallel) to the z axis and solves the resulting coupled differential equations. We adopt the same approach, but include the parity-violation effect. The cross section is written as

---

[1] U.S. Naval Academy, Annapolis, MD

$$\sigma = a + b\,P^n + c\,P^T + d\,P^n\,P^T, \qquad (1)$$

where P^n is the z component of the neutron polarization. Terms a and d are parity conserving, while terms b and c violate parity. Explicit expressions were derived for all terms for projectile spin 1/2 and target spin 1/2, and the resulting coupled differential equations solved. If the initial beam polarization is zero and bulk depolarization processes are neglected, a simple expression for the longitudinal asymmetry results:

$$\varepsilon = -\,n\,c\,P^T t + nbt\,\tanh(ndP^T t) \qquad (2)$$

For only two cases, low-energy resonances in ^{113}Cd and ^{117}Sn, are all the resonance parameters even claimed to be known. We calculated the relative value of the two terms (which we call the thin-target and the acquired-polarization terms) for these nuclei, including all nuclear spectroscopic information. For the 7.0-eV p-wave resonance in ^{113}Cd the results are mildly suprising: for reasonable target thicknesses the acquired-polarization term is comparable to the thin-target term. However, for the 1.3 -eV p-wave resonance in ^{117}Sn the acquired-polarization term is about 100 times larger than the thin-target term.

The origin of this extremely large effect lies in the details of the nuclear spectroscopy. In the limit as the thickness t becomes very large, the ratio of the two terms in the asymmetry is $-b/c = (x - 2y) / (x + 2y)$, where x and y are the entrance-channel-spin mixing ratios. For the 1.3-eV resonance in ^{117}Sn, these mixing ratios are such that $b = 1.99$ and $c = 0.01$. Thus, by accident, the acquired polarization term dominates by orders of magnitude.

This analysis can also be extended to targets with higher spin. We considered the 0.7-eV resonance in ^{139}La. Although the resulting expressions are much more complicated, they can be reduced to a form similar to Eq. 1, and the analysis carried through similarly to that for spin 1/2. When experimental values were not available for the channel mixing parameters, we assumed typical values.

These calculations are intended as illustrations. However, they make the point that the spectroscopic details must be included in realistic analyses. For the proposed time-reversal-invariance violation measurements, where one must be concerned about very small systematic errors in both experiment and analysis, such details are even more important. We plan to perform a similar analysis for the threefold-correlation experiment. This is a much more complicated problem since one must consider three polarization directions. We plan to maintain the spirit of the present approach, and continue to formulate the problem in terms of coupled differential equations.

[Gou90] C.R. Gould *et al.*, Int. J. Mod. Phys. **A5** (1990) 2181
[Haa88] D.G. Haase *et al.*, Hyperfine Interactions **43** (1988) 127
[Pos62] H. Postma *et al.*, Phys. Rev. **126** (1962) 979
[Van89] J.R. Vanhoy *et al.*, Z. Phys. A **333** (1989) 229

1.2 Time-Reversal-Invariance Experiments

We are making a three-pronged attack on the problem of limits to time-reversal invariance in the strong interaction as manifested in low-energy experiments. The first series of experiments is being mounted by the TRIPLE collaboration at LANL/LANSCE to look for evidence of time-reversal-invariance in epithermal-neutron scattering. The second type of experiment, performed at TUNL, is a test of time-reversal invariance in the direct-reaction regime. The third method is to look for interference effects between nearby resonances in tests of detailed balance.

The following subsections provide more detail on each of these research directions.

1.2.1 Measurements at LANSCE of Neutron Depolarization in Holmium

D.G. Haase, J.D. Bowman[1], P.P.J. Delheij[2], C.M. Frankle[1], J.E. Koster, C.R. Gould, J.N. Knudson[1], G.E. Mitchell, S. Penttila[1], H. Postma[3], N.R. Roberson, S.J. Seestrom[1], S.H. Yoo[1], V.W. Yuan[1]

The TRIPLE collaboration is investigating violations of fundamental symmetries in neutron scattering in cases where the particular symmetry violation would be enhanced by nuclear resonances. One such test is the fivefold-correlation (FC) test for time-reversal invariance which has been conducted at TUNL in the MeV region, i.e. without resonant enhancements [Kos 91]. At lower neutron energies time-reversal-violating effects would be diminished by the precession (depolarization) of the neutrons in the internal magnetic fields of the holmium domains.

Because domain structure is very sample specific, it is necessary to measure the domains in the particular crystal that would be used for the FC experiment. Most domain measurements either require thin samples or only probe surface domains. We have measured the depolarization of epithermal neutrons in the 2.3-cm-diameter single crystal cylinder of ^{165}Ho that was used in the TUNL experiment. The large enhancement of parity violation in the 0.734-eV resonance in ^{139}La was used to analyze the neutron polarization [Yua 91]. Our experiment is the first practical application of parity violation in nuclear reactions to a measurement problem in condensed matter physics.

A beam of longitudinally polarized neutrons of polarization f_{no} incident on a target becomes depolarized through the action of the component of the internal magnetic field B_{perp} perpendicular to the polarization axis. The polarization of the exiting beam is $f_n = f_{no} \exp(-2Dt)$ where D is the polarization parameter, the mean free path for a neutron spin reversal. If the sample is composed of small randomly oriented magnetic domains of average size δ then

$$D \approx \frac{\mu_n}{h} \left\langle B_{perp}^2 \delta^2 \right\rangle_{avg} \frac{n}{v_n^2}$$

---

[1] Los Alamos National Laboratory, Los Alamos, NM
[2] TRIUMF, Vancouver, BC, Canada V6T 2A3
[3] The University of Technology, Delft, The Netherlands

where μ_n is the magnetic moment of the neutron, v_n is the speed of the neutron and n is the number of domains per unit length [Pos 62]. In an unpolarized single crystal of ^{165}Ho at 4.2 K there is a net magnetic field in each domain of 0.6635 T parallel or antiparallel to the c crystalline axis. Therefore, if θ is the angle between the c axis and the neutron polarization direction, then

$$\left\langle B_{perp}^2 \delta^2 \right\rangle_{avg} = (0.6635\ T)^2 \sin^2\theta \, \langle \delta^2 \rangle_{avg}$$

Thus, by measuring f_n/f_{no} one can determine the average magnetic domain size. The preliminary depolarization data are displayed in fig. 1.1-4. For $\theta > 30^o$ the data are a strongly-varying function of θ, as expected by the elementary model of the domains in the bulk of the crystal, and the indication is that the average domain size is 2 to 3 microns. The orientation independence of f_n/f_{no} for small angles may indicate the presence of closure domains on the surface of the crystal, which will be investigated further.

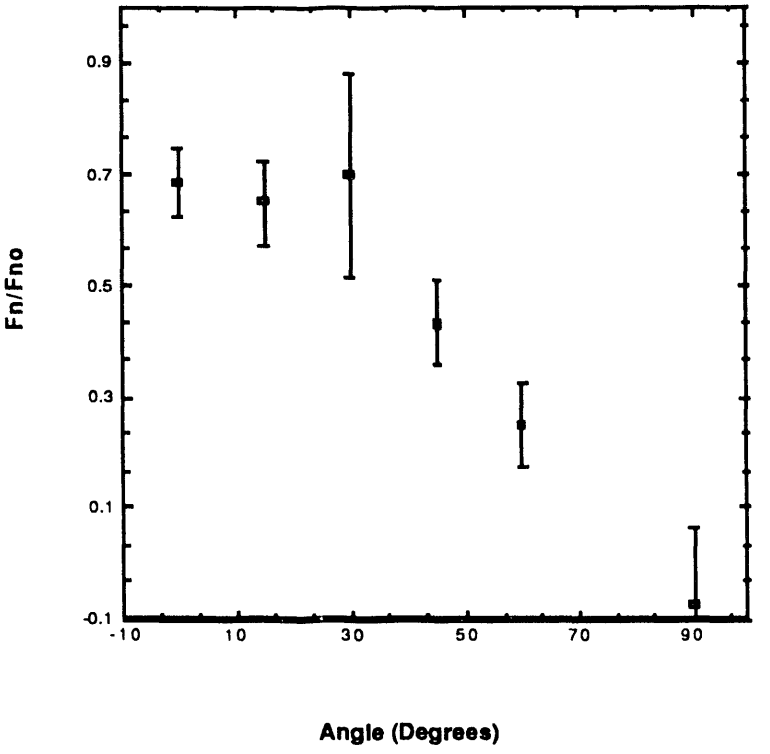

Fig. 1.2-1 The depolarization of longitudinally polarized neutrons in a ^{165}Ho single crystal. The quantities f_{no} and f_n are the polarizations of the incident and exiting neutron beams. The horizontal axis is the relative angle between the neutron polarization axis and the c crystalline axis of the target.

We have demonstrated that such depolarization measurements are possible at LANSCE. There is the possibility of extending the technique to other neutron energies using the parity enhancement effects in other neutron resonances [Fra 91]. Finally, it appears that the effect of neutron depolarization in the FC experiment can be analyzed by these measurements.

[Fra91] C.M. Frankle *et al.*, Phys. Rev. Lett. **67** (1991) 564

[Kos91] J.E. Koster, C.R. Gould, D.G. Haase and N.R. Roberson, Phys. Lett. B, to be published

[Pos62] H. Postma, H. Marshak, V.L. Sailor, F.J. Shore and C.A. Reynolds, Phys. Rev. **126** (1962) 979

[Yua91] "Parity Nonconservation in Polarized-Neutron Transmission Through ^{139}La," V.W. Yuan, C.D. Bowman, J.D. Bowman, J.E. Bush, P.P.J. Delheij, C.M. Frankle, C.R. Gould, D.G. Haase, J.N, Knudson, G.E. Mitchell, S. Penttila, H. Postma, N.R. Roberson, S.J. Seestrom, J.J. Szymanski and X. Zhu, Phys. Rev. C, to be published

1.2.2 Direct-Reaction Test of T-Violation in 2-MeV Neutron Scattering from Aligned ^{165}Ho

J.E. Koster, E.D. Davis[1], C.R. Gould, D.G. Haase, N.R. Roberson, L.W. Seagondollar, S. Wilburn, X. Zhu

Neutron transmission measurements are presently of considerable interest in studies of symmetry violation in hadronic systems [Bow90]. The fivefold correlation (FC) test searches for a T-odd P-even term in the forward elastic scattering amplitude of the form $(\mathbf{s} \cdot \mathbf{k} \times \mathbf{I})(\mathbf{k} \cdot \mathbf{I})$; **s** and **k** are the neutron spin and momentum, and **I** is the target spin. While P-even time-reversal violation is not expected within the standard model, the experimental limits established in hadronic systems [Hen89] are only of order 10^{-3}.

We recently carried out the first search for this term, using 2-MeV polarized neutrons and an aligned ^{165}Ho target ($I^{\pi} = 7/2^{-}$). The results have been published in Physics Letters. The energy spread in the beam was about 100 keV, and any T-violating effect is due to direct reaction contributions (CN contributions are averaged to zero). T-violation in direct reactions arises from the presence of T-odd interactions in the target and residual nucleus — in this instance, non-zero matrix elements of the T-odd interaction coupling the ground state to $7/2^{-}$ excited states in ^{165}Ho. Moldauer [Mol68] has inferred a limit of about 25 keV on T odd interaction matrix elements from detailed balance studies with direct reactions.

A novel feature of the experiment is that we vary the angle θ between the axis of alignment (c-axis) of the holmium and the beam direction. This eliminates many systematic errors associated with neutron analyzing power effects, misalignments of the beam and target, and target thickness variations [Kos90]. The magnitude of the FC effect can be obtained by a fit to the angular dependence of the transmission asymmetry

---

[1] University of Arizona, Tuscon, AZ 85721

$$\varepsilon_5(\theta) = \frac{N_+(\theta) - N_-(\theta)}{N_+(\theta) + N_-(\theta)}, \tag{1}$$

where $N_+(\theta)$ and $N_-(\theta)$ denote the number of neutrons transmitted when the incident neutron spins are parallel and anti-parallel to **k** x **I**.

The neutrons were produced in the $T(\vec{p},\vec{n})$ reaction using a 0.8 Ci/cm^2 tritiated titanium foil and a 1μA beam of 3.2-MeV polarized protons. The neutron polarizations were flipped at 10 Hz and were monitored by two detectors placed at ±45° with respect to the beam. Typical holmium target temperatures were around 285 mK, yielding 65% of the maximum alignment.

Results for the transmitted neutron asymmetries are shown in fig. 1.2-2. The data for $\varepsilon_5(\theta)$ are plotted on an expanded vertical scale and are consistent with zero asymmetry. Deformation effect asymmetries ($\varepsilon_{def}(\theta) = (N_+(\theta) + (N_-(\theta))/N_{AV} - 1/2$) show the expected large $P_2(\cos\theta)$ variation.

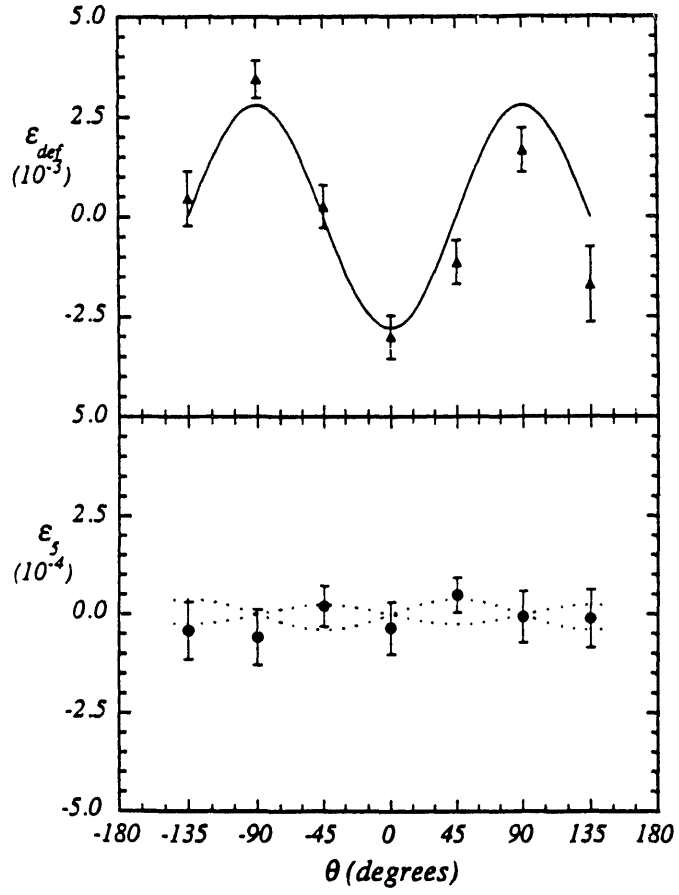

Fig. 1.2-2 Deformation effect asymmetries $\varepsilon_{def}(\theta)$, and T-violating spin-flip asymmetries $\varepsilon_5(\theta)$, as a function of the angle θ between the ^{165}Ho alignment axis and the beam direction. Note the different vertical scales. The solid line is a fit to the deformation effect data and the dotted lines are the bounds from a fit to the ±45° and ±135° spin flip asymmetry data.

The spin-flip asymmetries are related to the T-odd analyzing power A_5 by

$$\varepsilon_5(\theta) = \sqrt{15/8}\,\sin(\theta)\,\cos(\theta)\,\hat{t}_{20}(7/2)P_n n\sigma_{TOT}\,A_5 \qquad (2)$$

where $P_n \approx 0.40$ is the average neutron polarization, $n = 0.058$ atoms/b is the effective target thickness of the holmium cylinder and $\sigma_{TOT} = 7.04$ b at 2MeV. From an analysis of the ±45° and ±135° data, we find $A_5 = (1 \pm 6) \times 10^{-4}$, consistent with time-reversal-invariance. The bounds implied for $\varepsilon_5(\theta)$ are shown in fig. 1.2-20. as the dotted lines.

We identify the analyzing power A_5 with the ratio of energy-averaged elastic-scattering matrix elements of the anti-symmetric and symmetric parts (S^a and S^s, respectively) of the S-matrix:

$$A_5 \approx \langle S^a_{c\alpha_0;\alpha_0}\rangle / \langle S^s_{c\alpha_0;\alpha_0}\rangle, \qquad (3)$$

where $\langle\cdots\rangle$ denotes the energy-averaging operation and (c,α) the quantum numbers of reaction channels, α specifying the $7/2^-$ eigenstates of the ^{165}Ho target. Following Moldauer [Mol68], we attribute the anti-symmetric part of $\langle S^a \rangle$ to T-odd interaction matrix elements, $H_{\alpha_0\alpha_n}$, which couple the ground state α_0 of ^{165}Ho with excited $7/2^-$ states α_n. Retaining only the first excited state α_1, we have

$$\langle S^a_{c\alpha_0;c'\alpha_0}\rangle \sim \left(\frac{H_{\alpha_0\alpha_1}}{E_{\alpha_0} - E_{\alpha_1}}\right)\langle S^s_{c\alpha_0;c'\alpha_1}\rangle \qquad (4)$$

Thus, a bound on A_5 is related to a bound on $H_{\alpha_0\alpha_1}$ by

$$H_{\alpha_0\alpha_1} \sim \left(E_{\alpha_0} - E_{\alpha_1}\right)\left(\left\langle S^s_{c\alpha_0 c\alpha_0}\right\rangle / \left\langle S^s_{c\alpha_0 c'\alpha_1}\right\rangle\right) A_5. \qquad (5)$$

The first-excited $7/2^-$ state at 637.8 keV is one of three levels excited in the (n,n') reaction with cross section ≈600 mb. Assuming an equal division of the cross-section among these three levels, the inelastic cross section, σ_{inel}, for the 638-keV state is 200 mb. From coupled channels calculations, the total elastic scattering cross section, σ_{el}, at 2MeV is 3.7 b. Substituting the ratio of S-matrix elements in Eq. (5) by the square root of the ratios of the cross sections, we obtain a bound on $H_{\alpha_0\alpha_1}$ of about 1.3 keV, which is a factor of 20 smaller than the direct-reaction T-odd matrix element bound quoted by Moldauer [Mol68].

[Bow90] J.D. Bowman *et al.* in: Fundamental symmetries in nuclei and particles, eds. H. Hendrikson and P. Vogel (World Scientific, Singapore, 1990) p.1

[Hen89] E.M. Henley, in: Weak and electromagnetic interactions in nuclei, ed. P. Depommier (Editions Frontiéres, 1989) p. 181

[Kos90] J.E. Koster, Ph.D. thesis, N.C. State University 1990, unpublished

[Mol68] P.A. Moldauer, Phys. Lett. **26B** (1968) 713

1.2.3 Search for Resonances Suitable for Tests of Detailed-Balance Violation

J.M. Drake, E.G. Bilpuch, C.R. Bybee, G.E. Mitchell, J.F. Shriner, Jr.[1], J.T. Slayton[1]

It has recently been suggested that large enhancements of time-reversal-invariance (TRI) violations might be observed by tests of detailed balance near two interfering resonances [Bun89]. We have searched our large collection of (p,α) resonance data for pairs of resonances which might be particularly suitable for such a test; targets include ^{23}Na, ^{27}Al, ^{31}P, ^{35}Cl, and ^{39}K.

We found 33 cases in which adjacent resonances had the same J^{π}; these include seven different combinations of target spin and compound state spin/parity. While Bunakov and Weidenmüller examined the total cross section, the differential cross section is much more relevant for (p,α) measurements; thus, in the spirit of [Bun89], we have examined the quantity

$$\Delta(E,\theta) \equiv 2\,\frac{\frac{k_p^2}{g(p,\alpha)}\frac{d\sigma}{d\Omega_{(p,\alpha)}}(E,\theta) - \frac{k_\alpha^2}{g(\alpha,p)}\frac{d\sigma}{d\Omega_{(\alpha,p)}}(E,\theta)}{\frac{k_p^2}{g(p,\alpha)}\frac{d\sigma}{d\Omega_{(p,\alpha)}}(E,\theta) + \frac{k_\alpha^2}{g(\alpha,p)}\frac{d\sigma}{d\Omega_{(\alpha,p)}}(E,\theta)}\ ,$$

where $k = 2\pi/\lambda$ and g is the usual statistical factor. We have evaluated the differential cross-section expression for all seven spin/parity combinations for which data are available. Collision matrix elements have been derived for a Hamiltonian $H=H_0+iW$, following the approach used by Moldauer [Mol68], assuming only internal mixing and only two states. With these assumptions Δ is to first order proportional to W. A computer program to calculate Δ in the region of each of these 33 pairs has been written. We are currently evaluating the results.

[Bun89] V.E. Bunakov and H.A. Weidenmüller, Phys. Rev. **C39** (1989) 70

[Mol68] P.A. Moldauer, Phys. Rev. **165** (1968) 1136

1.3 Fluctuation Properties of Nuclear States

There is much interest in studying the fluctuations of energy levels in quantum systems and in understanding their role as a signature for quantum chaos. Several recent studies have suggested that agreement with the Gaussian orthogonal ensemble (GOE) version of random matrix theory is indicative of chaotic behavior and that agreement with Poisson statistics is indicative of regular behavior. The fluctuation properties of a collection of high-quality neutron and proton resonance data have been analyzed in depth and show both the short-range and long-range order required by GOE [Haq82, Boh85]. This approach has also been applied to levels of the nucleus ^{26}Al [Mit88, Shr90]; there the fluctuation proper-

---

[1] Tennessee Technological University, Cookeville, TN

ties show behavior intermediate between GOE and Poisson over an excitation energy range of E_x=0-8 MeV.

Application of this approach to nuclear levels from the ground state to the resonance region, as was done with ^{26}Al, is very difficult. There are severe limitations imposed, since the data set must be pure (correct spin assignments) and complete (no missing levels). For ^{26}Al, the first 100 positive-parity states have been identified and the spectroscopic assignments have been confirmed by detailed comparisons with the nuclear shell model. Negative-parity states are also known experimentally, but no detailed comparison with theory is available. The fluctuation properties appear to be independent of isospin, which is thought to be a rather good, but not perfect, symmetry in this nucleus. This result is consistent with general predictions by Dyson [Dys62] and Pandey [Pan81] that even a small breaking of a symmetry yields fluctuation patterns like those which would be present in the complete absence of the symmetry. A study by Guhr and Weidenmüller [Guh90] confirms this prediction specifically for the isospin symmetry. This result is significant for symmetry-breaking tests using fluctuations, since a weak perturbation can drive the system from Poisson toward GOE behavior.

During the past year, we have made progress in several areas of fluctuation studies, as we now summarize.

1.3.1 Energy Levels of ^{30}P for Fluctuation Studies

S.C. Frankle, J.F. Shriner, Jr.[1], *G.E. Mitchell, E.G. Bilpuch, C.R. Westerfeldt*

To further clarify the ^{26}Al results, additional data would be helpful. The best candidates for the study of nuclear levels from the ground state into the resonance region are the odd-odd nuclei ^{22}Na, ^{30}P, ^{34}Cl, and ^{38}K. These nuclei have several properties which make them excellent candidates for this type of study; they have a low proton separation energy, T=0 and T=1 states coexist over the entire energy range, and there is a sufficient number of levels for statistical tests. Of the above candidates, ^{30}P has the target which is easiest to fabricate for study with proton beams (^{29}Si) and the most convenient to use in practice. Therefore, ^{30}P was chosen for study.

As a first step, the ^{29}Si(p,γ), ^{29}Si(p,p$_1\gamma$), and ^{29}Si(p,p$_2\gamma$) reactions were studied over an energy range E_p=2.0-3.3 MeV. A total of 15 previously unobserved resonances were identified; a portion of the data is shown in fig. 1.3-1. Absolute strengths were obtained for resonances in the ^{29}Si(p,γ) reaction, and relative strengths were obtained for resonances in the ^{29}Si(p,p$_1\gamma$) and ^{29}Si(p,p$_2\gamma$) reactions.

When these new data are combined with the ^{29}Si(p,γ) studies of Reinecke *et al.* [Rei85] and p+^{29}Si studies of Nelson *et al.* [Nel83], there is a total of 23 resonances in the range E_p=0.95-3.33 MeV which had not previously been observed in charged-particle scattering. Each of these 23 resonances has been studied with the reactions ^{29}Si(p,p), ^{29}Si(p,p$_1$) and ^{29}Si(p,p$_2$). Data for one of the resonances are shown in fig. 1.3-2, along with an R-matrix fit to the elastic scattering data and a Gaussian/Lorentzian fit to the γ-ray data. This

[1] Tennessee Technological University, Cookeville, TN

resonance shows nicely the need for studying a variety of channels when one is interested in a complete level scheme.

A compilation of currently known spectroscopic information for ^{30}P has been made. To date, 156 levels have been identified. The excitation-energy region in which it is most difficult to identify all the levels is that slightly below the proton separation energy. We are designing a Compton-suppressed γ-ray spectrometer (see Section 5.5) to search for levels in this region.

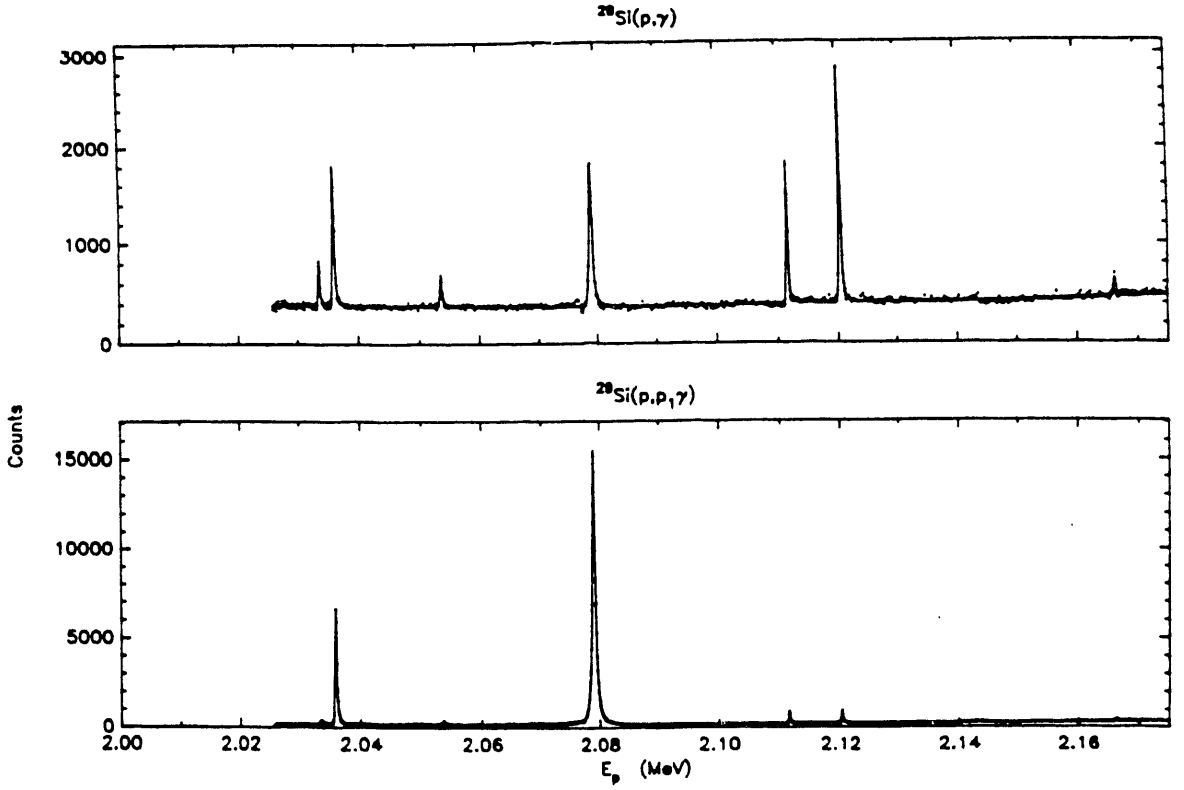

Fig. 1.3-1 Data and fits for the ^{29}Si(p,γ) and ^{29}Si(p,p$_1$γ) reactions over the energy range E_p=2.000-2.175 MeV.

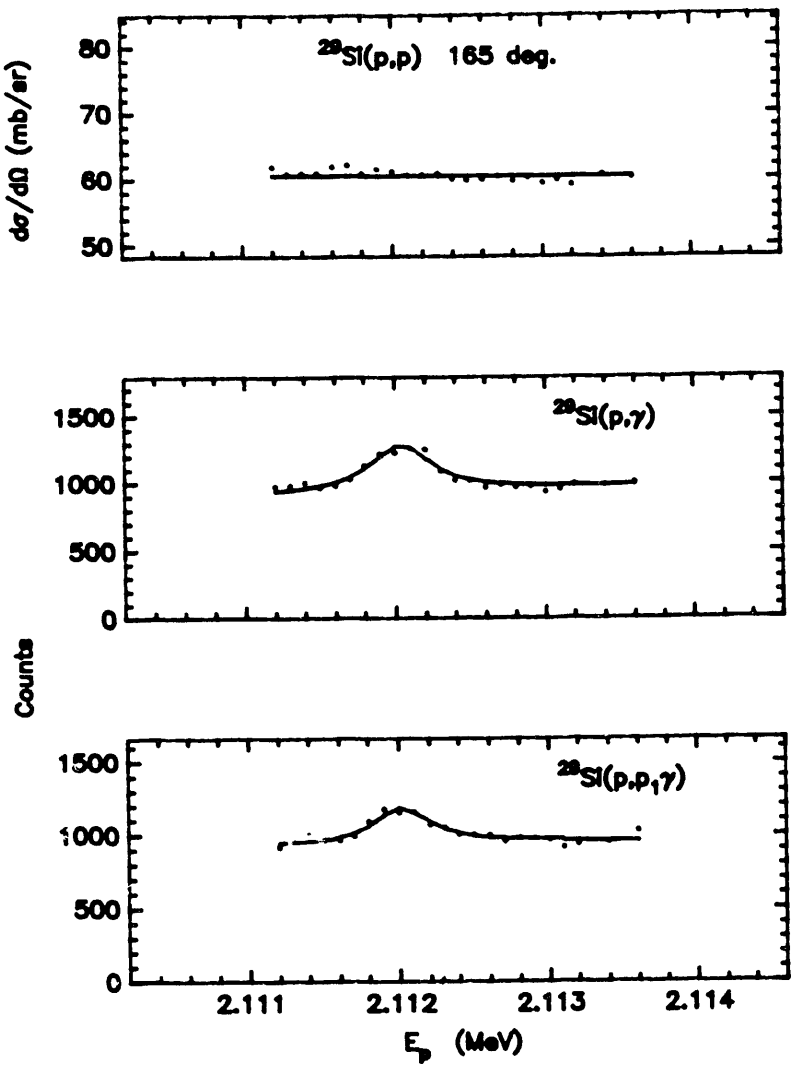

Fig. 1.3-2 Data and fits in the region of the resonance at E_p=2.1120 MeV.

[Boh85] O. Bohigas, R.U. Haq and A. Pandey, Phys. Rev. Lett. **54** (1985) 1645

[Dys62] F.J. Dyson, J. Math. Phys. **3** (1962) 1191

[Guh90] T. Guhr and H.A. Weidenmüller, Ann. Phys. **199** (1990) 412

[Haq82] R.U. Haq, A. Pandey and O. Bohigas, Phys. Rev. Lett. **48** (1982) 1086

[Mit88] G.E. Mitchell *et al.*, Phys. Rev. Lett. **61** (1988) 1473

[Nel83] R.O. Nelson *et al.*, Phys. Rev. **C27** (1983) 930

[Pan81] A. Pandey, Ann. Phys. **134** (1981) 110

[Rei85] J.P.L. Reinecke *et al.*, Nucl. Phys. **A435** (1985) 333

[Shr90] J.F. Shriner, Jr. *et al.*, Z. Phys. **A335** (1990) 393

1.3.2 Fluctuation Properties of Low-lying Nuclear States

G.E. Mitchell, J.F. Shriner, Jr.[1], *T. von Egidy*[2]

As discussed in the introduction to Section 1.3, it appears that the fluctuation properties of quantum energy levels may be used as a signature to determine whether the system is chaotic or regular. To study the behavior of nuclear levels near the ground state, we have analyzed data from 90 different nuclides which appear to be sufficiently complete and pure over some limited range of energy and angular momentum [Shr91]. Because of the limited number of levels in any single nuclide, we had to combine data from different nuclides to obtain statistically significant results. The nearest-neighbor spacing (NNS) distributions as a function of mass are shown in fig. 1.3-3. The lightest nuclei show GOE behavior, and the heaviest show Poisson; there is a relatively smooth transition from one extreme to the other as the mass increases.

Other effects are also present in the data, however. Figure 1.3-4 shows a spin dependence in even-even deformed nuclides. For example, 0^+ and 3^+ states show different behavior than do 2^+ and 4^+ states. There is also an effect due to deformation, as shown in fig. 1.3-5; the 2^+ and 4^+ states in deformed nuclides show different behavior than other states in the same nuclides, while no such distinction is observed in the spherical nuclides.

The significance of these results is not completely clear. One possible explanation of the mass dependence is that another symmetry (perhaps the projection quantum number K) is necessary to understand the fluctuations in the heavier nuclides. However, the spin results then suggest different amounts of symmetry-breaking for different spins. Clearly, more data are needed. It would also be helpful to find alternate signatures of chaos which do not place such stringent requirements on the quality of data. We are currently beginning to explore the use of the Fourier transform as a tool for identifying chaos in nuclear spectra; this technique has been used in molecular physics to analyze anticrossing spectra [Lev86]. We hope to apply the technique to the analysis of the nearly 700 levels found recently in p+^{48}Ti [Li91].

---

[1] Tennessee Technological University, Cookeville, TN
[2] Technical University of Munich, FRG

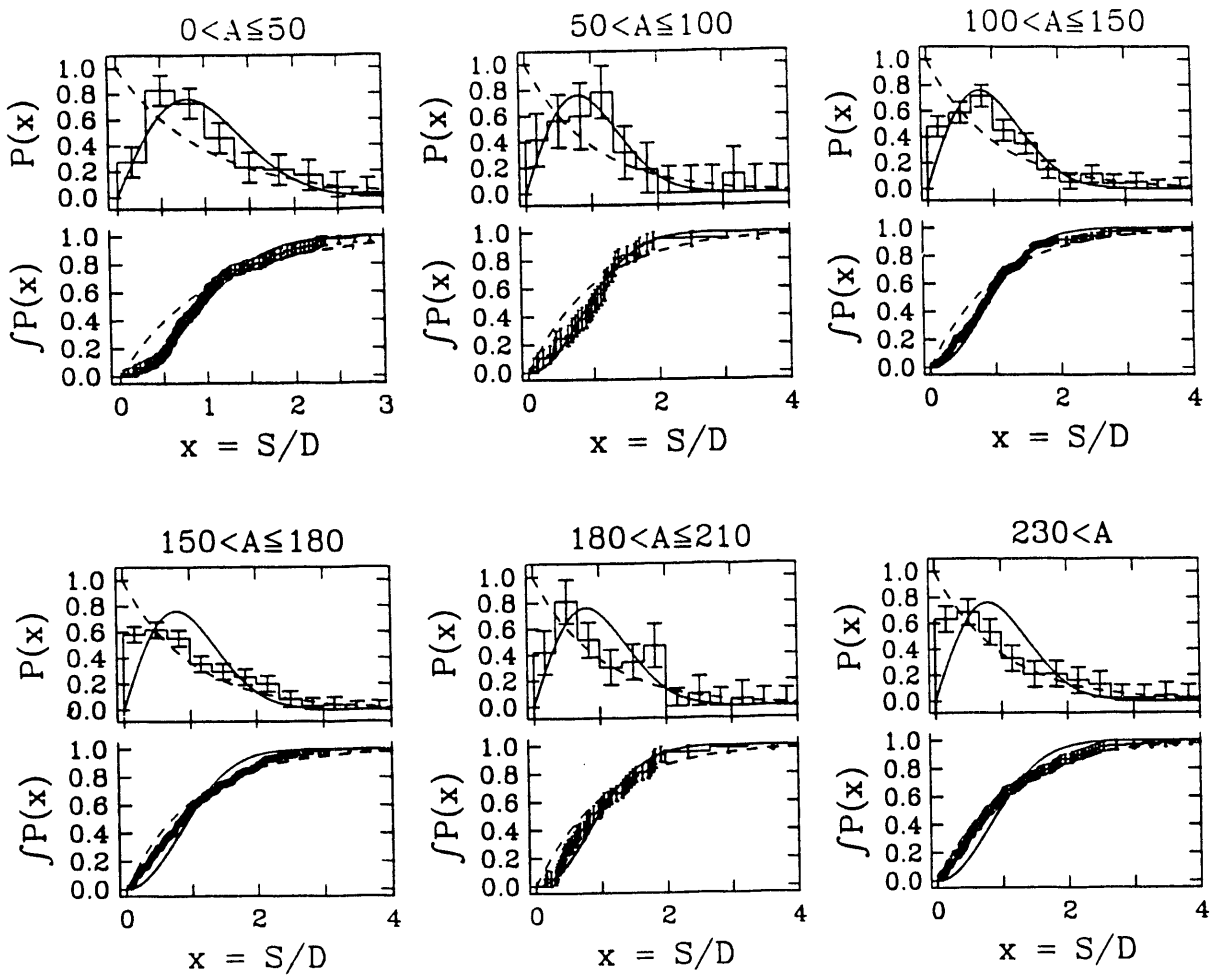

Fig. 1.3-3 Nearest-neighbor-spacing distributions and cumulative distributions for levels in six different mass regions. The dashed lines show the behavior for a Poisson distribution and the smooth solid lines show it for a GOE distribution.

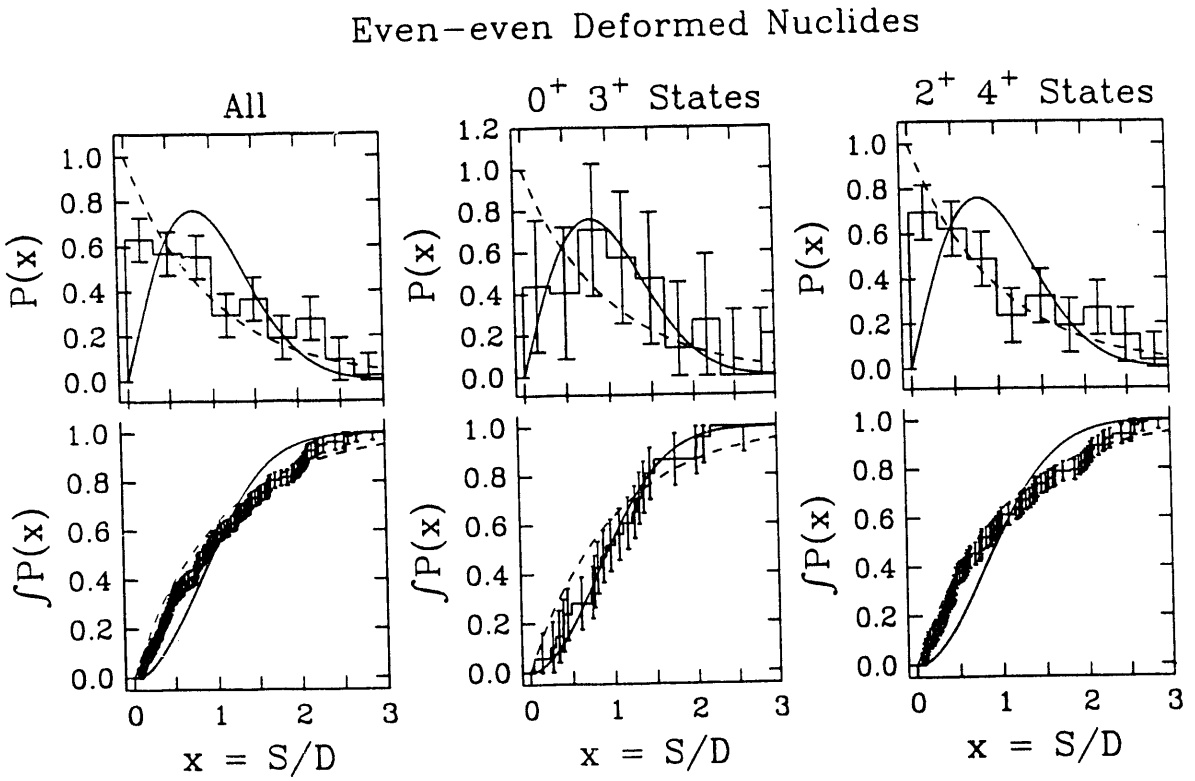

Fig. 1.3-4 Nearest-neighbor-spacing distributions and cumulative distributions for levels in even-even deformed nuclides. The dashed lines show the behavior for a Poisson distribution and the smooth solid lines show it for a GOE distribution.

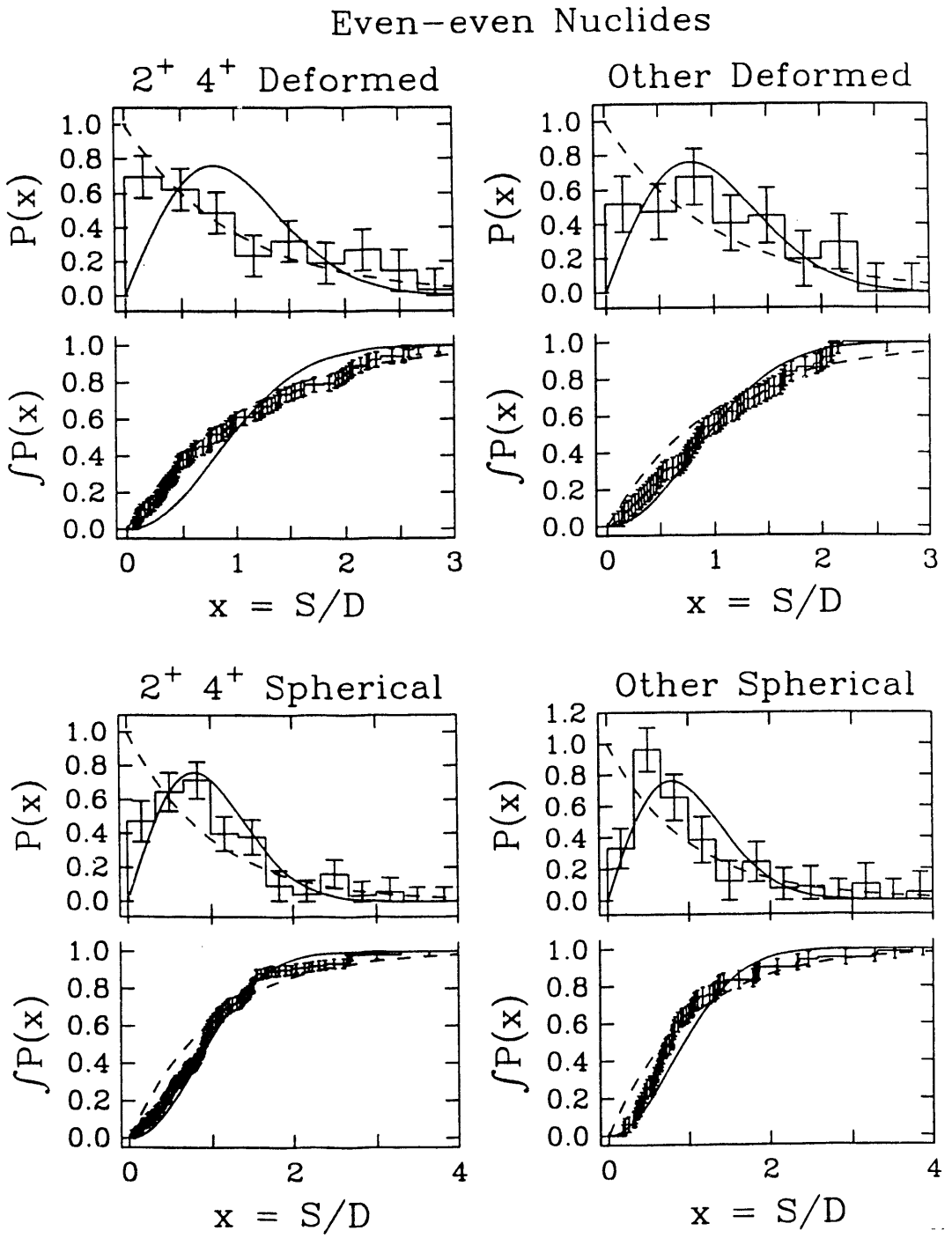

Fig. 1.3-5 Nearest-neighbor-spacing distributions and cumulative distributions for several groups of levels in even-even nuclides. The dashed lines show the behavior for a Poisson distribution and the smooth solid lines show it for a GOE distribution.

[Lev86] L. Levianıler *et al.*, Phys. Rev. Lett. **56** (1986) 2449

[Li91] J. Li, E.G. Bilpuch, C.R. Westerfeldt, G.E. Mitchell and F. Yang, Phys. Rev. **C44** (1991) 345

[Shr91] J.F. Shriner, Jr., G.E. Mitchell and T. von Egidy, Z. Phys. **A338** (1991) 309

2. INTERNUCLEON INTERACTIONS

During the past year we have made considerable progress towards elucidating some of the puzzling aspects of the low-energy internucleon interaction. Much of this progress has been made for the nucleon-nucleon tensor force, for charge-symmetry-breaking effects in the 3P channels of this interaction, and towards finding sensitive measures of three-nucleon-force effects in few-nucleon systems, especially in their scattering and breakup.

In the following sections we summarize our extensive experimental and theoretical results obtained over the past year.

2.1 Neutron-Proton Scattering

In neutron-proton scattering we have made considerable headway in the difficult low-energy experiments at TUNL that require polarized-neutron scattering from polarized-proton targets produced by brute-force cryogenic polarization of hydrogen in titanium, and we have also carefully measured the vector analyzing power at low energies.

2.1.1 NN Tensor Force from Polarized-n / Polarized-p Scattering

W.S. Wilburn, C.R. Gould, D.G. Haase, P.R. Huffman, C.D. Keith, N.R. Roberson, W. Tornow

Although the existence of a tensor component of the nucleon-nucleon interaction has been known since the discovery of the quadrupole moment of the deuteron, its strength is still not well determined, especially at low energies. Two observables that are very sensitive to the tensor interaction are the transverse and longitudinal spin-dependent differences in total cross section, $\Delta\sigma_L$ and $\Delta\sigma_T$. These measurements are difficult, since they require both a polarized proton target and a polarized neutron beam. An experiment is in progress at TUNL to measure these observables and the energies at which they cross through zero [Tor90]. The spin-dependent total cross-section differences are defined as

$$\Delta\sigma_L = \sigma(\rightrightarrows) - \sigma(\rightleftarrows) \qquad \Delta\sigma_T = \sigma(\uparrow\uparrow) - \sigma(\uparrow\downarrow),$$

where the first (top) arrow refers to the proton target spin and the second (bottom) refers to the neutron beam spin. The measured asymmetry in neutron count rate depends linearly (to a good approximation) on the proton polarization P_p, the neutron polarization P_n, and the target thickness x, as

$$\varepsilon_L = -\frac{1}{2}P_pP_nx\Delta\sigma_L \qquad \varepsilon_T = -\frac{1}{2}P_pP_nx\Delta\sigma_T$$

As a result, measurements at the zero crossing points are insensitive to uncertainties in these systematic quantities.

In the past year, a new collimation and detector system has been installed and extensive testing of systematic uncertainties has been performed. These tests revealed that the target is not as polarized as was expected, and that the analyzing power associated with the neutron beam production can make a substantial contribution to the measured asymmetry if the beam position is not carefully controlled. Also, a preliminary measurement of the zero

crossing of $\Delta\sigma_T$ has been made using a tritiated titanium foil on a ^{58}Ni backing.

The polarized neutron beam is produced through the reaction ^{3}H(p,n)^{3}He. The polarized proton beam is produced in the TUNL Intense Polarized Ion Source, which gives microampere beam currents with about 70% polarization. The polarization of the proton beam is monitored by a carbon-foil polarimeter. Solid-state detectors at ±40° measure the asymmetry of elastically-scattered protons from ^{12}C. The position of the beam on the tritium foil is controlled by a combination of analog slit-feedback loops and a computer-controlled steerer. The output of a beam profile monitor is read into the computer and the x and y centroids of the beam are calculated to give the steering signal [Gou85]. We are working to improve both the short-term stability and to reduce the long-term drift of the scanner feedback system. Precise control of the beam position is required since the analyzing power associated with the neutron production reaction can produce an asymmetry in the neutron count rate if the detectors are off-axis. R-matrix calculations indicate that at small angles (<1°) the analyzing power varies almost linearly with angle [Hal91]. Since the neutron detector consists of two liquid scintillators with phototubes placed above and below 0° (fig. 2.1-1), misalignments can be monitored by taking advantage of the ^{3}H(p,n)^{3}He analyzing power and observing the difference in asymmetry between the two detectors. Measurements made in this manner agree with the calculations.

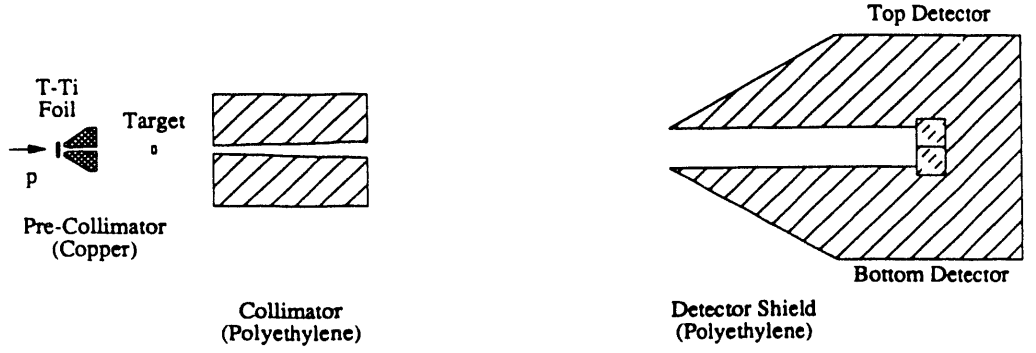

Fig. 2.1-1 Collimation system showing polarized target and neutron detectors.

The polarized proton target is produced using the TUNL polarized target facility. This apparatus consists of a ^{3}He-^{4}He dilution refrigerator with an ultimate temperature of 8 mK and a superconducting split-coil solenoid capable of producing a 7 T magnetic field. The target used is a TiH_2 powder pressed into a solid which is machined and connected to the dilution refrigerator cold finger with a high purity silver clamp. The target polarization can be monitored by measuring the temperature with two ^{3}He melting curve thermometers which have an absolute accuracy of 1 mK and a resolution of 10 μK [Gre82]. At present, a target polarization of 15% is obtained, whereas 40 – 50% should be possible. The target polarization was determined by measuring the asymmetry at 1.9 MeV neutron energy. At

this low energy, the contribution of the tensor interaction is small and calculations from effective-range parameters are considered accurate [Aur84]. Residual resistivity measurements indicate that impurities in the TiH_2 are probably limiting the thermal conductance. We plan to remake the target using higher purity material.

In a recent experiment, a pair of preliminary measurements of $\Delta\sigma_T$ was made at 3.9 and 5.7 MeV. The experiment was performed by flipping the neutron spin at 10 Hz and observing the difference in asymmetry between the two spin states. To remove systematic errors, the measurements were made with the target both polarized and unpolarized . The results of these two measurements predict a zero crossing of $\Delta\sigma_T$ at an energy of $E_n = 5.55 \pm 0.44$ MeV. Here, the error gives the one-standard-deviation statistical uncertainty. This result can be compared to the values predicted in fig. 2.1-2. More experiments are needed to improve the accuracy of this value.

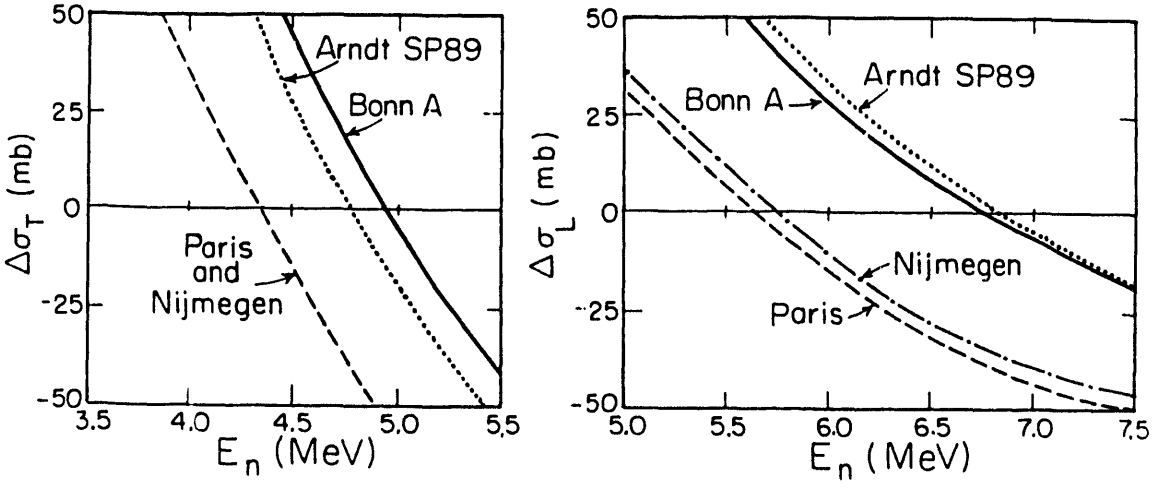

Fig. 2.1-2 Predicted zero-crossings of $\Delta\sigma_L$ (left side) and $\Delta\sigma_T$ (right side).

Once the zero-crossing measurement for $\Delta\sigma_T$ is completed, the next step will be to measure the longitudinal cross section, $\Delta\sigma_L$. We can switch to this geometry by simply rotating the superconducting magnet by 90° and selecting a different spin orientation for the incident beam. Once this measurement is accomplished, we will pursue absolute measurements of $\Delta\sigma_L$ and $\Delta\sigma_T$ at several energies in the range 4 – 10 MeV.

[Aur84] R. Aures *et al.*, Nucl. Instrum. and Methods **224** (1984) 347
[Hal91] G. Hale, private communication, 1991
[Gou85] C. Gould *et al.*, *TUNL Annual Report* (1985) 156
[Gre82] D. Greywall and P. Busch, J. Low Temp. Phys. **46** (1982) 451
[Tor90] W. Tornow *et al.*, *Physics with Polarized Beams on Polarized Targets*, eds. J. Sowinski and S.E. Vigdor (World Scientific , Singapore, 1990) 75

2.1.2 Neutron-Proton Analyzing Powers between 7.6 and 18.5 MeV

G.J. Weisel, W. Tornow, C.R. Howell, P.D. Felsher, M. AlOhali, Z.P. Chen[1], R.L. Walter, J.M. Lambert[2], P.A. Treado[2], I. Slaus[3]

We have completed a high-accuracy measurement of $^1H(n,n)^1H$ $A_y(\theta)$ between 7.6 and 18.5 MeV. A paper on this work has been submitted to Physical Review C, the abstract of which follows, along with a table of the final data and uncertainties at each energy and angle.

Measurements of the analyzing power $A_y(\theta)$ for neutron-proton scattering have been performed at 7.6, 12.0, 14.1, 16.0, and 18.5 MeV. The experimental setup is described as are the finite geometry corrections applied to the data. One of these corrections, due to the presence of carbon in the scintillators used for neutron detection, is discussed in detail. The $A_y(\theta)$ data are compared to the predictions of the Paris and Bonn nucleon-nucleon potentials and the predictions of two phase-shift analyses, one of which incorporates charge-independence-breaking effects in the ^3P waves.

Table 2.1-1 Summary of final TUNL n-p $A_y(\theta)$ data.

E_n (MeV)	θ^oc.m.	$A_y \pm \Delta A_y$	E_n (MeV)	θ^oc.m.	$A_y \pm \Delta A_y$
7.6	65.8	0.0072 ± 0.0008	14.1	45.9	0.0193 ± 0.0013
	90.6	0.0041 ± 0.0008		65.6	0.0212 ± 0.0009
	108.0	0.0039 ± 0.0008		90.8	0.0167 ± 0.0013
	124.8	0.0035 ± 0.0006		107.8	0.0141 ± 0.0009
				125.2	0.0078 ± 0.0015
12.0	46.0	0.0134 ± 0.0007			
	65.6	0.0177 ± 0.0010	16.0	46.0	0.0264 ± 0.0018
	90.6	0.0129 ± 0.0010		65.6	0.0291 ± 0.0016
	99.4	0.0122 ± 0.0012		90.6	0.0260 ± 0.0012
	107.8	0.0076 ± 0.0010		107.8	0.0195 ± 0.0010
	112.4	0.0073 ± 0.0015		125.2	0.0085 ± 0.0014
	116.4	0.0056 ± 0.0010			
	125.2	0.0051 ± 0.0007	18.5	65.6	0.0401 ± 0.0029
				90.6	0.0354 ± 0.0015
				108.0	0.0220 ± 0.0015
				125.0	0.0147 ± 0.0014

[1] Department of Physics, Tsinghua University, Beijing, The People's Republic of China
[2] Department of Physics, Georgetown University, Washington, DC 20007
[3] Rudjer Boskovic Institute, 41001 Zagreb, Yugoslavia

2.2 Testing Internucleon Potentials Through n – d Scattering

It is well-known that the details of both the two- and the three-nucleon interactions can probably best be determined through scattering and breakup in three- and four-body systems. Several aspects of these interactions have been elucidated in experiments at TUNL during the past year. We summarize in the following the advances that we have made.

2.2.1 Asymptotic S-wave Normalization of the Deuteron by n-d Scattering

C.R. Howell, N. Al-Niemi[1], R.T. Braun, C.E. Brient[1], D.E. Gonzalez, S.M. Grimes[1], G. Mertens[2], R.S. Pedroni[1], C.D. Roper, W. Tornow

The present experimental value for the asymptotic S-wave normalization of the deuteron wavefunction, A_S, is extracted (in a nearly model independent way) from data for *e-d* elastic scattering in the low-q^2 region [Eri84]. The average value of A_S extracted from the *e-d* data of [Bér73] and [Sim80] is $A_S = 0.8802 \pm 0.0020$. In this work, we consider an alternate method for determining the value of A_S. This method will utilize the strong relationship between A_S and the differential cross section, $d\sigma(\theta)/d\Omega$, for *n-d* elastic scattering to backward angles [Koi86]. The value of A_S obtained in the present work will provide an independent check of the results from *e-d* scattering [Eri84].

Koike and Taniguchi [Koi86] have shown in an almost model-independent way that there is a strong relationship between A_S and $\sigma(180°)$ for *n-d* elastic scattering. They showed that the $d\sigma(\theta)/d\Omega$ for *n-d* elastic scattering to c.m. angles beyond 150° at incident neutron energies below 20 MeV is mainly due to the $^3S_1$ part of the nucleon-nucleon NN interaction. Below 20 MeV the $^1S_0$ force only accounts for about 3% of $d\sigma(\theta)/d\Omega$ in the angular range $\theta_{c.m.}$ = 150° - 180° [Koi86]. At 10 MeV the P-wave part of the NN force accounts for about 3% of $d\sigma(\theta)/d\Omega$ at backward angles and the contribution by the D-waves is less than 1%, while at 20 MeV less than 2% of $d\sigma(\theta)/d\Omega$ at backward angles is due to the P-wave NN force and about 3% is due to the D-waves [Koi86]. Since A_S is defined by the strength of the $^3S_1$ force, it follows that $d\sigma(\theta)/d\Omega$ for low-energy *n-d* elastic scattering to backward angles, which mainly depends on the $^3S_1$ NN force, is a good observable for determining A_S. The relationship between $d\sigma(\theta)/d\Omega$ for *n-d* elastic scattering to 180° and A_S is shown in fig. 2.2-1. The calculations for this figure were taken from [Koi86]. The line is a fit to the points.

There have been two recent measurements [Sch83, Jan84] of $d\sigma(\theta)/d\Omega$ for backward-angle *n-d* elastic scattering at incident neutron energies below 20 MeV. Above 10 MeV the data from these two measurements disagree with each other by several standard deviations. The *n-d* data from one of the measurements [Sch83] suggest a value for A_S that is inconsistent with the results of *e-d* scattering data [Ber73, Sim80]. To resolve the discrepancy between the *n-d* data and to corroborate the value of A_S determined from *e-d* scattering data by

---

[1] Ohio University, Athens, Ohio
[2] University of Tübingen, Tübingen, Federal Republic of Germany

making an independent measurement using a strongly interacting probe, we have made $d\sigma(\theta)/d\Omega$ measurements to an accuracy better than ±4% for *n-d* elastic scattering to backward angles ($\theta_{c.m.}$ = 140° - 178°) at incident neutron energies of 8.0, 10.0, and 14.0 MeV.

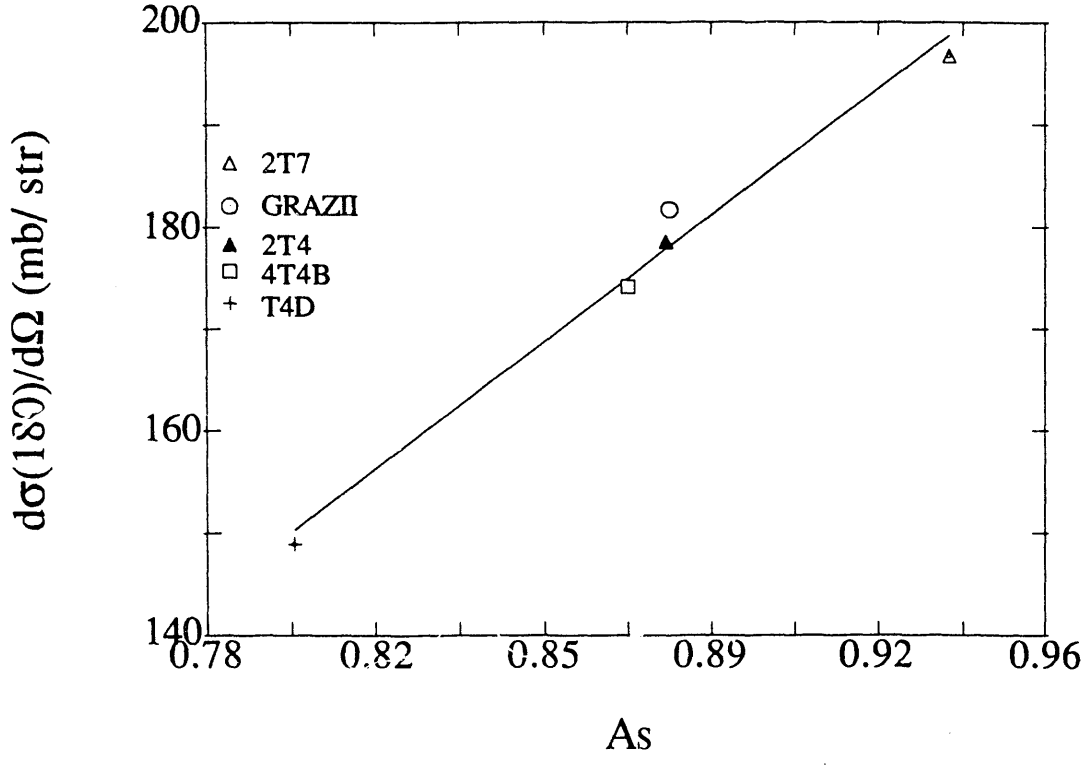

Fig. 2.2-1 Relation between $d\sigma(180°)/d\Omega$ for *n-d* elastic scattering and A_S. The calculations are for E_n = 10.0 MeV. Data points are from [Koi86]. The line is a fit to the points.

All measurements were made by detecting the recoil deuterons in a charged-particle spectrometer [Ahn85] which was developed at Ohio University for A(n,z) measurements. A diagram of the spectrometer is shown in fig. 2.2-2. The neutrons are produced by the $^2H(d,n)^3He$ source reaction. The neutron production target was a 3-cm-long cell filled with deuterium gas. The center of the neutron source was about 45 cm from the scatterer, which was a mixed CD_2-CH_2 foil about 4-mg/cm^2 thick. By simultaneously measuring *n-d* and *n-p* elastic scattering, the *n-d* yields could be normalized to those for *n-p* scattering to give an absolute cross section based on the well-known *n-p* cross section. The deuterium-to-hydrogen ratio in our scatterer was determined in an independent measurement [How89].

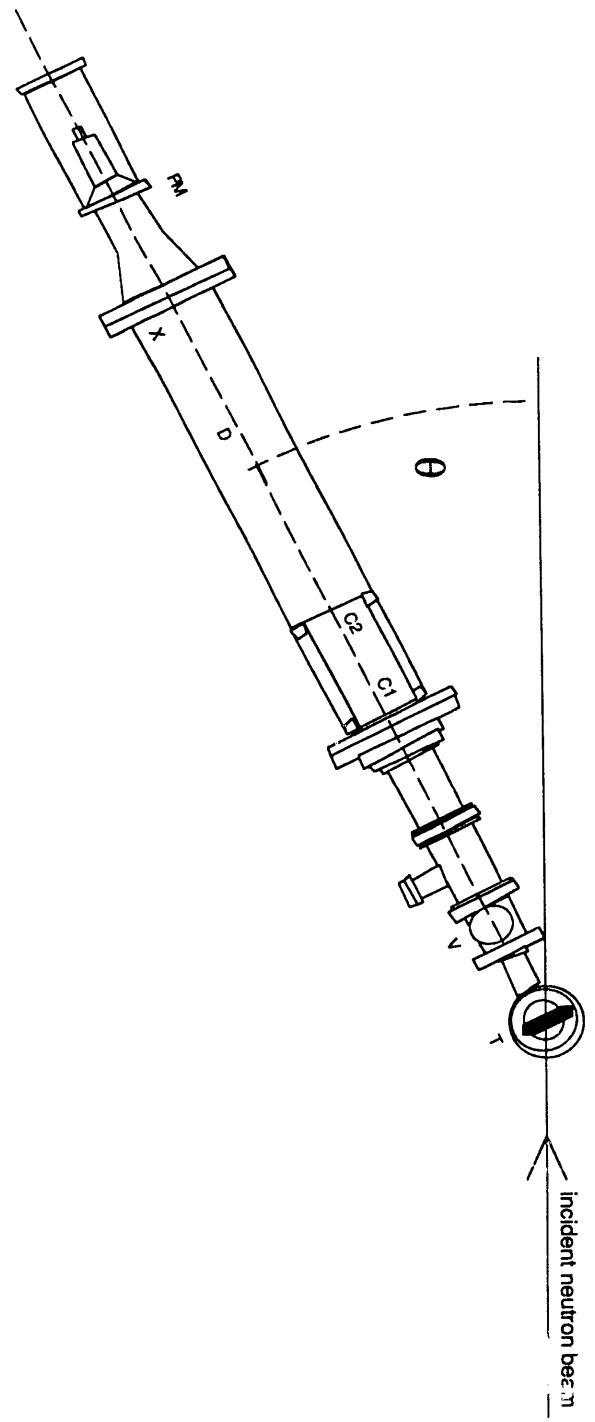

Fig. 2.2-2 Charged-particle spectrometer used in the backward-angle *n-d* elastic scattering measurements. T = target, V = isolation valve, (C_1,C_2) = two halves of proportional counter, D = drift tube, X = scintillator, PM = photomultiplier tube.

The outgoing deuterons and protons were detected in a plastic scintillator shown in fig. 2.2-2. The energy loss in the proportional counter was used for particle identification. The incident deuteron beam was pulsed to produce a pulsed neutron beam to enable time-

of-flight (TOF) measurements of the outgoing deuterons and protons. The TOF information gave another method of particle identification, thereby overdetermining the identity of the detected particles. This redundancy was used to reduce the experimental background.

To check our experimental techniques, the first measurements were made at 8 MeV, where the Karlsruhe [Sch83] and Uppsala [Jan84] data are in agreement. The 8-MeV and some 10-MeV measurements were made at the accelerator laboratory at Ohio University. Our results at 8 MeV are shown in fig. 2.3-3 in comparison to the Uppsala [Jan84] and Karlsruhe [Sch83] data and to three-nucleon 3N calculations which use the OBEPQ-B NN potential [Mac89]. The good agreement between our data and the existing data suggest that our experimental techniques are solid. For the 14-MeV measurements and the completion of the 10-MeV measurements, the spectrometer was moved to TUNL and installed in the neutron time-of-target target room in July of this summer. The 14-MeV data are shown in fig. 2.2-4. Our 14-MeV data are in good agreement with the 3N calculations and indicate that the Karlsruhe data are too high beyond 150°.

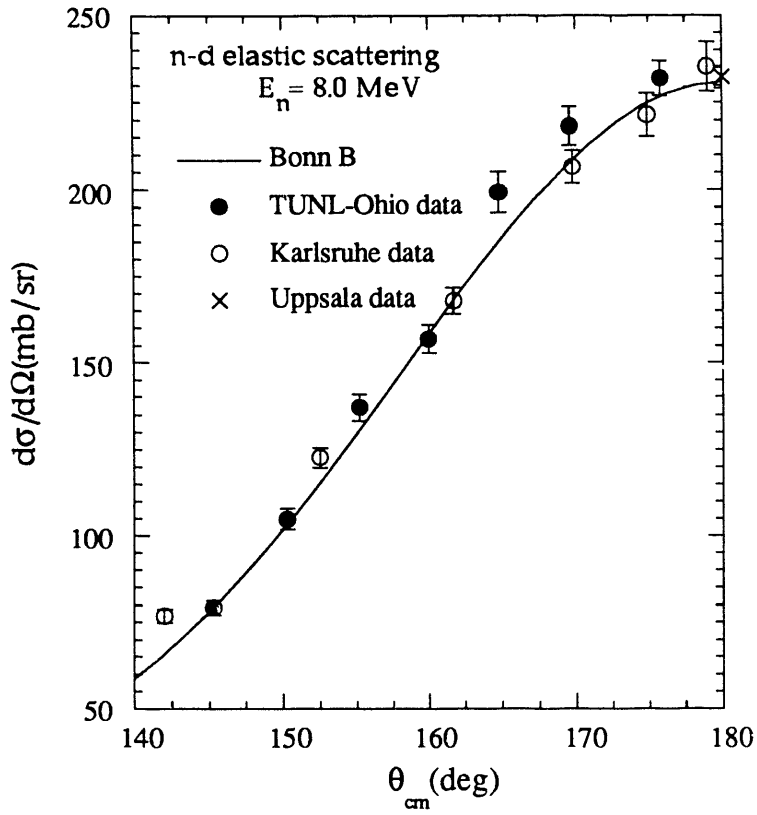

Fig. 2.2-3 Backward-angle $d\sigma(\theta)/d\Omega$ for *n-d* elastic scattering at 8.0 MeV. The data are described in the figure and text. The curve is a 3N calculation which uses the OBEPQ-B NN potential.

We expect that our data at 8.0, 10.0 and 14.0 MeV will enable us to determine A_S to 5

parts per thousand. The 3N calculations to establish the relationship between backward-angle $d\sigma(\theta)/d\Omega$ for *n-d* elastic scattering will be performed by H. Witała [Wit91]. (See section 2.3 in this report for details of the *n-d* calculations in the continuum region.)

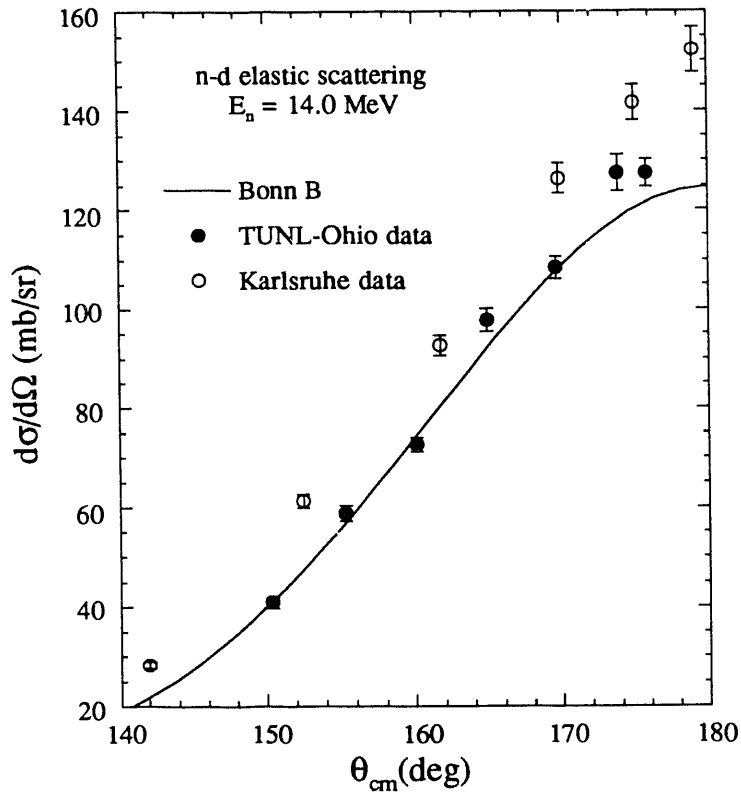

Fig. 2.2-4 Backward-angle $d\sigma(\theta)/d\Omega$ for elastic scattering at 14.0 MeV. The data are described in the figure and text. The curve is a 3N calculation which use the OBEPQ-B NN potential.

[Ahm85] M. Ahmad *et al.*, Nucl. Instr. and Methods **228** (1985) 349

[Bér73] R.W. Bérard *et al.*, Phys. Lett. **47B** (1973) 355

[Eri84] T.E.O. Ericson, Nucl. Phys. **A416** (1984) 281c

[How89] C.R. Howell *et al.*, TUNL Annual Report XXVIII (1989) 32

[Jan84] G. Janson *et al.*, Proceedings of the 10th International Conf. on Few-Body Problems, 1983, ed. B. Zeitnitz (North Holland, Amsterdam, 1984) p. 529

[Koi86] Y. Koike and Y. Taniguchi, Few Body Systems **1** (1986) 13

[Mac89] R. Machleidt, Adv. Nucl. Phys. **19** (1989) 189

[Sch83] P. Schwartz *et al.*, Nucl. Phys. **A398** (1983) 1

[Sim80] G.G. Simon *et al.*, Nucl. Phys. **A333** (1980) 381

[Wit91] H. Witała, private communications 1991

2.2.2 Dynamics of n-d Elastic Scattering above E_n = 70 MeV

C.R. Howell, X. Aslanoglou[1], F.P. Brady[2], J.R. Drummond[2], R.W. Finlay[1], R.C. Haight[3], N.S.P. King[3], A. Ling[3], P.W. Lisowski[3], C.L. Morris[3], B.K. Park[1], J. Rapaport[1], J.L. Romero[2], D.S. Sorenson[2], W. Tornow, J.L. Ullmann[3], B. Vlahovic

Computational advances [Wit87] permit three-nucleon (3N) scattering observables [How88] to be calculated using the exact forms of the Paris [Lac80] and Bonn [Mac89] potentials as input for the basic nucleon-nucleon (N-N) force. The underlying assumptions used in most 3N calculations are: (1) nucleons only interact via pairwise forces, thus no 3N force; (2) the dynamics of the interacting nucleons can be treated nonrelativistically; and (3) charge symmetry and charge independence are assumed to hold for all N-N angular momentum states with $\ell \geq 1$. In addition to the above assumptions, the Coulomb force cannot be included in these calculations in an exact way at energies above the deuteron breakup threshold. Therefore, these calculations are limited to *n-d* scattering observables.

High-accuracy measurements of *n-d* scattering observables at low energies ($T < 20$ MeV) are critically testing assumptions (1) and (3) above. The 3N calculations at c.m. energies above 50 MeV made by Witała during his visit to TUNL this summer (1991) (see section 2.3 for rigorous *n-d* elastic calculations) will be useful for investigating the soundness of item (2) above. The comparison of the "exact" nonrelativistic 3N calculations to nucleon-deuteron (N-d) scattering data over an incident nucleon energy range from 50 to 300 MeV should provide a continuous map of the reaction dynamics in the 3N scattering system. Since inelasticities in the pion-nucleon vertices start to become important at energies above the pion-production threshold, it is important to conduct these studies at energies below this threshold so that these inelastic effects will not be confused with 3N reaction dynamics. This study should give a measure of the the importance of relativity in 3N scattering systems at incident nucleons between 70 and 300 MeV. In a more general context, the relativistic treatment of nucleons in nuclear systems is a bridge the nuclear physics community must cross to advance our understanding of nuclear systems at medium and high energies. The 3N system is an excellent starting place, since we currently can solve "exactly" the 3N scattering problem using nonrelativistic formalism. The relativistic treatment of the interacting nucleons in this system is a natural progression in the field.

Both *n-d* and *p-d* elastic scattering data can be used for testing the calculations since the effect of the Coulomb interaction has been demonstrated to be negligible at cm angles beyond 35 degrees for incident energies above 60 MeV [Dec89]. For *n-d* cross-section data there is a gap between 70 and 200 MeV, and only 180-degree data are available above 200 MeV [Til87]. The situation for *p-d* scattering is only slightly better [Til87].

To fill the large gap in the database for *n-d* scattering, we have measured backward-angle ($\theta_{c.m.}$ = 155° - 180°) cross sections for *n-d* elastic scattering for incident neutron energies from 60 to 260 MeV. All measurements were conducted at the LAMPF/WNR continuous energy neutron beam facility. The same spectrometer used in the A(n,p) project

[1] Ohio University, Athens, OH
[2] University of California, Davis, CA
[3] Los Alamos National Laboratory, Los Alamos, NM

(see section 4.2.1) was employed for these measurements. The analysis of these data is underway and should be completed by the end of fall 1991.

[Dec89] B. Dechant *et al.*, Proc. XII Intern. Conf. on Few Body Problems in Physics, Vancouver, B.C., Canada (1989)
[How88] C.R. Howell *et al.*, Phys. Rev. Lett. **61** (1988) 1565
[Lac80] M. Lacombe *et al.*, Phys. Rev. **C21** (1980) 861
[Mac89] R. Machleidt, Adv. in Nucl. Phys. **19** (1989) 189
[Til87] D.R. Tilley, H.R. Weller and H.H. Hasan, Nucl. Phys. **A474** (1987) 1
[Wit87] H. Witała, W. Glöckle and T. Cornelius, Few-Body Systems Suppl. **2** (1987) 555

2.2.3 Three-Nucleon-Force and Off-Shell Effects in ^{2}H(n,nnp) Breakup

H.R. Setze, C.R. Howell, J.M. Lambert[1] , G. Mertens[2], I. Slaus,[3] W. Tornow, R.L. Walter, G.J. Weisel

The influence of three-nucleon forces (3NF) is expected to be critically dependent on the spatial arrangement of the interacting nucleons [Fri82]. The kinematic richness of the n+d → n+n+p breakup reaction makes it excellent for studying 3N systems in extreme geometric configurations, since one has the ability to vary continuously the arrangement of the nucleons in the exit channel. Meier and Glöckle [Mei84] have done a systematic study of the influence of the 3NF on cross sections for n+d → n+n+p breakup in several exit-channel configurations. Their calculations, which used the Malfliet-Tjon [Mal69] two-nucleon (2N) potential and a simplified 2π exchange 3NF, confirmed that the influence of the 3NF is extremely angle and energy dependent. They found the cross section for the colinear configuration (the three outgoing nucleons form a line in the c.m. system) to be enhanced by 10% at E = 14.4 MeV, and that for the star configuration (the three outgoing nucleons have equal momenta and interparticle angles of 120° in the c.m.) to be enhanced by 5% at E = 18.5 MeV when the 2π exchange 3NF was added to their calculations.

Our motivation for measuring cross sections for the n-d breakup reaction stems from the results of recent measurements by Strate *et al.* [Str88]. Using an array of neutron detectors, they measured cross sections over a large region of 3N phase space for ^{2}H(n,nnp) breakup at 13.0 MeV. There are sizeable disagreements between their data and the 3N calculations using the Bonn and Paris nucleon-nucleon potentials. Their data for the space-star configuration is about 25% larger than the 3N calculations, which use only 2N forces [Str88, Wit88]. In addition, their spectrum containing the colinear point has an enhancement which is not predicted by calculations which use only 2N forces. These discrepancies between data and theory are consistent with the trends found in the study by Meier and Glöckle [Mei84]. If the data of Strate *et al.* are correct, the above results would be the clearest evidence of the 3NF yet observed in a scattering system. Because of the sig-

---

[1] Georgetown University, Washington, D.C.
[2] University of Tübingen, Tübingen, FRG
[3] Ruder Boskovic Institute, Zagreb, Yugoslavia

nificant consequences of these results, we are planning a series of measurements to verify the experimental results of Strate *et al.*

The shielded neutron source to be used in n+d → n+n+p breakup measurements has been constructed and tested [How89]. The shielding was found to be adequate for our measurements. The neutron production target will be a water cooled deuterium gas cell. The cylindrical wall of the cell is made of copper for good heat conduction to the water lines, and the beam stop is made of gold to provide good heat conduction with minimum background in the neutron beam. It has been built and is ready for installation. The fabrication of the collimator to accommodate the larger deuterated scatterer has been completed. The collimator will be installed in the shielding wall, and the neutron beam from the collimator will be profiled during the fall 1991. The efficiencies of the 11 neutron detectors to be used in the breakup experiment have been measured using a ^{252}Cf source. (See section 5.8.1 for details of the neutron-detector efficiency measurements.) The efficiency data are currently being analyzed. We hope to start our first measurements of D(n,nnp) breakup in December 1991. Based on the yields obtained in our tests [How89], we estimate a cross-section measurement to a statistical accuracy of ±5% will require 30 24-hour shifts with 3 μA of beam on target.

[Fri82] J.L. Friar, Proc. Conf. on the Interaction between Medium Energy Nucleons in Nuclei, Indiana Univ., 1982, AIP Conf. Proc. No. **97**, p. 378
[How89] C.R. Howell *et al.*, TUNL Annual Progress Report XXVIII (1989) 38
[Mal69] R.A. Malfliet and J.A. Tjon, Nucl. Phys. **A127** (1969) 161
[Mei84] W. Meier and W. Glöckle, Phys. Lett. **138B** (1984) 329
[Str88] J. Strate *et al.*, J. Phys. G: Nucl. Phys. **14** (1988) L229
[Wit88] H. Witała, W. Glöckle and T. Cornelius, Few Body Systems **5** (1988) 89

2.3 Rigorous Three-Nucleon Elastic Scattering and Breakup Calculations

During a two-month visit at TUNL H. Witała, Jagellonian University, Cracow, Poland, installed his 3N continuum Faddeev code on the local Cray Y-MP at the North Carolina Supercomputation Center (NCSC) in Research Triangle Park. Witała's code, developed in collaboration with W. Glöckle, Bochum, Germany, is presently the only code that calculates rigorously elastic and breakup processes in the neutron-deuteron reaction above the deuteron breakup threshold for any given NN interaction.

The following subsections summarize the status of projects initiated during Witała's visit.

2.3.1 Charge-Symmetry Breaking Effects in ^{3}P NN Forces

H. Witała, W. Glöckle, W. Tornow

The 2N systems provide insufficient information about some details of the NN force. One of the open questions deals with such aspects as the charge-independence and charge-symmetry breaking (CIB, CSB) in higher angular momentum NN states. Experimental information on these effects coming from 2N scattering data is sparse. The Nd analyzing

power A_y is a good candidate to search for CIB and CSB effects in ^3P_J NN states. In contrast to most low energy Nd elastic scattering observables, A_y cannot be described by rigorous Faddeev type 3N calculations [Glö90] with either the Paris [Lac80] or Bonn [Mac89] potentials.

In [Wit91] we investigated what kind of modifications to the ^3P_J phase shifts is required to bring the calculated nd A_y in closer agreement with the data. Starting from the Bonn-B potential parameters, the ^3P_J phases were varied by searching on 2N and 3N observables simultaneously. We demonstrated that it is possible to simultaneously describe the A_y data in the pp and np systems together with the A_y data in the 3N pd system by modifying the 2N interaction in the ^3P_J states. This approach introduces CIB in these NN interactions. The nd analyzing-power data, which are slightly higher in the maximum than the pd data, can also be very well reproduced by assuming an additional CSB the ^3P_J forces. In this case the modification of the ^3P_J phase shifts is more uncertain than that for the pp system, since two-nucleon nn data do not exist. We obtained in our simultaneous analysis of 2N and 3N data a sizeable CIB and CSB only in the $^3P_0$ phase shift, while the $^3P_1$ and $^3P_2$-$^3F_2$ phase shifts were found to be essentially charge-independent.

Since we neglect the Coulomb interaction totally in our 3N calculations, we assumed that the entire difference in the maxima of the pd and nd analyzing power distributions is due to charge-symmetry breaking effects. There exists a plausible argument that the incident proton slows down in the Coulomb field of the deuteron [Tor91]. Therefore, the A_y for pd should be slightly smaller than that for nd. If this argument is correct, then the charge-symmetry breaking effects in the ^3P_J NN interactions are probably not as large as found in our analysis [Wit91]. However, with decreasing bombarding energy an interesting effect can be seen (see fig. 2.3-1). While at E_N=8.5 MeV the nd and pd A_y data support our modifications of the ^3P_J forces obtained at higher energies, our nd prediction overestimates the data at E_N=6 MeV and especially at E_N=5 MeV. On the other hand the difference between the nd and pd A_y data decreases with decreasing energy, and our pd prediction at 5 MeV agrees with both the pd and nd data set rather well. These observations may indicate the smallness of Coulomb effects. Furthermore, it indicates an energy dependence of the charge-symmetry breaking interaction. In view of this result, it would be extremely interesting to measure the n-d analyzing power at even lower energies.

[Glö90] W. Glöckle, H. Witała and Th. Cornelius, Nucl. Phys. **A508** (1990) 115c

[Lac80] M. Lacombe, *et al.*, Phys. Rev. **C 21** (1980) 861

[Mac89] R. Machleidt, *et al.*, Adv. Nucl. Phys. **19** (1989) 189

[Sag91] K. Sagara, private communication, 1991

[Tor91] W. Tornow, Int. Conf. on Spin and Isospin in Nuclear Interactions, Telluride, Colorado USA, 11-15 March 1991, to be published in Adv. Nucl. Phys

[Tor91] W. Tornow, *et al.*, Phys. Lett. **257B** (1991) 273

[Wit91] H. Witała and W. Glöckle, Nucl. Phys. **A528** (1991) 48

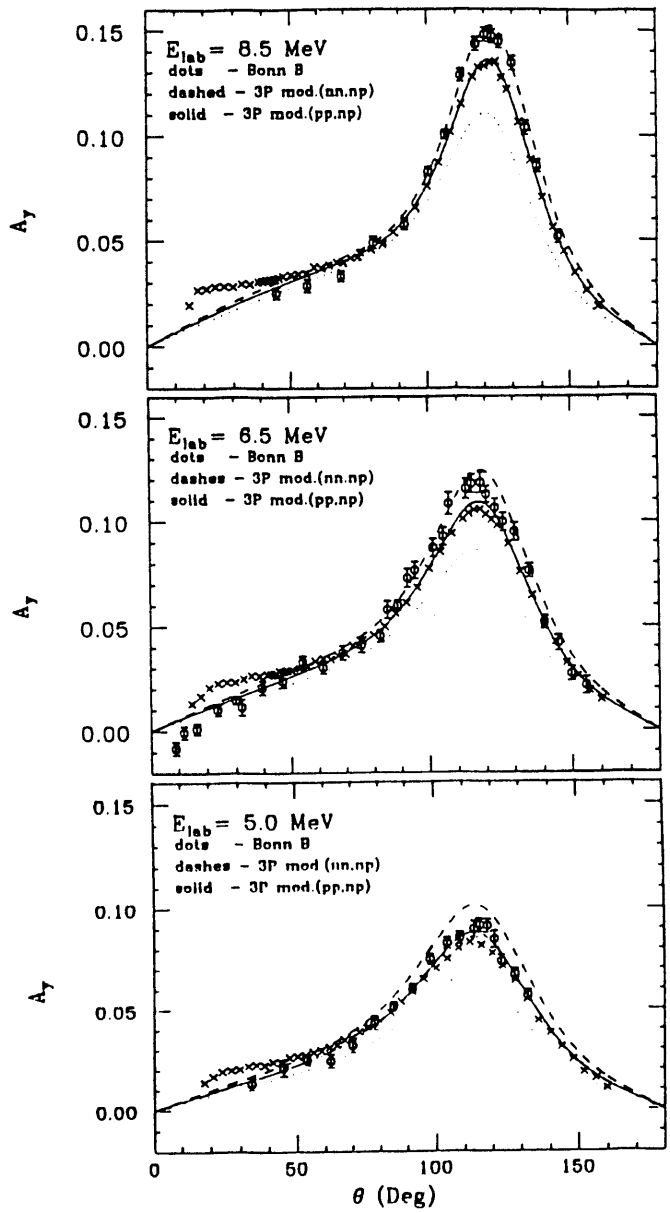

Fig. 2.3-1 Low-energy nd (circles) [Tor91] and pd (crosses) [Sag91] analyzing-power data compared to the Bonn-B potential predictions and to the ^3P_J nd and pd dynamics as proposed in [Wit91].

2.3.2. Energy Dependence of Nucleon-Deuteron Scattering and ^3P Interactions

W. Tornow, H. Witała, W. Glöckle

The energy dependence of neutron-deuteron elastic scattering observables was calculated from 5 to 45 MeV by rigorous three-nucleon calculations using the Bonn-B nucleon-nucleon interaction. The goal of these calculations was to identify energy and angular regions which may be investigated experimentally to study the question of charge-symmetry

breaking and/or Coulomb effects in the ^3P_J nucleon-nucleon interactions.

We propose the accurate measurement of $A_y(\theta)$ in nd elastic scattering at E_{lab} = 16 and 22.7 MeV in order to compare to existing pd data at the same bombarding energies. Suppose that the simple picture of a slow-down of the incident proton is correct, then according to fig. 2.3-2c, the pd A_y data must be slightly lower in magnitude at 16 MeV than the corresponding nd data in the angular region around $\theta_{c.m.}$ = 125°, while at 22.7 MeV both data sets should coincide. According to fig. 2.3-2b, exactly the opposite behavior is expected around $\theta_{c.m.}$ = 100°. Here, the pd and nd data should agree at 16 MeV while the magnitude of the pd data should be slightly lower than the corresponding nd data at 22.7 MeV. Possible CSB effects are unlikely to exhibit a similar variation in energy dependence over such a small energy range. In fact, the CSB introduced in [Wit91] predicts larger nd than pd A_y values around $\theta_{c.m.}$ = 125° at both 16 and 22.7 MeV. Similarly at $\theta_{c.m.}$ = 100°, where the calculated A_y is more negative for nd than for pd scattering at both energies.

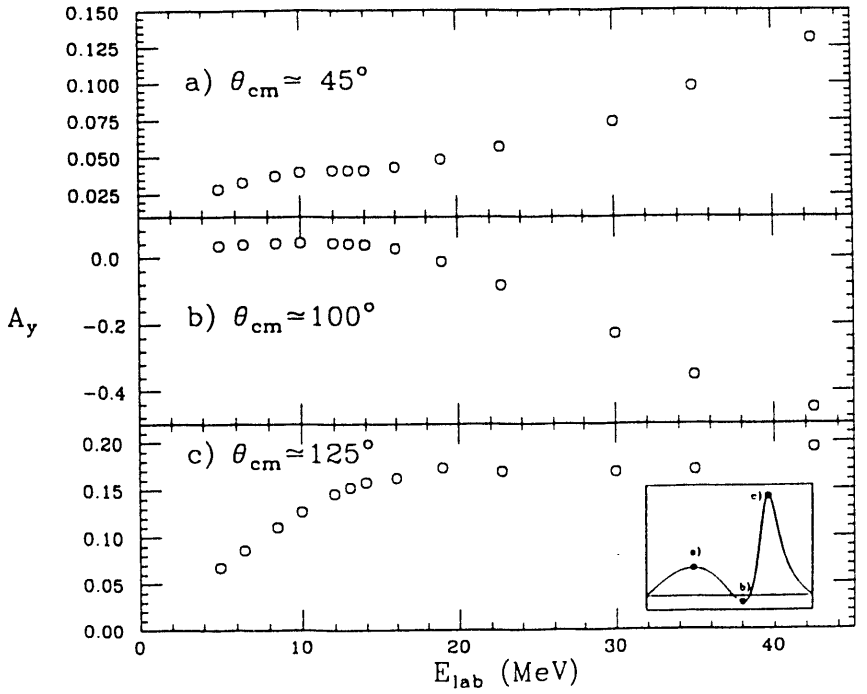

Fig. 2.3-2 Excitation functions of the neutron-deuteron elastic analyzing power A_y at characteristic angles. The angles of interest are indicated in the inserts by solid dots.

If the "proton slow-down" hypothesis should turn out to be correct, then, as a by-product of our present work, we have identified both the angular and energy regions in which pd data must be corrected slightly to obtain accurate information about the ^3P_J NN interactions and the $^3S_1$–$^3D_1$ NN tensor force from the comparison with rigorous nd scattering calculations.

[Wit91] H. Witała and W. Glöckle, Nucl. Phys. **A528** (1991) 48

2.3.3 Two-Nucleon j=4 Contributions to 3N-Scattering Observables

H. Witała, W. Glöckle, W. Tornow

In the first rigorous 3N scattering calculations [Wit87] using realistic NN potentials nucleons were allowed to interact in all partial wave states with two-nucleon total angular momentum $j \leq 2$. The restriction to $j_{max} = 2$ is justified for incident nucleon laboratory energies below about 30 MeV. With the improvements in computational speed and memory of supercomputers during the last three years, the $j_{max} = 2$ limit was pushed to $j_{max} = 3$ [Wit89], allowing for the accurate calculations of 3N observables at higher energies, possibly up to about 100 MeV. In order to extend the calculations into the 100 to 200 MeV energy regime and to simultaneously check on the reliability of the $j_{max} = 3$ restriction at lower energies, the influence of $j = 4$ contributions ($^3G_4$, $^1H_4$, $^1G_4$ and $^3F_4$-$^3H_4$) must be carefully investigated. However, until now this has not been possible.

Prior to the installation at NCSC, the Cray Y-MP at the Supercomputation Center in Jülich, Germany, has been the only computer on which Witała's code is installed. There, 15 Mword of "running" memory is available for a single user. This amount of memory is not enough for a $j_{max} = 4$ calculation. At NCSC up to 40 Mword is available, at a very low priority, however. Since the demand for CPU time is large at NCSC and a $j_{max} = 4$ calculation requires about 7 hours of CPU time at a speed of 100 Mflops, it turned out to be impossible to complete such a calculation within a period of 2 weeks. After modification of the program by dividing the calculation into smaller segments each of which require 21 Mword and a combined total of about 10 hours of CPU time, it was possible to perform a complete $j_{max} = 4$ calculation using the Bonn-B NN potential at an incident nucleon laboratory energy of 116 MeV.

The dashed curve in fig. 2.3-3 shows the calculated n-d differential cross section $\sigma(\theta)$ obtained with $j_{max} = 4$ in comparison to a $j_{max} = 3$ calculation (solid curve). As expected, the higher partial wave NN interactions contribute to $\sigma(\theta)$ mainly in the forward-angle region. Figure 2.3-4 displays the analyzing power $A_y(\theta)$. Here, the difference between $j_{max} = 3$ and $j_{max} = 4$ is very small throughout the entire angular region. Finally, fig. 2.3-5 shows the nucleon-to-nucleon polarization transfer coefficient $K_y^{y'}(\theta)$. Sizeable differences are noticed, not only at forward angles but also near 125°.

We conclude from this first rigorous $j \leq 4$ 3N scattering calculation that $j = 4$ NN interactions play a nonnegligible role for most 3N observables at incident nucleon energies of about 100 MeV. Except for a few observables, $j_{max} = 3$ calculations are sufficient if only backward angles are of interest. We will extend the $j_{max} \leq 4$ 3N calculations up to about $E_{lab} = 250$ MeV.

[Wit87] H. Witała, W. Glöckle and Th. Cornelius, Few-Body Syst. Suppl. **2** (1987) 55

[Wit89] H. Witała, W. Glöckle and T. Cornelius, Nucl. Phys. **A491** (1989) 157

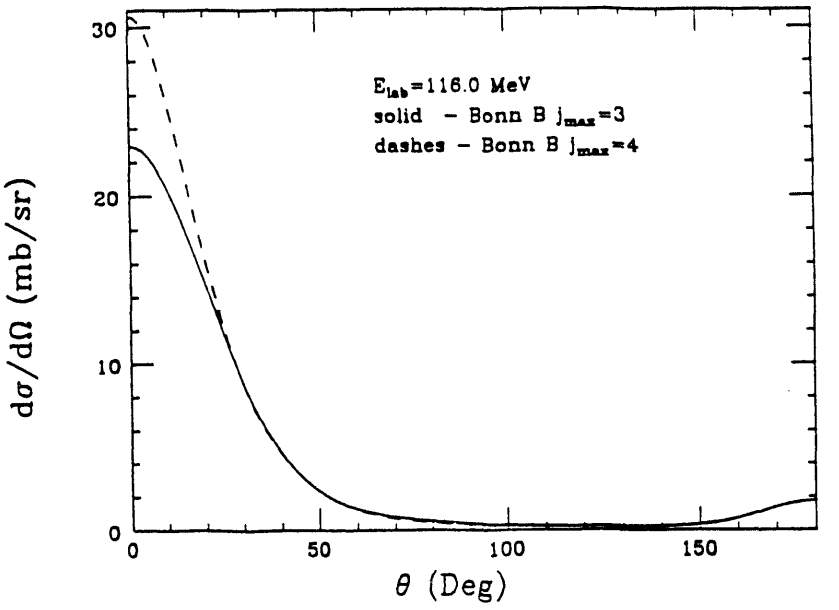

Fig. 2.3-3 Calculated neutron-deuteron differential elastic cross section at $E_{lab} = 116$ MeV using the Bonn-B NN interaction with two-nucleon total angular momentum $j \leq 3$ (solid curve) and $j \leq 4$ (dashed curve).

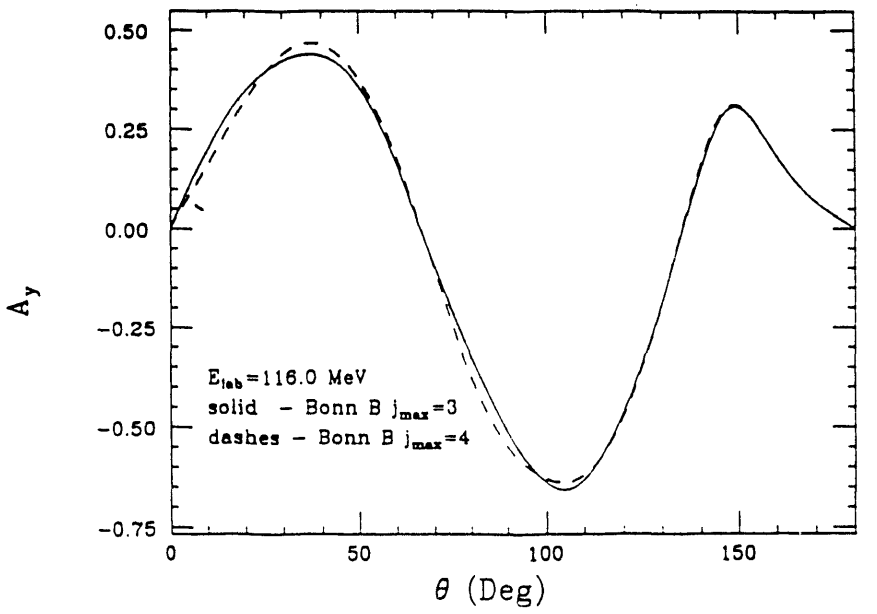

Fig. 2.3-4 Same as fig. 2.3-3 for neutron-deuteron elastic analyzing power.

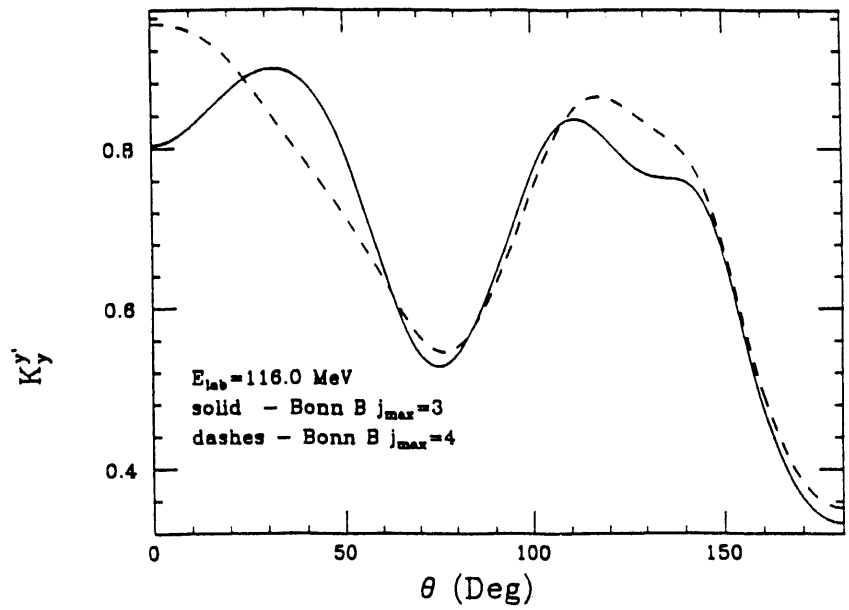

Fig. 2.3-5 Same as fig. 2.3-3 for neutron-deuteron nucleon-to-nucleon polarization transfer coefficient.

2.3.4 Perturbative Treatment of the Three-Nucleon Force in the 3N Continuum

H. Witała, W. Glöckle, W. Tornow

With the advent of vectorized supercomputers, the three-nucleon (3N) scattering equations of the Faddeev type can now be solved for any two-nucleon (2N) force in a numerically precise way [Glö90a]. This new tool of rigorous 3N continuum calculations makes it possible to test the assumption whether free 2N forces describe 3N scattering data quantitatively. The results obtained until now with modern, meson-exchange based NN interactions seem to support this assumption [Glö90b]. The comparison of such numerically precise solutions with experimental 3N data is expected to shed light on several important issues such as charge-independence and/or charge-symmetry breaking effects in ^3P_J forces [Wit91] or the magnitude of the $^3S_1$-$^3D_1$ tensor force [Cla90]. However, the usefulness of the 3N system as a tool for studying these questions relies heavily on the smallness of three-nucleon force (3NF) contributions to Nd elastic scattering observables. There are indications that the 3NF plays a non-negligible role in specific kinematically-complete configurations of the nucleon-deuteron (Nd) breakup process [Mei84].

The inclusion of a 3NF requires an extension of the calculational scheme used to solve the 3N equations [Glö87]. The qualitatively very good description of the triton properties [Fri84] and of many 3N scattering observables using 2N forces alone [Glö90a] indicates that the 3NF must be only a weak additional contribution. Therefore, it is natural to formulate a perturbative expansion in order to include the 3NF.

The 2π-exchange process is the most important and elaborated one among possible 3NF mechanisms [Coo81]. In our preliminary study we took this 3NF together with the Bonn-B 2N interaction [Mac89] and restricted the treatment of the 3NF to the first-order (n = 1) in the perturbation approach. Both 2N- and 3N- forces were allowed to act only in $^1S_0$ and $^3S_1$–$^3D_1$ partial wave states. This corresponds to a 5-channel calculation in case of the 3N bound state. While the 2NF was allowed to act in all total angular momenta of the 3N system up to J = 17/2, the 3NF was restricted to $J \leq 3/2$. It is well known that 3NF contributions to the triton binding energy depend dramatically on the cut-off parameter Λ_π in the πNN form factor [Had90], resulting in larger binding energies with increasing Λ_π. Because of this unpleasant feature, we performed calculations of Nd elastic scattering and breakup observables at an incident nucleon laboratory energy of E_{lab} = 10 MeV using two values for Λ_π in generating the 2π-exchange 3NF: Λ_π^2 = 17.0 fm^{-2} and Λ_π^2 = 25.0 fm^{-2}. In figs.2.3-6 and 2.3-7 the Nd elastic scattering analyzing power A_y and the nucleon-to-nucleon polarization transfer coefficient $K_y^{y'}$ are shown. Surprisingly, no significant difference in the calculated observables was found with these two values for Λ_π. It is interesting to note that the addition of the 3NF caused non-negligible changes to both of these observables. As another example, we show in fig. 2.3-8 the effects of the 3NF on the differential cross section for the space-star configuration (in the c.m. system all three nucleons have equal momenta with an angle of 120° between them) as a function of the c.m. angle between the plane formed by the three outgoing nucleons and the incident beam direction.

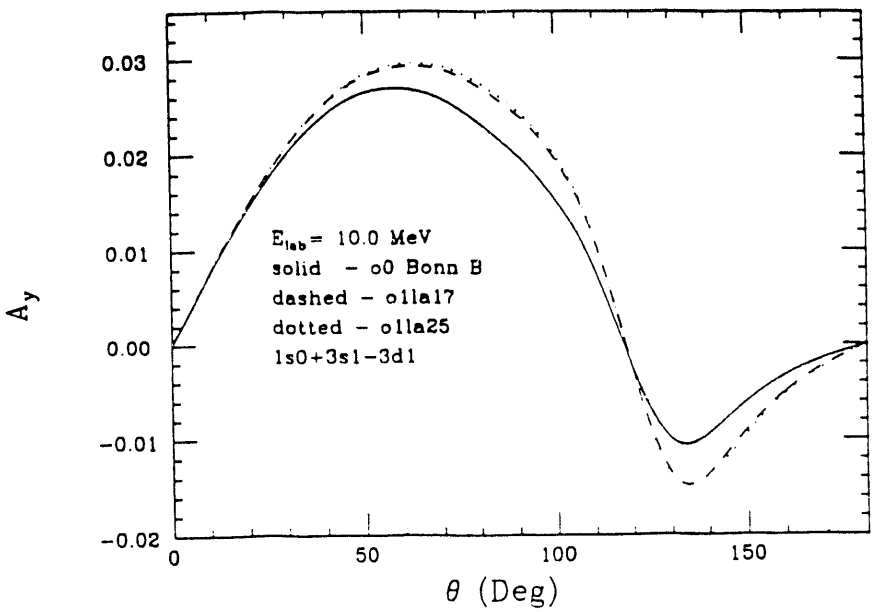

Fig. 2.3-6 Nd elastic scattering analyzing power A_y. The solid curve was obtained with 2N forces only. The dashed and dotted curves were calculated by adding a 3NF characterized by cut-off parameters Λ_π^2 = 17.0 fm^{-2} and Λ_π^2 = 25.0 fm^{-2}, respectively.

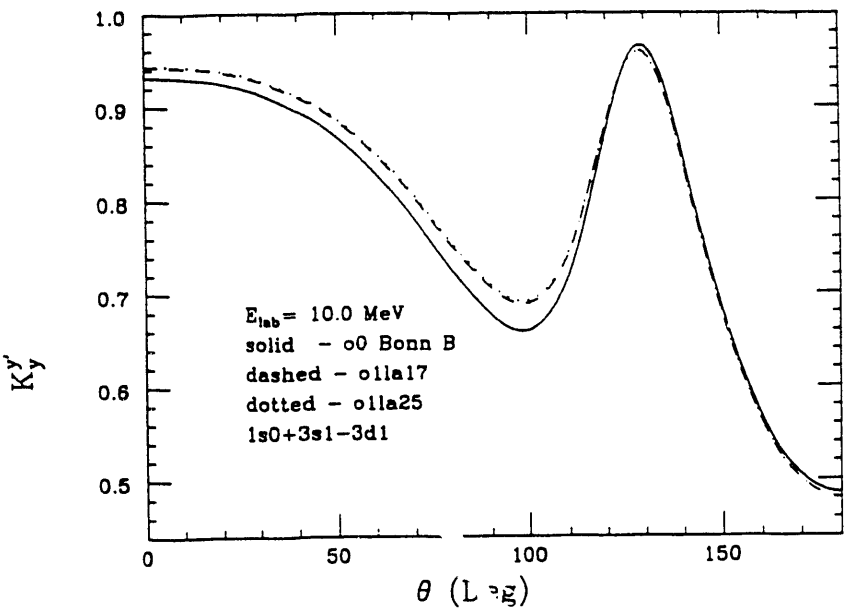

Fig. 2.3-7 Nd elastic scattering nucleon-to-nucleon spin transfer coefficient $K_y^{y'}$. For explanation of the curves see fig. 2.3-6.

For several reasons, it is impossible to draw quantitative conclusions about the magnitude of 3NF effects in the 3N continuum from a comparison of our results with experimental data. First, both of these observables depend significantly on higher partial wave states [Wit90, Cla90]. Second, it is known from 3N bound-state calculations that the magnitude of the 3NF contribution to the binding energy depends on higher partial wave states, and finally, the calculations were restricted to the first order in perturbation theory.

In summary, our preliminary studies indicate that a 3NF may have non-negligible effects on some observables in Nd elastic scattering and in the breakup process. However, before quantitative conclusions can be drawn, calculations with 2N and 3N forces acting in higher partial wave states and using higher orders in the perturbation approach must be performed.

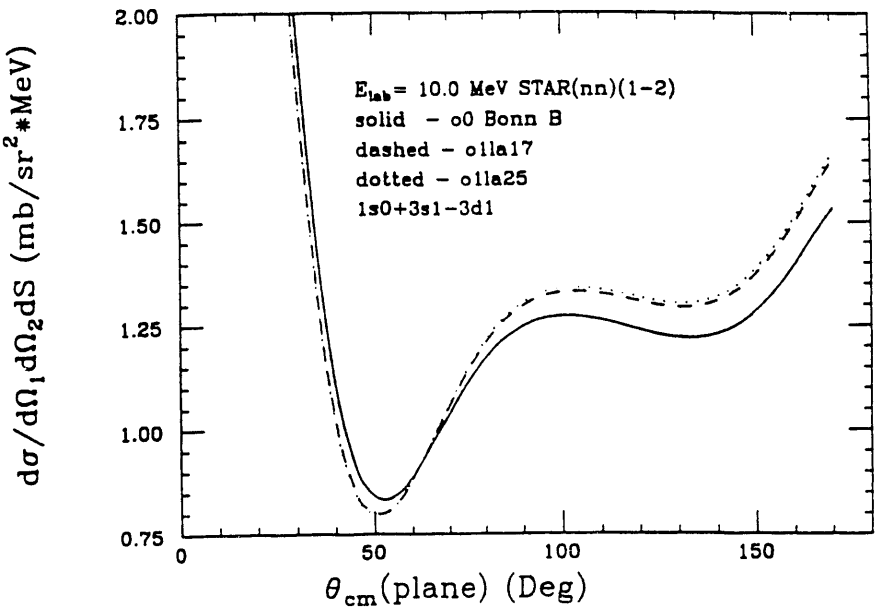

Fig. 2.3-8 Cross section for the space-star configuration in nd breakup as function of the c.m. angle between the plane formed by the momenta of the outgoing nucleons and the incident beam direction. For explanation of the curves see fig. 2.3-6.

[Cla90] M. Clajus *et al.*, Phys. Lett. **B245** (1990) 333

[Coo81] S.A. Coon, W. Glöckle, Phys. Rev. **C23** (1981) 1790

[Fri84] J.L. Friar, B.F. Gibson and G.L. Payne, Ann. Rev. Nucl. Sci. **34** (1984) 403

[Glö87] W. Glöckle, Lecture Notes in Physics **273** (1987) 3

[Glö90a] W. Glöckle, H. Witała and Th. Cornelius, Nucl. Phys. **A508** (1990) 115c

[Glö90b] W. Glöckle, H. Witała and Th. Cornelius, Proc. of the 25th Zakopane School on Physics, Vol. 2, ed. J. Styczen and Z. Stachura, (World Scientific, Singapore, 1990) p. 300

[Had90] E. Hadjimichael, Nucl. Phys. **A508** (1990) 161c

[Mac89] R. Machleidt, Adv. Nucl. Phys. **19** (1989) 189

[Mei84] W. Meier and W. Glöckle, Phys. Lett. **138B** (1984) 329

[Wit91] H. Witała and W. Glöckle, Nucl. Phys. **A528** (1991) 48

2.3.5 N-d Elastic Scattering at Backward Angles between 60 and 260 MeV

H. Witała, W. Glöckle, C.R. Howell, W. Tornow, B. Vlahovic

The neutron-deuteron elastic scattering differential cross section was calculated between 60 and 260 MeV using the Bonn-B NN potential. This is the first time that rigorous 3N calculations were performed at such high energies. The purpose of the present calculations

is to compare to backward-angle n-d differential cross-section data in the 60 to 250 MeV energy range which have recently been obtained in a Duke-LANL-Ohio-Davis collaboration at the WNR facility at LAMPF.

In the calculations nucleons were allowed to interact in two-nucleon states with total angular momentum $j_{max} = 3$. As shown in section 2.3.3, the $j_{max} = 3$ limitation is certainly justified for this observable in the angular region of interest up to about 150 MeV. Figure 2.3-9 displays the calculated 180° n-d differential cross section (open dots) in comparison to data (crosses) obtained at different laboratories. In general, there is very good agreement between data and calculation, except above 200 MeV. At these energies, the $j_{max} = 3$ limitation may come into play. Future calculations with $j_{max} = 4$ will focus on this question. It should be noted, that the only rigorous 3N calculation performed to date with $j_{max} = 4$ at E = 116 MeV (see section 2.3.3) gives slightly lower cross sections at 180° than the corresponding $j_{max} = 3$ calculations, exactly opposite to what one might expect from fig. 2.3-9. It would be very interesting to extend the calculations up to 320 MeV in order to explore possible explanations for the flat energy dependence of the measured cross section around 300 MeV.

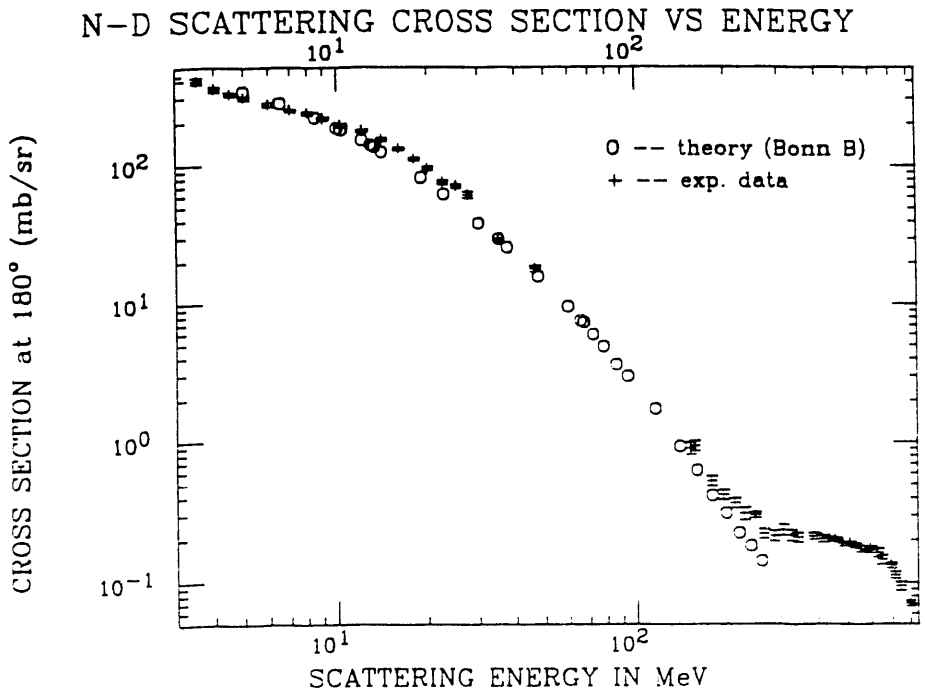

Fig. 2.3-9 Comparison of data (crosses) for the 180° neutron-deuteron differential cross section and rigorous 3N calculations (open circles) using the Bonn-B NN potential with $j_{max} = 3$.

2.3.6 Calculation of n-d Breakup at 12.8, 13.0, and 13.2 MeV

H. Witała, W. Glöckle, C.R. Howell, H.R. Setze, W. Tornow, B. Vlahovic

Neutron-deuteron breakup ($n+d \rightarrow n_1+n_2+p$) experiments performed in specific configurations of the outgoing three nucleons are of fundamental interest for studying the question of possible three-nucleon forces (3NF). The comparison of experimental results obtained at Erlangen [Str90, Str89] at 10.3 and 13 MeV with rigorous three-nucleon (3N) calculations using realistic, meson-exchange based two-nucleon potentials suggests the existence of rather large 3NF effects especially in the space star (Mercedes star) configuration of the three outgoing nucleons. A recent p-d breakup experiment at 13 MeV [Sch91] is also at variance with n-d calculations for this configuration. In addition, the experimental p-d and n-d results do not agree with each other. Since the Coulomb effects acting in the p-d reaction cannot be treated in the rigorous 3N calculations, at the present time accurate conclusions cannot be drawn from p-d breakup data.

The important consequences of the Erlangen experiments require an independent verification of the experimental results. Therefore, a n-d breakup experiment at E_n = 13 MeV is in preparation at TUNL. Similarly to the Erlangen setup, we will measure in kinematically-complete arrangements several different breakup configurations simultaneously.

Because of the finite geometry of the experimental setup, the experimental data are distributed around the point-geometry locus in the $E_{n_1} - E_{n_2}$ plane, where E refers to the energies of the detected neutrons. Before comparing to theoretical predictions, the data must be projected onto the point-geometry locus. However, this projection causes problems, especially in regions where the locus has a large curvature, since a unique projection procedure does not exist. Therefore, contrary to the Erlangen approach, we will treat the theoretical breakup results exactly in the same way as the experimental data. For that purpose the breakup cross section must be calculated for a large number of angles in the incident neutron energy range of interest. We calculated the n-d elastic scattering and breakup amplitudes at 12.8, 13.0 and 13.2 MeV. From these amplitudes cross sections can be calculated for any given combination of nucleon angles. Interpolations in energy must be performed to obtain cross sections at any given incident neutron energy in the energy interval between 12.8 and 13.2 MeV.

Figures 2.3-10 and 2.3-11 show n-d breakup cross sections along the locus for the space star ($\theta_1 = \theta_2 = 50.5°$, $\phi_{12} = 120°$) and collinear ($\theta_1 = 39°$, $\theta_2 = 75.5°$, $\phi_{12} = 180°$) configurations calculated at 12.8, 13.0 and 13.2 MeV with the Bonn-B NN potential with $j_{max} = 3$ and correct treatment of the charge-dependence of the $^1S_0$ NN interaction. We are using the calculated amplitudes to generate a detailed library of cross sections that will be used in both the Monte Carlo simulation of our experimental setup and the projection procedure mentioned above.

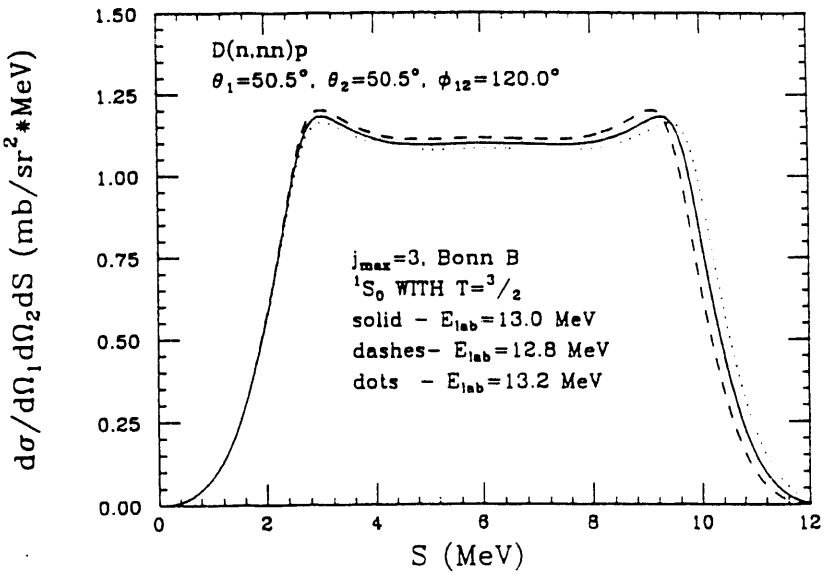

Fig. 2.3-10 Rigorous 3N calculations for the ^{2}H(n,nn)p breakup cross section (along the locus) in the space star geometry using the Bonn-B NN potential.

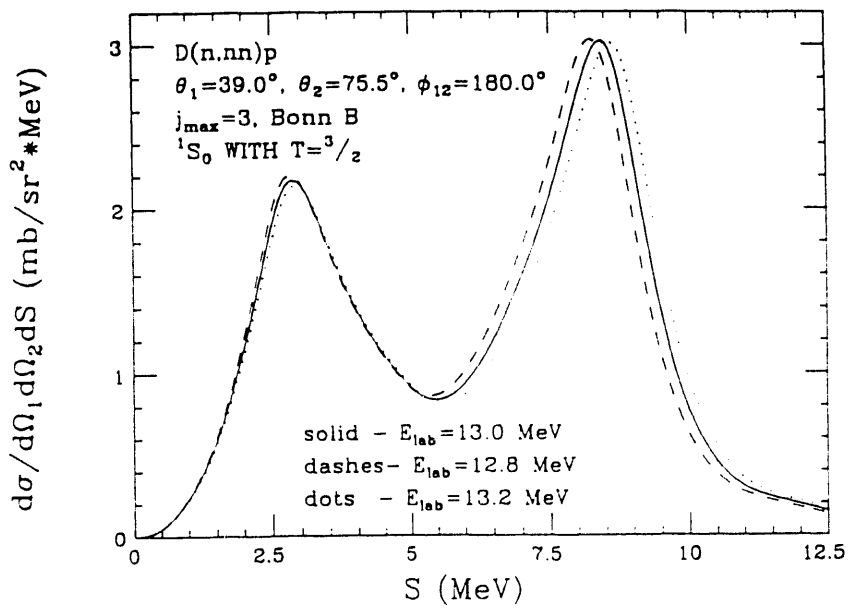

Fig. 2.3-11 Same as fig. 2.3-10 for colinear configuration.

[Str89] J. Strate *et al.*, Nucl. Phys. **A501** (1989) 51
[Str90] J. Strate, private communication
[Sch91] H. Paetz gen. Schieck, private communication

2.3.7 Small-Angle Proton Energy Spectra from ^{2}H(n,p)nn and the NN Scattering Length

H. Witała, W. Glöckle, R. Braun, W. Tornow

The accurate determination of the neutron-neutron scattering length a_{nn} is of fundamental interest. Due to the lack of a suitable free neutron target the deuteron breakup reaction has been frequently used to extract values for a_{nn}. It is well known that $a_{nn} = -18.50 \pm 0.42$ fm obtained from the reaction ^{2}H(π^-,γ)2n is in disagreement with the mean value $\bar{a}_{nn} = -16.73 \pm 0.47$ fm obtained from a number of experiments using the reaction ^{2}H(n,nn)p (neutron-pickup geometry) [Mil90]. There are indications that the latter result is incorrect due to the action of a three-nucleon force (3NF). A 3NF is not present in the reaction ^{2}H(π^-,γ)2n. Sensitivity calculations performed by [Sla82] that included a 3NF showed that the magnitude of a_{nn} is reduced by 1.9 fm in the neutron-pickup configuration [^{2}H(n,nn)p] and enlarged by about 0.3 fm in the proton-knock-on configuration [^{2}H(n,p)nn]. In fact, a recent proton-knock-on experiment [Koo89] at 63 MeV gave $a_{nn} = -18.8 \pm 1.0$ fm.

In order to further investigate a possible 3NF influence on the determination of a_{nn}, a ^{2}H(n,p)nn experiment is in preparation at TUNL. The Enge split-pole magnet (section 5.4) will be used for measuring the energy distribution of the protons emitted around $\theta_1 = 0°$. Since the experiment will be performed in finite geometry, the extraction of a_{nn} requires a Monte Carlo simulation of the experimental setup. To create an input library, proton energy spectra are needed for angles around $\theta_1 = 0°$ and incident energies within the region of interest using different values for a_{nn}. As an example, fig. 2.3-12 shows a proton energy spectrum at $\theta_1 = 3°$ for an incident neutron energy of 13 MeV calculated with the Bonn-B NN interaction with $j_{max} = 3$ and correct charge-dependent treatment of the $^1S_0$ NN interaction. The width of the high-energy peak is a measure of a_{nn}.

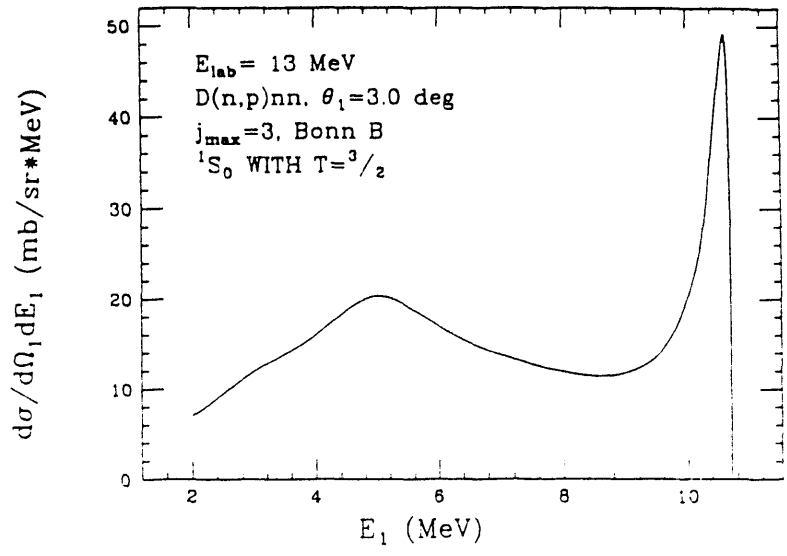

Fig. 2.3-12 Rigorous 3N calculation of proton energy spectrum at θ_1=3° for ^{2}H(n,p)nn at E_{lab} = 13 MeV using the Bonn-B NN interaction with j_{max} = 3.

[Koo89] N. Koori *et al.*, in Approaches to Nuclear Reactions in Tandem and Cyclotron Energy Region, eds. S. Oryu and T. Sawada (World Scientific, Singapore 1989) p. 129
[Mil90] G.A. Miller *et al.*, Phys. Rep. **194** (1990) 1
[Sla82] I. Slaus *et al.*, Phys. Rev. Lett. **48** (1982) 993

2.3.8 NN D-Wave Sensitivity of the n-d Elastic Analyzing Power

W. Tornow, H. Witała, W. Glöckle

In [Wit91] it was shown that charge-independence breaking (CIB) and charge-symmetry breaking (CSB) in the ^3P_J NN interaction can account for the difference between the N-d analyzing power $A_y(\theta)$ at $\theta \approx 120°$ c.m. and rigorous 3N calculations using modern, meson-exchange based NN interactions. Figure 2.3-13 clearly demonstrates that the modified Bonn-B ^3P_J NN interactions of [Wit91] describe $A_y(\theta)$ data at 10 MeV very well in the angular range of the maximum of A_y (solid and dashed curves). However, contrary to the better agreement noticed between n-d data at forward angles and calculations using the original Bonn-B potential (dotted curve), the ^3P_J modified potential calculations are at variance with the data in this angular range. It was found earlier [Tor88] using separable NN interactions that the forward angular region of $A_y(\theta)$ is quite sensitive to the strength of the $^3D_2$ NN interaction, while the maximum of A_y depends only slightly on this phase shift.

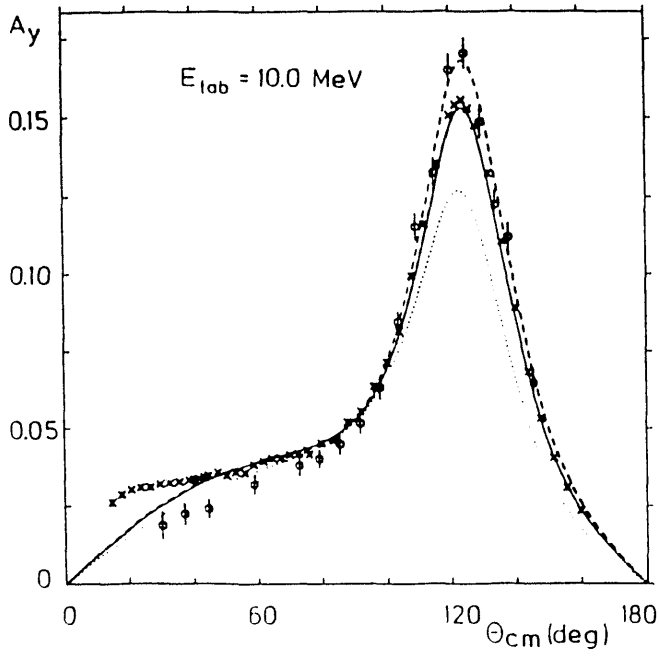

Fig. 2.3-13 Neutron-deuteron (open circles) and proton-deuteron (crosses) analyzing power data at 10 MeV in comparison with rigorous 3N calculations using the original Bonn-B NN potential (dotted curve), a ^3P_J CIB modified Bonn potential (solid curve) and a ^3P_J CSB modified Bonn potential (dashed curve).

Figure 2.3-14 shows the sensitivity of $A_y(\theta)$ at 10 MeV to modifications of the $^3D_2$ NN interaction. Here, the solid curve represents the full calculation using the original Bonn B NN potential. The dotted curve was obtained by setting the $^3D_2$ phase shift to zero. In agreement with [Tor88], the entire angular region below 90° is affected rather strongly by this manipulation. At the maximum of A_y a slightly lower magnitude is observed. Comparing the solid and dotted curves in fig. 2.3-14 and considering the discrepancy between n-d data and the modified ^3P_J calculations shown in fig. 2.3-13, one may argue that an increase in the $^3D_2$ NN phase shift is needed to bring the modified ^3P_J calculation in better agreement with the data. In fact, the dashed-dotted and dashed curves in fig. 2.3-14 were obtained by multiplying the strength of the $^3D_2$ NN interaction in the original Bonn-B potential by factors of 1.2 and 1.4, respectively. This procedure not only brings the calculations in better agreement with the n-d data at forward angles but also increases A_y at the maximum. The latter finding is equivalent to a small reduction in the amount of CIB required by modifying ^3P_J NN interactions only. It has to be seen whether the proposed increase in the $^3D_2$ phase shift is consistent with 2N and other 3N data.

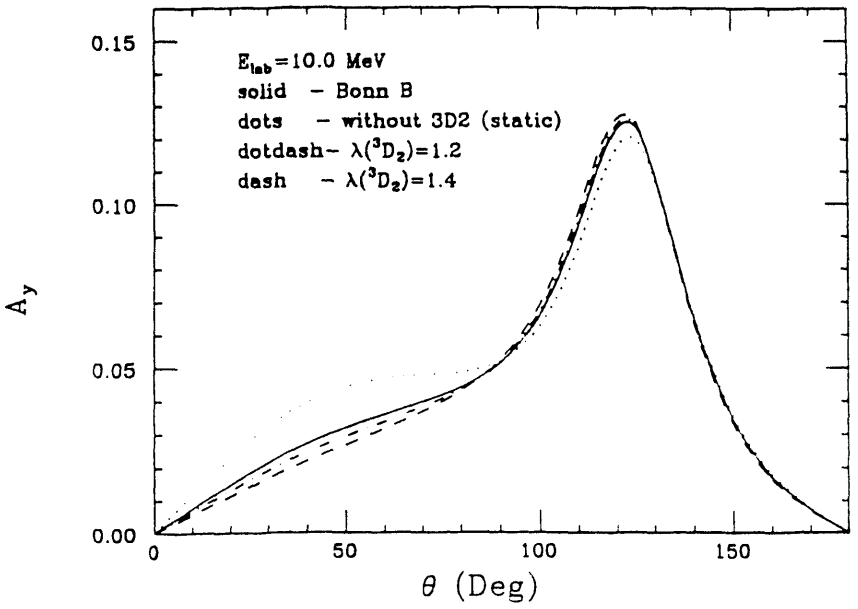

Fig. 2.3-14 Rigorous n-d calculations at 10 MeV using the original Bonn-B potential (solid curve), the Bonn-B potential with the $^3D_2$ phase shift turned off (dotted curve) and modified Bonn-B potentials with increased strength in the $^3D_2$ NN interaction (dotted-dashed curve: factor 1.2; dashed curve: factor 1.4).

[Tor88] W. Tornow *et al.*, Phys. Lett. **B203** (1988) 341
[Wit91] H. Witała and W. Glöckle, Nucl. Phys. **A528** (1991) 48

2.4 Charge-Symmetry-Breaking Effects

The problems of charge-independence and charge-symmetry-breaking in the nucleon-nucleon interaction remain provocative and puzzling. During the past year we have designed and performed at TUNL several tests that bear on these problems, as we now describe.

2.4.1 Charge-Symmetry Breaking Versus Coulomb Effects in Three-Nucleon Scattering

W. Tornow, C.R. Howell, R.L. Walter, I. Slaus[1]

In [Tor90] it was shown that, besides charge-symmetry breaking (CSB) [Wit91], the Coulomb interaction may be an alternative explanation for the small difference observed experimentally between the proton-deuteron and neutron-deuteron analyzing power $A_y(\theta)$ around $\theta_{c.m.} = 120°$. To further investigate the effect of the Coulomb repulsion in p-d scattering the n-d $\sigma(\theta)$ and $A_y(\theta)$ data at 10 MeV were "fitted" using an optical-model approach with Woods-Saxon form factors that is standard for heavier nuclei. The solid line in fig. 2.4-1 was obtained by searching on the data, but restricting the potential parameters to values close to those commonly accepted for heavier nuclei. For the real central potential we obtained $V_R = 38.6$ MeV, $r_R = 1.24$ fm and $a_R = 0.75$ fm. The spin-orbit potential parameters are $V_{so} = 2.24$ MeV, $r_{so} = 1.105$ fm and $a_{so} = 0.65$ fm and the imaginary (surface absorptive) potential is characterized by $W_I = 2.70$ MeV, $r_I = 1.24$ fm and $a_I = 0.675$ fm. The shape of the measured $A_y(\theta)$ is qualitatively reproduced.

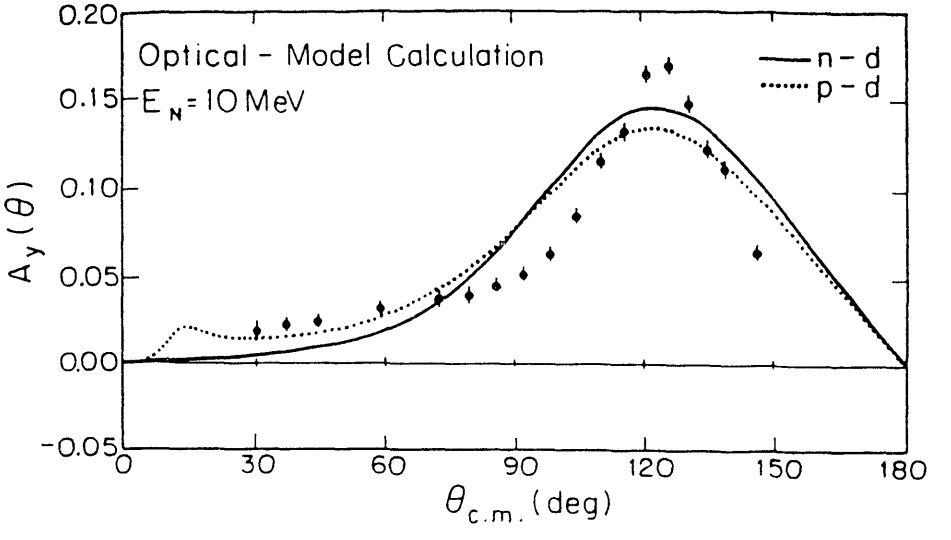

Fig. 2.4-1 Optical-model calculations for n-d (solid curve) and p-d (dotted curve) $A_y(\theta)$ at 10 MeV compared to n-d data [Tor82].

The dotted curve in fig. 2.4-1 was calculated for p-d scattering using exactly the same nuclear potential as for n-d. For the Coulomb potential we used that of a uniform charge

[1] Rudjer Boskovic Institute, Zagreb, Croatia, Yugoslavia

distribution of radius parameter r_c = 1.24 fm. Since our result does not depend strongly upon the value of r_c, for simplicity we set $r_c = r_R$, so that we used a Coulomb radius R = 1.24 • $A^{1/3}$ = 1.56 fm. Of course, a folding-model approach would give a value that is closer to the rms value of 1.953 fm. A polarization potential was not included since it was shown to be negligible [Ben87]. Qualitatively, the curves exhibit the same difference at A_y(max) as observed experimentally. In addition, the forward-angle difference is also predicted. Carrying this optical-model approach farther, we used an energy dependence for the real potential that is common for heavier nuclei ($V_0 - 0.3E_N$, V_0 = 41.6 MeV) and calculated the solid curve in fig. 2.4-2. This prediction compares favorably with the experimental trend. It also should be noted that $\sigma(\theta)$ is described quite well at scattering angles forward of 120° c.m. As expected, beyond 120° c.m. where nucleon-pickup dominates, the optical-model calculation does not reproduce $\sigma(\theta)$. However, in agreement with data [Rau88], we find that the n-d backward-angle $\sigma(\theta)$ is slightly larger than that for p-d scattering.

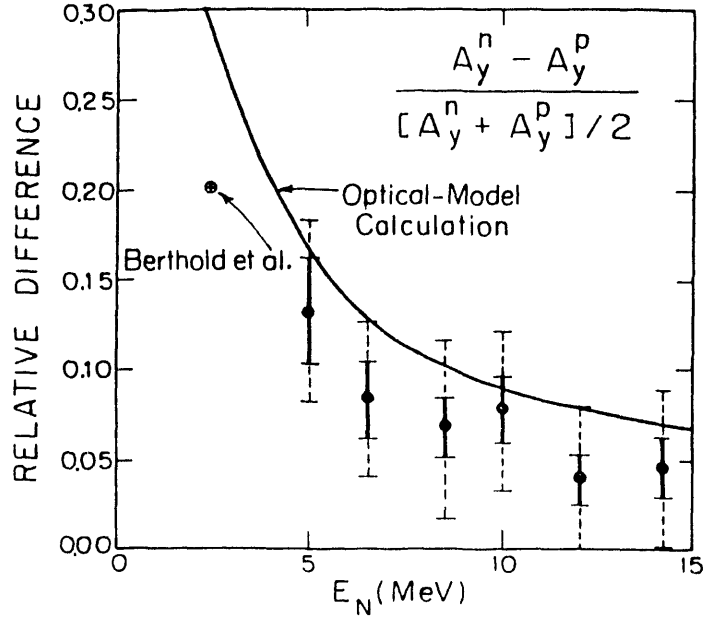

Fig. 2.4-2 Relative difference between n-d and p-d analyzing power near $\theta_{c.m.}$ = 120°. The point at 2.5 MeV was obtained from [Ber88]. The solid curve is an optical-model calculation.

In summary, the comparison of n-d and p-d $A_y(\theta)$ data has been extended down to 5 MeV, with a particular focus on differences at the maximum of $A_y(\theta)$. To first order, these differences can be reproduced by applying a simple correction to remove the effect of the Coulomb interaction in p-d scattering. This approach to the Coulomb correction should also be applicable to other p-d and d-p observables, for example $\sigma(\theta)$, but the quality of the available n-d $\sigma(\theta)$ data is insufficient for a meaningful comparison. Reiterating our conclusion, we find that a straightforward treatment of the Coulomb correction has revealed that

the major part of the observed differences between n-d and p-d $A_y(\theta)$ data is most likely an electromagnetic effect and not a charge-symmetry-breaking effect. It now appears likely that CSB effects in the ^3P NN interactions are too small to be observed in the Nd scattering systems at low energies with present techniques. It might well be that CSB effects account for only about 10% of the discussed differences, similar to what was found for the 3N bound-state binding energy difference [Bra78]. However, rigorous Faddeev calculations that include the Coulomb interaction exactly will be important for supporting the present conclusions.

[Ben87] G. Bencze, Phys. Lett. **B202** (1987) 289; S.K. Adhikari and T.K. Das, Phys. Rev. **C37** (1988) 1376, and references therein

[Ber88] G.H. Berthold, A. Stadler and H. Zankel, Phys. Rev. Lett. **61** (1988)1077 and Phys. Rev. **C41** (1990) 1365

[Bra78] R.A. Brandenburg, S.A. Coon and P.U. Sauer, Nucl. Phys. **A294** (1978) 305

[Fri87] J.L. Friar, B.F. Gibson and G L. Payne, Phys. Rev. **C35** (1987) 1502

[Ish90] Y. Wu, S. Ishikawa and T. Sasakawa, Phys. Rev. Lett. **64** (1990) 1875, and references therein

[Rau88] G. Rauprich *et al.*, Few Body Systems **5** (1988) 67, and references therein

[Tor82] W. Tornow *et al.*, Phys. Rev. Lett. **49** (1982) 312

[Tor90] W. Tornow *et al.*, TUNL Annual Report XXIX (1989-90) p. 33

2.4.2 Low-Energy n-d Analyzing Powers and ^3P Interactions in NN Potentials

W. Tornow, C.R. Howell, M. AlOhali, Z.P. Chen[1], P.D. Felsher, J.M. Hanly[2], R.L. Walter, G.J. Weisel, G. Mertens[3], I. Slaus[4], H. Witała[5], W. Glöckle[6]

This work was published recently in Phys. Lett. **B257** (1991) 273. The abstract follows:

Data for the analyzing power $A_y(\theta)$ for elastic scattering of neutrons from deuterons have been measured at 5.0, 6.5 and 8.5 MeV to an accuracy of ±0.0035. Surprisingly large differences have been observed at these low energies between the data and rigorous Faddeev calculations using the Paris and Bonn-B NN potentials (see figs. 2.4-3 and 2.4-4). The $A_y(\theta)$ data provide a stringent test for our present understanding of the on-shell and off-shell ^3P_J NN interactions.

[Cub89] J. Cub *et al.*, Few-Body Systems **6** (1989) 151

---

[1] Department of Physics, Tsinghua University, Beijing, The People's Republic of China
[2] Present address: Booz-Allen & Hamilton, Inc., Arlington, VA
[3] Physikalisches Institut, Universität Tübingen, FGR
[4] Rudjer Boskovic Institute, Zagreb, Croatia, Yugoslavia
[5] Institute of Physics, Jagellonian University, Cracow, Poland
[6] Institut für Theoretische Physik II, Ruhr Universität Bochum, FGR

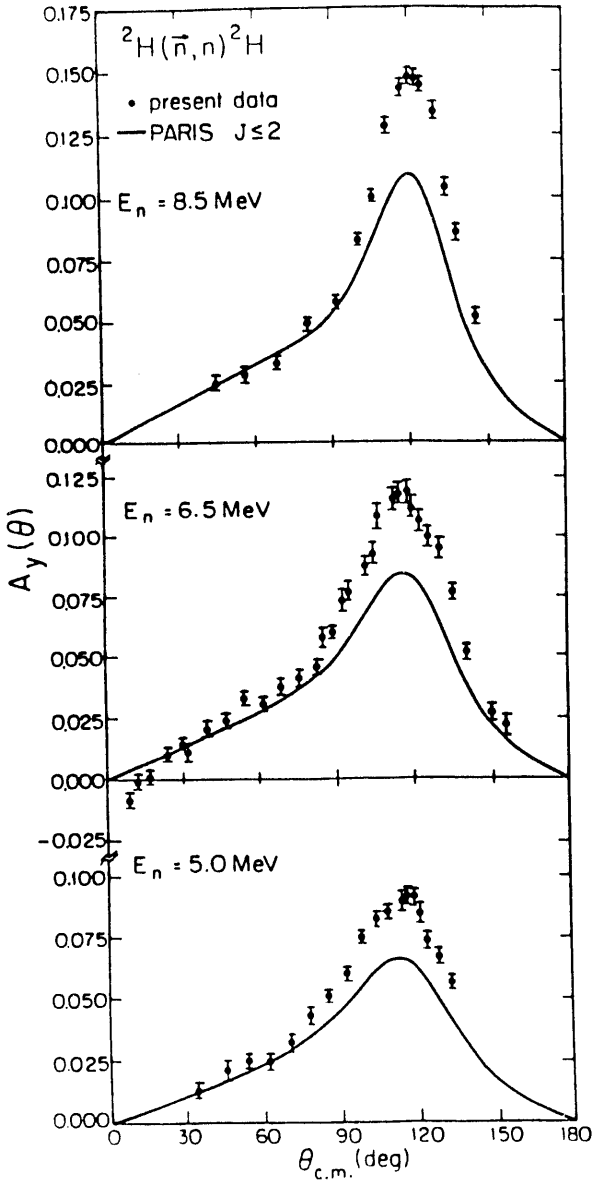

Fig. 2.4-3 Neutron-deuteron elastic analyzing power $A_y(\theta)$ data at E_n=5.0, 6.5 and 8.5 MeV in comparison to rigorous Faddeev calculations using the Paris NN potential.

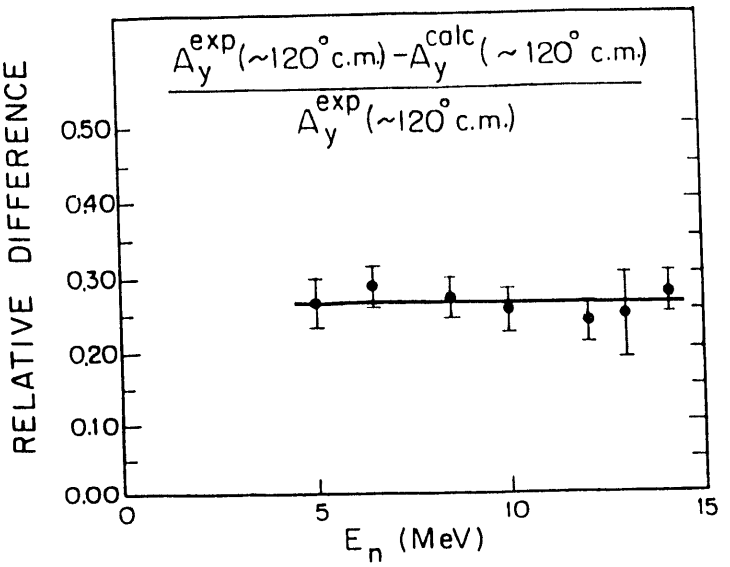

Fig. 2.4-4 Energy dependence of the relative difference between the measured and calculated $A_y(\theta)$ at the maximum of $A_y(\theta)$. The solid line represents the average relative difference. The datum at 13 MeV is from [Cub89]. The other data were obtained at TUNL.

2.4.3 Search for Charge-Symmetry Breaking in Deuteron-Induced Deuteron Breakup

P.D. Felsher, C.R. Howell, I. Slaus[1], W. Tornow, M.L. Roberts[2], J.M. Hanly[3], G.J. Weisel, M. Al Ohali, R.L. Walter, J.M. Lambert[4], P.A. Treado[4,], G. Mertens[5], Y. Koike[6]*

Consistent information now exists to verify that charge symmetry is broken [Mil90]. This information, obtained from a variety of observables and systems, is also leading to an understanding of the fundamental causes of the breaking of this symmetry [Mil90]. In particular, the difference between the $^1S_0$ *nn* and *pp* scattering lengths [Sla89], and the observed ^{3}H-^{3}He mass difference [Wu90, Fri87] are fully explained by the Coulomb interaction and charge symmetry breaking (CSB) in the *S*-wave part of the nucleon-nucleon (*NN*) force. However, very little is known about CSB in *NN* angular momentum states for $\ell \geq 1$.

---

[1] Ruder Boskovic Institute, Zagreb, Yugoslavia
[2] Present address: Lawrence Livermore National Laboratory, Livermore, CA 94550
[3] Present address: Booz Allen and Hamilton, Huntsville, Al 35806
[4] Department of Physics, Georgetown University, Washington, DC 20057
[5] University of Tübingen, Tübingen, Germany
[6] Department of Physics, Hosei University, Tokyo, Japan
*Deceased

In the A = 3 system, differences between data for neutron-deuteron (*nd*) and proton-deuteron (*pd*) elastic scattering provide a measure of CSB. The main difficulty in interpreting the results of *nd-pd* comparisons is discerning between differences that are due to CSB and those that are due to the electromagnetic (e.m.) force [Tor91]. Because the Coulomb repulsion of the incident proton in *pd* scattering reduces the effective interaction energy of the proton, *pd* data must be compared to *nd* data at a lower energy. The calculation of the Coulomb energy shift in *pd* scattering has a large uncertainty due to the large diffuseness of the deuteron.

In the A = 4 system, attempts have been made to observe CSB by comparing data for the $D(\vec{d},p)^3H$ and $D(\vec{d},n)^3He$ stripping reactions [Grü89]. Although the Coulomb force in the entrance channel is identical for these two reactions, there are difficulties in interpreting the results. First, because of the differences in the Q-values, the reactions must be compared at different incident deuteron energies in order to match the c.m. energy in the exit channel. Second, the effect of the Coulomb force in the exit channels is clearly different.

In this work we investigate the use of spin observables from the $D(\vec{d},dp)n$ and $D(\vec{d},dn)p$ charge symmetric reactions as a probe of CSB. Even though the four-nucleon (4*N*) system is inherently more complicated than the three-nucleon (3*N*) system and rigorous calculations do not exist for these reactions, we use this probe because of three advantages over the comparisons of *nd* and *pd* elastic scattering data:

1) Since the entrance channels are identical, the ambiguity of the Coulomb energy shift in the entrance channel in *pd* scattering is avoided.

2) Unlike the A_y data for the *nd-pd* comparisons, the $D(\vec{d},dp)n$ and $D(\vec{d},dn)p$ data can be measured simultaneously, thereby cancelling most instrumental asymmetries and all uncertainties in the incident beam polarization.

3) The use of tensor polarized deuteron beams enables, with only minor technical difficulties, the measurements of several CS spin observables, rather than of only A_y as in the case of *Nd* elastic scattering which requires a tensor polarized deuteron target to make *nd* tensor analyzing power measurements. In addition, the $\vec{d}+d\rightarrow d+p+n$ breakup reaction is favored over the comparison of data from the $^2H(d,p)^3H$ and $^2H(d,n)^3He$ reactions because the complications in the comparisons due to the Q-value differences in the latter two reactions are avoided. Also, because of the kinematic flexibility of the $d+d\rightarrow d+p+n$ breakup reaction, the Coulomb force in the exit channel of the $D(\vec{d},dp)n$ and $D(\vec{d},dn)p$ reactions can be made very similar by choosing particle emission angles to match the relative momenta between the emitted proton and deuteron.

We investigated the reactions $D(\vec{d},dp)n$ and $D(\vec{d},dn)p$ at an incident energy of 12 MeV for several *d-N* angle pairs. The angle pairs were chosen to make measurements in the kinematic region corresponding to *dN* quasi-free scattering (QFS). The observed A_y values are roughly equal to those for *Nd* elastic scattering, and the tensor analyzing powers are comparable to, although sometimes appreciably larger than, those for $\vec{d}p$ elastic scattering [Whi79]. The strong resemblance between the analyzing powers for the $D(\vec{d},dN)N$ reactions and those for *Nd* elastic scattering, suggest that the present data should have similar sensitivity to the *NN P*-waves as *Nd* elastic scattering.

In a kinematically-complete three-body (3B) breakup reaction five kinematical variables uniquely define the point in 3B phase space at which the observable is measured. In measurements of the $\vec{d}+d \rightarrow d+p+n$ reaction, we specify the angles and energies of the two detected particles (θ_1, ϕ_1, θ_2, ϕ_2, E_1, E_2), thus kinematically over-determining the reaction. Since in our measurements the detectors were always located in the xz plane, the notation (θ_1,θ_2) will be used to represent the angles of the detected particles, with $\theta > 0°$ for $\phi = 0°$ and $\theta < 0°$ for $\phi = 180°$. For example, in the case of the dn coincidence measurements, we specify the tensor analyzing powers as $A_{ij}(\theta_d, \theta_n, E_d, E_n)$, where i and j represent either x, y, or z.

We made measurements at two angle pairs for the CS tests: (θ_d,θ_N) = (+17.0°, –17.0°) and (+17.0°, –34.5°). If charge symmetry (CS) is valid, then the observables for D($\vec{d}$,dp)n and D($\vec{d}$,dn)p with (θ_d,θ_p) = (θ_d,θ_n) should be equal. Also, we investigated the process D($\vec{d}$,pn)d with (θ_p,θ_n) = (+17.0°,–17.0°), where if CS is valid then the A_{yy} and A_{zz} along the kinematic locus in a plot of E_p versus E_n should be symmetric (A_y is antisymmetric) with respect to the $E_p = E_n$ point. This feature can be proven as follows: since tensor analyzing powers measured with the spin quantization axis of the beam along a coordinate axis are invariant under a 180° rotation about the z axis [Hae74],

$$A_{ii}(\theta_p = +\theta, \theta_n = -\theta, E_p = E_1, E_n = E_2) = A_{ii}(\theta_p = -\theta, \theta_n = +\theta, E_p = E_1, E_n = E_2),$$

where the particle angles and energies are specified as above. If charge symmetry holds, then

$$A_{ii}(\theta_p = -\theta, \theta_n = +\theta, E_p = E_1, E_n = E_2) = A_{ii}(\theta_p = +\theta, \theta_n = -\theta, E_p = E_2, E_n = E_1).$$

Therefore, we obtain the symmetric relationship

$$A_{ij}(\theta_p = +\theta, \theta_n = -\theta, E_p = E_1, E_n = E_2) = A_{ij}(\theta_p = +\theta, \theta_n = -\theta, E_p = E_2, E_n = E_1).$$

This simply means that if CS holds, then tensor analyzing powers such as A_{yy} and A_{zz} must be symmetric about the E_p=E_n point along the locus of E_p *vs.* E_n. On the other hand, since A_y is antisymmetric under a 180° rotation about the z axis [Hae74], the A_y for the breakup reaction must be antisymmetric about the E_p=E_n point on the locus.

Figure 2.4-5 shows the A_y, A_{yy} and A_{zz} data for (θ_d,θ_N) = (+17.0°, –17.0°) plotted as a function of arc length along the kinematically allowed curve S. The data for the two reactions are indistinguishable within statistical uncertainties, except for the A_y data around $S = 6$ MeV. To more closely investigate the difference in A_y, the uncertainties were reduced by summing all the data between $S = 3.9$–7.4 MeV. The differences in the above interval in A_y, A_{yy} and A_{zz} between the two processes in the above interval are 0.006 ± 0.004, 0.002 ± 0.005 and 0.004 ± 0.006, respectively.

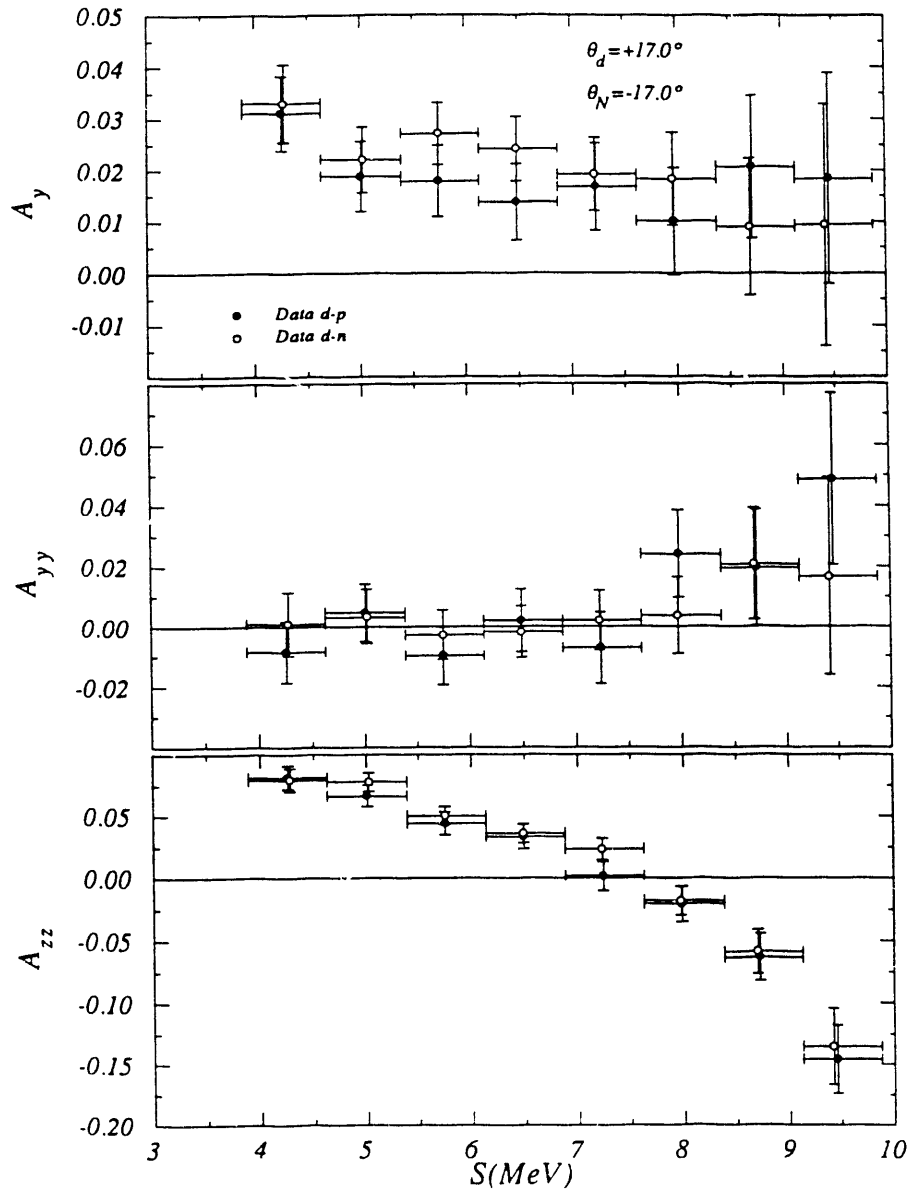

Fig. 2.4-5 Vector A_y and tensor A_{yy} and A_{zz} analyzing powers for the reactions D($\vec{d}$,dp)n (closed circles) and D($\vec{d}$,dn)p (open circles) along the locus as a function of the arc length S with (θ_d,θ_N) = (+17.0°, -17.0°). The horizontal *bars* indicate the interval along the arc which that point spans.

The data for (θ_d,θ_N) = (+17.0°, –34.5°) are shown in fig. 2.4-6. These data were summed over the region on the locus in which the D($\vec{d}$,dn)p and D($\vec{d}$,dp)n measurements overlapped, that was S=4.6–9.9 MeV. The A_y and A_{yy} data for the two processes agree within their statistical errors of ±0.017 and ±0.022, respectively. However, there is a significant difference of 0.060±0.025 between the A_{zz} data.

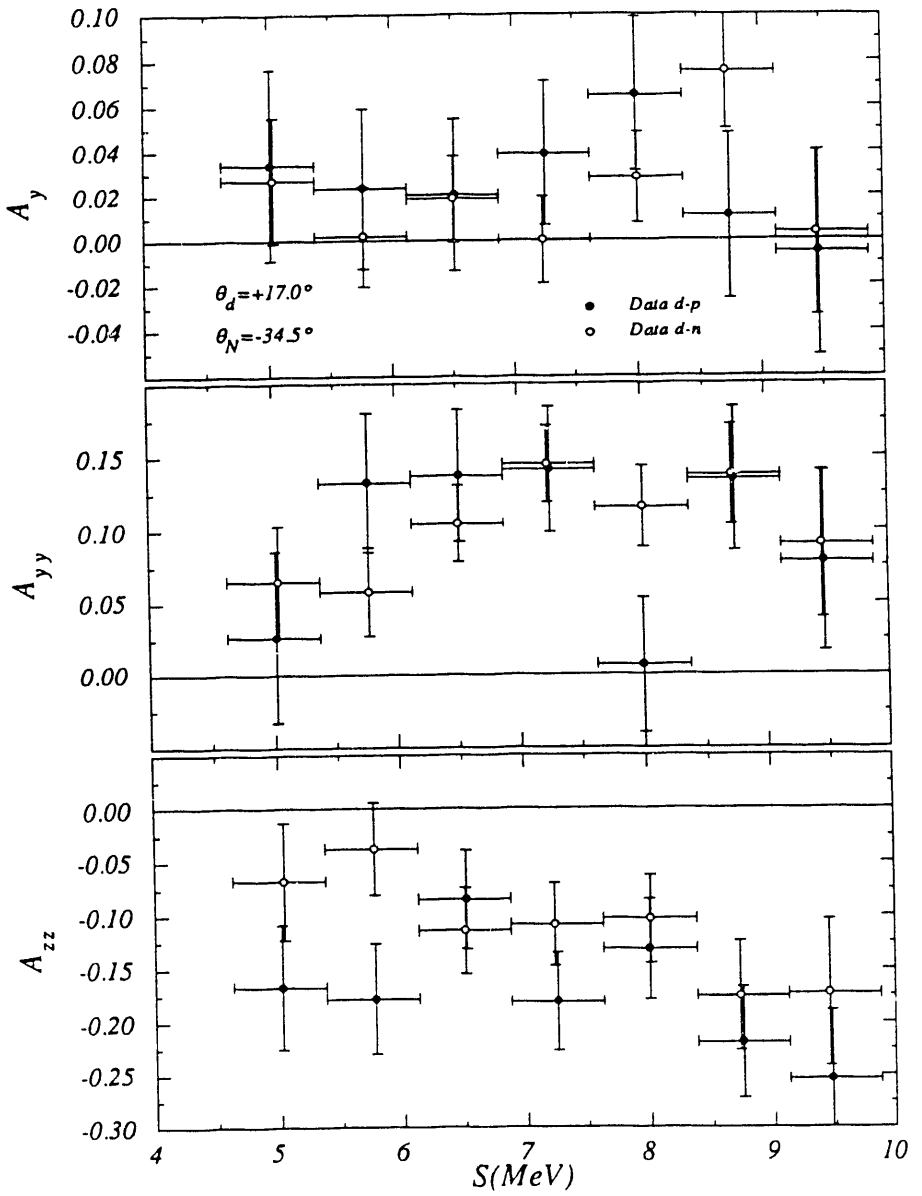

Fig. 2.4-6 Same as fig. 2.4-5 except for (θ_d,θ_N) = (+17.0°, -34.5°)

The analyzing powers A_y, A_{yy} and A_{zz} for the reaction D($\vec{d}$,pn)d with the angles (θ_p,θ_n) = (+17.0°,–17.0°) are shown in fig. 2.4-7 and are compared in the two regions S = 3.9–6.6 and 7.6–10.4 MeV. These regions are symmetric in energy with respect to the E_p=E_n point (S = 7 MeV). The A_{yy} and A_{zz} data are symmetric to within the statistical errors of ±0.02, and the A_y data are antisymmetric to within their statistical errors of ±0.016. However, in the interval S = 6.4–7.9 MeV around the $E_p = E_n$ point, the value of A_y is 0.031 ± 0.012, but it should be zero if CS is valid.

Thus, it is seen that, with two exceptions, our study has found excellent agreement between CS observables to within an absolute uncertainty of ±0.006 to ±0.02. These exceptions are the two observables A_{zz} for (θ_d,θ_N) = (+17.0°, -34.5°) at S = 4.6-9.9 MeV and A_y for (θ_p,θ_n) = (+17.0°,-17.0°) at S = 6.4-7.9 MeV.

A manuscript on our results is near completion for submission to Physical Review Letters.

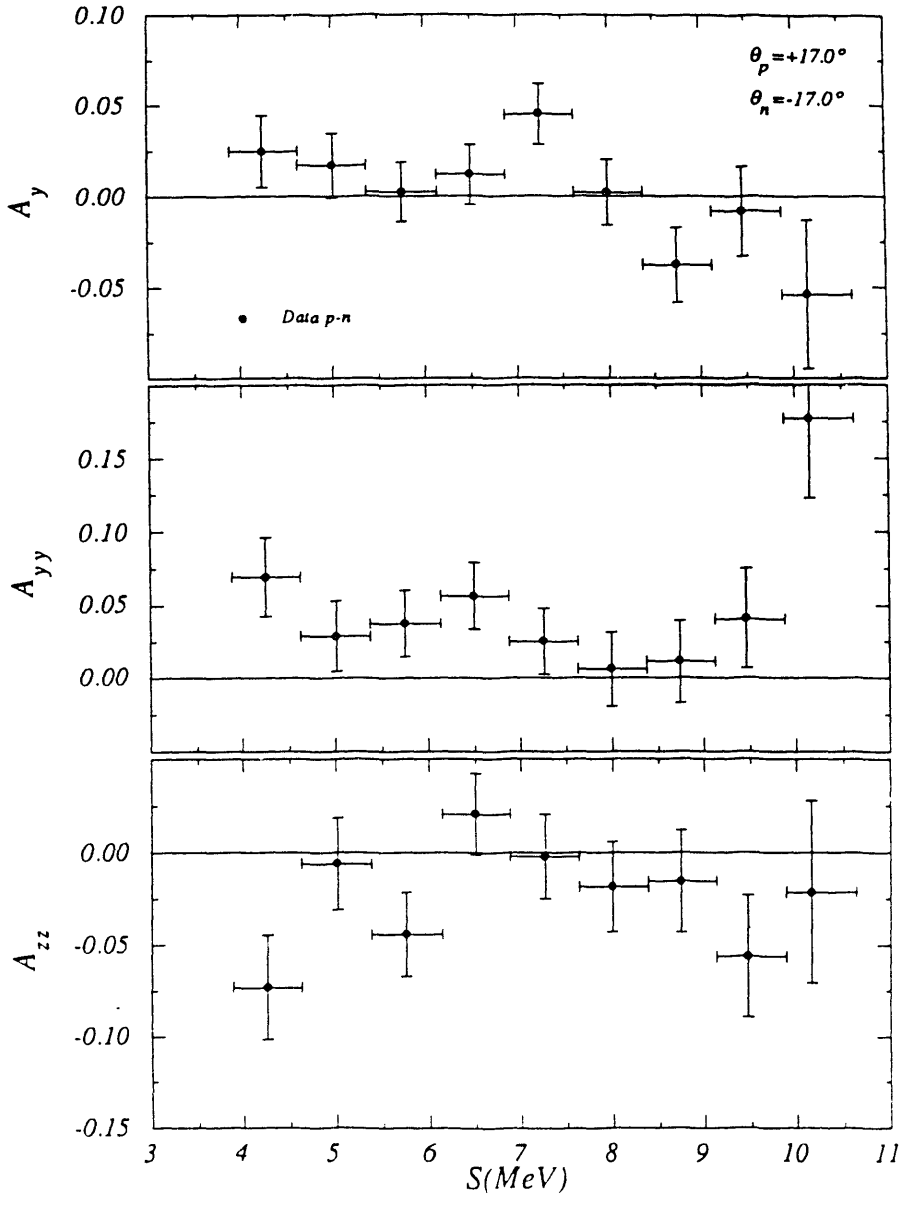

Fig. 2.4-7 Vector A_y and tensor A_{yy} and A_{zz} analyzing power data for the D($\vec{d}$,pn)d reaction at (θ_p,θ_n) = (+17.0°,-17.0°). The horizontal bars indicate the interval along the kinematic arc which that point spans.

[Fri87] J.L. Friar, B.F. Gibson and G.L. Payne, Phys. Rev. **C35** (1987) 1502; R.A. Brandenburg *et al.*, Phys. Rev. **C37** (1988) 781

[Grü89] W. Grüebler, Proc. of symposium on Spin and Symmetries, eds. W.D. Ramsay and W.T.H. van Oers, TRIUMPF, Vancouver, Canada (1989) and references therein

[Hae74] W. Haeberli, Nuclear Spectroscopy and Reactions, Part A, ed. J. Cerny, 1974 (Academic Press, New York) p. 151

[Mil90] G.A. Miller, B.M.K. Nefkens and I. Slaus, Phys. Rep. **194** (1990) 1

[Sla89] I. Slaus, Y. Akaishi and H. Tanaka, Phys. Rep. **173** (1989) 257

[Tor91] W. Tornow, C.R. Howell, R.L. Walter and I. Slaus, submitted to Phys. Rev. C

[Whi79] R.E. White *et al.*, Nucl. Phys. **A321** (1979) 1

[Wu90] Y. Wu, S. Ishikawa and T. Sasakawa, Phys. Rev. Lett. **64** (1990) 1875, and references within

2.4.4 Analyzing Powers in d+d → d+p+n at 12 MeV

P.D. Felsher, M. Al Ohali, J.M. Hanly[1], C.R. Howell, Y. Koike[2], J.M. Lambert[3], G. Mertens[4], M.L. Roberts[5], I. Slaus[6], W. Tornow, P.A. Treado[3,], R.L. Walter, G. Weisel*

In recent years, partially driven by the interest in fusion energy, astrophysical studies, and the search for three-nucleon (3N) forces, much effort has been devoted to study of the four-nucleon (4N) system. As a result of this concerted effort and the increasing capabilities of supercomputers, much progress has occurred on the theoretical front. Recent advances in realistic microscopic theories have led to 4N calculations of the bound-state of ^{4}He [Car89, Fon89a] as well as for some polarization observables for the 4N scattering systems ^{2}H($\vec{d}$,d) and ^{2}H($\vec{d}$,p) [Fon89b]. However, compared to the 3N situation, the 4N calculations are still quite elementary due to the increased complexity of the 4N system.

One aspect of the 4N system that has received considerable attention is three-body breakup. In particular, the $\vec{d}+d \rightarrow d+p+n$ breakup process has been studied at a variety of energies for kinematic conditions favorable to *d-p* and *d-n* quasi-free scattering (QFS). From a theoretical perspective, this breakup reaction is an excellent candidate for studying the reaction dynamics of QFS in the 4N scattering system since it is essentially free of contamination from nucleon-nucleon final-state interactions [Val72]. In addition, to within the validity of the impulse-approximation, *d-p* and *d-n* QFS data should resemble *d-p* and

[1] Booz-Allen Hamilton, Inc., Huntsville, AL 35806
[2] Hosei University, Tokyo, Japan
[3] Georgetown University, Washington, DC
[4] University of Tübingen, Tübingen, FRG
[5] Lawrence Livermore National Laboratory. Livermore, CA
[6] Ruder Boskovic Institute, Zagreb, Yugoslavia
[*] Deceased

d-n elastic scattering. Insight into the role of the Coulomb force in 4N breakup reactions could be gained by comparison between *d-p* and *d-n* QFS data. Furthermore, the symmetry properties of the $\vec{d}+d \rightarrow d+p+n$ breakup reaction makes it ideal for studying charge-symmetry breaking (see section 2.4.3).

We have made measurements at TUNL of the vector and tensor analyzing powers A_y, A_{yy}, and A_{zz}, for *d-p* and *d-n* QFS in the $\vec{d}+d \rightarrow d+p+n$ breakup reaction. Although there exist cross-section data for deuteron-nucleon QFS in the *d+d* system [Val72, Fuk89], prior to the present work and the recent *d-p* QFS A_y measurements of Fukunaga *et al.* at 60 MeV [Fuk89], data for spin observables for this reaction did not exist. The present measurements were conducted using a 12-MeV tensor-polarized deuteron beam incident on a deuterium-filled gas cell. The momenta of two (*d-n*, *d-p*, or *p-n*) of the three outgoing particles were detected in coincidence, thereby completely defining the reaction kinematics. A list of the angle pairs measured in this work is shown in table 2.4-1. A portion of these data were used in a charge-symmetry breaking study (see section 2.4.3).

Table 2.4-1 Angle Pairs used in coincidence measurements. The + and - refer to left and right scattering respectively and the angle θ is lab scattering angle.

Deuteron-Proton		Deuteron-Neutron		Proton-Neutron	
θ_d (deg.)	θ_p (deg.)	θ_d (deg.)	θ_n (deg.)	θ_p (deg.)	θ_n (deg.)
±17.0	±17.0	±17.0	±17.0	±17.0	±17.0
±19.4	±19.4	±17.0	±34.5	±17.0	±34.5
		±19.4	±28.9	±19.4	±28.9
±10.0	±10.0				
±10.0	±41.2				
±17.0	±17.0				
±17.0	±34.5				
±34.5	±17.0				

Our data have been compared to three plane-wave impulse approximation PWIA calculations. Two of the calculations (P-ON and Y-ON) restricted the *d-N* vertices to be on the energy shell, while the other (Y-OFF) allowed the *d-N* vertices to go off the energy shell. All calculations were made using the computer codes NMPWIA and NMPWIAOFF, which were developed at TUNL. The *d-N* vertices were computed using the T matrices for *n-d* elastic scattering. The Coulomb force was neglected in the calculations. The matrix elements for the P-ON on-shell calculations, which were done with the code NMPWIA, were generated with Koike's 3N computer code [Koi86]. In this calculation the *n-d* T matrices were generated using the PEST NN potential, which is a separable form of the Paris potential. The NN partial waves included in the calculations were: $^1S_0$, $^3S_1$ - $^3D_1$, $^1P_1$, $^3P_{0,1,2}$, and $^3D_{2,3}$. The *n-d* T matrices for the Y-ON on-shell and Y-OFF off-shell calculations were computed by Fonseca [Fon90]. A Yamaguchi NN potential, which predicted a 5.5% D-state probability of the deuteron, was used to generate the T matrices for

the Y-ON and Y-OFF calculations. The NN partial waves included in these calculations were: $^1S_0$ and $^3S_1$ - $^3D_1$.

Comparisons of some of our data to the PWIA calculations are shown in figs. 2.4-8 and 2.4-9. The influence of P and D waves on A_y, A_{yy} and A_{zz} is shown in the comparison of the Y-ON and P-ON calculations. The importance of off-shell effects is demonstrated in the comparison of the Y-ON and Y-OFF calculations.

P.D. Felsher received his Ph.D. degree this year for his work on this project. A manuscript on our results is being prepared for publication.

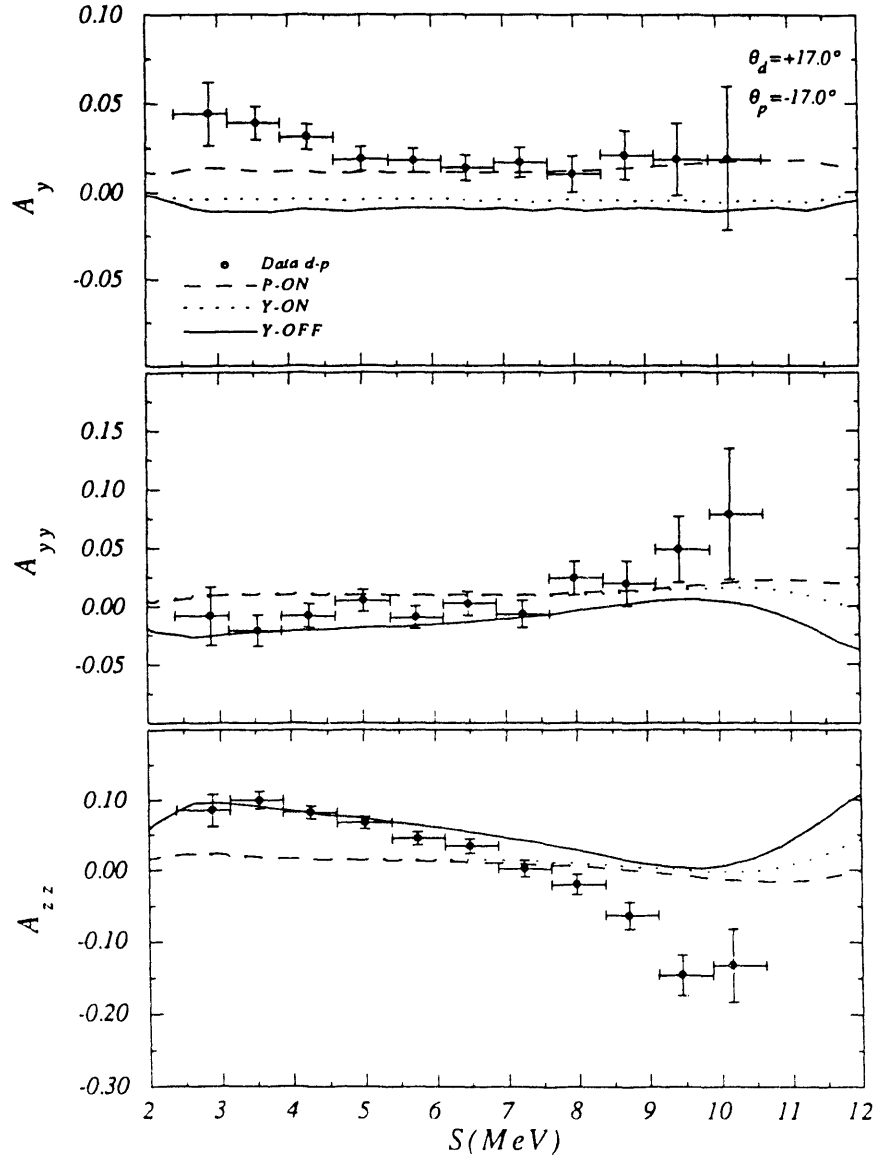

Fig. 2.4-8 Comparison of on-shell and off-sheli PWIA calculations to D($\vec{d}$,dp)n data with $(\theta_d,\theta_p) = (+17.0°, -17.0°)$. Details of the calculations are given in text.

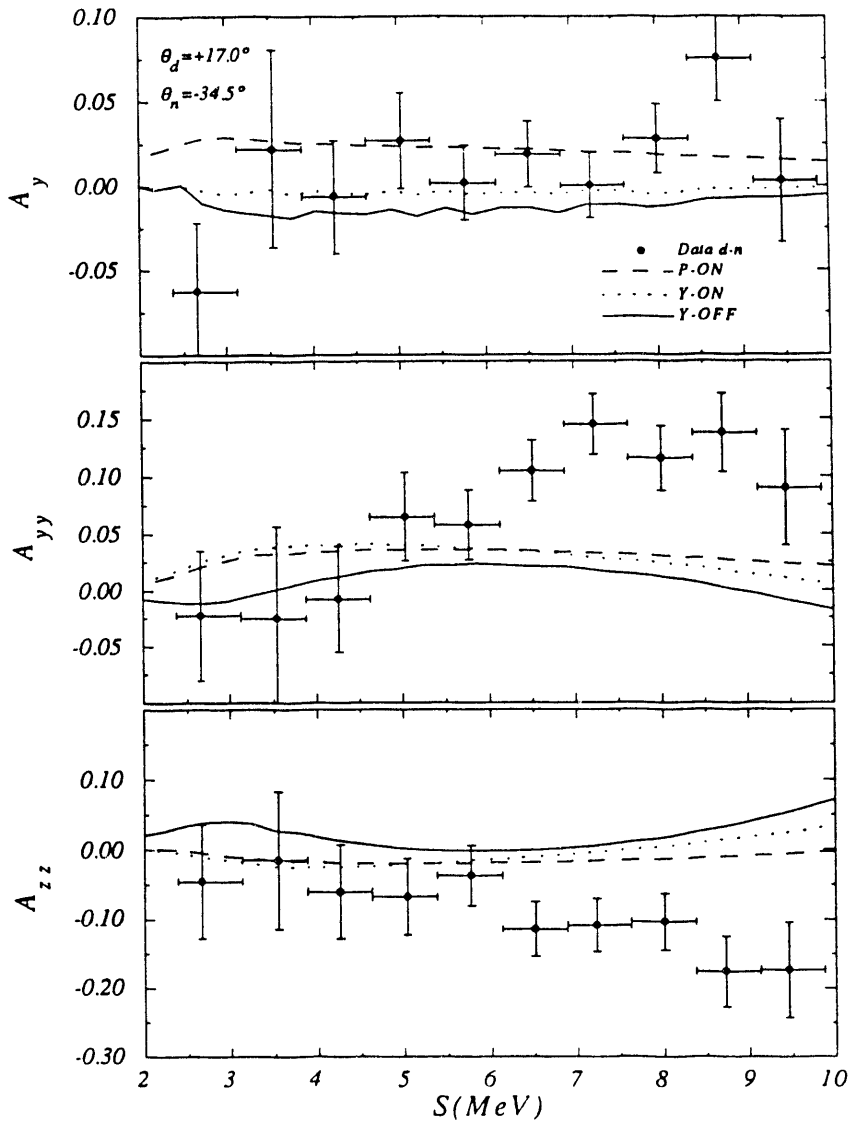

Fig. 2.4-9 Same as fig. 2.4-8, except for (θ_d,θ_n) = (+17.0°, –34.5°).

[Car89] J. Carlson, Proceedings of Few Body XII, Vancouver (1989)
[Fon89a] A.C. Fonseca, Phys. Rev. **C40** (1989) 1390
[Fon89b] A.C. Fonseca, Phys. Rev. Lett. **63** (1989) 2036
[Fon90] A.C. Fonseca, private communication 1990
[Fuk89] K. Fukunaga *et al.*, Few-Body Systems **7** (1989) 119
[Koi86] Y. Koike and Y. Taniguchi, Few Body Systems **1** (1986) 13
[Val72] V. Valkovic *et al.*, Nucl. Phys. **A183** (1972) 126, and references therein

3 DYNAMICS OF VERY LIGHT NUCLEI

This section on the dynamics of very light nuclei summarizes our progress of the past year in understanding how internucleon interactions are manifested in the structure of light nuclei. In particular, consequences of the nucleon-nucleon tensor interaction are the occurrence of D states in ^{3}H, ^{3}He, and ^{4}He. In nuclei above the nominally 1s shell, D states of relative motion may also arise from higher shell-model orbitals. It is therefore of interest to investigate how this interplay of tensor forces and higher-orbital effects evolves as the number of nucleons in the system increases.

All of the measurements summarized here have involved use of tensor-polarized deuterons produced by the TUNL Intense Polarized Ion Source (section 5.3). Thus, such devices are very important to our continuing program of studying internucleon dynamics in very light nuclei.

3.1 D(d,p)^{3}H and D(d,n)^{3}He Spin Observables at Very Low Energies

A.W. Ackley, R.K. Das, K. Fletcher, E.J. Ludwig, H.J. Karwowski, W.J. Thompson

There has been renewed interest in the D(d,p)^{3}H and D(d,n)^{3}He scattering states of the four-nucleon system in recent years, even though these reactions are among the earliest studied (see [Pae88] and references cited therein). Higher order partial waves contribute to these reactions even at very low energies. For example, recent differential cross-section measurements indicate that entrance channel P-waves and D-waves are important even at center of mass energies below 50 keV [Bro90]; this dramatically increases the number of non-vanishing matrix elements needed to describe the reactions, and, therefore, increases the number of observables needed for unambiguous determination of the matrix elements. A group from the Universität Köln has just published a set of the reaction matrix elements for these reactions below 500 keV, based on a fit to the available data [Lem90].

Using beams from the TUNL Intense Polarized Ion Source, we are measuring tensor analyzing powers for these reactions for deuteron energies below 100 keV at the Low Energy Beam Facility (LEBF). The protons, tritons, and ^{3}He nuclei produced in these high Q-value fusion reactions are detected in solid-state detectors. Carbon foils of appropriate thickness are placed in front of the detectors to stop elastically-scattered deuterons. Thin deuterated titanium films are used as targets. To circumvent the possibility that depletion of deuterium under bombardment might introduce errors into analyzing power measurements, a rapid state-changing mode is used in our data collection. Left, right, up, and down detectors are mounted in back of the scattering chamber at a scattering angle of 10° to monitor the beam polarization by the D(d,p) reaction. This monitor will be calibrated using the Lamb Shift Polarimeter, described in section 5.3.3.

Preliminary analyses of A_{zz} angular distributions at 60 keV and 80 keV are shown in fig. 3.1-1. The D(d,p) branch has twice as many data points as the D(d,n) branch because both reactants are detected for this case. In analyzing the data, the $A_{zz}(10°)$ of the uncalibrated monitor has been set to –0.951 for 80 keV and to –0.905 for 60 keV. These values were obtained from the ongoing R-matrix analysis of A=4 reactions by G. Hale at LANL

[Hal91]. Once the Lamb Shift Polarimeter is on-line and the LEBF monitor is calibrated, these data will be reanalyzed.

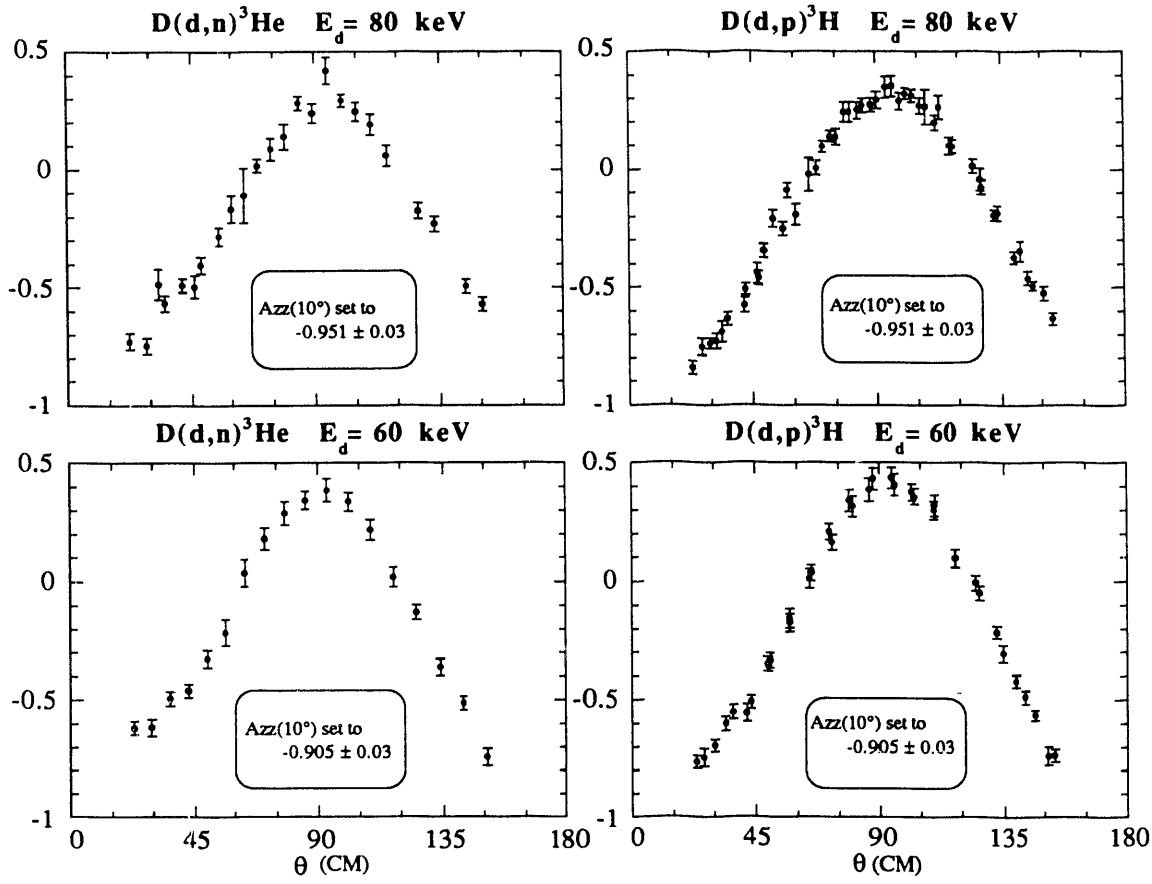

Fig. 3.1-1 Preliminary analyses of Azz(θ) data for the reactions $D(d,p)^3H$ and $D(d,n)^3He$ at 60 keV and 80 keV. For these plots, the analyzing power of the polarization monitor has been set to values obtained by the LANL R-matrix analysis of the A=4 system. This monitor will be independently calibrated.

Increasing the deuterium content of the targets is one of our on-going projects. At present, our procedure begins with floating 20 $\mu g/cm^2$ carbon films onto target rings and depositing a titanium film of desired thickness using an electron gun. The carbon backing provides extra mechanical support for the delicate film. The films are heated in vacuum to a temperature of 400°C, the chamber is then isolated from the pump and backfilled with deuterium gas. In bulk samples, it is possible to achieve concentrations approaching TiD_2 (see, for example, [McQ50]). To date, we have been unable to approach this ratio in a thin film. Tests are currently underway to improve the deuterium concentration by varying the film deposition and deuterating procedures.

[Bro90] R.E. Brown and N. Jarmie, Phys. Rev. **C41** (1990) 1391
[Hal91] G. Hale, private communication
[Lem90] S. Lemaître and H. Paetz gen. Schieck, Few-Body Systems **9** (1990) 155
[McQ50] A.D. McQuillan, Proc. R. Soc. London, Series A **204** (1950) 309
[Pae88] H. Paetz gen. Schieck, Few-Body Systems **5** (1988) 171

3.2 D-state Parameters for Light Nuclei using Transfer Reactions

One manifestation of the nucleon-nucleon tensor force in light nuclei is the presence of non-spherical components in the nuclear wave function, or D states. Effects of the D states of composite nuclei formed in transfer reactions show up strongly in tensor analyzing powers (TAP) measured using polarized deuteron beams. We are continuing our program to precisely determine parameters for ^{3}H, ^{3}He, and ^{4}He, such as the asymptotic D/S state ratios, η, and the related D_2 parameters, using TAP measurements in (d,t), (d,^{3}He), and (d,α) reactions.

3.2.1 Triton D-state Parameters by Transfer Reactions

T.B. Clegg, E.R. Crosson, R.K. Das, H.J. Karwowski, E.J. Ludwig, W.J. Thompson

Our program to establish the D-state component of light nuclei has proceeded with the analysis of sub-Coulomb (d,t) reactions in order to extract the triton asymptotic D/S ratio η_t. The incident energy has been chosen to be sufficiently below the Coulomb barrier that the reaction can be reliably analyzed using very few parameters. Such reactions have low cross sections, which necessitates the use of high-intensity polarized beams. However, there are experimental advantages to measuring these reactions at sub-Coulomb energies, since the largest effects in tensor analyzing powers from the D state occur at backward angles where cross sections are largest and background-producing elastic-scattering yields are smallest.

We have obtained angular distributions of $d\sigma/d\Omega$, A_{zz}, and A_{yy} for three nuclear reactions having different angular momentum transfers. They are summarized in table 3.2-1.

Table 3.2-1 Reactions investigated for sub-Coulomb measurements of triton D-state parameters.

Reaction	E_d	J^π	Q-value
^{95}Mo(d,t)^{94}Mo	7 MeV	5/2$^+$	-1.11 MeV
^{119}Sn(d,t)^{118}Sn	6 & 7 MeV	1/2$^+$	-0.23 MeV
^{149}Sm(d,t)^{148}Sm	8 MeV	7/2$^-$	0.38 MeV

The reactions were chosen using the following criteria:

1) The neutrons are transferred with $j = l + 1/2$, since this condition provides maximum triton D-state contribution [Bha88].

2) Only a single orbital angular momentum transfer is allowed in each reaction.

3) The Q-values of the reactions are near zero in order to have adequate overlap of the deuteron and triton sub-Coulomb trajectories.

4) The spectroscopic factors should be large in order to maximize the triton yield at these bombarding energies.

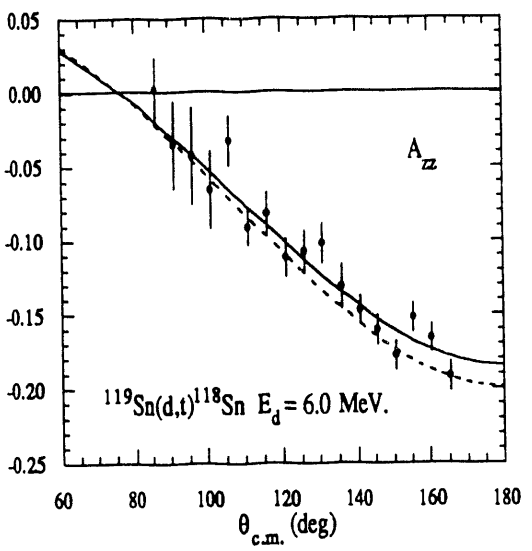

Fig. 3.2-1 Angular distribution of $A_{zz}(\theta)$ for the ^{119}Sn(d,t)^{118}Sn at E_d = 6 MeV. The solid curves result from an exact, finite-range DWBA analysis using best fit η_t = –0.44, while the dashed curves result from η_t = –0.46.

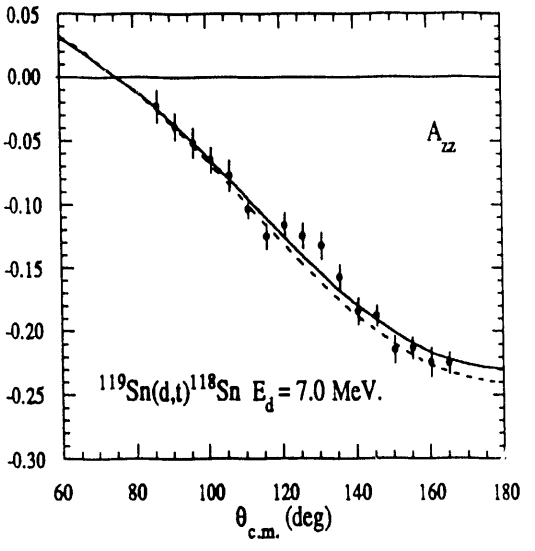

Fig. 3.2-2 Angular distribution of $A_{zz}(\theta)$ for the ^{119}Sn(d,t)^{118}Sn at E_d = 7 MeV. The solid curves result from an exact, finite-range DWBA analysis using best-fit η_t = –0.42, while the dashed curves result from η_t = –0.46.

Using the TUNL Intense Polarized Ion Source, data were taken at $85^o \leq \theta_{lab} \leq 165^o$ where analyzing powers exhibit considerable sensitivity to the presence of a D-state component. Figures 3.2-1 and 3.2-2 show preliminary data in comparison with finite-range DWBA predictions incorporating best fits to the data (solid curves) at 6 and 7 MeV and a theoretical prediction [Fri88] using η_t = –0.46 (dashed curve). The calculations for this transition are insensitive to the choice of optical model parameters (OMP), and interaction potentials for both the heavy and light systems. An analysis incorporating a tensor potential for the entrance channel and two-step amplitudes has begun in order to establish a relatively parameter-free value for η_t, with smaller uncertainties than previous determinations [Vua89]. Moreover, by using a variational method, d+n amplitudes have been generated

by Schiavilla *et al.* in momentum space [Sch86]. Fourier transforms of these functions will be obtained to provide wave functions in coordinate space. The incorporation of these functions will provide stringent tests of the Urbana and Argonne effective nucleon-nucleon interactions.

3.2.2 The d-d Configuration in ^{4}He from (d,α) Reactions

T.B. Clegg, E.R. Crosson, R.K. Das, H.J. Karwowski, S.K. Lemieux, E.J. Ludwig, W J. Thompson, A.M. Eiro[1], F.D. Santos[1]

Previous experiments leading to the extraction of the D-state parameters for ^{4}He using the (d,α) reaction have been complicated by an uncertainty in the mixture of L values contributing to the reaction. This has resulted in a wide range of extracted D_2 values (-0.31 fm^2 < D_2 < -0.08 fm^2). Improved determinations are needed to test four-body calculations of the ^{4}He ground state which are becoming available. At present, variational calculations generated by a realistic Hamiltonian which includes a three-nucleon interaction, suggest that D_2 for ^{4}He is very sensitive to the short-range tensor part of the N-N interaction [Eir90].

We are continuing our investigations of (d,α) reactions populating stretched states which involve a unique L transfer. Reactions investigated include ^{58}Ni(d,α)^{56}Co at 12, 16, and 22 MeV, ^{50}Ti(d,α)^{48}Sc at 16 MeV and ^{48}Ti(d,α)^{46}Sc at 22 MeV. Each of the residual nuclei have states characterized by $J^\pi = 7^+$, and these are states which are populated by a unique L=6 transfer. Angular distributions of $d\sigma/d\Omega$, A_y, A_{yy}, and A_{xx}, obtained at forward angles, are compared to exact finite-range DWBA calculations incorporating the realistic $<$d,dl α$>$ overlap functions of Schiavilla *et al.* [Sch86].

Optical-model potential parameters have been obtained from the global parameter set of Daehnick *et al.* [Dae80] for the deuteron and from an analysis of ^{59}Co(α,α)^{59}Co and ^{58}Ni(α,α)^{58}Ni at 24 MeV and ^{48}Ti(α,α)^{48}Ti for the alpha particle. The results of calculations for the lowest $J^\pi = 7^+$ state excited in the ^{58}Ni(d,α)^{56}Co reaction at 22 MeV including the Argonne (AV14) and Urbana (UV14) interactions are shown in fig. 3.2-3 by the solid and dashed curves, respectively, along with a calculation which includes no D-state component (dotted curve). Similar comparisons are presented in fig. 3.2-4 for the ^{50}Ti(d,α)^{48}Sc data measured at 16 MeV.

There is a possibility that transitions to 7^+ states take place by two-step processes such as (d,t) (t,α) and (d,^{3}He) (^{3}He,α). An exact evaluation of these components is impossible, since there do not exist stable targets that would allow the necessary cross sections to be measured. Calculations based on published spectroscopic factors have been made, however, assuming maximum estimates for two-step amplitudes. These indicate that the maximum (d,t) (t,α) cross section is about 2% of the maximum measured cross section, while the maximum (d,^{3}He) (^{3}He,α) cross section is 5% of this value. When these amplitudes were combined with the direct amplitude the resulting predictions for A_{xx} exhibited only small variations from the predictions shown in fig. 3.2-3.

---

[1] University of Lisbon, Portugal.

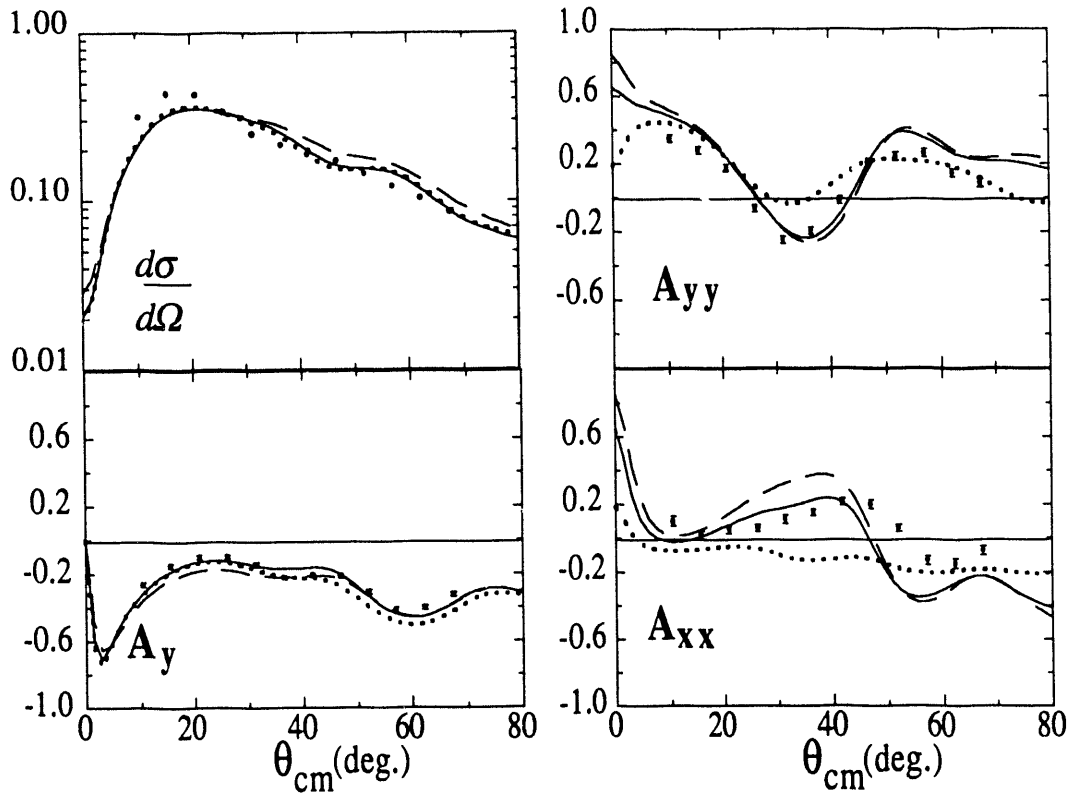

Fig. 3.2-3 Angular distributions of the cross section (arbitrarily normalized), A_y, A_{xx} and A_{yy} at 22-MeV deuteron energy for ^{58}Ni(d,α)^{56}Co to the lowest 7$^+$ state in ^{56}Co. Solid curves are predictions for AV14, dashed curves are for UV14, and dotted curve for the inclusion of an S state of d - d relative motion only.

Our analyses show that A_{xx} is especially sensitive to the presence of a D-state component and, in fact, quite sensitive to the form of the interaction. Moreover, A_{xx} appears to be insensitive to inclusion of a two-step amplitude (even an unrealistically large amplitude) and to the choice of optical-model-potential parameters. The quantity A_{xx} will be an important observable in (d,α) reactions at higher energies where high-momentum components in the alpha-particle wave function can be probed and compared to results from electron-scattering experiments.

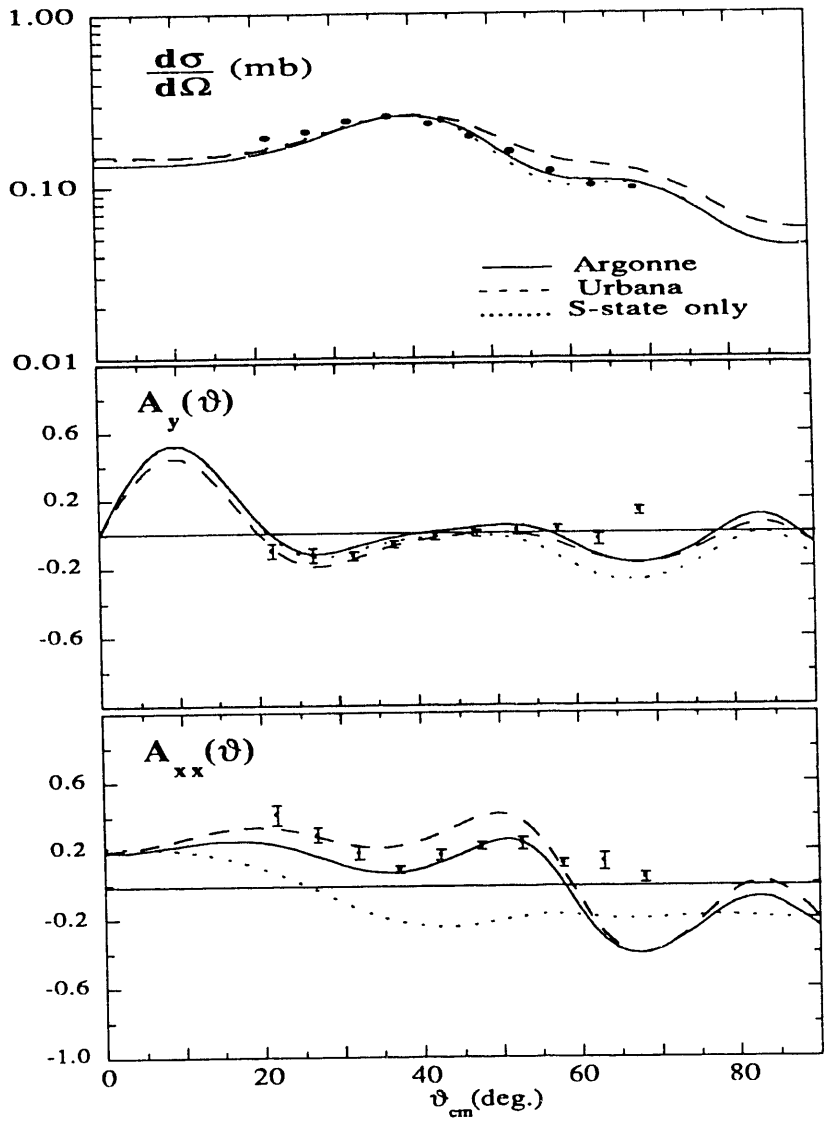

Fig. 3.2-4 Angular distributions of the cross section (arbitrarily normalized), A_y and A_{xx} at 16-MeV deuteron energy for ^{50}Ti$(d,\alpha)^{48}$Sc to the lowest 7^+ state in ^{48}Sc. The solid curves are predictions for AV14, dashed curves for UV14, and dotted curve for the S state of d - d relative motion only.

[Bha88] C.M. Bhat *et al.*, Phys. Rev. **C38** (1988) 1537

[Dae80] W.W. Daehnick *et al.*, Phys. Rev. **C21** (1980) 2253

[Eir90] A.M. Eiro and F.D. Santos, Jour. of Phys. **G16** (1990) 1139

[Fri88] J.L. Friar *et al.*, Phys. Rev. **C37** (1988) 2859

[Sch86] R. Schiavilla, V.R. Pandharipande and R.B. Wiringa, Nucl. Phys. **A449** (1986) 219

[Vua89] B. Vuaridel *et al.*, Nucl. Phys. **A499** (1989) 429

3.3 Analyzing Powers in $^2H(d,\gamma)^4He$ at Low Energies and the D-State of ^4He

L.H. Kramer, M.J. Balbes, R.M. Chasteler, M.A. Godwin, E. Hayward, R.M. Prior, G. Schmid, D.R. Tilley, H.R. Weller, J.Z. Williams

The low energy $^2H(d,\gamma)^4He$ cross section has been shown to be much larger than that predicted if the reaction proceeds by E2 capture from the $^1D_2$ scattering state to the $^1S_0$ component of the ^4He ground state [Wel88]. The larger cross section is thought to come from $^5S_2(E2)$ capture to the $^5D_0$ component of the ^4He ground state, since this eliminates the centrifugal barrier. If capture proceeds purely through s-wave capture to the D-state, then the analyzing powers A_y and A_{yy} are isotropic with values of 0.0 and 0.25, respectively.

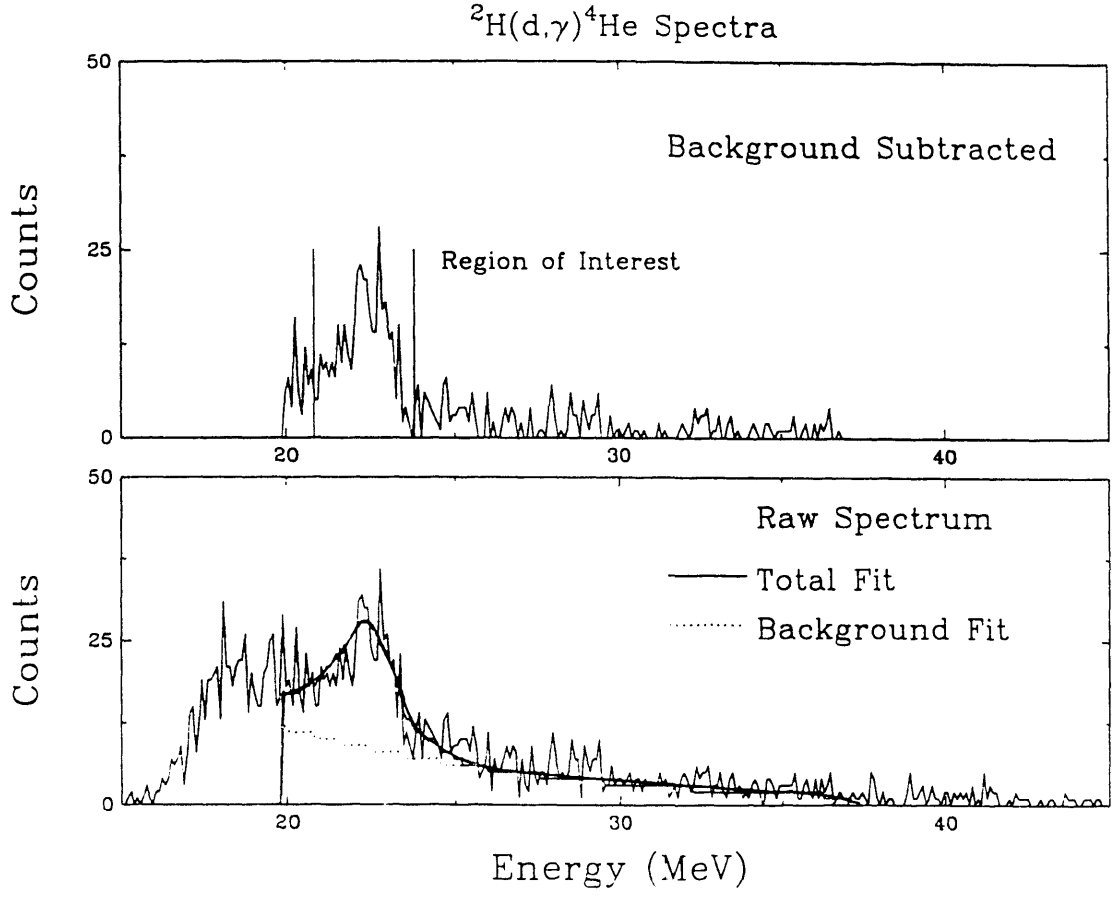

Fig. 3.3-1 γ-ray spectrum from the $^2H(\vec{d},\gamma)^4He$ reaction at $E_d(lab) = 80$ keV and $\theta(lab) = 0°$. Spectrum is the result of 2 1/2 days of beamtime. The lower frame is the raw spectrum with a fit which includes a lineshape and a background function; both the total fit and the background are shown. The upper frame is the raw spectrum with the background subtracted, and the region of interest is highlighted.

We have begun a program to investigate the $^2H(\vec{d},\gamma)^4He$ reaction at very low energies through measurement of the vector and tensor analyzing powers. A new low energy radiative-capture experimental facility, designed to utilize the maximum beam from the TUNL Intense Polarized Ion Source, has been constructed at the 60° port of the polarized ion source analyzing magnet. The experimental setup consists of a short beamline with a deuterated-titanium foil mounted at the end. An anticoincidence-shielded 10" x 10" NaI detector is used to detect γ-rays and a solid-state detector is used to monitor target thickness. The source has delivered polarized beam currents of 25 - 45 μA on-target and γ-rays were detected at the rate of 5-10 counts/hr.

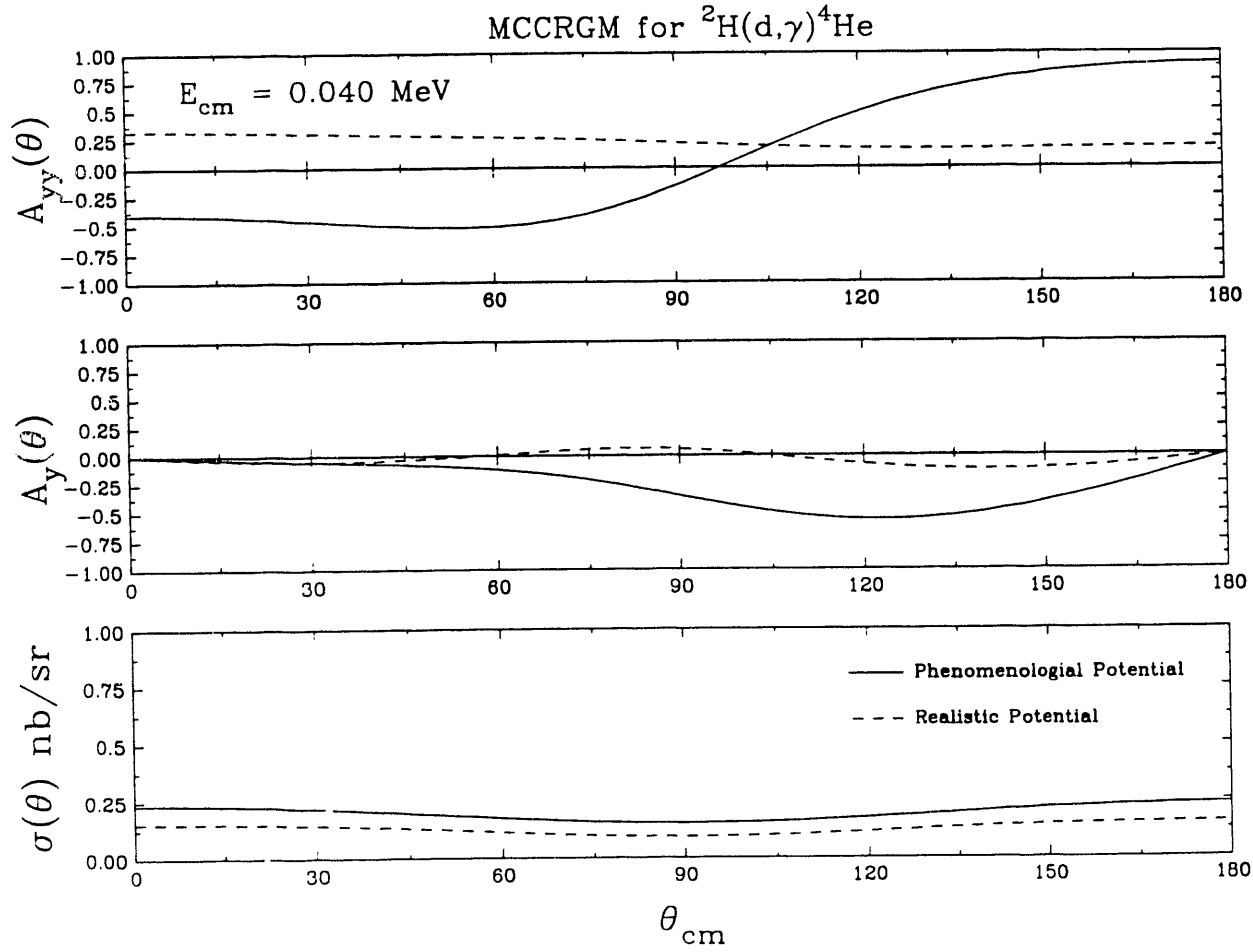

Fig. 3.3-2 Microscopic coupled-channel resonating group model calculation results for E_d(lab) = 80 keV. The solid line represents a Realistic potential and the dashed line represents a Phenomenological potential. Both potentials are explained in the text.

We have measured the analyzing powers, A_y and A_{yy}, for the reaction at E_d(lab) = 80 keV and θ(lab) = 0°, 45°, and 82°. A sample spectra from the 0° measurements is shown in fig. 3.3-1. Precisely tuned electronics providing 99.8% cosmic-ray rejection, along with pulse-shape discrimination electronics, were crucial in producing this spectrum. Data analysis is underway and should be completed by early fall 1991. At θ(lab) = 0°, we have extracted a preliminary result for the analyzing powers and find $A_y = 0.001 \pm 0.140$ and $A_{yy} = -0.419 \pm 0.085$, indicating that the reaction does not proceed purely by s-wave capture to the D-state.

A recent microscopic coupled-channel resonating-group-model calculation has been obtained from Hofmann *et al.* at Erlangen [Wac88] and will be used for comparison. Two potentials were used in this calculation. One, the Realistic (Bonn) potential, is dominated by s-wave capture to the D-state and predicts some E1 and M2 p-wave capture (about 12% and 8%, respectively). The other potential, the Phenomenological potential, has a much greater percentage of E1 and M2 p-wave, about 30% each. Results from these calculations are shown in fig. 3.3-2. If the preliminary results for 0° are plotted, one sees that there is good agreement with the Phenomenological potential, indicating that there may be large E1 and/or M2 p-wave contributions. Once data analysis has been completed, we will perform a transition-matrix element analysis to deduce the p-wave strength in the reaction directly from the $\sigma(\theta)$, $A_y(\theta)$, and $A_{yy}(\theta)$ data.

A second anticoincidence-shielded NaI detector and in-line polarimeter have been added to the setup and further measurements are scheduled for late summer and early fall 1991. Present plans include measurement of T_{20} at E_d(lab) = 80 keV and an extension of the measurements to lower energies. A calculation of $^2H(d,\gamma)^4He$ at low energies ($E_{cm} < 500$ keV) by Arriaga *et al.* [Arr91] using a variational Monte Carlo method has recently been completed. An attempt is being made to extend the calculation to our energies. We hope to be able to compare our results with this calculation to further our understanding of the $^2H(d,\gamma)^4He$ reaction as we approach the energy region of astrophysical relevance.

[Arr91] A. Arriaga, V.R. Pandharipande, R. Schiavilla, Phys. Rev. **C43** (1991) 983 and private communication

[Wac88] B. Wachter, T. Mertelmeier and H.M. Hofmann, Phys. Lett. **B200** (1988) 246 and private communication

[Wel88] H.R. Weller and D.R. Lehman, Ann. Rev. Nucl. Part. Sci. **38** (1988), 563

3.4 Radiative Capture of Polarized Deuterons by ^{3}He

M.J. Balbes, R. Chasteler, L.H. Kramer, M.A. Godwin, G. Schmid, D.R. Tilley, H.R. Weller, J.Z. Williams

The tensor analyzing power $T_{20}(\theta)$ of the $^3He(d,\gamma)^5Li$ reaction has been measured at 6 angles (θ_{lab} = 30°, 50°, 70°, 90°, 120°, and 150°) with a deuteron-beam energy integrated from 0-800 keV using the Intense Polarized Ion Source (IPIS) at TUNL. The rf power to the Strong Field 2 (SF2) cavity of the IPIS was turned on and off to alternate the beam between the polarized and unpolarized modes. The spherical tensor moments of the beam

were measured in the new polarimeter [TUNL90a], and the polarization was found to be 57% of the theoretical maximum. This low polarization was due to instabilities in the source which have subsequently been corrected. The cross section for a pure t_{20} beam can be expressed as $\sigma_p(\theta)= \sigma_u(\theta)[1+t_{20}T_{20}(\theta)]$. By measuring $\sigma_p(\theta)$ and $\sigma_u(\theta)$ in our NaI spectrometers, and t_{20} in our polarimeter, we can calculate $T_{20}(\theta)$ using the above relation. Figure 3.4-1 shows all data taken in this energy region, including the new $T_{20}(\theta)$ data.

Table 3.4-1 Transition Matrix Element (TME) simultaneous fit to the measured observables, $\sigma(\theta)$, $A_y(\theta)$, $A_{yy}(\theta)$, and $T_{20}(\theta)$ yields two solutions of equal statistical validity. The percentage contribution of each incident partial wave to the total cross section is quoted in the table. In both solutions E1 radiation dominates the reaction. However, both solutions have a non-negligible M1 contribution. Solution 1 reflects the original prediction of dominant $^4s_{3/2}$(E1) capture due to the $J^\pi = 3/2^+$ fusion resonance at this energy.

	Solution 1	Solution 2
% $^2s_{1/2}$(E1)	3.1 ± 2.8	47.9 ± 5.5
% $^4s_{3/2}$(E1)	89.3 ± 2.7	43.9 ± 4.9
% ^{2}p(M1)	0.7 ±0.6	1.2 ± 0.7
% ^{4}p(M1)	6.9 ± 1.6	7.1 ± 1.6

We expect that at this low energy, s-wave-capture contributions to the cross section will dominate. Also, the $3/2^+$ fusion resonance, lying just above the d+^{3}He threshold, is expected to make the $^4s_{3/2}$ partial wave contribution (where the notation is $^{2S+1}\ell_J$) dominate over the $^2s_{1/2}$-partial-wave contribution. Measurements of the vector and tensor analyzing powers, $A_y(\theta)$ and $A_{yy}(\theta)$, discussed previously [TUNL89], have left an ambiguity in the fitting of transition matrix elements to the data. Unfortunately, this ambiguity was not resolved by the inclusion of $T_{20}(\theta)$ in the fit. The two indistinguishable solutions are shown in figure 3.4-1 and summarized in table 3.4-1.

The observables $\sigma_u(\theta)$, $A_y(\theta)$, and $A_{yy}(\theta)$ have also been measured for a beam which entered the target with E_d = 600 keV and exited with 300 keV. The results of a preliminary analysis of the data (fig. 3.4-2) are consistent with the above measurement, although a detailed analysis and final results are not yet available.

We have continued to improve our calculations of capture observables by using the Resonating Group Model (RGM). This model uses the cluster description of nuclei and the variational principle to calculate dynamical quantities such as phase shifts and absolute cross sections, using Gaussian functions as the basis set. Clusters are represented as sums of Gaussians. For example, the deuteron can be represented with two Gaussians whose separation has been set according to the best reproduction of known observables. The

alpha particle, being much more tightly bound, can be represented by one Gaussian, although more may be used for a more complete calculation. The distance between clusters and the relative size of the clusters are calculated in the RGM code using the variational principle, but the strength of the spin-orbit and tensor force must be set by the user.

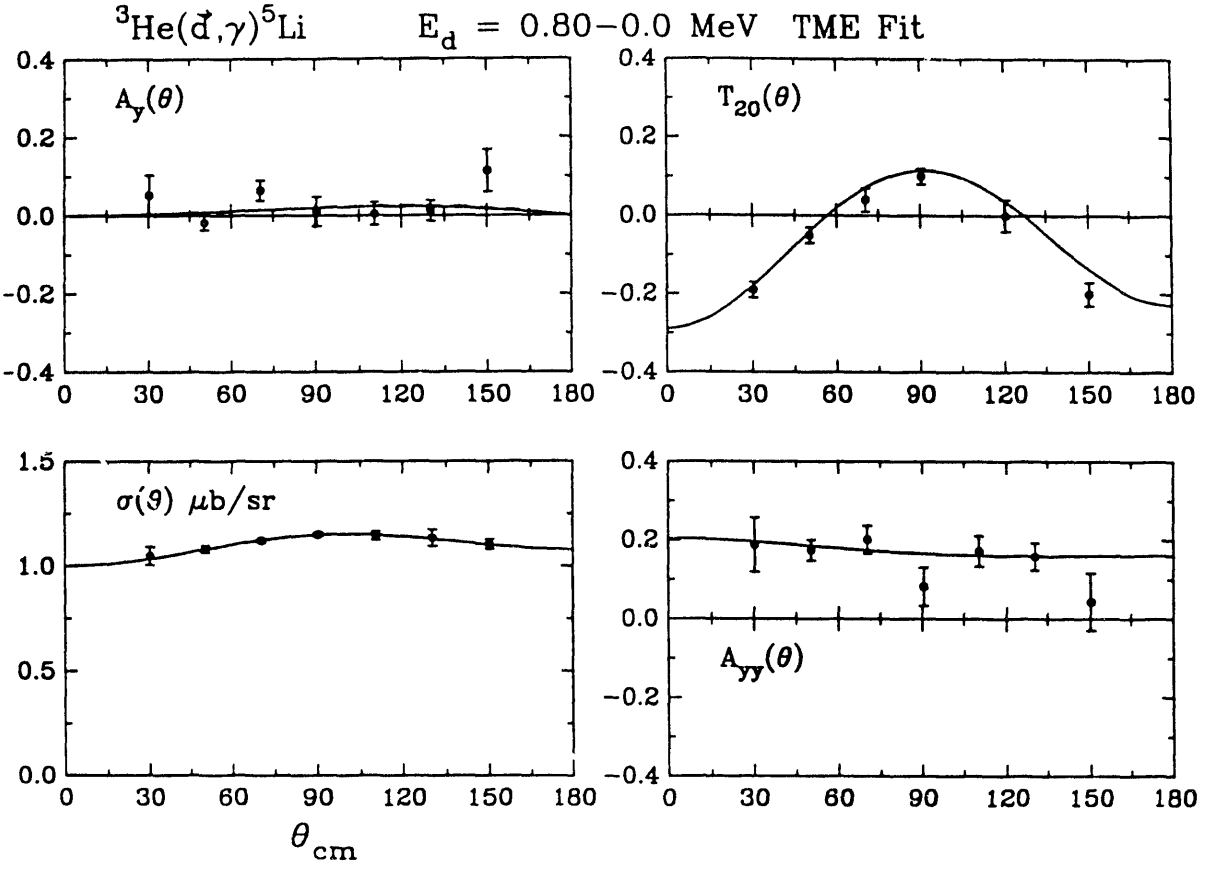

Fig. 3.4-1 The two indistinguishable fits corresponding to table 3.4-1.

For calculating the ^{3}He(d,γ)^{5}Li matrix elements, three channels were used: [p+^{4}He]$^{S=1/2}$, [d+^{3}He]$^{S=1/2}$, and [d+^{3}He]$^{S=3/2}$. The ground state wave function was found to consist of about 99% [p+^{4}He]$^{1/2}$, 14% [d+^{3}He]$^{1/2}$, and <1% [d+^{3}He]$^{3/2}$. Since the first two configurations have the same spin, they are not orthogonal states and therefore the percentages can add to greater than 100%. The current calculations have been improved over previously reported calculations [TUNL90b] by finding better values for the strengths of the spin-orbit and tensor forces. This is accomplished by adjusting the two-body values of these forces so as to reproduce existing ^{4}He(p,p)^{4}He phase shifts in the energy range of interest.

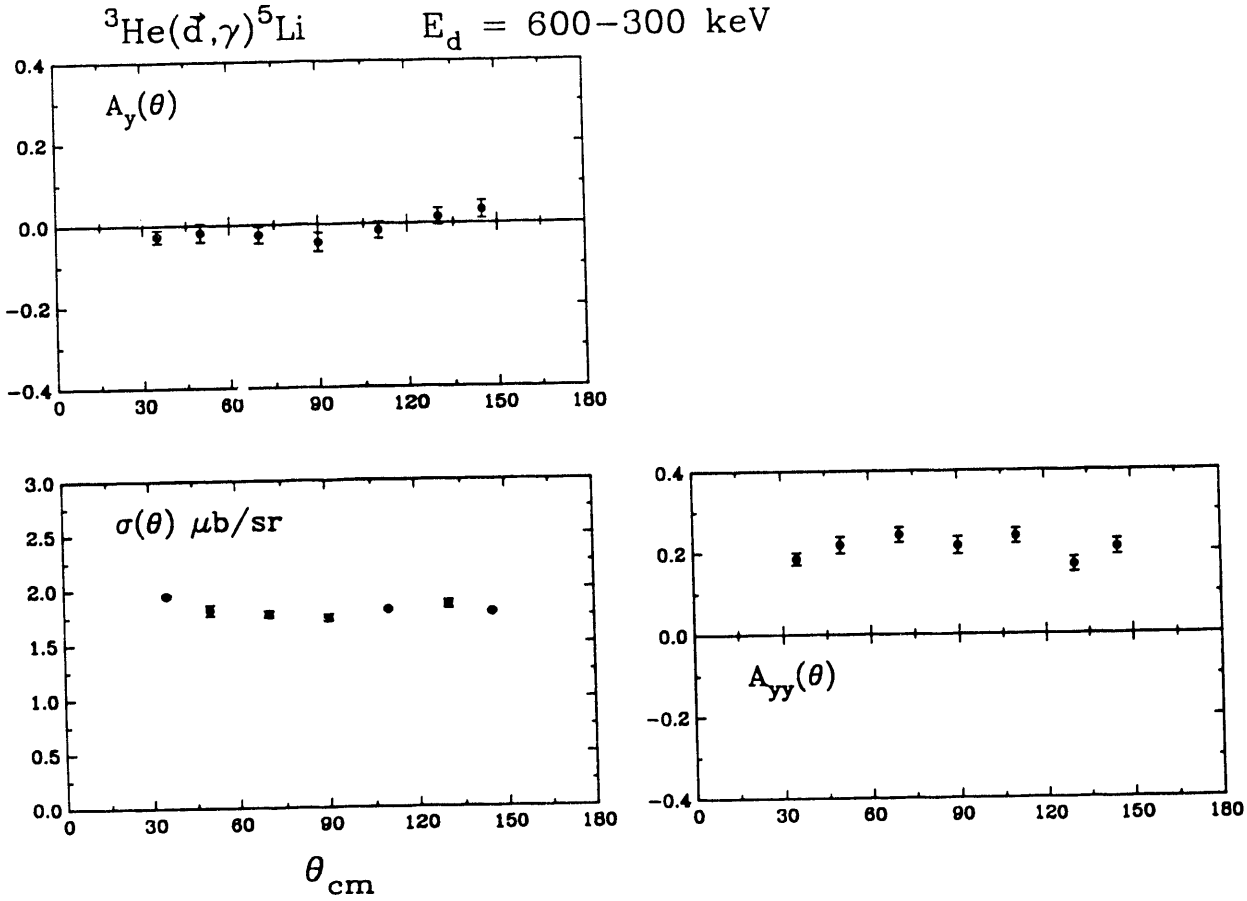

Fig. 3.4-2 The results of a preliminary analysis for a 600-keV beam which loses 300 keV in the target.

Transition matrix elements of the form $< \Psi_{g.s} \mid EM \mid \Psi_{sc} >$, denoted by their continuum state quantum numbers in the notation $^{2S+1}\ell_J$, were also calculated at the $3/2^+$ fusion resonance and at E_d = 8.6 MeV. At the fusion resonance, the $^4s_{3/2}$ (E1) transition matrix element was found to dominate the photonuclear cross section. The incident $^2s_{1/2}$ partial wave can couple directly to the p-α scattering channel, giving the S=1/2 state in the resonance a very short lifetime and consequently a large width that spreads the $^2s_{1/2}$ (E1) strength over all energies. For this reason it contributes < 1% of the strength of the photonuclear cross section. The tensor force, and to a lesser degree the spin-orbit force, is important because it couples the $[d+^3He]^{S=3/2}$ incoming channel to the $[p+^4He]^{S=1/2}$ channel, allowing the photonuclear transition to the S=1/2 ground state to proceed by the dominant ΔS=0 term of the E1 operator. Figure 3.4-3 compares the calculation with the measured observables.

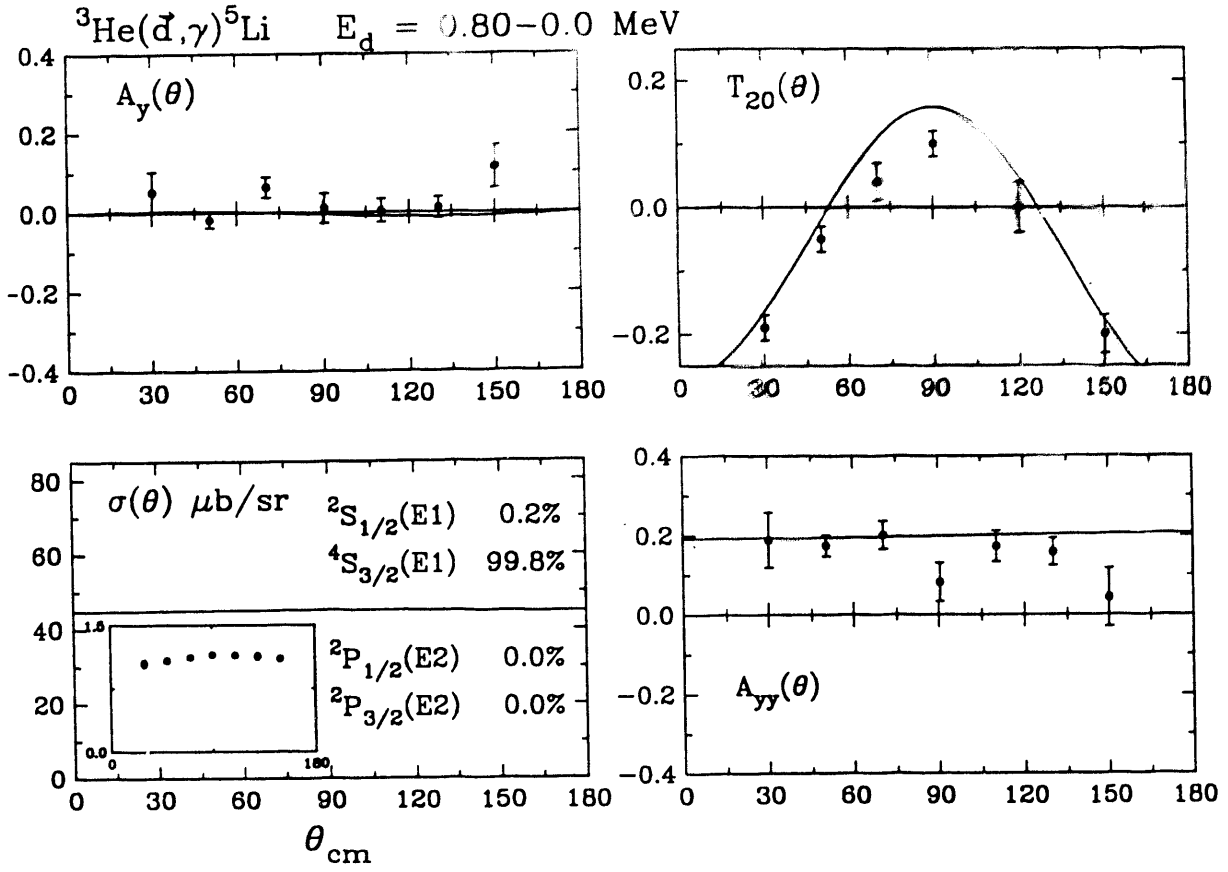

Fig. 3.4-3 Results of the RGM calculation at the $3/2^+$ fusion resonance.

At E_d = 8.6 MeV, the $^4s_{3/2}$ (E1) transition matrix element contributes only 45% of the cross section while 22% comes from the $^2d_{5/2}$ (E1) TME and 6% from the $^2p_{3/2}$ (E2) TME. No significant contribution is made by M1 radiation. Figure 3.4-4 compares the calculated and measured observables. Note that, although the curves do not reproduce the data well, the fractional strengths are in fair agreement with the results of the TME analysis. By reducing the distance between the α-p clusters, the calculation can be made to reproduce the data almost exactly. However, this causes the binding energy to be off by as much as 4 MeV.

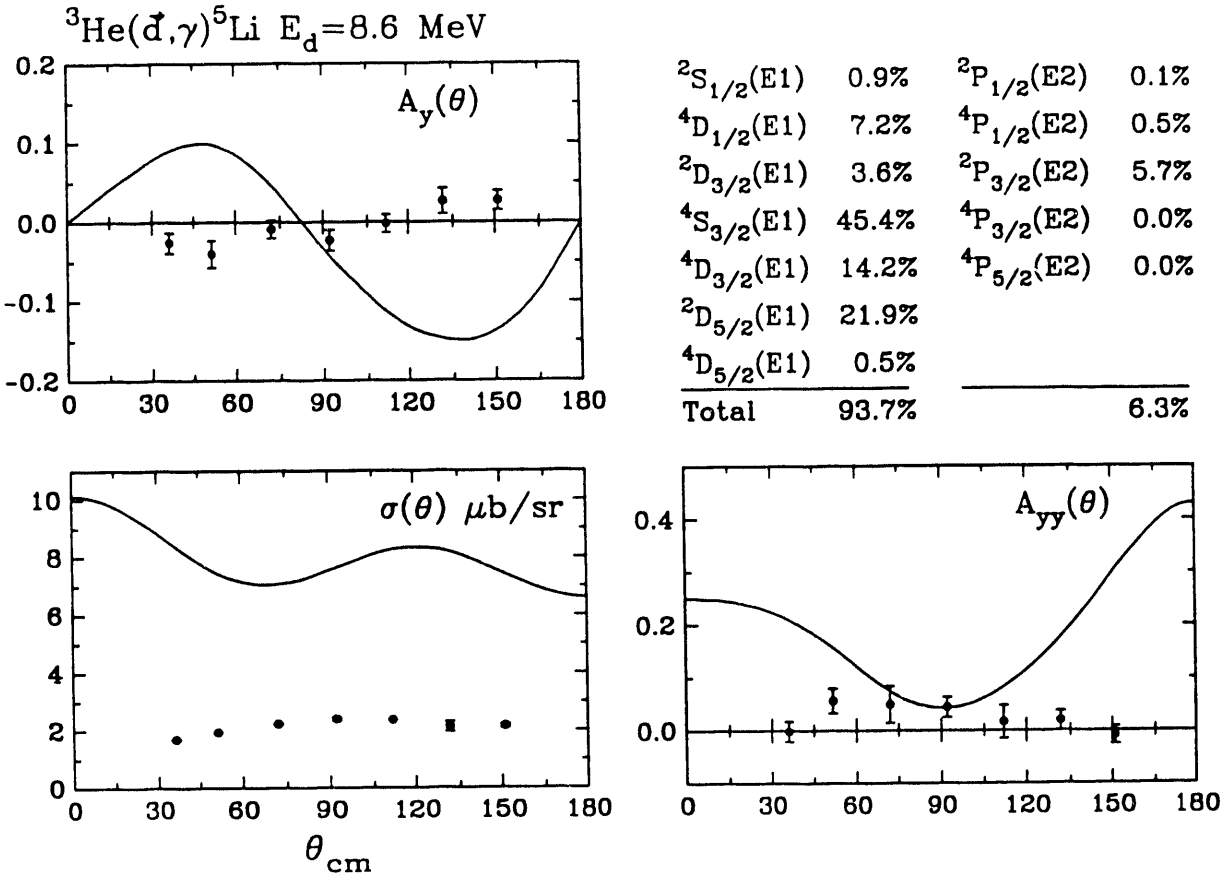

Fig. 3.4-4 Results of the RGM calculation at 8.6 MeV. The percentages give the strength of the corresponding Transition Matrix Elements in the cross section.

[TUN90a] TUNL Annual Report (1989/90) A Polarimeter for Tensor Polarized Deuteron Beams

[TUN90b] TUNL Annual Report (1989/90) Capture Observables and the Resonating Group Model

[TUN89] TUNL Annual Report (1988/89) pp. 60-62

3.5 The ^{6}Li(d,γ) Be Reaction and the D State of ^{8}Be

J.Z. Williams, M.J. Balbes, R.M. Chasteler, G. Feldman, M. Godwin, L.H. Kramer, G. Schmid, D.R. Tilley, H.R. Weller

The study of the D-state of ^{8}Be through the reaction ^{6}Li(d,γ) ^{8}Be with tensor-polarized deuterons was continued this past year with new measurements and improvements in theoretical calculations. The new data which were obtained include polarized-beam data at 9.0 MeV and at 2.0 MeV.

The data at 9.0 MeV include new measurements of the tensor analyzing power, $T_{20}(\theta)$, over the angular range of 50° to 135°. The addition of the $T_{20}(\theta)$ data allows for a more complete transition matrix element (TME) analysis to be performed. Without this measurement, the data were not sensitive to s-wave capture and prior TME analyses did not include this amplitude. The TMEs included in the present analysis and their values are given in table 3.5-1, and the results are shown in fig. 3.5-1. The current analysis results in two solutions with similar χ^2 (≈4.5). Both solutions yield approximately the same $^1d_2$ strength (72%). The main differences between the two solutions are the amount of spin-flip $^3p_1$(E1) strength needed in each fit (≈11% for fit 1 and ≈3% for fit 2) and the relative amount of s=2 capture strength (≈7% for fit 1 and ≈15.5% for fit 2). This s=2 strength is contained in different amplitudes for each solution. From the fits we see that both solutions have similar angular dependence except at the extreme angles in $A_{yy}(\theta)$ and $T_{20}(\theta)$. The present data set makes it impossible to choose one of the solutions over the other.

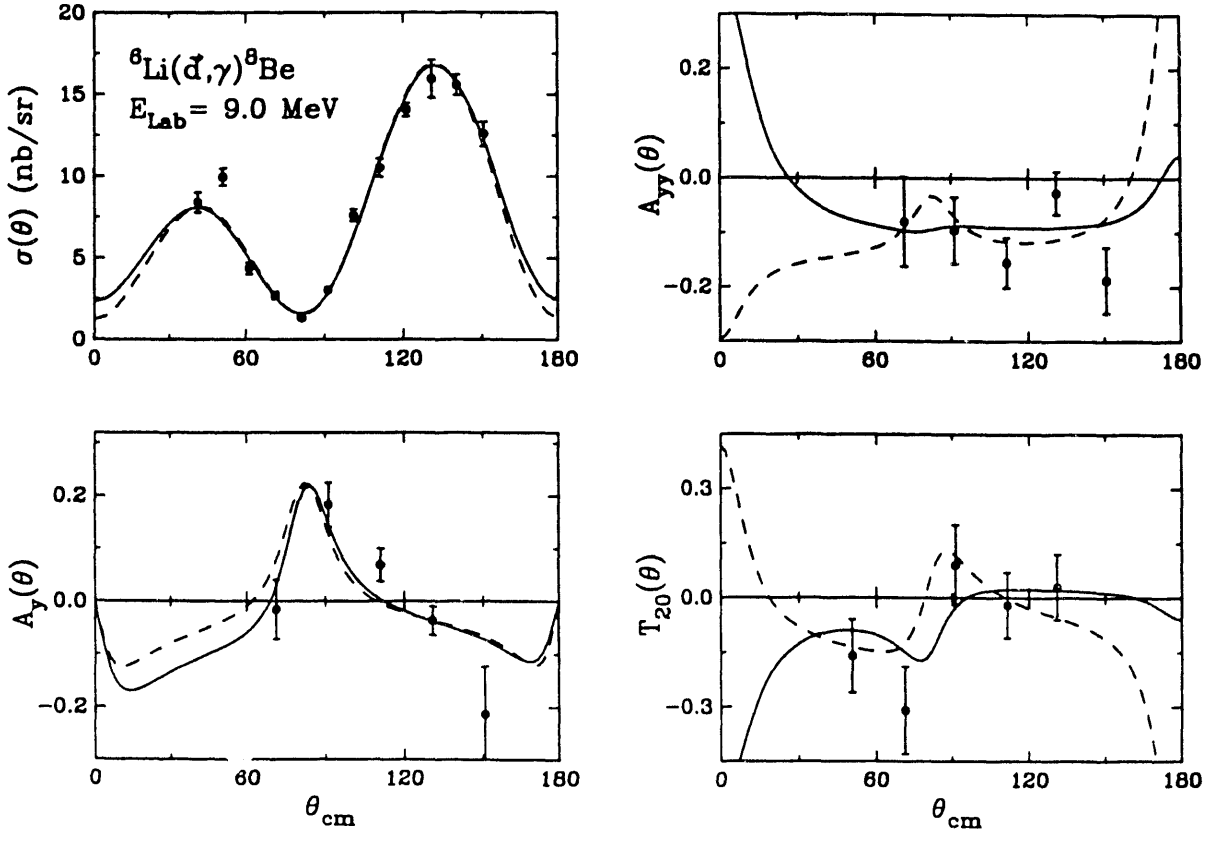

Fig. 3.5-1 Angular distributions of the data at $E_{d(lab)}$ = 9.0 MeV plotted in the center-of-mass frame. The solid curve represents Fit 1 and the dashed curve represents Fit 2, which were both obtained by simultaneously fitting the selected transition matrix elements to the data. Error bars represent statistical uncertainties associated with the data.

Table 3.5-1 The contributions to the cross-section from the transition matrix elements (TME) obtained from the the TME fits, calculated by the Direct-Capture model, and calculated from the MCRGM at 9.0 MeV.

	Fit 1	Fit 2	Direct-Capture	MCRGM
$^1d_2$(E2)	0.722 ± 0.022	0.717 ± 0.024	0.993	0.827
$^5s_2$(E2)	0.065 ± 0.021	0.023 ± 0.018	0.003	0.037
$^5d_2$(E2)	0.004 ± 0.003	0.132 ± 0.034	0.004	0.003
$^3d_2$(E2)	——	——	——	0.004
$^1p_1$(E1)	0.103 ± 0.014	0.094 ± 0.010	——	0.119
$^3p_1$(E1)	0.106 ± 0.036	0.034 ± 0.016	0.00	0.001
$^5p_1$(E1)	——	——	——	0.009

Polarized-beam measurements have also been recently made at 2.0 MeV. These measurements include the tensor analyzing power, $A_{yy}(\theta)$, and the vector analyzing power, $A_y(\theta)$, at θ_{Lab}= 45°, 90°, and 140°. A TME analysis with the same amplitudes as in the 9.0 MeV analysis has been performed. The results of this analysis are given in table 3.5-2 and fig. 3.5-2. This TME analysis shows that the cross section is dominated not by E2 radiation as expected, but by E1 radiation (≈80%). In addition, the results of the analysis do not indicate the presence of any s-wave capture, which was expected to be enhanced at lower beam energies as a result of angular momentum barrier considerations.

Table 3.5-2 The contributions to the cross-section from the transition matrix elements (TME) obtained from the the TME fit and from the MCRGM at 2.0 MeV.

	Fit	MCRGM
$^1d_2$(E2)	0.147 ± 0.033	0.239
$^5s_2$(E2)	——	0.061
$^5d_2$(E2)	0.041 ± 0.071	0.001
$^3d_2$(E2)	——	0.001
$^1p_1$(E1)	0.363 ± 0.049	0.681
$^3p_1$(E1)	0.449 ± 0.076	0.014
$^5p_1$(E1)	——	0.002

The results of a direct-capture calculation are shown in fig. 3.5-3 and are summarized in table 3.5-1. The amount of D-state between the two point particles is proportional to the predicted value of A_{yy}. A D-state admixture of 3.0% was found to give the best fit to the data. It must be noted, however, that this is only the probability of having L=2 for the relative motion of the ^{6}Li cluster and the deuteron in the ground state of ^{8}Be, and assumes that the ground state of ^{8}Be is a pure d + ^{6}Li configuration. An estimate of the spectroscopic factor was obtained from the MCRGM calculation of Hofmann *et al.*, who predict S = 0.5. Using this spectroscopic factor, the d+^{6}Li D-state percentage of the ground state of ^{8}Be is predicted to be 1.5%.

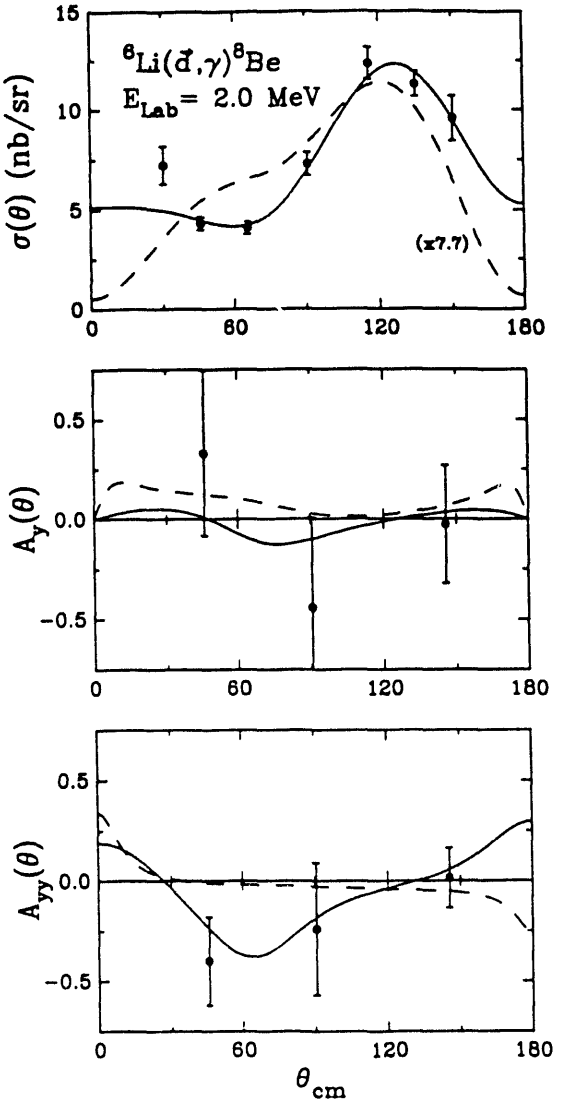

Fig. 3.5-2 Angular distributions of the data at $E_{d(lab)}$= 2.0 MeV plotted in the center-of-mass frame. The solid curve represents the TME analysis and the dashed curve represents the MCRGM calculation. Error bars represent statistical uncertainties associated with the data.

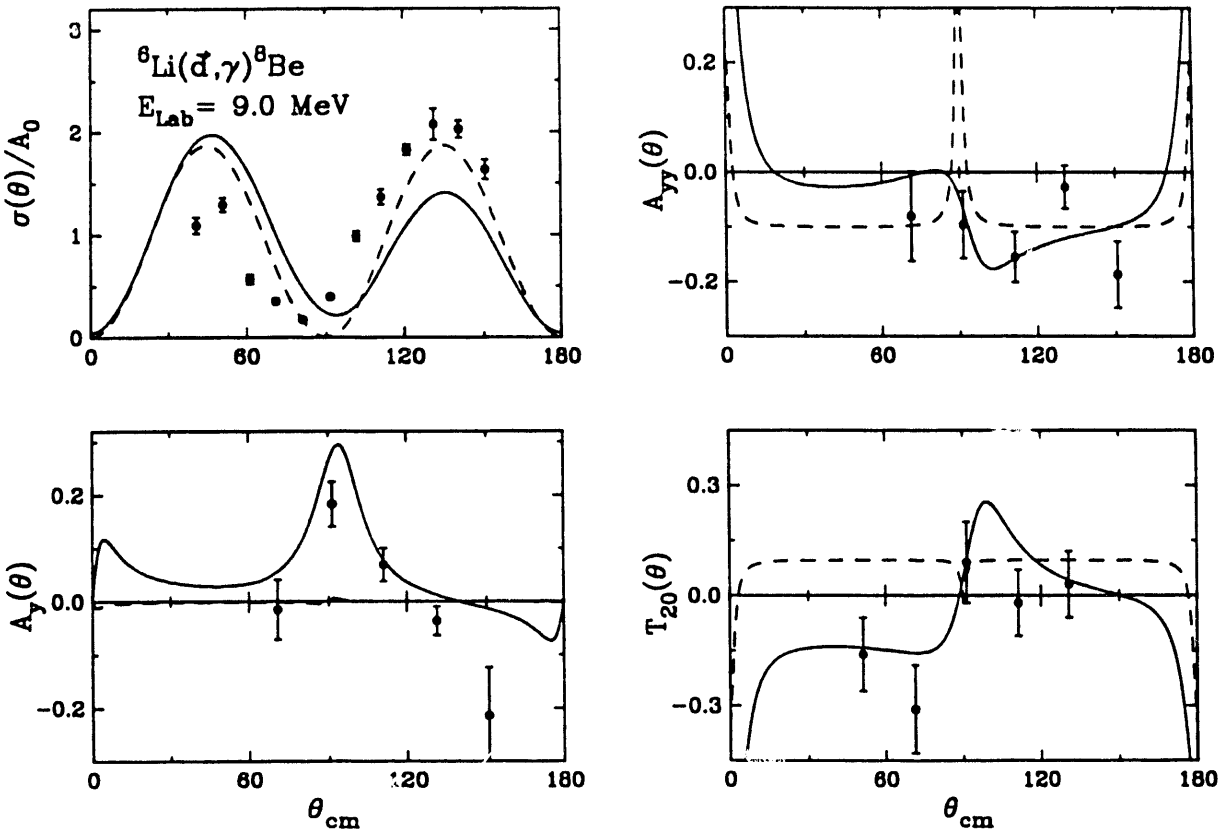

Fig. 3.5-3 Angular distributions of the data at $E_{d(lab)}$ = 9.0 MeV plotted in the center-of-mass frame. The solid curve represents the MCRGM calculation and the dashed curve represents the direct-capture calculation. Error bars represent statistical uncertainties associated with the data.

Work has also continued on the MCRGM calculation, performed by Dr. Harmut Hofmann and Dr. Michael Unkelbach. In this MCRGM calculation, the ground-state wave function was calculated using three cluster configurations : $[^4He + ^4He]^{S=0}$, $[^6Li + d]^{S=0}$, and $[^6Li + d]^{S=2}$. In addition to these channels, the scattering wave function included $[^7Li + p]^{S=1,2}$ and $[^7Be + n]^{S=1,2}$ channels. For the $[^7Li + p]$ and $[^7Be + n]$ channels, only relative s- and p-waves are considered, while for the $[^6Li + d]$ channels s-, p-, and d-waves are considered. The $[^4He + ^4He]$ E2 channel can only have d-waves. While the ground state is 99% $[^4He + ^4He]^{S=0}$, the overlap of the $[^6Li + d]^{S=0}$ configuration (non-orthogonal) was calculated to be 0.73. The D-state probability in the ground state of ^{8}Be, which is the $[^6Li + d]^{S=2}$ configuration (orthogonal), was calculated to be 0.3%. As in the direct-capture calculation, this is the probability for the L=2 relative motion of the ^{6}Li + d clusters. However, unlike the direct-capture calculation, the MCRGM does not assume the ground state of ^{8}Be to be a pure ^{6}Li + d configuration. The results of this calculation are given in

fig. 3.5-3 and table 3.5-1 for 9.0 MeV and in fig. 3.5-2 and table 3.5-2 for 2.0 MeV. The lower D-state probability found in the direct-capture calculation may be a result of neglecting tensor-force effects in the continuum in that calculation.

Plans for this project include more measurements of the tensor and vector analyzing powers, $A_{yy}(\theta)$ and $A_y(\theta)$, at 2 MeV, and attempting an improved MCRGM calculation that includes D states in all fragments, a more realistic two-body force, and a careful computation of E1 radiation.

4 FACETS OF THE NUCLEAR MANY-BODY PROBLEM

As a condensed-matter system of finite size that is dominated by short-range interactions between its particles, the nucleus is a fertile ground for developing understanding of the many-body problem. During the past year we have made progress in measuring and interpreting several facets of the nuclear many-body problem. These aspects include measurements and analyses of nuclear reactions that are relevant to nuclear astrophysics, various excitation mechanisms that can be fruitfully investigated by using low- and medium-energy probes, and the characterization of nuclear elastic scattering at low energies, especially through spin-dependent scattering phenomena, in the measurement of which TUNL has considerable expertise.

4.1 Nuclear Astrophysics

In the past year we have initiated a research program in nuclear astrophysics. This developing program has already made use of several facilities at TUNL, at Princeton University, and at ORNL, to carry out innovative measurements of nuclear reaction processes that are of interest in astrophysics.

Several of the new instrumentation capabilities at TUNL are very useful in the nuclear astrophysics program. The facilities include the upgraded FN tandem (section 5.1), the Low Energy Beam Facility (section 5.6), and the split-pole magnetic spectrometer (section 5.4). The bolometric detector development project (section 5.8.5) also has potential for nuclear astrophysics applications.

4.1.1 The ^{8}Li(α,n)^{11}B Reaction and Primordial Nucleosynthesis

According to recent theoretical studies, a quark-hadron phase transition in the early universe may have given rise to inhomogeneities in the baryon density. These non-uniformities could have produced high-density, proton-rich regions and low-density, neutron-rich regions at the onset of nucleosynthesis. The discussion of the nuclear physics of such regions was the subject of a recent TUNL workshop [Tho90]. For some parts of the allowed parameter space, the calculated abundances of the light elements (with the notable exception of ^{7}Li) are in good agreement with observations, but are also not noticeably different from predictions based upon a standard (homogeneous) big bang.

An inhomogeneous big bang may produce observational signatures in the elements beyond ^{7}Li [Kaj90, Ter90]. A branch point in the reaction flow to these elements appears to occur at ^{8}Li, where the ^{8}Li(α,n)^{11}B reaction, which leads to the production of heavy elements, competes with the ^{8}Li(n,γ)^{9}Li and ^{8}Li(d,n)^{9}Be reactions, which turn the reaction flow back toward ^{6}Li. Because of the short half life of ^{8}Li ($T_{1/2}$ = 838 ms), a direct measurement of the (α,n) reaction is difficult at best. Consequently, we have approached this problem by two different routes: First, we have investigated the structure of states in the compound nucleus ^{12}B which could correspond to ^{8}Li+α and/or ^{11}B+n resonances. From our measurements of excitation energies, widths and decay branches, we can estimate the rate of the (α,n) reaction. Second, since ^{11}B is stable, the inverse reaction ^{11}B(n,α)^{8}Li

can be studied in the relevant temperature region, i.e. at neutron energies between 7.5 and 8.1 MeV. By using the principle of detailed balance, this cross section can be transformed into the corresponding $^{8}Li(\alpha,n_0)^{11}B$ cross section.

Spectroscopic Studies of ^{12}B

A.E. Champagne, Z.Q. Mao[1] , R.B. Vogelaar[1]

We have studied states in ^{12}B by using the $^{11}B(d,p)^{12}B$ and $^{9}Be(\alpha,p)^{12}B$ reactions. The (d,p) reaction provides direct information about the single-neutron structure of ^{12}B. Information pertaining to the $^{8}Li+\alpha$ part of the reaction is not so easily obtained. While the (α,p) reaction will populate configurations in common with resonant alpha capture, the strengths of these configurations cannot be reliably extracted. These measurements were performed using beams of deuterons (E_d=24 MeV) and alpha particles (E_α=35 MeV) provided by the Princeton AVF cyclotron. Outgoing reaction products were momentum-analyzed using a QDDD magnetic spectrometer.

Spectra from each of these reactions, showing states of astrophysical interest, are displayed in fig. 4.1-1. Careful energy calibrations and measurements of line-shapes were obtained by using the $^{19}F(\alpha,^{3}He)^{20}F$, $^{14}N(d,^{3}He)^{13}C$, $^{23}Na(d,^{3}He)^{22}Ne$, and $^{35}Cl(d,^{3}He)^{34}S$ reactions. From this information, we have determined excitation energies and total widths, which are listed in table 4.1-1. Angular distributions have also been measured for both the (α,p) and (d,p) reactions. Unfortunately, neither reaction produces angular distributions with definitive shapes. This may seem surprising for the (d,p) reaction, but since the states of interest are unbound to neutron emission by more than 7 MeV, the usual diffractive shape of the angular distribution is largly washed out. Tentative spin assignments are listed in table 4.1-1 and we are currently estimating the (α,n) reaction rate by using our results.

Table 4.1-1 Experimental results for states in ^{12}B of astrophysical interest.

E_x (MeV)	E_{res}(cm) (keV)	Γ (keV)	J^π
10.201(3)	200(3)	7(4)	$(1,2)^-$
10.417(14)	416(14)	70(30)	≥ 5
10.564(4)	563(4)	9(4)	$(1,2)^-$
10.879(4)	878(4)	15(6)	$(0\text{-}3)^+$
11.328(10)	1.327(10)	85(25)	
11.571(6)	1.570(6)	55(15)	

As mentioned above, a measurement of the $^{11}B(n,\alpha)^{8}Li$ reaction can be used to determine the (α,n_0) cross section by detailed balance. However, this provides only a lower

[1] Princeton University, Princeton, NJ

limit to the the total (α,n) cross section, which will have contributions from neutron decays to excited states in ^{11}B (see fig. 4.1-2a). In order to determine the strengths of decays to excited states, we have performed a preliminary measurement of neutron-decay branches in ^{12}B by using the $^{9}Be(\alpha,p)^{12}B^{*}(n)^{11}B$ reaction. Neutrons were detected in coincidence with outgoing protons at $\theta_{cm} = 55°$ using a 12.7 cm x 5.1 cm NE-213 scintillator. Neutron energies were obtained from the time of flight referenced to the cyclotron RF phase. A sample spectrum is shown in fig. 4.1-2b. Better statistics and measurements at other angles are needed in order to determine accurate neutron branching ratios. Nonetheless, these preliminary results suggest that neutron decays to excited states are not negligible. We plan to complete this measurement at Yale University during fall 1991.

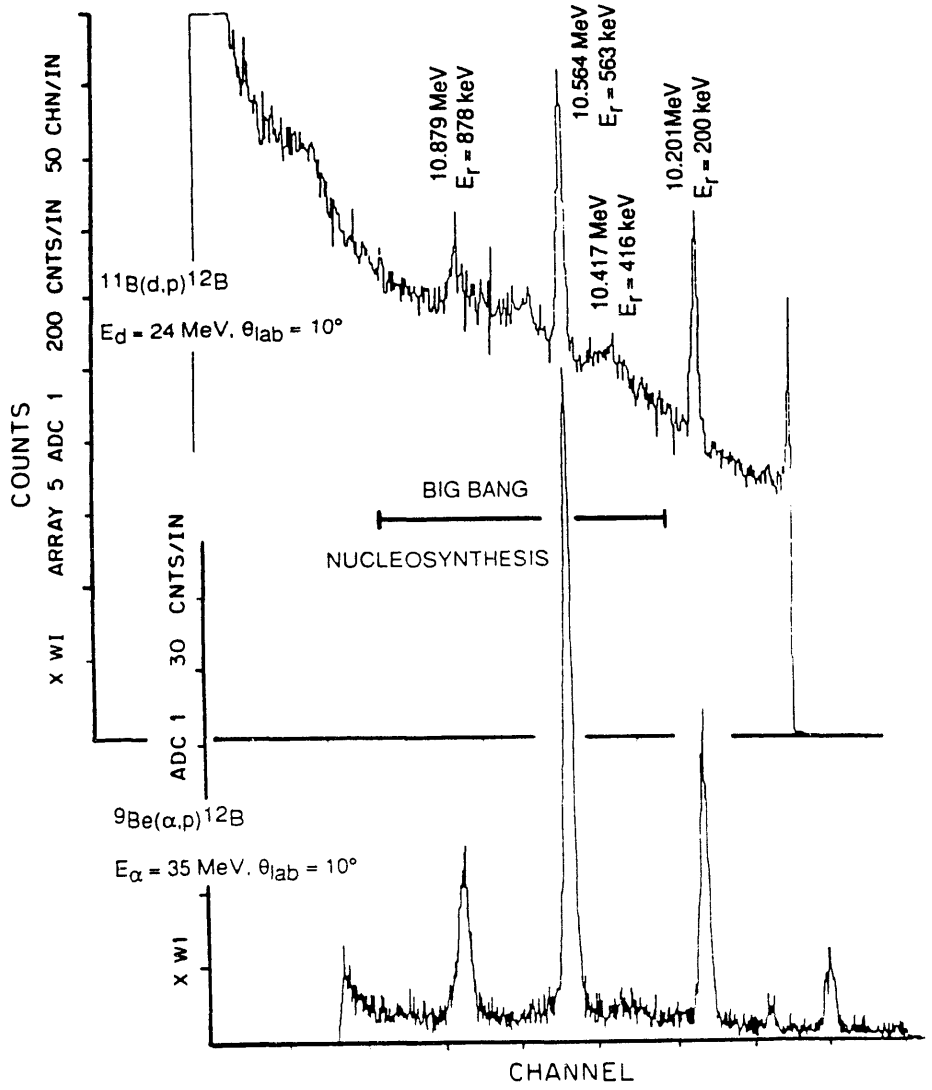

Fig. 4.1-1 Spectra of the $^{9}Be(\alpha,p)^{12}B$ and $^{11}B(d,p)^{12}B$ reactions showing states just above the $^{8}Li+\alpha$ threshold (Q = 10.001 MeV). Also shown is the region of interest for big-bang nucleosynthesis.

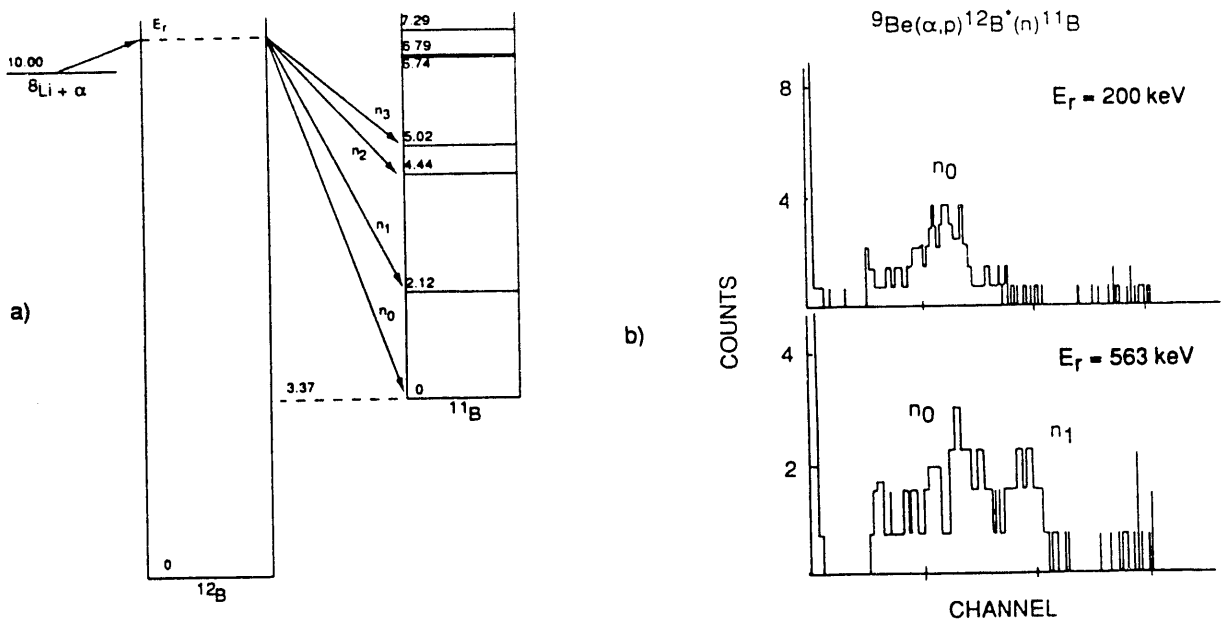

Fig. 4.1-2 Neutron decays from ^{8}Li+α resonances may have sizable branches to the excited states in ^{11}B shown in part a). A preliminary measurement of the reaction ^{9}Be(α,p)^{12}B*(n)^{11}B (part b) suggests than the (α,n_0) channel may account for only 60-70% of the total cross section for the 563-keV resonance.

[Kaj90] T. Kajino and R.N. Boyd, Ap. J. **359** (1990) 267
[Ter90] N. Terasawa and K. Sato, Ap. J. **362** (1990) L47
[Tho90] *Primordial Nucleosynthesis*, ed. W.J. Thompson, B.W. Carney and H.J. Karwowski, (World Scientific) (1990)

Initial Measurements of the ^{11}B(n,α)^{8}Li Reaction

W.Tornow, C.R. Howell, G.J. Weisel, R.L. Walter, A.E. Champagne, C.G. DePree, L.A. Jones, B. Smith[1], J. Görres[1], M. Wiescher[1], R.B. Vogelaar[2], Z.Q. Mao[2]

A measurement of the ^{11}B(n,α)^{8}Li reaction has recently been published by Paradellis *et al.* [Par90] and further work has been completed [Rol91]. The astrophysical S-factor for the ^{8}Li(α,n_0)^{11}B reaction, as obtained from these measurements, is shown in fig. 4.1-3. The S-factor shows several pronounced resonant structures, most notably a resonance near 550 keV. Within experimental errors, this energy is consistent with the prediction of a 563-keV resonance from our spectroscopic studies. However, the S-factor curve implies a total width of about 100 keV while our results show unambiguously that the width of the 563-keV resonance is only 9±4 keV.

---

[1]University of Notre Dame, Notre Dame, IN
[2] Princeton University, Princeton, NJ

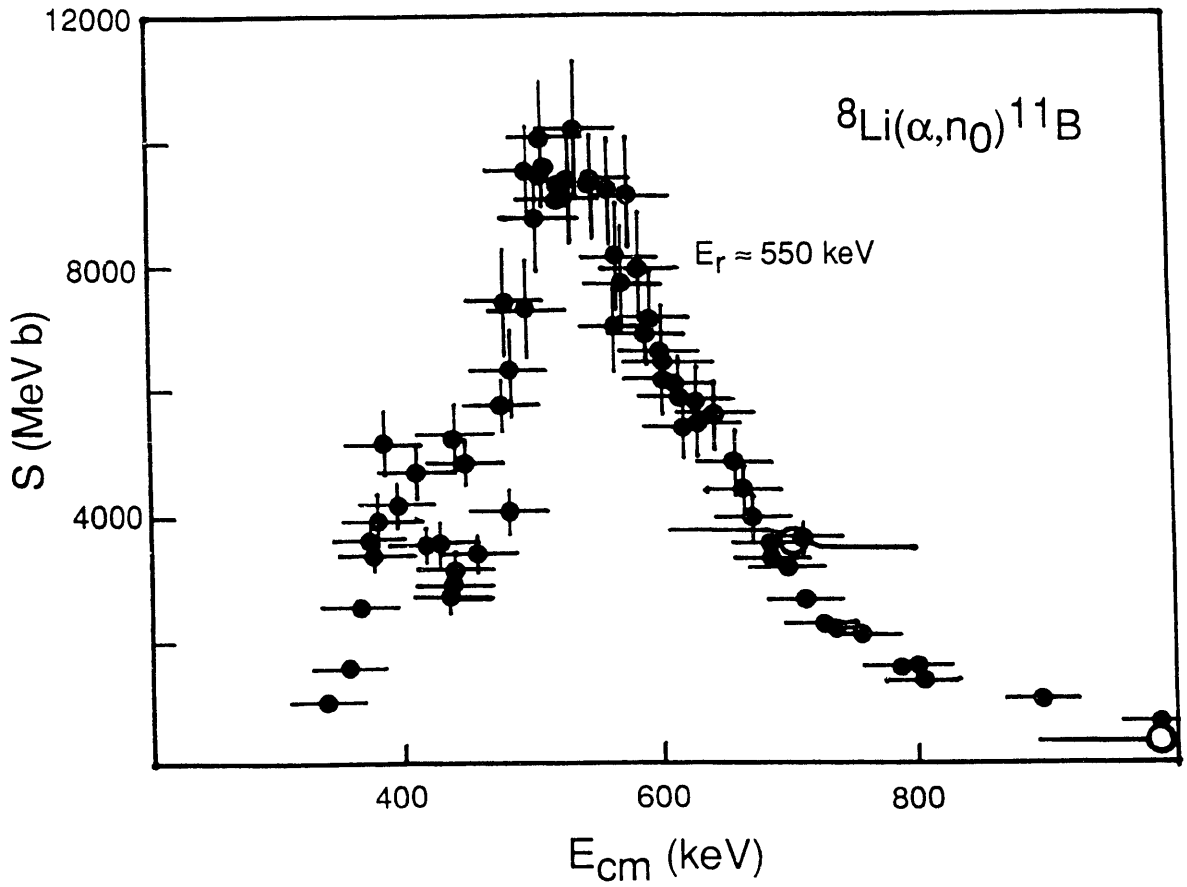

Fig. 4.1-3 S-factor for the $^8Li(\alpha,n_0)^{11}B$ reaction at energies of interest for primordial nucleosynthesis. The solid points are based on data from [Rol91]. The open circles are preliminary TUNL data.

In order to check these results, we have begun a measurement of the $^{11}B(n,\alpha)^8Li$ reaction. Our target and detection system consisted of a 100 $\mu g/cm^2$-thick ^{11}B foil supported between two Si(SB) detectors (fig. 4.1-4). The use of a solid target (rather than a BF_3-filled proportional counter as in [Par90]) ensures that the reaction kinematics and the cone of incident neutrons can be precisely measured and controlled. Neutrons were produced by the $D(d,n)^3He$ reaction using a deuteron beam incident on a D_2 gas cell. The energy spread of the exiting neutrons was governed primarily by energy loss of the deuteron beam in the gas cell and was typically ±100 keV.

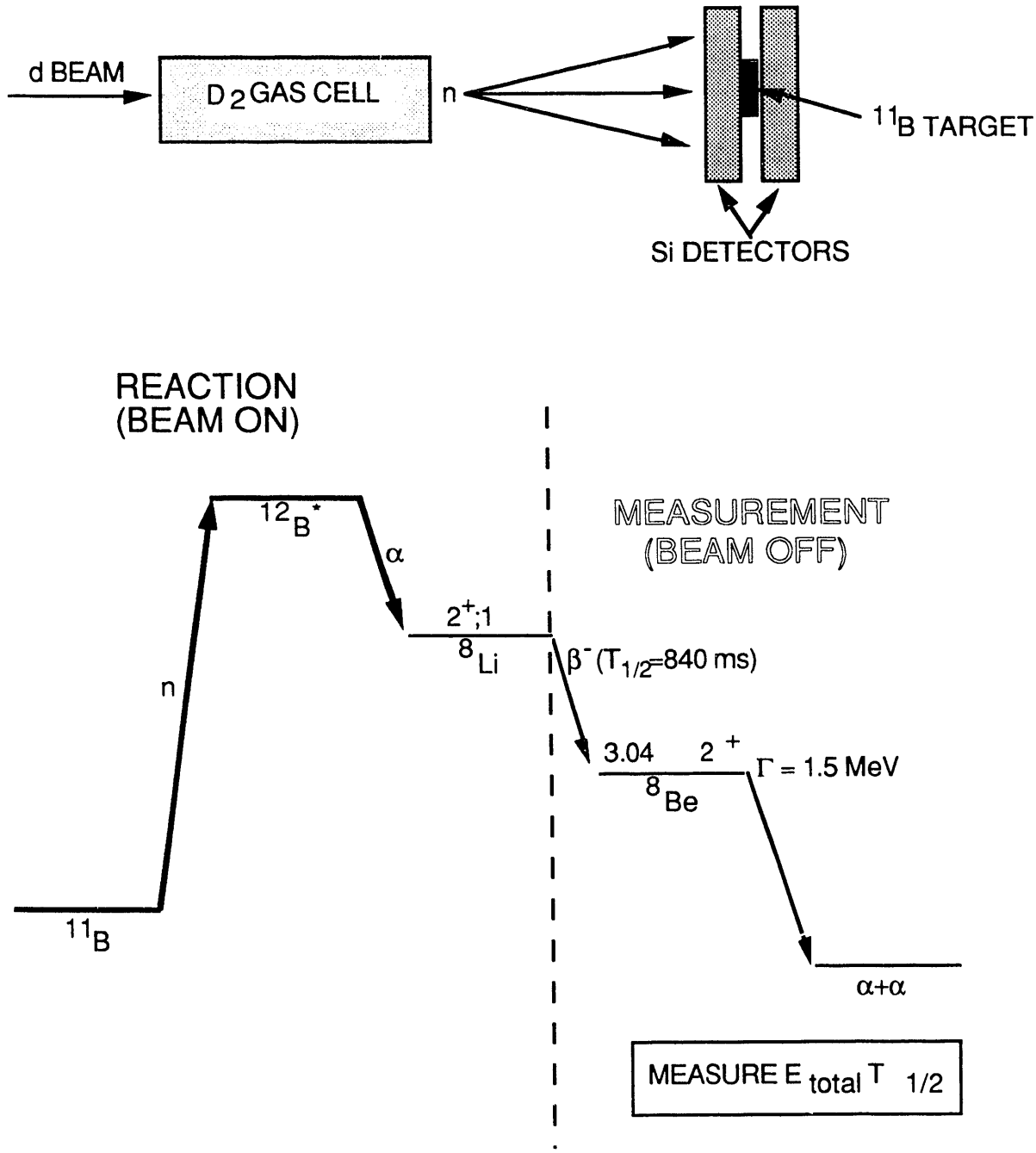

Fig. 4.1-4 Schematic of the TUNL $^{11}B(n,\alpha)^{8}Li$ measurement.

Data were collected in cycles consisting of 5 sec of neutron activation (about six ^{8}Li halflives), followed by 5 sec of counting (fig. 4.1-4). The signature of ^{8}Li production was taken to be the beta-delayed breakup of ^{8}Be into two alpha particles, and we measured both the total energy deposited in the detectors and the decay half-life. Most of the ^{8}Li recoils had enough energy to implant themselves in the downstream detector. These events showed up as singles events with an energy equal to the total decay energy. About 10-20%

of the events (depending upon the neutron energy) involved back-to-back coincidences. Cross sections were measured at incident neutron energies of 8.0, 8.5, 8.75, 10.0, and 14.0 MeV.

In a preliminary analysis, we have normalized the yield at our highest neutron energy to the cross section of [Par90] and it appears that our results at the lower energies are consistent with those of [Par90]. However, only our lowest two measurements are at astrophysically-interesting energies (fig. 4.1-3). In order to map out the cross section at these energies, we will need to run with finer energy steps and with a lower neutron-energy spread. The energy spread can be lowered by running the D_2 cell at lower pressure. However, we will have to improve our current system in order to make up for the resulting decrease in neutron-production efficiency.

Changes that we are planning to implement include a new gas cell that can stand higher beam currents, lowering the data-collection cycle from 10 sec to 6 sec, a thicker target, and a new target chamber that will permit the target to be mounted closer to the neutron source. Together, these improvements should increase our count rate by a factor of 10, which will be adequate for final measurements

---

[Par90] T. Paradellis *et al.*, Z. Phys. **A337** (1990) 211
[Rol91] C. Rolfs, private communication 1991

4.1.2 Development of the $^{17}O(p,\alpha)^{14}N$ Measurement

A.E. Champagne, J.C. Blackmon, L.A. Jones, K.A. Fletcher, E.J. Ludwig

We have constructed and have completed initial testing of hardware intended for measurements of low-energy cross sections. Our primary goal is a measurement of the strength of the E_p=70 keV resonance in the $^{17}O(p,\alpha)^{14}N$ reaction. These results, combined with observations of the ^{17}O abundance in the atmospheres of some red giants, may shed some light on mass flow and mixing in main-sequence stars more massive than the sun. However, the strength of this resonance is expected to be in the range 3-30 neV (i.e. $\sigma_{res} = 0.2 - 2$ nb) [Lan89]. Consequently, we require both high beam current and high detection efficiency. A schematic of our apparatus (as presently constructed) is shown in fig. 4.1-5.

The beam passes through a LN_2-cooled shroud, 28.5 cm long by 2.5 cm in diameter. At the end of the shroud is a 1.4-cm-diameter collimator followed by a 1.6-cm-diameter aperture located 3.9 cm from the target and biased at –300 V in order to suppress secondary electrons. Targets of $W[^{17}O]_3$ were prepared by resistance heating of 0.25-mm-thick tungsten disks in an oxygen atmosphere. Analyses of these targets by Rutherford backscattering indicated that a uniform oxide layer was established over a thickness corresponding to an energy loss of 25 keV for a 70-keV incident proton. The target is directly water cooled and is viewed by four 5 cm x 5 cm implanted Si detectors. In combination, these detectors provided a detection efficiency of 24%. Because we are interested in detecting low-energy alpha particles (E_α<1 MeV), we could not shield the detectors against backscattered beam.

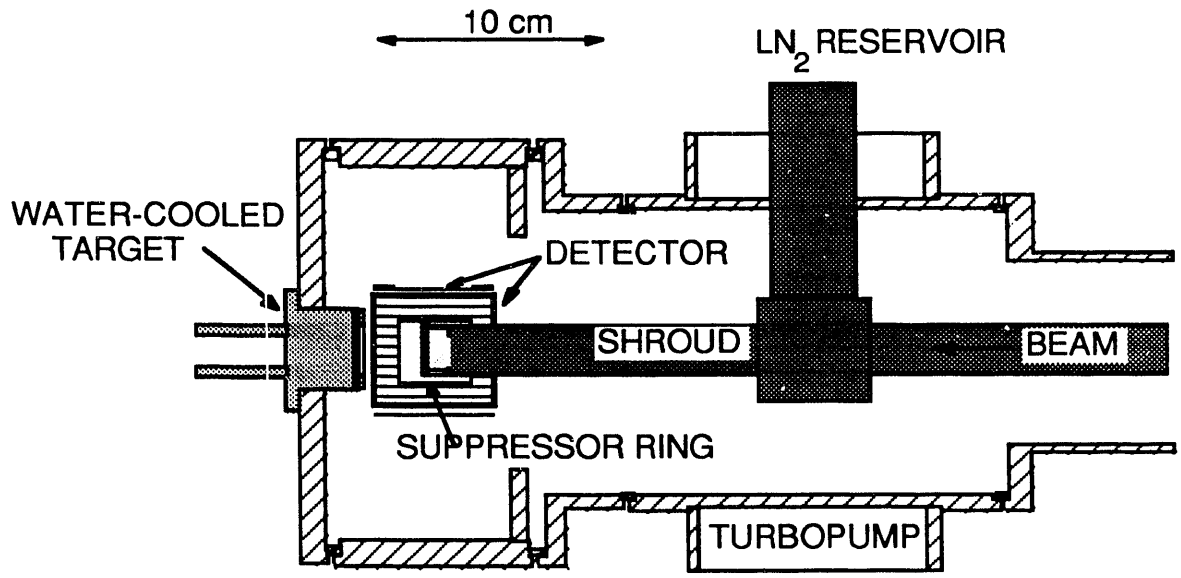

Fig. 4.1-5 Schematic of the target chamber to be used for measuring the $^{17}O(p,\alpha)^{14}N$ reaction.

This chamber was recently installed for initial testing on the 60° port of the TUNL polarized-ion-source inflection magnet. At this location it was possible to put 100 μA of beam on target, but it was not possible to transport the beam cleanly. This produced severe backgrounds, the most troublesome being low-energy secondary electrons produced at beam-defining slits upstream of our apparatus. Overall, the background could be reduced by a factor of 6000 simply by flipping the detectors, so that their ground electrodes faced the target, and by careful tuning of the beam.

This experience has suggested that minor modifications to the shroud and suppressor assembly are required in order to provide increased electron suppression. However, it is also clear that our major difficulty is the poor beam quality at our present location. As a result, we plan to move our equipment to an unused port on the planned switching magnet for the Low Energy Beam Facility, where experience indicates that we will have more control over beam quality. Finally, by removing some of the PC board supporting each detector, we will be able to pack the detectors in a closer geometry and thereby gain an additional 10% in efficiency. These changes will be made for data taking beginning late in 1991.

[Lan89] V. Landre *et al.*, Phys. Rev. **C40** (1989) 1972

4.1.3 Nuclear-Astrophysics Studies with Radioactive Ion Beams

A.E. Champagne, J.C. Blackmon, L.A. Jones, J.D. Garrett[1], I.Y. Lee[1], D. Winchel[1]

The recent initiative to develop radioactive ion beams at the Holifield Heavy Ion Research Facility (HHIRF) promises exciting new capabilities for nuclear astrophysics

---

[1] Oak Ridge National Laboratory, Oak Ridge, TN

studies of explosive nucleosynthesis. We have begun to assess the requirements for targets and detection systems that will take advantage of these new beams and we have just completed a development run using a stable-ion beam at the HHIRF.

Nuclear-astrophysics measurements with radioactive beams involve reversing the traditional roles of projectile and target, i.e. beams of low-energy heavy ions with hydrogen or helium targets. In order to minimize background, the target must be thin enough so that the beam can be transported away from the detectors. However, it must be robust enough to survive bombardment over several hours. These requirements imply the use of gas targets, or for hydrogen targets, of thin plastics.

Our initial tests involved thin polyethylene and Kapton foils (thicknesses of 2.5 μm and 12.5 μm, respectively) which were bombarded by a beam of ^{28}Si (E_{lab} = 49 MeV, E_{cm} = 1.704 MeV) provided by the HHIRF 25-MV-tandem Van de Graaff accelerator. Beam currents were restricted to about 5 pnA which is comparable to what might be optimistically expected for a radioactive beam. At this bombarding energy, each target was thick enough to populate the known E_{cm} = 1.595-MeV resonance in the $H(^{28}Si,\gamma)^{29}P$ reaction. This resonance gamma decays 91% of the time directly to the ground state of ^{29}P (E_γ = 4.343 MeV). Gamma rays were detected with the Oak-Ridge Spin Spectrometer which, for this run, comprised 18 Compton-suppressed Ge detectors and 51 NaI detectors in a 4π geometry.

Although the beam was defocussed to a fairly large spot (2 mm x 4 mm), the targets were found to have a lifetime of only about 2 hours, with no obvious degradation before failure. We do not yet understand how the targets are destroyed, but thermal stress is probably not responsible, since the target should reach radiative equilibrium in a short time. Also, because the carbon (and in the case of Kapton, nitrogen and oxygen) in these targets produced substantial background, we could not discern any evidence for the 1.595-MeV resonance.

Further tests were carried out using TiH_2 targets prepared by heating 12.5-μm-thick Ti sheet in a hydrogen atmosphere. These targets are too thick to be suitable for radioactive beams, but they were useful for the purpose of evaluating the properties of the Spin Spectrometer. A sum of the raw Ge spectra showed no evidence for the 1.595-MeV resonance. However, the portion of the data corresponding to single-detector events clearly shows a feature at $E_\gamma \approx$ 4.3 MeV (shown in fig. 4.1-6), as would be expected for the dominant decay of this resonance.

These data are currently being analyzed, from which it is clear that some sort of multi-element gamma-ray detector is desirable for use with radioactive beams. However, since we will be studying states with comparatively low spin, our final detector need not have as many elements as the Spin Spectrometer. About 10 elements would most likely be sufficient and this would also have the benefit of increased efficiency for individual detectors. Further tests of a prototype detection system are planned. We also plan to continue our investigation of targets, including gas targets.

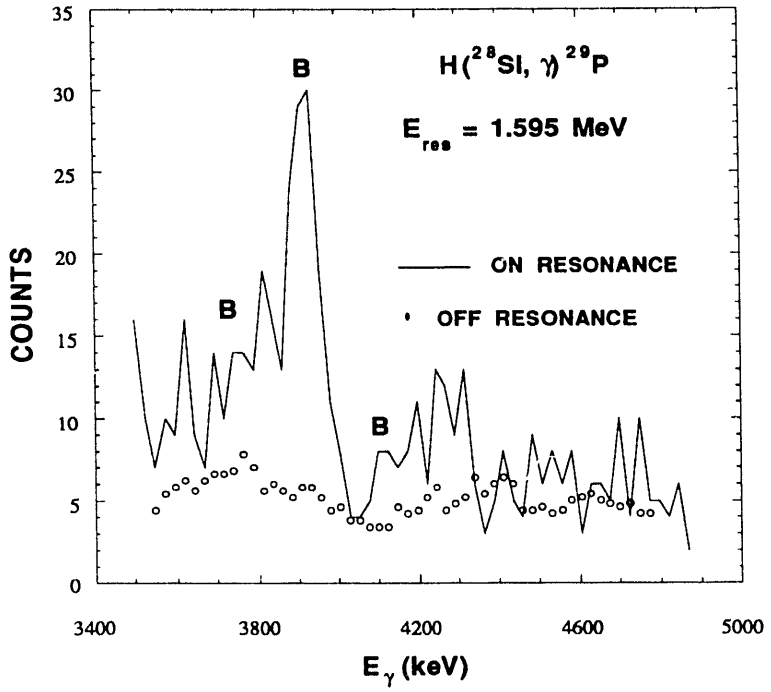

Fig. 4.1-6 A sum of the 18 individual Ge spectra (after corrections for Doppler shifts) showing γ rays in the energy range 3.4 to 4.9 MeV from single-detector events. Peaks labelled by B have been identified as background arising from carbon and oxygen in the target. The width of the peak at 4.3 MeV is consistent with Doppler broadening combined with the natural width of the 1.595-MeV resonance (Γ = 50 keV). On-resonance corresponded to E_{lab} = 49 MeV (E_{cm} = 1.704 MeV), while the off-resonance run was at E_{lab} = 41 MeV (E_{cm} = 1.426 MeV). This spectrum represents about 1/5 of the available data.

4.2 Excitation Mechanisms of the Nucleus

During the past year we have studied several aspects of nuclear-excitation mechanisms, using facilities at LAMPF/WNR and at LBL. We have also collaborated extensively with physicists at these facilities, as well as with collaborators at the University of Saskatchewan, Ohio State University, and George Washington University in order to develop studies of photonuclear reactions induced by polarized photons – a field of research which is likely to develop significantly as new electronuclear physics facilities come on-line.

4.2.1 Gamow-Teller Strength Functions for Light- and Medium-Mass Nuclei

C.R. Howell, X. Aslanoglou[1], F.P. Brady[2], J.R. Drummond[2], R.W. Finlay[1], R.C. Haight[3], N.S.P. King[3], A. Ling[3], P.W. Lisowski[3], C.L. Morris[3], B.K. Park[1], J. Rapaport[1], J.L. Romero[2], D.S. Sorenson[2], W. Tornow, J.L. Ullmann[3], X. Yang[1]

Our collaboration is making the most complete measurements of differential cross sections for the (n,p) charge-exchange reaction near zero momentum transfer (q) and zero energy loss (ω) on light and medium mass nuclei. All measurements are made using the continuous-energy neutron beam from target 4 of the LAMPF/WNR facility. The combination of the continuous-energy neutron beam and the multiple target chamber array in our spectrometer (see fig. 4.2-1) makes our experimental setup extremely efficient for (n,p) cross-section measurements. Our data enables, for the first time, the extraction of the Gamow-Teller GT strength function at all neutron energies continuously between 60 and 260 MeV.

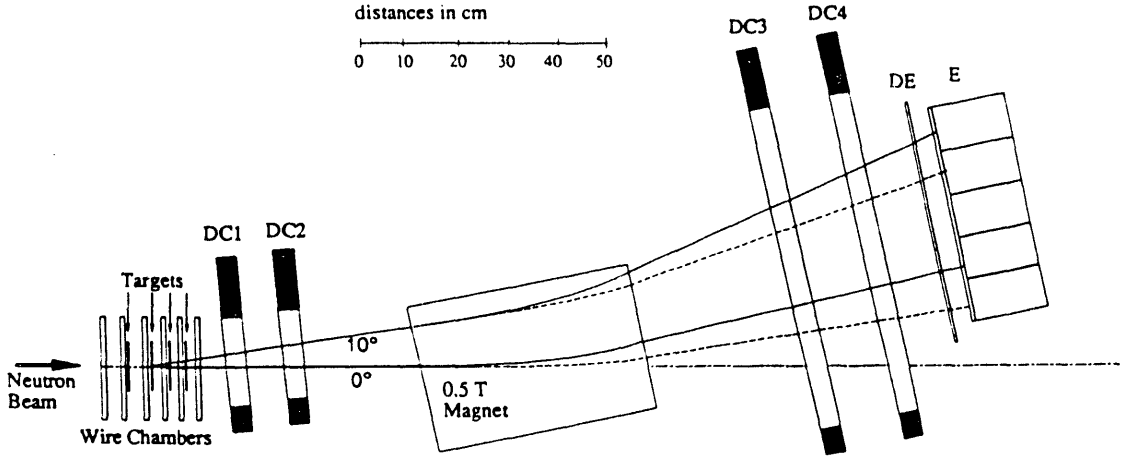

Fig. 4.2-1 Experimental setup for (n,p) cross-section measurements at medium energies.

So far, we have completed measurements on ^{6}Li, ^{12,13}C, ^{NAT}S, ^{40}Ca, and ^{60,64}Ni. The analyses on the data from these measurements, except for ^{60}Ni, are completed. A manuscript on our results for the ^{6}Li and ^{12,13}C nuclei has been submitted to Physical Review Letters. To illustrate the quality of our data, the volume integrals for the spin-flip isospin-flip part of the effective NN interaction obtained in our analysis are shown in

[1] Ohio University, Athens, OH
[2] University of California, Davis, CA
[3] Los Alamos National Laboratory, Los Alamos, NM

fig. 4.2-2. The result of the ^{64}Ni analysis has been submitted to Physical Review C. The abstract from the ^{64}Ni paper follows.

Cross sections have been measured for the reaction ^{64}Ni(n,p)^{64}Co at laboratory angles between 0° and 10° for incident neutron energies from 90 to 240 MeV. The ground-state cross sections together with the ß decay *ft* value for the transition ^{64}Co(*g.s.*)→^{64}Ni(*g.s.*) are used to normalize the q=0 differential cross section in units of mb/sr-GT. This is the first absolute measurement of the A(*n,p*) unit cross section for a nucleus in the (*fp*)-shell and it may be used to calibrate the GT strength measured in other (*n,p*) reactions of similar mass nuclei. Since the (e^-,ν_e) channel involves the same nuclear matrix element as the (*n,p*) channel, knowledge of GT strength in these nuclei is important for supernova modeling codes which depend on knowledge of e^- capture rates of (*fp*)-shell nuclei to determine parameters of stellar core collapse.

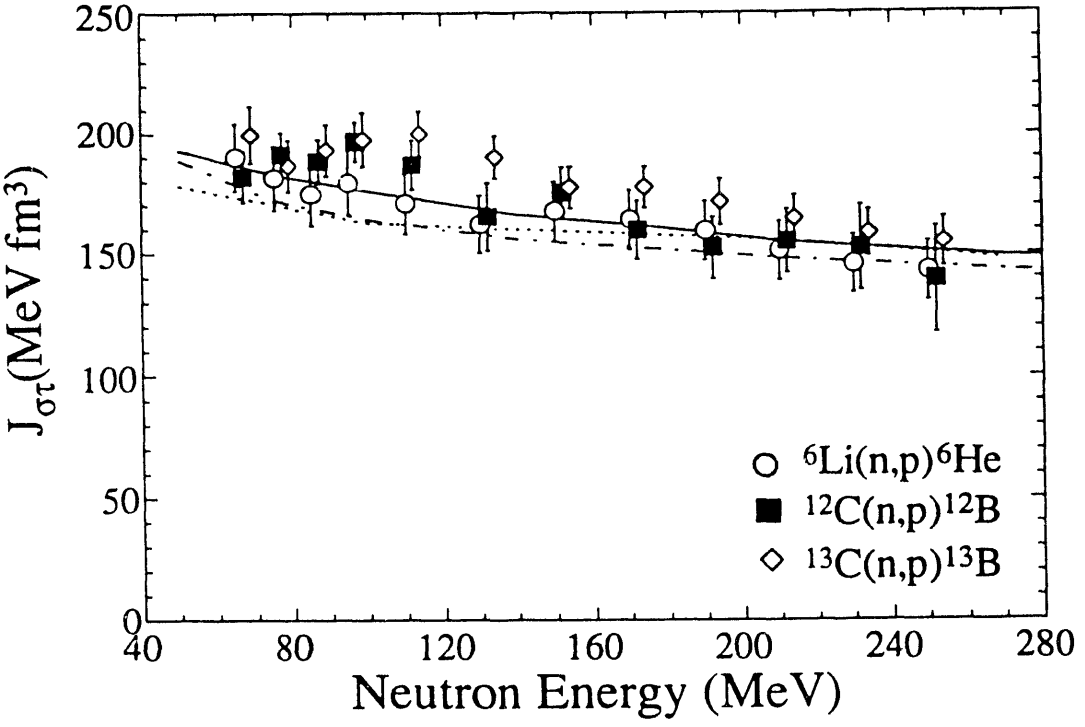

Fig. 4.2-2 Volume integrals for the spin-flip isospin-flip part of the effective NN interaction derived from the present data. The ^{12}C points are shifted to the right by 2 MeV and the ^{13}C points by 4 MeV for clarity. Theoretical values of the volume integrals derived from the free Love-Franey t-matrix [Fra85] (dotted curve) and the Nakayama-Love F=Matrix [Nak88] at k_f = 1.36 (solid curve) and k_f = 0.0 fm^{-1} (dot-dash curve) are shown.

A manuscript on the results of the ^{NAT}S and ^{40}Ca analyses is being prepared for publication. The analysis of the ^{60}Ni data is underway.

In summer 1991 the emphasis of our experimental program switched from measuring GT strength functions to investigating energy dependences of giant resonances and studying the NN tensor force by measuring stretched transitions in the $^{10}B(n,p)$ reaction. Because these new projects required (n,p) measurements at lab angles greater than 20°, the spectrometer shown in fig. 4.2-1 had to be modified. The target assembly was moved to the downstream side of the magnet and target chamber 1 was removed from the setup along with drift chambers DC1 and DC2. The frame supporting DC3, DC4, DE and E detectors was rotated to cover the angular region between 20° and 50°. This summer we acquired large-angle (θ_{lab} = 20° - 50°) data for $^{12}C(n,p)$ and $^{10}B(n,p)$.

[Fra85] M.A. Franey and W.G. Love, Phys. Rev. **C31** (1985) 488
[Nak88] K. Nakayama and W.G. Love, Phys. Rev. **C38** (1988) 51

4.2.2 Isovector Giant Quadrupole Resonance in (p, γ) Reactions

H.R. Weller, G. Feldman, M. Godwin, E. Hayward, L.H. Kramer

Polarized proton capture reactions offer several unique advantages in the search for resonant E2 strength. First, real photons are detected, which restricts the contributing multipoles to relatively low order ($\lambda \leq 3$). Second, E1/E2 interference effects can give rise to noticeable signatures in the measured observables, such as cross-section asymmetry or vector analyzing power (especially at 90°).

We have begun a program of polarized (p,γ) studies using the polarized proton beam of the 88-inch Cyclotron at the Lawrence Berkeley Laboratory in an effort to identify the isovector giant quadrupole resonance (IVGQR) and to understand its systematics. In the first part of this work, we have measured the cross section $\sigma(\theta)$ and the vector analyzing power $A_y(\theta)$ at 9 points in the angular range θ_γ = 37.5°–145° for the $^{30}Si(\vec{p},\gamma)\,^{31}P$ reaction using polarized protons at E_p = 25.5 MeV. We have also measured the vector analyzing power at θ_γ = 90° at 11 energies over the proton energy range E_p = 20-36 MeV. A transition matrix element analysis of $\sigma(\theta)$ and $\sigma(\theta)A_y(\theta)$ at E_p = 25.5 MeV reveals substantial E2 strength ($\sigma_{E2}/\sigma_{tot} \approx 26\%$) in the (p,γ_1) channel, in excess of a direct E2 capture estimate (~7%). The energy dependence of $A_y(90°)$ for γ_1 shows a resonance structure which can be reproduced by a direct-semidirect calculation including an E2 resonance (E_{IVGQR} = 38.6 MeV, Γ_{IVGQR} = 5.0 MeV, Σ_{IVGQR} = 50%) built on the first excited state of ^{31}P. By contrast, the γ_0 data can be equally well described by a DSD calculation with or without an IVGQR. Further details can be found in our recent publication on these results.

In work currently underway, we have measured $\sigma(\theta)$ and $A_y(\theta)$ at 6 angles in the range θ_γ = 38.8°–130° for the $^{89}Y(\vec{p},\gamma)^{90}Zr$ reaction at E_p = 22.5 MeV. The γ-ray spectra show the ground-state transition (γ_0) clearly resolved from the strong cluster of three states near $E_x \approx$ 2.3 MeV. The angular distributions for γ_0 reveal large asymmetries about θ_γ = 90° in both $\sigma(\theta)$ and $\sigma(\theta)A_y(\theta)$, indicative of E1/E2 interference effects. Legendre polynomial fits give non-zero Legendre coefficients of order k = 3,4, thus confirming the presence of E2 radiation. A transition-matrix analaysis (TME) analysis of the γ_0 transition

reveals two solutions, both of which give an E2 contribution of 28%. The direct E2 capture strength given by a DSD calculation is 6%, indicating a substantial concentration of non-direct E2 strength in the reaction at this energy.

The quality of the TME fits to these angular distributions can be improved significantly by adding two E3 transition matrix elements ($^7d_{5/2}$ and $^7g_{7/2}$) and then fitting the data with Legendre functions up to order k = 5. The E3 strength falls in the range 2-6%, while the E2 contribution is 22-32%. The analyzing powers for transitions to the first three excited states are much larger than those leading to the ground state, as in the case of ^{30}Si. Final results for the angular distribution of γ_0 and γ_{123} are shown in fig. 4.2-3 along with Legendre fits.

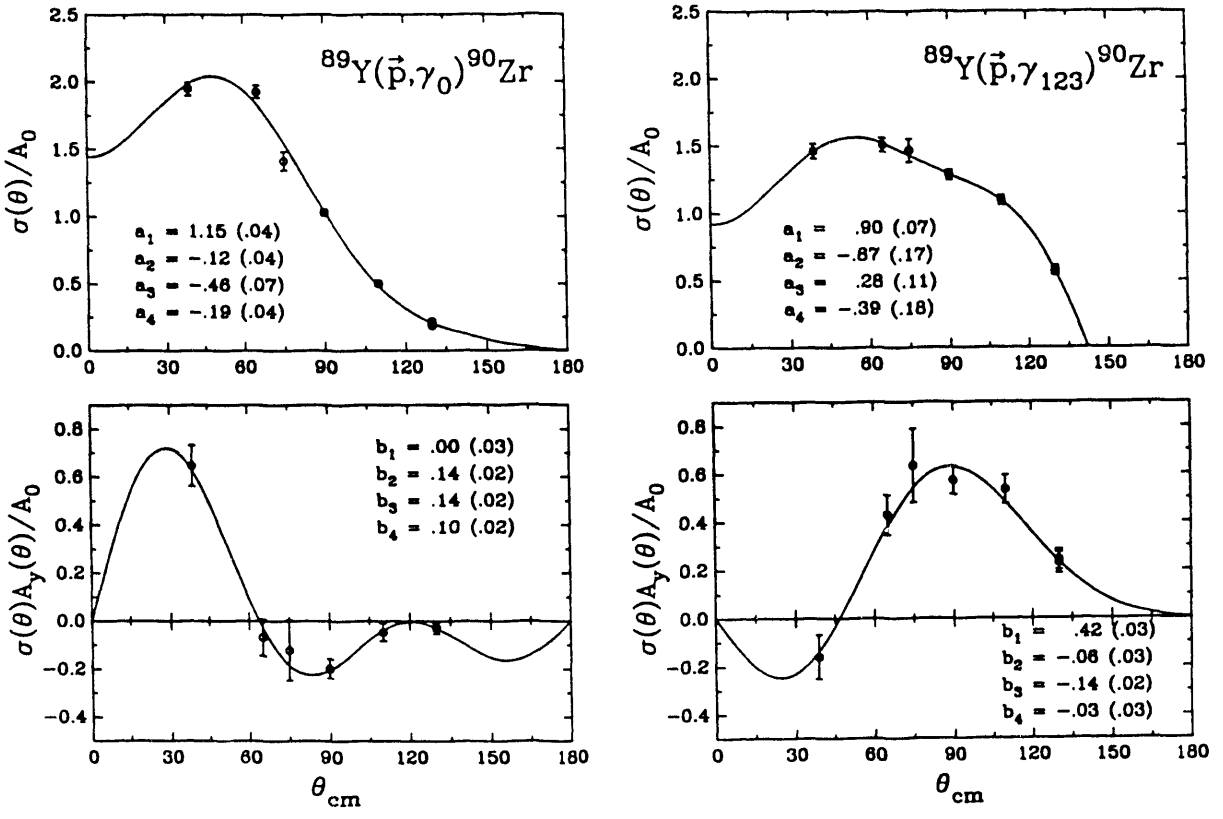

Fig. 4.2-3 Angular distributions of cross section and analyzing power for the γ_0 and γ_{123} transitions from the $^{89}Y(\vec{p},\gamma)^{90}Zr$ reaction at E_p = 22.5 MeV. The solid curves are Legendre polynomial fits.

Recently, we have also measured the analyzing power at 90° in 2-MeV steps for E_p = 16.5 to 30.5 MeV. Analysis of this data is currently underway. Two typical spectra for E_p = 16.5 MeV and E_p = 30.5 MeV are shown in fig. 4.2-4. A direct-semidirect model calculation for the 90° analyzing powers between 16.5 and 30.5 MeV has been performed and is shown in fig. 4.2-5. An attempt to interpret the angular distribution and

energy dependence results and to determine the IVGQR parameters for ^{90}Zr using the DSD model is also underway.

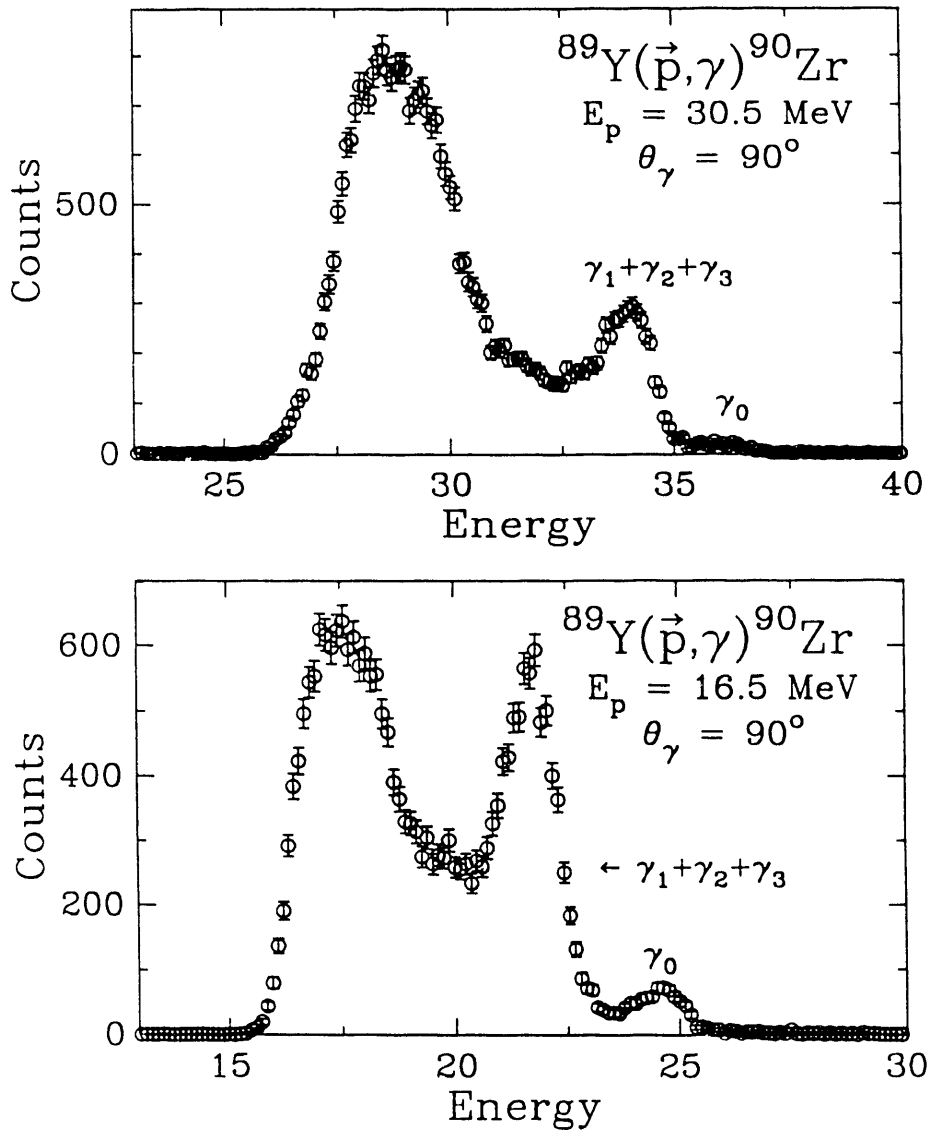

Fig. 4.2-4 Typical spectra from the ^{89}Y($\vec{p}$,γ)^{90}Zr reaction for θ = 90° and E_p = 16.5 and 30.5 MeV. Curves are the total lineshape fit to the data (solid curve) along with the γ_0 and γ_{123} transitions (dashed curves).

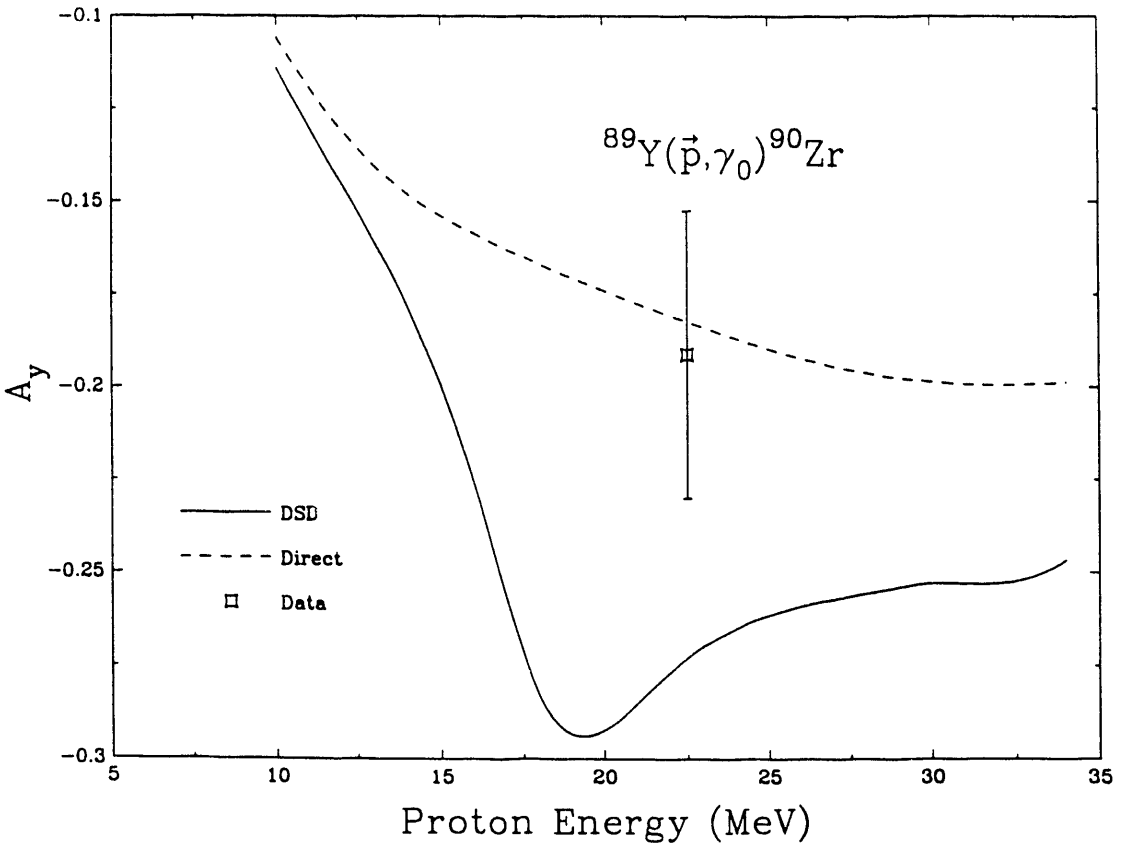

Fig. 4.2-5 Results of the direct-semidirect model calculations for vector analyzing powers Ay(90°) as a function of energy for the γ_0 transitions for $^{89}Y(\vec{p},\gamma)^{90}Zr$. Included is the result from the angular distribution at 22.5 MeV.

[Fel91] G. Feldman *et al.*, Phys. Rev. **C43** (1991) 223

4.2.3 Angular Distribution Coefficients for (γ,x) Reactions with Linearly Polarized Photons

R.M. Chasteler, H.R. Weller, J. Langenbrunner, E.L. Tomusiak[1], J. Asai[1], R.G. Seyler[2], D.R. Lehman[3]

Polarized photon beams have been available for a considerable time, and their use in the study of photonuclear reactions is expected to increase in future years. A general formalism which permits one to write down expressions for observables in terms of reduced transition matrix elements exists [Wel63], but has neither been generally applied nor put in a

1 University of Saskatchewan, Saskatoon, Saskatchewan, Canada.
2 The Ohio State University, Columbus, Ohio.
3 The George Washington University, Washington, D.C.

useful and convenient form similar to that which exists for the case of polarized capture reactions [Sey79].

We have evaluated specific formal expressions for a linearly polarized gamma-ray-capture particle-out reaction. They allow one to generate the expression for the cross section as a function of the detected particle angle, θ, and the photon-polarization angle, ϕ, in terms of the reduced transition matrix elements for any multipolarities and any particle spins. Tables, which allow one to construct these expressions, are presented for target spins and parities of 0^+, $1/2^+$, 1^+ and $3/2^+$; outgoing particle spins and parities of 0^+, $1/2^+$ and 1^+; residual-nuclei spins and parities of 0^+, $1/2^\pm$, 1^+ and $3/2^\pm$; and multipolarities E1, M1, and E2. Some simple examples – ^{4}He($\vec{\gamma}$,d)d assuming pure E2 radiation and ^{2}H($\vec{\gamma}$,p)n for pure M1 or pure E1 radiation – are described and are shown to reduce to familiar results [Hay70, Sat55]. This work is in press at *Atomic Data and Nuclear Data Tables.*

[Hay70] Evans Hayward, in "Photonuclear Reactions", National Bureau of Standards Monograph **118** (1970) 34

[Sat55] G.R. Satchler, Proc. Phys. Soc. **68A** (1955) 1041

[Sey79] R.G. Seyler and H.R. Weller, Phys. Rev. **C20** (1979) 453

[Wel63] T.A. Welton in *Fast Neutron Physics*, edited by J.B. Marion and J.L. Fowler (Wiley Interscience, New York, 1963), Vol. II, p. 1317

4.3 Dispersion Relations and Nucleon Scattering

Many current optical-model (OM) developments are including the dispersion relations (DR) for the OM potential. The DR relates the real and imaginary parts of the mean potential field as follows:

$$M(r,E) = V(r,E) + i\,W(r,E)$$

$$V(r,E) = V_{HF}(r,E) + \Delta V(r,E)$$

$$\Delta V(r,E) = (P/\pi) \int_{-\infty}^{\infty} [W(r,E')/(E'-E)]\, dE'$$

where W(r,E) is the usual absorptive potential that is a combination of a surface and volume contributions, V_{HF} (r,E) is the Hartree-Fock contribution, and $\Delta V(r,E)$ is the dispersive contribution to the mean field V(r,E). The P denotes a principal-value integral. The DR introduces a surface contribution to the real central potential that has a moderately strong variation with energy in the region below 10 MeV. So far, DR models for nucleon-nucleus scattering have been studied in detail mainly for the single-particle (SP) nuclei ^{208}Pb, ^{90}Zr, and ^{40}Ca.

In the following subsections we summarize some of our recent progress in relating DR and nucleon scattering.

4.3.1 Volume-Absorptive Potentials and DR Contribution to the Mean Field

J. Vanderkam, W. Tornow

The energy dependence of the volume absorptive potentials W_V is commonly parameterized by

$$W_V(E) = A\frac{(E-E_F)^n}{(E-E_F)^n + B^n} \tag{1}$$

where E_F is the Fermi energy. The constants A, B and n can be obtained from fits to nucleon-nucleus scattering data. With even n, $W_V(E)$ is symmetric with respect to the Fermi energy. In the past we evaluated the volume dispersive term

$$\Delta V_V(E) = \frac{1}{\pi}\int_{-\infty}^{+\infty} W_V(E')\left[\frac{1}{E'-E} - \frac{1}{E'-E_F}\right] dE' \tag{2}$$

by using a numerical integration method. In order to save computer time, we have instead derived analytical solutions of Eq. (2) for n=2 (Brown-Rho parametrization):

$$\Delta V_V(E) = \frac{AB(E-E_F)}{(E-E_F)^2 + B^2}, \tag{3}$$

for n=4 (Jeukenne-Mahaux parametrization):

$$\Delta V_V(E) = \frac{AB(E-E_F)\,[(E-E_F)^2 + B^2]}{\sqrt{2}\,[(E-E_F)^4 + B^4]}, \tag{4}$$

and for n=6:

$$\Delta V_V(E) = \frac{AB(E-E_F)\,[2(E-E_F)^4 + B^2(E-E_F)^2 + 2B^4]}{3[B^6 + (E-E_F)^6]} \tag{5}$$

Formulas (3) and (4) were given in [Bro81] and [Mah87], respectively.

Recently, it was pointed out by Mahaux and Sartor [Mah91] that the absorptive potentials must be zero on both sides of the Fermi energy E_F between the particle and hole states. The parametrizations of Eq. (1) gives zero absorption only at exactly $E = E_F$. Therefore, we rewrite Eq. (1)

$$W_V = A\frac{(|E-E_F| - F)^n}{(|E-E_F| - F)^n + B^n}, \tag{6}$$

where $W_V(E)$ is set to zero for $|E-E_F| < F$ with $F > 0$. We derived analytical solutions of Eq. (2) with Eq. (6) and n=2, 4, and 6. The solutions are rather lengthy and will not be given here.

Equations (1) and (6) given above assume that the absorptive potential $W_V(E)$ is symmetrical around the Fermi energy E_F. This assumption is plausible for small values of $|E-E_F|$ but, according to [Mah91], the symmetry assumption no longer holds for larger values of $|E-E_F|$. Calculations performed for nuclear matter indicate that the nonlocality of

the imaginary part of the microscopic mean field causes W_V to increase at large positive energies and to approach zero at large negative energies. Following [Mah91] the asymmetric volume absorption $W_V^{asym}(E)$ can be parameterized by

$$W_V^{asym}(E) = W_V(E) + a_V\left[\sqrt{E} + \frac{(E_F + E_A)^{3/2}}{2E} - \frac{3}{2}\sqrt{E_F + E_A}\right] \tag{7}$$

for $E > E_F + E_A$, $E_A > 0$ and

$$W_V^{asym}(E) = W_V(E)\left[1 - \frac{(E_F - E - E_A)^2}{(E_F - E - E_A)^2 + E_A{}^2}\right] \tag{8}$$

for $E \le E_F - E_A$, $E_A > 0$, while $W_V(E)$ is defined by Eq. (6) and E_A is the energy beyond which the volume absorption is asymmetric. The coefficient a_V in Eq. (7) is defined in [Mah91]. We calculated the volume dispersive term for $W_V^{asym}(E)$ given by Eq. (7) and for the volume dispersive term of $W_V^{asym}(E)$ given by Eq. (8) we found a close approximation:

$$\begin{aligned}\Delta V_V^{asym}(E) = \Delta V_V(E) - & \frac{A}{\pi\left[(E - E_F + E_A)^2 + E_A^2\right] * 2E_A^2} * \\ & \left\{\frac{\pi}{2}(E - E_F)(E_A^3 - E_A^2(E - E_F + E_A)) - E_A^2(E - E_F) * \right. \\ & (E - E_F + 2E_A)\, ln\, E_A + E_A^2 (E_F - E_A - E)^2 * ln\left|\frac{E_F - E_A - E}{E_A}\right| + \\ & \left. E_A^2\left[(E_A + E - E_F)^2\, ln\,|E_A + E - E_F| - E_A^2\, ln\,|E_A|\right]\right\}\end{aligned} \tag{9}$$

These closed-form solutions are useful for expediting DR calculations, particularly when one is employing a global, iterative search method as is being done in some of the analyses at TUNL.

[Bro81] G.E. Brown and M. Rho, Nucl. Phys. **A372** (1981) 397
[Mah87] C. Mahaux and R. Sartor, Nucl. Phys. **A468** (1987) 193
[Mah91] C. Mahaux and R. Sartor, Nucl. Phys. **A528** (1991) 253

4.3.2 DR Optical Model and Coupled-Channel Model for n+^{27}Al and n+^{59}Co

M.M. Nagadi, J.P. Delaroche[1], C.R. Howell, W. Tornow, R.L. Walter

The need for a good description for n+ ^{27}Al and n+ ^{59}Co total and differential cross-section data emerged from the fact that there exist spin-spin cross-section data for both nuclei that have not been satisfactorily described to date. For ^{27}Al, descriptions of the spin-spin cross-section data have been made by Gould *et al.* [Gou86], Hnizdo *et al.* [Hni87], and Heeringa *et al.* [Hee89]. Compound-nucleus analyses have been made for ^{59}Co spin-spin cross-section data by Thompson [Tho76], while Heeringa *et al.* [Hee76,77] and McAbee *et al.* [McA90] used direct-reaction models for data at higher energies.

Part of the problem these authors faced was the lack of a model designed specifically for the nucleus in question. Therefore we developed more complete models for neutron

scattering for both nuclei. For both ^{27}Al and ^{59}Co two models were developed; a dispersive optical model (DOM), and a coupled channel model (CCM). Predictions from the models were compared to the spin-spin cross section data.

Dispersive optical model and coupled channel model for n+^{27}Al

Although it is important in developing the DR optical model (DOM) to study single-particle (SP) nuclei in order to test the extension of the DOM to negative energies (SP bound states), it is also important to investigate the applicability of the DR to deformed nuclei, such as ^{27}Al and ^{59}Co. In earlier work we made preliminary calculations which showed that the strength of the spin-spin potential obtained in fitting the spin-spin data is sensitive to the inclusion of dispersive terms. Because of this, we developed a spherical OM for ^{27}Al with the DR as a constraint. The model gives a moderately good description of the differential cross-section data (fig. 4.3-1) over the range 7-26 MeV, the latter being the highest energy at which $\sigma(\theta)$ data are available. Analyzing-power data from TUNL at 14 and 17 MeV were also used in developing the DOM, as shown in fig. 4.3-2. These latter data, which were helpful in constraining the spin-orbit parameters, are also moderately well described. Table 4.3-1 lists the parameters of our potential. Here V_{HF} is the Hartree-Fock potential of the nuclear mean field and is shown in fig. 4.3-3.

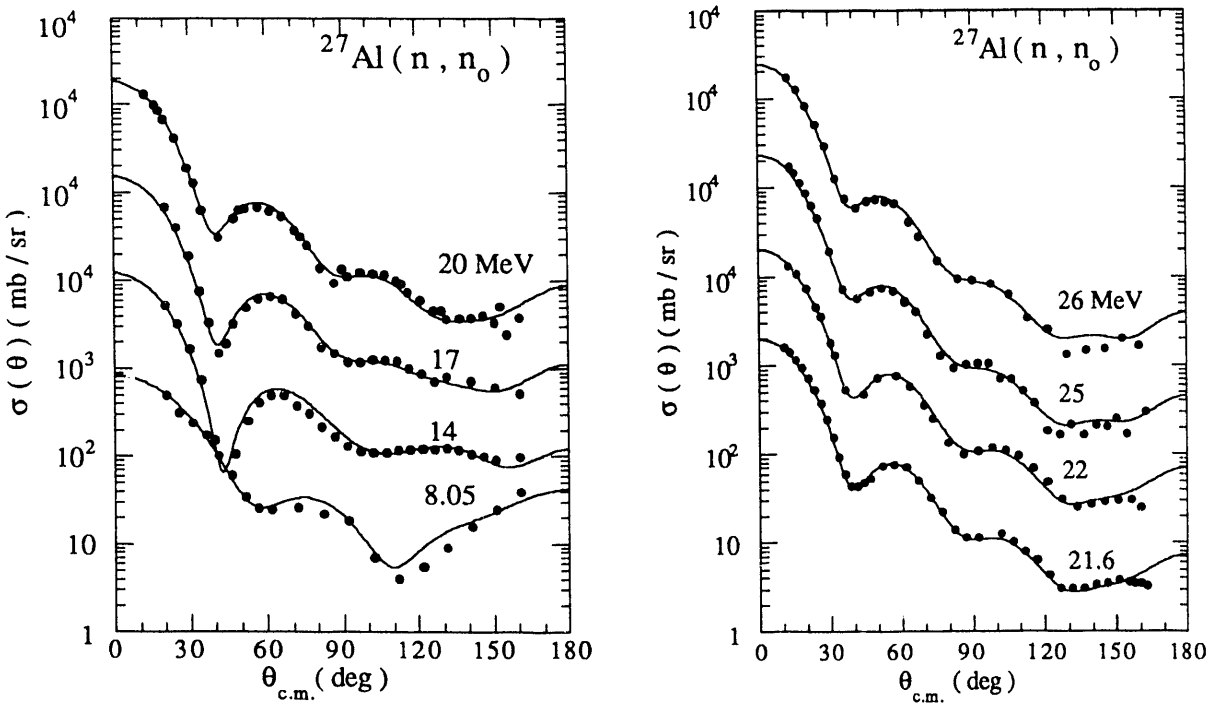

Fig. 4.3-1 Differential cross section using DOM.

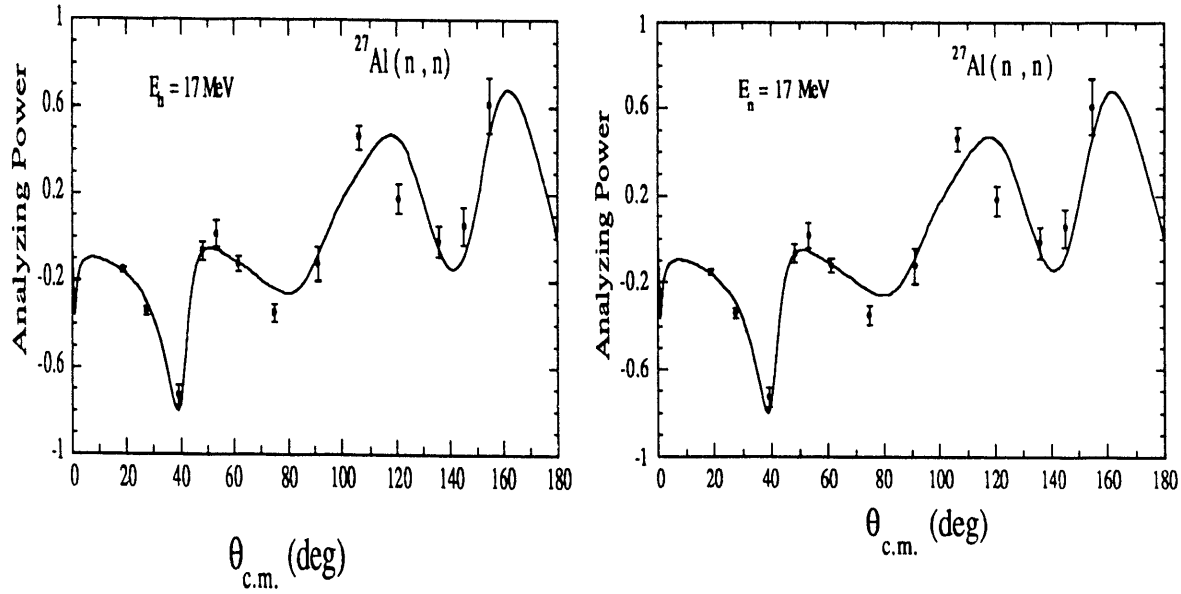

Fig. 4.3-2 The analyzing power fits at 14 and 17 MeV.

Figure 4.3-4 shows the dispersive corrections calculated from the imaginary volume and surface potentials of the mean field. The extension of the DOM to bound states is one of the main advantages of the DR approach; however due to the deformation of the ^{27}Al nucleus, bound states are severely fragmented. In addition, the Fermi energy as defined by Johnson [Joh87] and others loses its meaning due to the overlapping of the bound states in ^{27}Al. For this reason, we considered only the deeply-bound $1s_{1/2}$ states of ^{27}Al and ^{28}Si, which lie around –50 MeV, as shown in fig. 4.3-4.

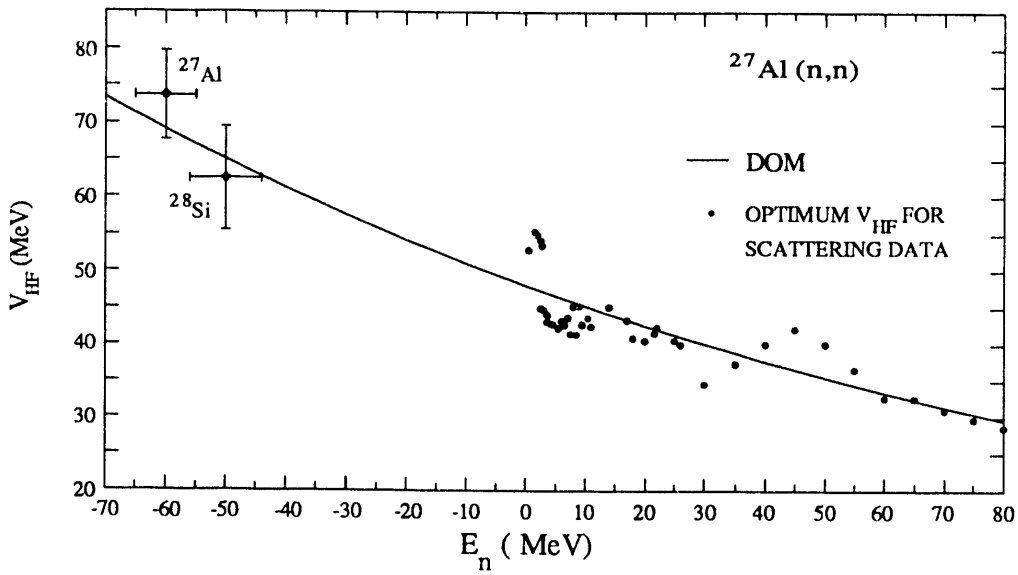

Fig. 4.3-3 Hartree-Fock potential

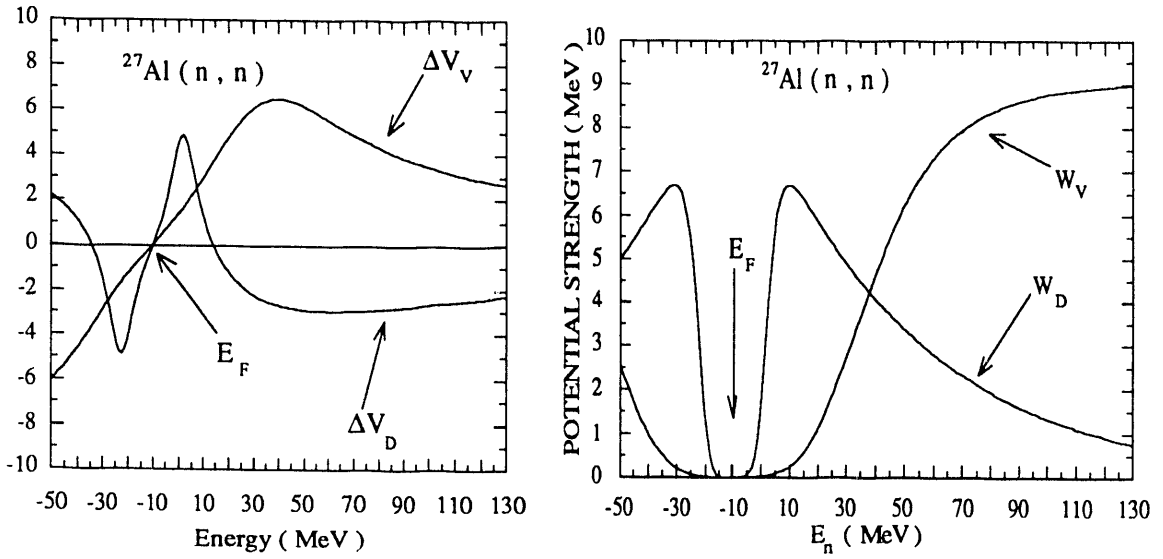

Fig. 4.3-4 The dispersive volume, and surface term. The absorptive surface and volume terms.

Table 4.3-1 Dispersive optical model parameters[a] for ^{27}Al(n,n)^{27}Al.

$V(r,E) = V_{HF}(r,E) + \Delta V(r,E)$

$V_{HF} = V_{HF}(E)\ f(r)$

$V_{HF}(E) = V_{HF}(E_F) \exp[-a\,(E - E_F)/V_{HF}(E_F)]$

$f(r) = [1+\exp((r-R_{HF})/a_{HF})]^{-1}$

$V_{HF}(E_F) = 51.163, \quad a = 0.31, \quad r_{HF} = 1.19, \quad a_{HF} = 0.66$

$W_V = a\,(E - E_F)^4 / [(E - E_F)^4 + b^4]$

$a = 9.13, \quad b = 50.0, \quad E_F = -10.39$

$W_D = g\,(E - E_F)^6 \exp(-c\,(E - E_F)) / [(E - E_F)^6 + h^6]$

$g = 10.413, \quad h = 12.98, \quad c = 0.0186$

$r_D = 1.28, \quad a_D = 0.55, \quad V_{so} = 5.70, \quad r_{so} = 1.00, \quad a_{so} = 0.41$

a) Potentials are in MeV and geometry parameters are in fm.

Although the dispersive DOM fit for the total cross section gives a very good description of the data at $E_n > 7$ MeV, the data below 5 MeV are not fit as well (see fig. 4.3-5). This total cross-section discrepancy is symptomatic of many DOM studies so far, but the problem seems to be the worst for the light nucleus ^{27}Al. This fact is attributed partially to angular-momentum dependencies and to reorientation effects.

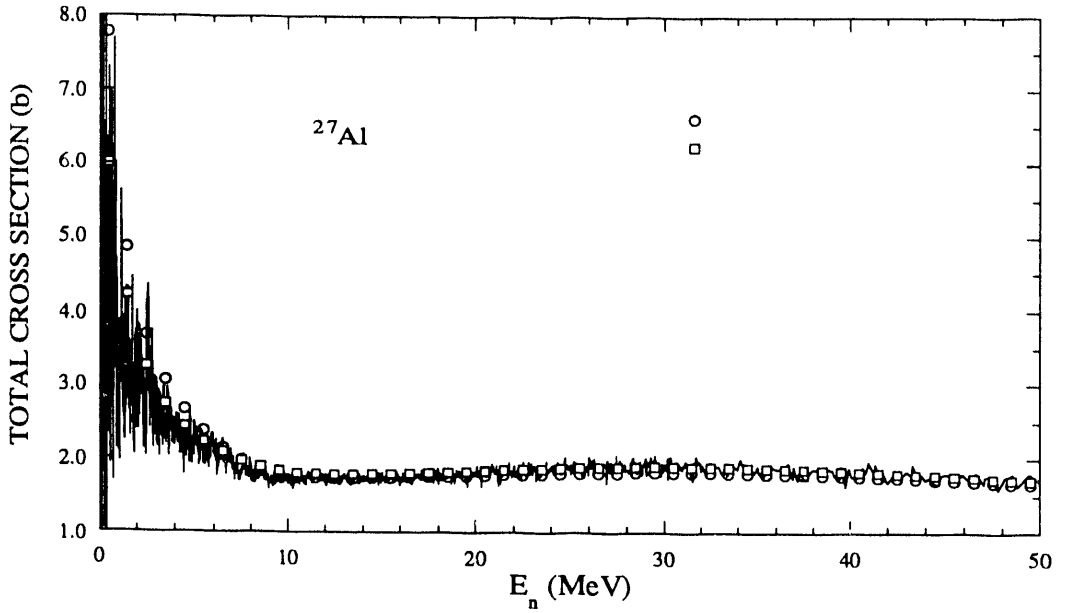

Fig. 4.3-5 Total cross section fits.

To investigate the problem of fitting the total cross section at low energy, a simple coupled channel model was developed that included only the coupling of the ground state to itself (reorientation effect). Starting with the CCM of ^{28}Si(n,n)^{28}Si by Howell *et al.* [How88], we obtained a model (table 4.3-2) that improved the description of the total cross section data at low energy, as shown in fig. 4.3-5.

Table 4.3-2 Coupled-channel model parameters[a] for ^{27}Al(n,n)^{27}Al.

$U(r_v,E)= V(E)\ f(r_v)$
$V(E) = 53.61 - 0.29 * E$
$f(r_v)= [1+\exp((r_v-R)/a_v)]^{-1}$
$r_v = 1.15, \quad a_v = 0.65$
$W_v = a\,(E - E_F)^4 /[(E - E_F)^4+b^4]$
$a = 9.13, \quad b = 50.0, \quad E_F = -10.39$
$W_D = g\,(E - E_F)^6 \exp(-c\,(E - E_F))/[(E - E_F)^6+h^6]$
$g = 10.413, \quad h = 12.98, \quad c = 0.0186$
$r_D = 1.25, \quad a_D = 0.58, \quad V_{so} = 5.7, \quad r_{so} = 1.0, \quad a_{so} = 0.41$

a) Potentials are in MeV and geometry parameters are in fm.

From our calculations of the spin-spin total cross section with both DOM and CCM for ^{27}Al we found that both give qualitatively a good description of the data except at 7.6 MeV. The results are compared to the data of Gould *et al.* [Gou86], and Heeringa *et al.* [Hee89] in fig. 4.3-6; except for the datum at 7.6 MeV, the data are qualitatively reproduced with a

surface spin-spin potential of strength of V_{SS} = 1.5 MeV, W_{SS} = 0 MeV, r_{SS} = 1.0 fm, and a_{SS}=0.654 fm for the coupled channel calculation. For the dispersion-model calculation we used a surface V_{SS} = 0.8 MeV, r_{SS} = 1.0 fm and a_{SS} = 0.654 fm. It is interesting to see that the calculated spin-spin cross section starts to decrease around 3 MeV, and then becomes negative at about 2 MeV (this behavior is similar to the behavior of ^{59}Co spin-spin cross section). This behavior would be a good motive for future spin-spin measurements up to 7 MeV.

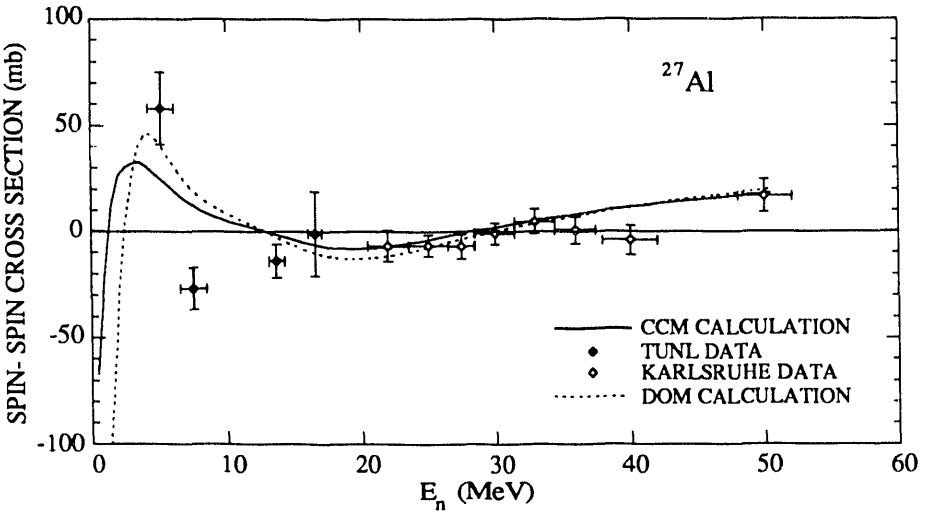

Fig. 4.3-6 Calculated spin-spin cross section.

Dispersive optical model and coupled channel model for n+^{59}Co

As for ^{27}Al, finding a good model for n+^{59}Co to describe the spin-spin cross-section data, especially at low energy, was the main motivation for this work. The spin-spin cross section for ^{59}Co was measured from 250 keV to 31 MeV by Heeringa *et al.* [Hee76,77] and by Fisher *et al.* [Fis72]. In developing a DOM and a CCM for ^{59}Co, we used total and differential cross-section data, as well as polarization data of the Stuttgart group.

A coupled-channel model was developed for ^{59}Co, starting from the coupled channel-model of Pedroni *et al.* [Ped88] for ^{58}Ni. Figure 4.3-7 shows the fit to $\sigma(\theta)$ using our model. A dispersive optical model is being developed. Both the DOM and the CCM will be used to calculate the spin-spin cross section for ^{59}Co in the same manner as for ^{27}Al.

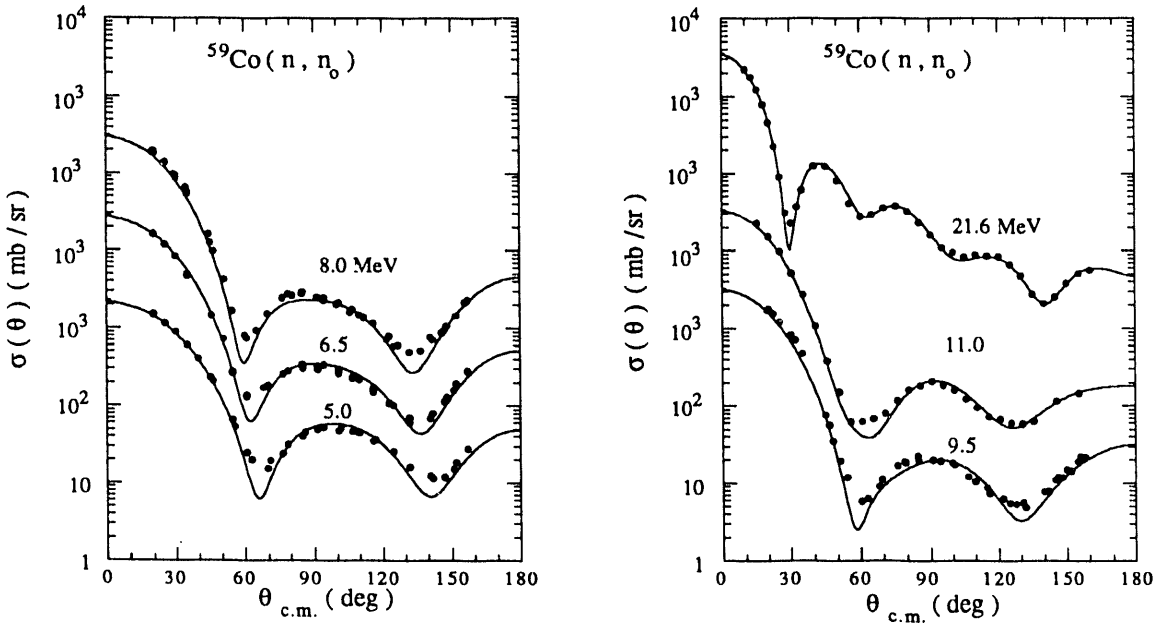

Fig. 4.3-7 Differential cross section fits using CCM.

Measurement of $\sigma(\theta)$ and $A_y(\theta)$ for ^{27}Al and ^{59}Co

M.M. Nagadi, M.Al-Ohali, G. Weisel, R. Setze, C.R. Howell, W. Tornow, R.L. Walter, J. Lambert[1]

In order to improve the models for neutron scattering from ^{27}Al and ^{59}Co, high accuracy $\sigma(\theta)$ and $A_y(\theta)$ measurements were performed at 15.5 MeV for both nuclei. In addition, high-accuracy $\sigma(\theta)$ data for ^{59}Co were obtained at 10, 12 and 14 MeV. The results of a preliminary analysis of the data for ^{59}Co are shown in fig. 4.3-8. More $\sigma(\theta)$ measurements at higher energies are planned for ^{59}Co to provide data for extending our analysis.

The measurement for $A_y(\theta)$ will also be extended to larger angles, where $\sigma(\theta)$ is small. However, in order to make these latter measurements to good statistical accuracy, it will be necessary to complete the development of a pre-bunching system for the TUNL Intense Polarized-Ion Source.

[1] Department of Physics, Georgetown University.

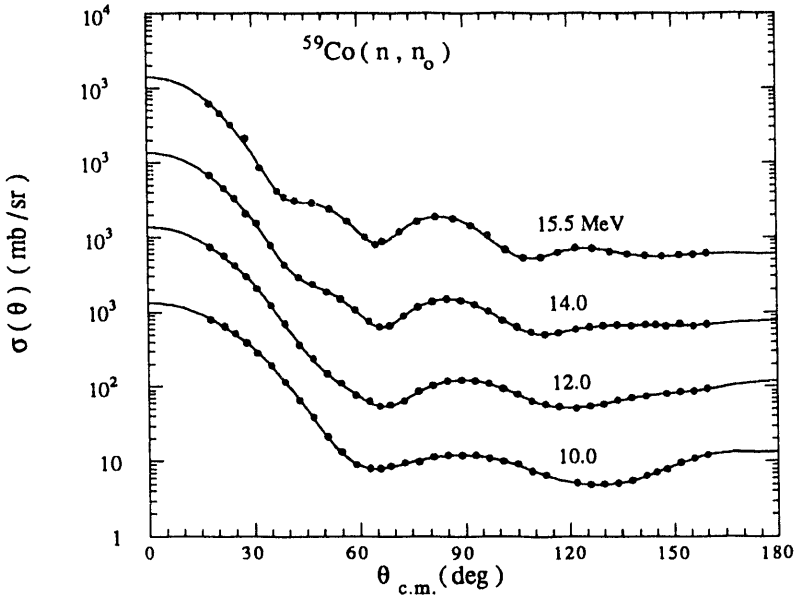

Fig. 4.3-8 Preliminary analysis of the experimental data. Curves are Legendre polynomial fits.

[Fis72] T.R. Fisher *et al.*, Nucl. Phys. **A179** (1972) 241
[Gou86] C.R. Gould *et al.*, Phys. Rev. Lett. **57** (1986) 2371
[Hee76] W. Heeringa *et al.*, Phys. Lett. **61B** (1976) 350
[Hee77] W. Heeringa *et al.*, Phys. Rev. **C16** (1977) 1389
[Hee89] W. Heeringa *et al.*, Phys. Rev. Lett. **63** (1989) 2456
[Hni87] V. Hnizdo *et al.*, Phys. Rev. Lett. **59** (1987) 1892
[How88] C.R. Howell *et al.*, Phys. Rev. **C38** (1988) 1552
[McA90] T. L. McAbee *et al.*, Nucl. Phys. **A509** (1990) 39
[Joh87] C.H. Johnson *et al.*, Phys. Rev. **C36** (1987) 2252
[Tho76] W.J. Thompson, Phys. Lett. **65B** (1976) 309
[Ped88] R.S. Pedroni *et al.*, Phys. Rev. **C38** (1988) 2052

4.3.3 The Nuclear Mean Field for n+^{28}Si between –60 and 80 MeV

M.A. Alohali, C.R. Howell, W. Tornow, R.L. Walter

Previously, Howell *et al.* [How88] reported a conventional spherical optical model (SOM) analysis of n+^{28}Si in the energy range from 8 to 40 MeV. The model gave a good representation for $\sigma(\theta)$ and $A_y(\theta)$ for both observables and for the total cross section σ_T. One constraint in the SOM, which followed the procedure that was conventional at that time, was that the strength of the surface and volume absorptive terms varied linearly with energy. Such approximations appear to be quite satisfactory for analyses when the projectile energy is greater than 8 MeV and the energy range is not too large. However, with such energy dependences the OM of [How88] fails to properly predict σ_T below about 5 MeV.

One advantage of the newer DOM formulation that ties the strength of the absorptive potential to the Fermi energy, E_F, is that the absorptive potential can be constrained to drop to zero at $E = E_F$ in a smooth fashion (as is expected from basic principles) and can be well represented by a simple energy-dependent function.

We applied the DOM method to the n+^{28}Si system. The data base consisted of $\sigma(\theta)$, $A_y(\theta)$ and σ_T data measured at TUNL and at many other labs. The energy range for $\sigma(\theta)$ extended from 2 to 40 MeV, for $A_y(\theta)$ from 10 to 17 MeV and for σ_T from 0.2 to 80 MeV. In order to search on this large data base, the global search code GENOA was modified to include the dispersion-relation correction terms given in section 4.3.1. We find that the DOM gives a fairly good description of σ_T up to 80 MeV. It gives less overestimation of σ_T than the SOM for E< 6 MeV. The fits to the $\sigma(\theta)$ and $A_y(\theta)$ data are moderately good and of similar quality to those of [How88] whose data base started at 8 MeV.

The DOM potential is of the same form as given in section 4.3.2 with an exponential E-dependence for $V_{HF}(r,E)$ and powers of 4 and 6 for $W_V(E)$ and $W_D(E)$, respectively. The parameters that describe the n+^{28}Si data are given in table 4.3-3.

Table 4.3-3 DOM parameters for ^{28}Si(n,n)^{28}Si.

V_{HF} (E_F)= 54	a = 0.54	r_{HF} = 1.17	a_{HF} = 0.69
a = 11.8	b = 73.3	E_F = -12.826	
g = 10.4	h = 6.3	c = 0.013	
r_D = 1.31	a_D = 0.57		
V_{so} = 5.8 - 0.015 E_n	r_{so} = 1.09	a_{so} = 0.5	

Here the potential strengths and energies are in MeV and geometries in fm.

An advantage of the DOM is the possibility of predicting bound-state properties by extending the model into the negative-energy (shell-model) region. However, in many cases the deformation of a nucleus such as ^{28}Si causes the single-particle states to be fragmented. One major problem is that the sum of the measured strengths does not always exhaust the expected shell-model sum rule. This fragmentation leads to difficulties in determining the centroid energies of the states. Nevertheless, we used as much information from the literature as could be obtained from stripping and pickup reactions on ^{28}Si [Endt 78] and from the (e,e'p) reaction [Fru84].

A comparison of the observed levels and the predicted levels with the DOM parametrized above is shown in fig. 4.3-9. The model gives reasonably close predictions of the energies of some of the levels, in particular of the particle states and the deepest hole state ($1s_{1/2}$), the latter of which is expected to have less fragmentation than other states.

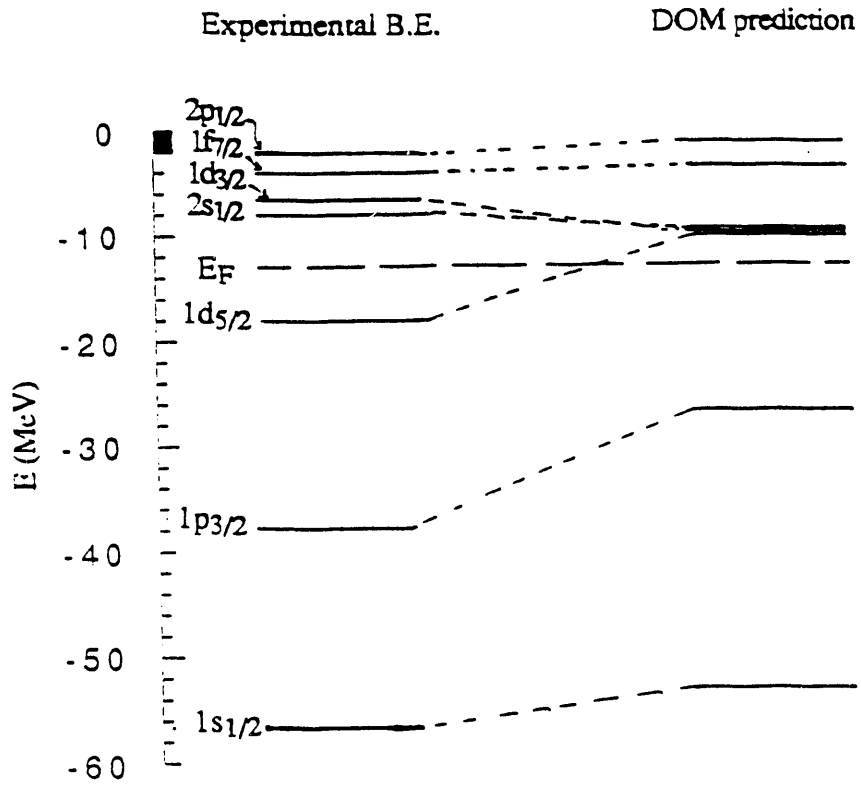

Fig. 4.3-9 Comparison of the neutron single-particle and single-hole levels predicted by DOM with the empirical values for n+^{28}Si.

Another approach to study the bound states energies in relation to the V_{HF} potential is to compare V_{HF} in the negative-energy range to that deduced from calculations which yield the empirical bound-state energies. That is, these latter calculations use the bound-state energies as well as the ΔV_V, ΔV_D and V_{so} of our DOM to predict the value that V_{HF} would have to be in order to place a calculated DOM state at the empirical value. In fig. 4.3-10 the energy dependence of our $V_{HF}(E)$ is shown (solid curve) alongside the V_{HF} for exact bound-state values (solid circles). As expected from the calculation above, the DOM prediction gives reasonable values for most of the particle states and for the deepest hole state; it underpredicts V_{HF} for the other hole states by a sizable amount.

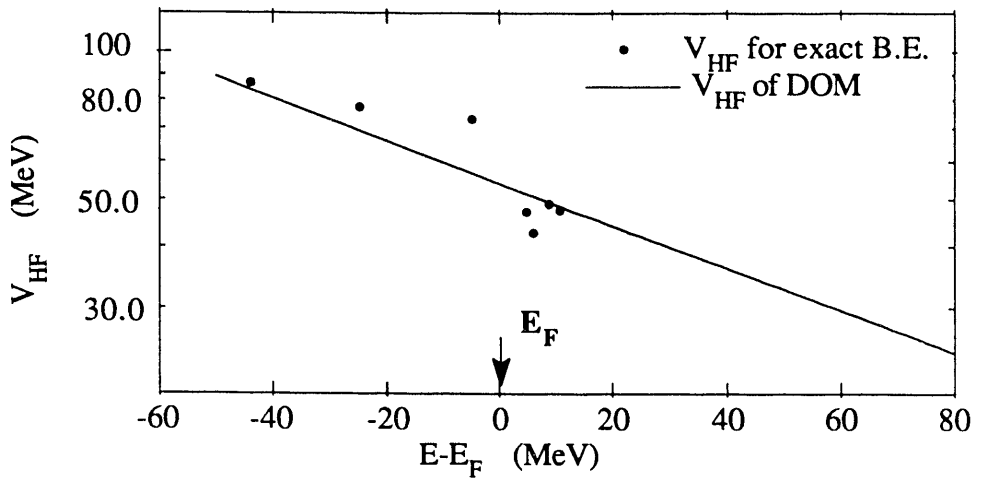

Fig. 4.3-10 Energy dependence of the depth of the Hartree-Fock potential V_{HF}.

We plan to investigate other energy dependences for $V_{HF}(E)$, W_D and W_V. We will also investigate p+^{28}Si scattering and use the large data base available for this reaction to give insight into the dispersion relation and Coulomb corrections.

[Endt78] Nucl. Phys. **A310** (1978) edited by P.M. Endt and Van Der Leun
[Fru84] S. Frullani and J. Mougey, Advances in Nuclear Physics **14** (1984) 194
[How88] C.R. Howell *et al.*, Phys. Rev. **C38** (1988) 1552

4.3.4 The n+^{93}Nb Interaction: Conventional and Dispersion Optical Models

R.L. Walter, R.S. Pedroni, C.R. Howell, M. Cheves, Z.M. Chen, G. Weisel, W. Tornow

A paper reporting our measurement of $\sigma(\theta)$ and $A_y(\theta)$ from 8-17 MeV and a conventional spherical OM analysis of the data was published in Phys. Rev. **C43** (1991) 2336. The abstract follows:

Differential cross sections and analyzing powers for neutron elastic scattering from ^{93}Nb have been measured at energies from 8 to 17 MeV using pulsed-beam time-of-flight methods. These data plus total cross-section data from 1 to 20 MeV are interpreted in terms of the spherical optical model. Several sets of optical potential parameters with systematic energy dependences have been derived in searches that used different initial parameter sets. In addition, comparisons of the data to calculations based on previously reported optical potentials are presented. It is concluded that the data favor the inclusion of a small imaginary spin-orbit term.

We have extended our interpretation of these data in the more exact framework of the DOM, to allow for energy dependencies in the potential parameters that are not inherent to the conventional spherical OM, and to test the model by comparing predictions of the model to known bound-state energies. Recently, Finlay and co-workers [Fin91] reported on total cross-section, σ_T, measurements from 5 to 100 MeV and we have formed a collaboration with him and P. W. Lisowski of LANL to include these data in the DOM analysis. Our analysis also includes $\sigma(\theta)$ and σ_T data from Smith *et al.* at ANL and data from several other labs.

We find that the DOM gives a good description of the data base (see figs. 4.3-11,-12,-13). Because we recently introduced the dispersion relation explicitly into our search code GENOA, and also sped up the integration for the dispersive corrections by using analytic forms of them, we are able to investigate sensitivities and parameter space in a more detailed fashion than has been possible before. The ^{93}Nb data base seems well-matched for DOM studies, in that the agreement shown in the figures is as good, if not better, than any DOM model for any other nucleus to date. Another reason for an in-depth study of ^{93}Nb is that it is an intermediate-mass nucleus and will allow comparisons of systematics that might exist between our studies of heavier nuclei (^{120}Sn, ^{208}Pb) and lighter nuclei (^{28}Si, ^{40}Ca).

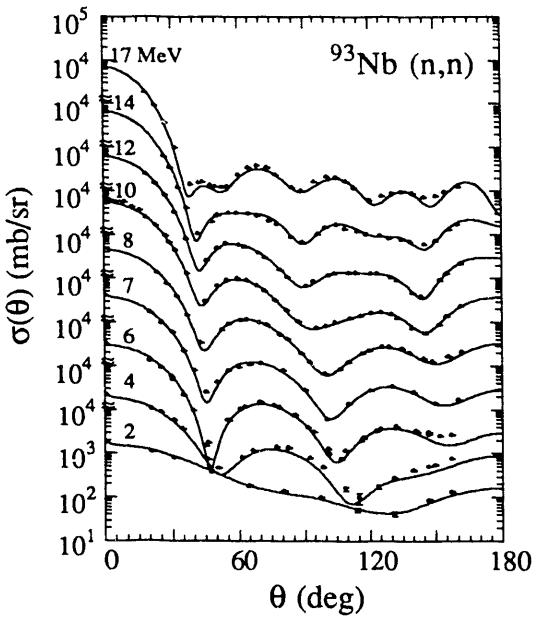

Fig. 4.3-11 The $\sigma(\theta)$ data compared to DOM calculations.

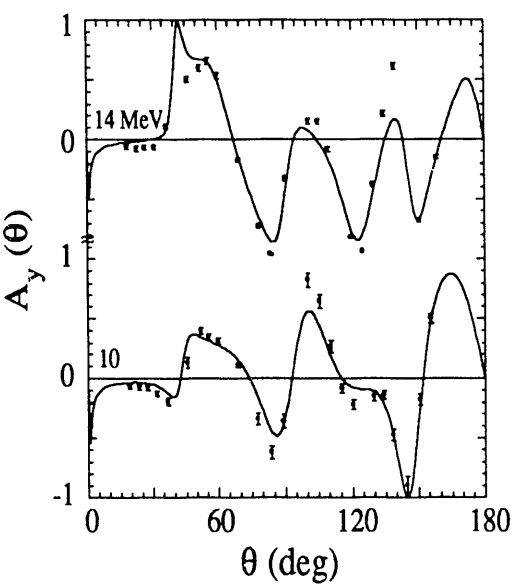

Fig. 4.3-12 The $A_y(\theta)$ data compared to DOM calculations.

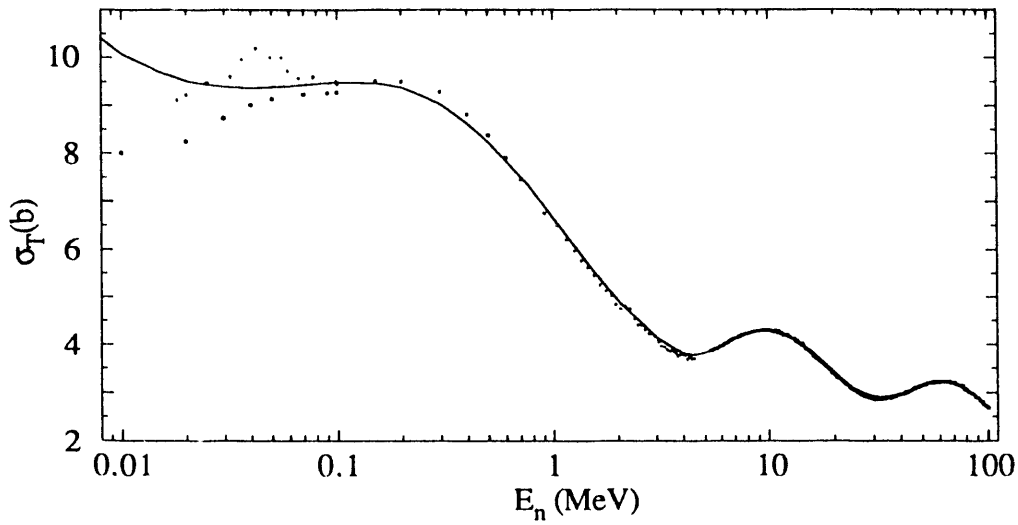

Fig. 4.3-13 The total cross section data comaped to DOM calculations.

[Fin91] R.W. Finlay *et al.*, Nuclear Data for Science and Technology, Jülich, Germany (1991) (to be published)

4.3.5 Dispersive Optical-Model Analysis for n+^{120}Sn

R.L. Walter, C.M. Cheves, Z.M. Chen, G. Weisel, W. Tornow

As for ^{93}Nb, spherical OM analyses have been made previously at a number of laboratories, including TUNL, where $\sigma(\theta)$ and $A_y(\theta)$ have been measured from 10 to 17 MeV. We have initiated a DOM analysis of these data in order to connect the wealth of scattering information up to 80 MeV with known bound-state energies at negative energies. The ^{120}Sn scattering data appear to be compatible with a DOM model whose parameters fall in a reasonable range when compared to those for ^{93}Nb and ^{208}Pb. The preliminary results for predicting bound-state energies look encouraging.

4.3.6 Improvements to Optical-Model Software and Analysis of n+^{208}Pb and n+^{209}Bi

G.J. Weisel, M.L. Roberts, W. Tornow, C.R. Howell, R.L.Walter

Over the past four years, TUNL has added significantly to the data base for ^{208}Pb(n,n) and ^{209}Bi(n,n). The work of Roberts *et al.* [Rob91] produced ^{208}Pb(n,n) cross-section data for 8.0 MeV and analyzing power, A_y, data for 6.0, 7.0, 8.0, 9.0, and 10.0 MeV. In addition, we have completed detailed A_y measurements of ^{209}Bi(n,n) at 6.0 and 9.0 MeV. We recently initiated a project to produce improved optical-model descriptions for these nuclei using the new data and new developments in computer hardware and software. While the new system of networked micro-VAX workstations recently installed at TUNL has greatly enhanced computing power, considerable effort has been expended on our main

optical model (OM) search code GENOA and other support software to incorporate the formalism of the dispersive optical model (DOM).

Our new version of GENOA makes it possible to search on the parameters describing the energy dependence of the imaginary volume (W_V) and surface (W_D) potentials. For each choice of W_V and W_D parameters, the code makes the dispersion relation integrations to obtain the two dispersive contributions to the real potential, ΔV_V and ΔV_D. We have taken the approach of treating W_V and W_D as we would any other OM parameters: to vary them to optimize the fit of the OM to the data. To expedite these OM parameter searches, many of the dispersion integrals have been evaluateded in closed form, as reported by Vanderkam in section 4.3.1. With this new software, all searches may be accomplished automatically and a minimum in chi-squared space found efficiently.

The project underway will make improvements over recent DOM analyses of ^{208}Pb(n,n) and ^{209}Bi(n,n). Roberts *et al.* [Rob91] reported a ^{208}Pb(n,n) DOM with a linearly segmented energy dependence for the imaginary volume and surface potentials, which is less physically reasonable than the continuous functions which our model will use. Secondly, because of the previous software complications in handling ΔV_V and ΔV_D, both the studies of Roberts *et al.* for ^{208}Pb(n,n) and of Das and Finlay [Das91] for ^{209}Bi(n,n) make only one iteration between the determination of dispersive corrections and the determination of the Hartree-Fock field. With the new GENOA software described above, further iterations are easily accomplished.

A third improvement we have made is to prepare two new OM data sets for ^{209}Bi(n,n) and ^{208}Pb(n,n), spanning the energy range 0.8 to 80.0 MeV. For ^{209}Bi we have included the new TUNL A_y data at 6.0 and 9.0 MeV as well as the new total cross-section data of Finlay *et al.* [Fin91]. In addition, the OM data sets for both ^{208}Pb and ^{209}Bi were corrected for the presence of compound nucleus (CN) contributions to the elastic channel by using a new TUNL analysis of CN reactions. As described in TUNL XXIX (section 4.7.3), these calculations are made more physical through the use of A_y data.

We have also developed a new version of OPSTAT, a CN code obtained from Ohio University. Our choice of OPSTAT was motivated by the fact that it includes the most recent width-fluctuation corrections, particularly those due to Moldauer [Mol80]. Our contribution was to cast OPSTAT in the DOM parametrization so that our DOM potentials may be used in CN calculations. This enables a feed-back loop which insures that the final DOM yields a CN correction consistent with the OM data set.

A DOM analysis enables the prediction of bound-state quantities, by extrapolating the real part of the potential derived in the analysis of scattering states to negative energies. We have automated a bound-state code, obtained from C.H. Johnson of ORNL, to enable quick and efficient comparison of predictions of bound-state quantities for different versions of scattering DOM potentials. Our version of the code can also determine the Hartree-Fock field for each bound state such that the experimental binding energy is reproduced. Using these results, an iteration is done between the bound and scattering-state parameters: after compromising between the requirements of the Hartree-Fock field for the bound and scattering states, the scattering data are used to re-tune all the OM parameters,

after which the bound-state predictions are checked again. This process may be repeated efficiently with the new computer codes now in place.

This work on state-of-the-art DOM analyses of ^{208}Pb(n,n) and ^{209}Bi(n,n) is now underway. We expect these analyses to be sufficiently thorough that definitive conclusions may be drawn, demonstrating the subtle similarities and differences between the ^{208}Pb(n,n) and ^{209}Bi(n,n) systems.

[Rob91] M. Roberts *et al.*, Phys. Rev. C (in press)
[Das90] R.K. Das and R. Finlay, Phys. Rev. C **42** (1990) 1013
[Fin91] R. Finlay *et. al.*, Nuclear Data for Basic and Applied Science (1991) Jülich, Germany, Proceedings (to be published)
[Mol80] P.A. Moldauer, Nucl. Phys. **A344** (1980) 185

4.4 Nuclear Scattering Phenomena

We have investigated several nuclear scattering phenomena during the past year, with the goal of improving our understanding of the interaction mechanisms, especially their spin dependence.

4.4.1 Microscopic Description of Nucleon-Nucleus Scattering for A=6-208 from 8 to 80 MeV

R.L. Walter, L.F. Hansen[1], F.S. Dietrich[1]

For several years we have had a project to study the suitability of microscopic models for describing $\sigma(\theta)$ and, in particular, $A_y(\theta)$ data for elastic neutron scattering obtained at TUNL. We have investigated data for about 20 isotopes in the range A=6–208. For some of the cases we also studied (p,p) data to obtain a measure of the isovector dependence of the real and imaginary terms of the microscopic potentials.

At present we are determining local averages of the scale factors for the strengths of the real, imaginary, and spin-orbit potentials for the effective interactions of Jeukenne, Lejeune and Mahaux, and of Yamaguchi, Nagata and Matsuda. We have found the Brieva and Rook interaction to be inferior to these two interactions. A status report of this project will be given at the Beijing International Fast Neutron Physics Conference in September 1991.

---

[1] Lawrence Livermore National Laboratory

4.4.2 Polarized-Neutron / Polarized-^{93}Nb Scattering and the Tensor Spin-Spin Potential

J.P. Soderstrum[2] , *C.R. Gould, D.G. Haase, N.R. Roberson, M.B. Schneider*[3] , *L.W. Seagondollar*

Spin-spin effects in nucleon-nucleus scattering may be analyzed in terms of central and tensor potentials given by:

$$U_{10}(\mathbf{r}) = -F_{10}(\mathbf{r})\hat{\mathbf{I}}\cdot\hat{\mathbf{s}} \tag{1}$$

and

$$U_{12}(\mathbf{r}) = -F_{12}(\mathbf{r})\,[3(\hat{\mathbf{I}}\cdot\hat{\mathbf{r}})(\hat{\mathbf{s}}\cdot\hat{\mathbf{r}})-(\hat{\mathbf{I}}\cdot\hat{\mathbf{s}})]\,/2 \tag{2}$$

where **I** is the target spin, **s** is the nucleon spin, **r** is the nucleon-nucleus separation vector, and F_{10} and F_{12} are the central and tensor radial form factors. Recent proton-depolarization measurements[Nak90] and polarized-neutron, polarized-target transmission measurements [Hee89] have indicated that the tensor potential could be large, of order 0.8 MeV or more. However, the measurements do not readily distinguish between the effects of the central and tensor terms. Solutions with predominantly central potentials also gave reasonable accounts of the data.

A technique for resolving this ambiguity involves polarized-neutron, polarized-target transmission in two geometries: transverse (with spins perpendicular to the beam direction) and longitudinal (with spins parallel to the beam direction). The central contribution is the same in the two geometries, but the tensor contribution changes in sign and magnitude between transverse and longitudinal. As a result the tensor contribution can be extracted unambiguously from the cross section difference between the two geometries.

We have carried out the first such two-geometry measurement at 7.5 MeV with polarized ^{93}Nb. We recently submitted the results for publication in Physics Review, along with an analysis of all existing spin-spin data in the literature. The ^{93}Nb longitudinal and transverse spin-spin cross sections were small, -2.2 ± 6.9 and -5.2 ± 5.3 mb respectively. In terms of the geometry used by Heeringa *et al.* [Hee89] the data imply a value of $V_{12} = -67 \pm 190$ keV and of $V_{10} = 460 \pm 460$ keV. The ^{93}Nb spin-spin data taken together are therefore well described by a predominantly central spin-spin potential of order 1 MeV, with a small tensor spin-spin potential of at most a few hundred keV.

We have compared the spin-spin potentials for ^{93}Nb to the potentials found for ^{13}C, ^{15}N, and ^{27}Al. Because of the differences in geometries, we consider volume integrals of the potentials rather than potential depths directly. In the valence model, the volume integral, J_{10}, of the central spin-spin potential V_{10}, is related to the volume integral, J_{ss}, of the central spin-spin term, v_{ss} of the effective nucleon-nucleon interaction [Sat71]. Explicitly:

$$J_{10} \equiv 4\pi V_{10} \int f(r)\, r^2 dr = -\,I/(\,l + 1/2)\, J_{\sigma\sigma} \tag{3}$$

---

[2] Present Address: E.G. and G Energy Measurements, PO Box 1912, Las Vegas, NV 89125
[3] Present Address: Physics Department, Grinnell College, Grinnell, IA 50112

We take J_{ss}(nn,pp) = 283 MeV.fm^3, and J_{ss}(np) = –213 MeV.fm^3 from the recent work of McAbee *et al.* [McA90). The comparison of the theoretical and experimental volume integrals J_{10} is given in table 4.4-1. The signs are in agreement. The experimental values tend to be slightly larger than the theoretical values, while for ^{13}C the values disagree by about a factor of two. However, Przewoski *et al.* [Prz90] pointed out that even a small amount of tensor potential, V_{12} = 25 keV, changed their central potential, V_{10}, solution drastically, from 350 keV to 250 keV. We conclude therefore that a smaller value of J_{10} is easily accommodated for ^{13}C, and similarly for the other nuclei.

Table 4.4-1 Volume integrals, J_{10}, in MeV.fm^3 for central spin-spin potentials in ^{13}C, ^{15}N, ^{27}Al, and ^{93}Nb. The theoretical values, J^{theory}_{10} in column 6 are calculated from Eq. (3), using J_{ss} values from [McA90]. The experimental values, J^{expt}_{10} in column 6 are calculated from unit normalized potentials, V_{10} derived from potentials given in [Nak90, Hee89, and Prz90].

Nucleus	I	l	J_{ss}	J^{theory}_{10}	J^{expt}_{10}
^{13}C	1/2	1	–213	71	140±20 [a]
^{15}N	1/2	1	283	–94	–133±7 [b]
^{27}Al	5/2	2	–213	213	237±98 [c]
^{93}Nb	9/2	4	–213	213	337±71 [c]

[a] [Prz90] [b] Set III from [Nak90] [c] [Hee89]

Interestingly, the overall agreement would have been poor using the early phenomenological value [Hus73] of J_{ss}(np) = –45 MeV.fm^3. It is clear that if the ambiguities between central and tensor contributions can be resolved, accurate depolarization and transmission measurements can show good sensitivity to the strength of the underlying spin-spin effective NN interaction

---

[Hee89] W. Heeringa *et al.*, Phys. Rev. Lett. **63** (1989) 2456
[Hus73] A.H. Hussein and H.S. Sherif, Phys. Rev. **C8** (1973) 518
[McA90] T.L. McAbee, W.J. Thompson and H. Ohnishi, Nucl. Phys. **A509** (1990) 39
[Nak90] T. Nakano *et al.*, Phys. Lett. **240B** (1990) 301
[Prz90] B. v. Przewoski *et al.*, Phys. Rev. Lett. **64** (1990) 368
[Sat71] G.R. Satchler, Part. Nuclei **1** (1971) 397

4.4.3 The Deuteron-Nucleus Tensor Interaction in $^{90}Zr(d,d)^{90}Zr$

D.J. Abbott, H.J. Karwowski, T.B. Clegg, E.J. Ludwig, E.R. Crosson, R.K. Das, S.K. Lemieux, K.A. Fletcher, T.C. Black, W.J. Thompson

An investigation into the form of, and possible contributions to, the deuteron-nucleus tensor interaction through measurement of polarization transfer observables (PTO) was completed in the past year. A complete description of $^{90}Zr(\vec{d},\vec{d})^{90}Zr$ and $^{90}Zr(d,p)^{91}Zr$ at 15 MeV, and of the analysis can be found in previous TUNL progress reports as well as in [Abb90a, Abb89]. We summarize here the results and comment on several issues concerning the finite-range coupled channels (FRCC) calculations described in last year's report [Abb90b].

Both an optical-model analysis and FRCC calculations coupling the elastic channel to several $^{90}Zr(d,p)^{91}Zr$ states were made. In the initial optical model calculations both the analyzing power A_{xz} and the PTO $K_y^{z'z'}$ were used almost exclusively to determine a form for the T_r tensor interaction. Table 4.4-2 shows the final optical model parameterizations determined from this analysis.

Table 4.4-2 Deuteron optical potential for $^{90}Zr(d,d)^{90}Zr$ at 15 MeV. The spin-orbit potential is the full Thomas form for both the real and imaginary terms. The real and imaginary tensor potentials are second and third derivative forms, respectively, taken from [God79].

	REAL			IMAGINARY		
POTENTIAL	DEPTH (MeV)	RADIUS (fm)	DIFFUSE (fm)	DEPTH (MeV)	RADIUS (fm)	DIFFUSE (fm)
Central	87.56	1.214	0.816	17.95	1.371	0.615
Spin-Orbit	5.15	0.70	0.54	2.07	0.71	0.35
T_r Tensor	4.00	1.40	0.45	2.00	1.21	0.70

The form of the T_r potential differs from previous analyses in that it is substantially stronger, particularly for the real part of the potential. Figure 4.4-1 shows the breakdown of contributions to the observables by the real and imaginary parts of the tensor interaction. It also serves to illustrate both the sensitivity that A_{xz} and K_A have to T_r as well as the supplementary nature of the information that they provide. K_A is sensitive to the magnitude of the tensor interaction, while the structure of A_{xz} is largely determined by interference between the the real and imaginary terms.

In a more sophisticated analysis we used a coupled-reaction-channels formalism in order to provide a quantitative measure of the spin dependent potential generated in the elastic channel from coupling to inelastic channels such as (d,p) and (d,n). Coupling to the (d,p) channel has been predicted to have a significant contribution to the T_r tensor interaction between the deuteron and nucleus [Tos87]. Another question to be considered was the effect of including non-orthogonal corrections to the FRCC calculations.

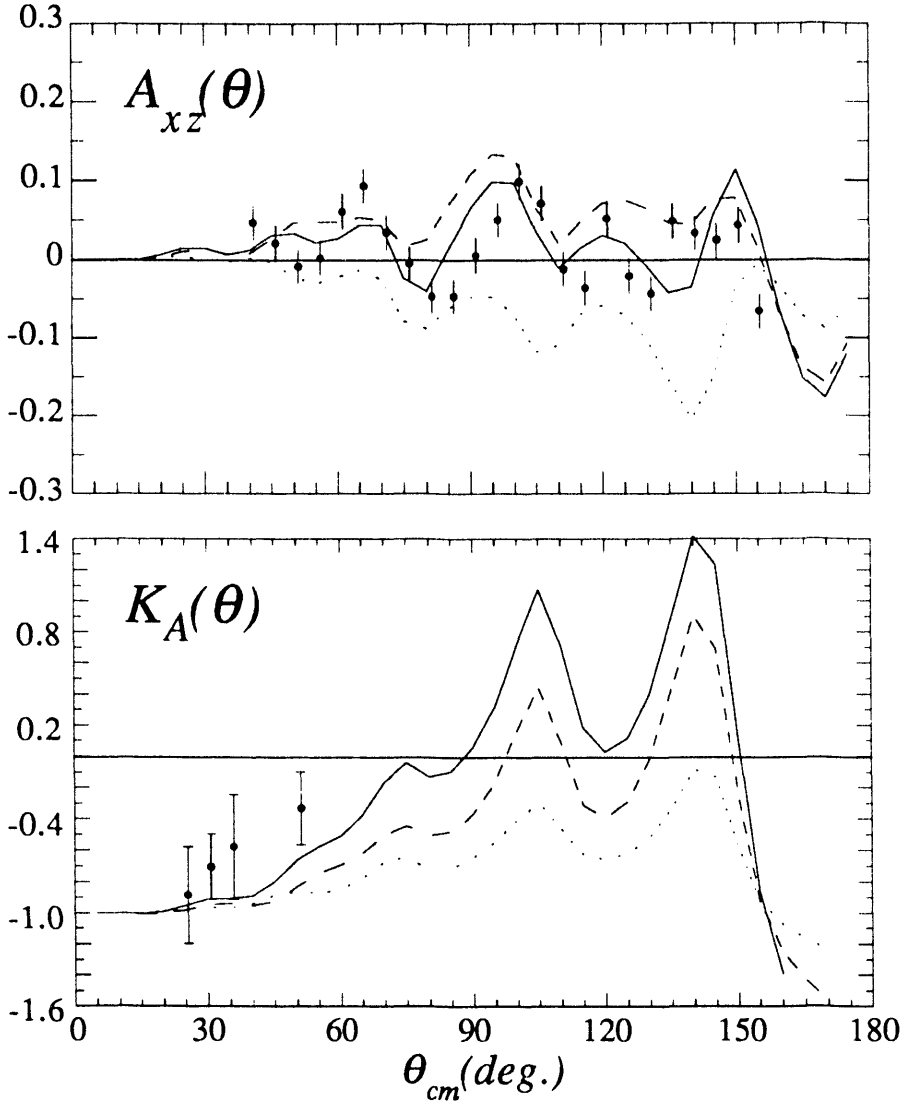

Fig. 4.4-1 Data for the observables A_{xz} and K_A for $^{90}Zr(\vec{d},\vec{d})^{90}Zr$ at 15 MeV are shown along with optical model calculations using the potential in Table 1. Effects of the T_r tensor potential are shown for the pure real (dashed), pure imaginary (dotted), and combined (solid) potentials.

Figure 4.4-2 shows the CC calculations for the observables A_{xz} and K_A, as well as an optical-model calculation with all explicit tensor dependence removed. In this manner, any changes in the tensor-sensitive observables may be associated primarily with the coupling. The first thing to note is that, while coupling effects are generally small, the addition of non-orthogonal corrections has an effect as large as the coupling itself. This result indi-

cates that in such calculations one should be careful in dismissing non-orthogonal corrections as a small perturbation.

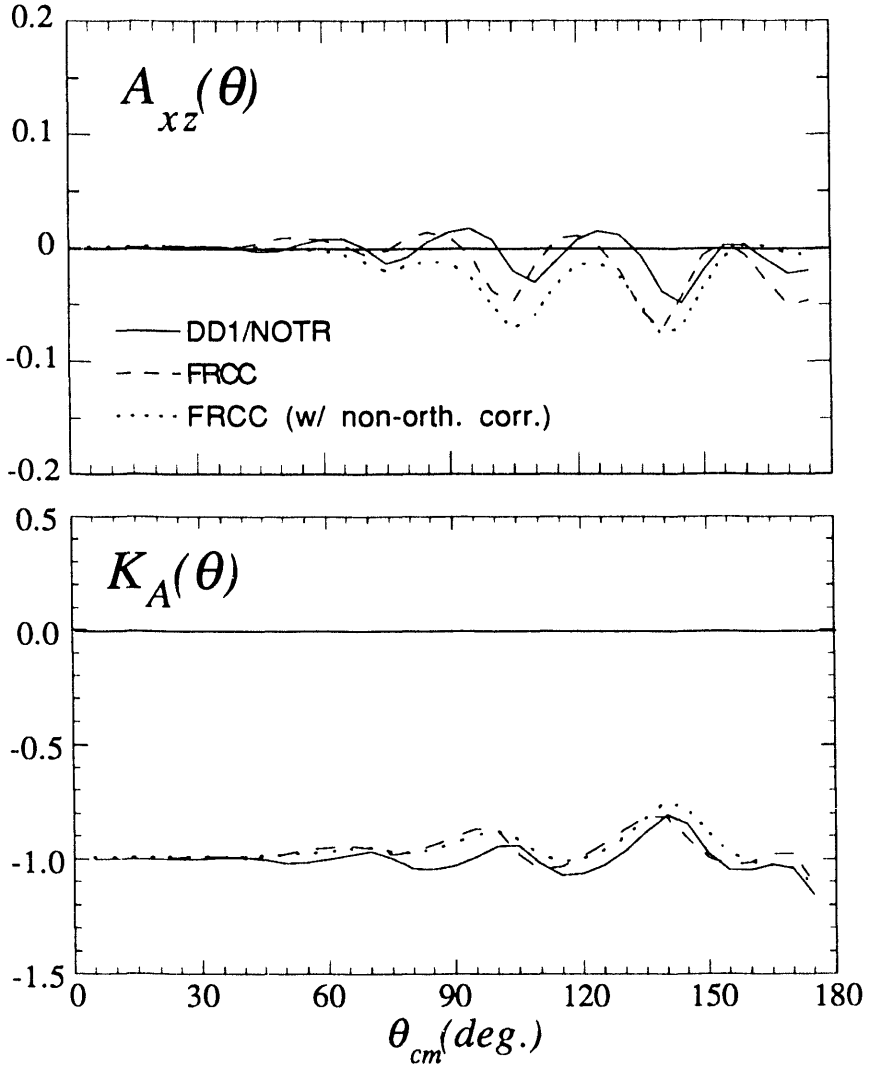

Fig. 4.4-2 T_r sensitive observables A_{xz} and K_A for $^{90}Zr(\vec{d},\vec{d})^{90}Zr$ at 15 MeV are shown, along with an optical model calculation using the potential in Table 1 with no T_r (solid curve), as well as finite-range coupled-channels calculations (coupling to the (d,p) channel) with and without non-orthogonal corrections (dotted and dashed curves respectively).

By examining the structure of both observables more closely, it can be seen that the CC effects can be associated with an imaginary T_r potential using a geometry similar to that in table 4.4-2 but having only about 15% of its strength. This is particularly encouraging

because these CC contributions are small perturbations to the direct elastic scattering potential, so one should essentially be able to add the CC-generated tensor potential to any explicit T_r potential included in the elastic channel.

[Abb89] D.J. Abbott *et al.*, Nucl. Inst. and Meth. **A284** (1989) 409
[Abb90a] D.J. Abbott, Ph.D. thesis, University of North Carolina at Chapel Hill, 1990 Available from University Microfilms International, Ann Arbor, Michigan
[Abb90b] D.J. Abbott *et al.*, TUNL Progress Report XXIV (1989-1990) 82
[God79] R.P. Goddard, Ph.D. thesis, University of Wisconsin, Madison, 1979 Available from University Microfilms International, Ann Arbor, Michigan
[Tos 87] J.A. Tostevin, Nucl. Phys. **A466** (1987) 349

4.5 Energy-Loss Phenomena and the Lewis Effect

G.E. Mitchell, C. Rolfs[1], H. Ebbing[2], W.H. Schulte[2], S. Wüstenbecker[2]

The quantized character of the energy loss of energetic charged particles in matter is manifested in the Lewis effect [Lew62] on the yield curves of narrow nuclear resonances. The standard signature of the Lewis effect is a peak in the thick target yield curve near the resonance energy, followed by a plateau. The physical basis for this effect is easily understood. Since the charged particles lose energy in discrete steps, some particles with an energy above the resonance will "jump over" the resonance and thence not contribute to the yield. This effect is only observed with very good energy resolution and with very clean targets.

As part of a continuing program oriented towards nuclear astrophysics and studies of chaotic properties of nuclear states, as well as for atomic and condensed matter applications, we have made major improvements [Wüs89] both in targetry (an ultra-high-vacuum target system constructed with many special features, such as *in situ* evaporation) and in the energy resolution characteristics of the 400-kV Münster accelerator, so that the ion beam resolution is now less than 20 eV. The energy resolution is such that we have observed larger Lewis effects in several solid targets than observed previously. The effects are so large that it becomes essential to quantitatively understand the Lewis effect in order to interpret the experimental data.

However, for these solid targets there is a large Doppler contribution. This Doppler contribution cannot be measured independently from the energy loss properties. The study of the Doppler broadening is of appreciable interest for condensed-matter applications. Since gas targets are free of the solid target complications, we decided to study the Lewis effect and the assoicated energy loss phenomena in a windowless gas target. This minimized the Doppler effects and provided a wide range of gas-target thicknesses by varying the gas pressure.

A promising reaction for studying these simultaneous atomic and nuclear excitations is $^{21}Ne(p,\gamma)^{22}Na$, where several narrow resonances occur below 300 keV. We have two

---

[1] Ruhr Universität Bochum
[2] Universität Münster

major results. The energy loss spectra were obtained for a variety of gas target thicknesses, ranging from ultrathin targets (less than one atomic monolayer) to rather thick targets. The data for very thin targets provide information on the atomic excitation mechanism at impact paramter b = 0, while studies on thick targets provide information on the energy-loss spectra of the projectiles integrated over all impact parameters b.

For thin targets the projectile passes through the electron cloud and with some probability knocks out an electron before forming the resonance; thus a replica or echo resonance should be formed. We clearly observe such an echo resonance. Naturally, for thicker targets the energy-loss process can take place in one atom at any impact parameter b and the nuclear reaction in another atom. In this case the relevant collision spectrum is the energy-loss spectrum integrated over all values of b. We observed a very pronounced Lewis peak for thick ^{21}Ne targets; this is the first observation of the Lewis effect in gas targets. The measured collision spectra were convoluted and integrated over target thickness to obtain the thick-target yield. The calculated curve is in excellent agreement with the data, including the magnitude of the Lewis peak. With these results one can now pursue both gas- and solid-target studies with confidence. Several papers on these results are now in preparation.

[Lew62] H. W. Lewis, Phys. Rev. **125** (1962) 937

[Wüs89] S. Wüstenbecker *et al.*, Nucl. Instrum. and Methods **A279** (1989) 448

4.6 Nuclear Data Evaluations for A = 3-20

D.R. Tilley, H.R. Weller, G.M. Hale[2], P. Atkinson, R. Huffman

The transfer of the project for evaluation of nuclear data in the mass range A = 5 – 20, carried out for many years by Professor Fay Ajzenberg-Selove at the University of Pennsylvania, has been completed during the past year, thus implementing the recommendation to DOE by the Panel on Basic Nuclear Data Compilations(PBNDC). As detailed below, TUNL carried out continuing literature coverage for A = 3-20, worked on the A = 16, 17 review and, in collaboration with Los Alamos, brought the review on A = 4 to completion. In August 1991 TUNL was able to fill the position of full-time editorial assistant for the project with a staff member (R. Huffman) who is now learning existing procedures and working along with the present editorial assistant (P. Atkinson) who will be leaving during the coming year.

A = 4 system. During the 1990-1991 period TUNL, in collaboration with Gerry Hale of Los Alamos National Laboratory, completed a preliminary version of the A = 4 review and prepared a preprint. The preprint was mailed out in May 1991. During the summer, revisions based on the responses received were carried out to complete the manuscript to be submitted in September 1991 for publication in Nuclear Physics A.

A = 5 - 20 systems. Since the recommendation by PBNDC, Professor Ajzenberg-Selove has worked closely with TUNL to insure a smooth and successful transfer. During late 1990 while she was carrying out her final review (A = 13 - 15) she transferred reference cards for each item, reprints, reports and conference proceedings, as well as original drawings of all level diagrams that are included in the A = 5 - 20 reviews. In addition, she

consulted extensively with Tilley and Weller at TUNL in response to numerous questions concerning procedures and policies. Her coverage of the literature continued through December 1990, at which time she provided full and up-to-date printouts and computer files of all reaction-by-reaction bibliographical lists for A = 5 - 20 and TUNL assumed the responsibility for further literature coverage and data compilations.

TUNL is preparing the review of the A = 16, 17 systems with the intention of completing most of the review during 1991. Tilley visited the National Nuclear Data Center at Brookhaven National Laboratory in June 1991 to learn the procedures for entering data for A = 5 - 20 into ENSDF format. During this visit NNDC installed the computer software onto the TUNL VAX to enable convenient ENSDF data entry at TUNL.

5. NUCLEAR INSTRUMENTS AND METHODS

In the past year we have completed improvements to several instruments at TUNL, such as the upgrading of the FN tandem Van de Graaff accelerator (section 5.1.2), and improvements to the KN Van de Graaff accelerator (section 5.2) and to the new Intense Polarized Ion Source (section 5.3). The Enge split-pole magnetic spectrometer is being installed with several enhancements (section 5.4), and a Compton-suppressed γ-ray spectrometer has been designed (section 5.5) and will soon be under construction. The Low Energy Beam Facility at TUNL is being developed (section 5.6) and is now being used routinely for experiments that need the intense, low-energy proton or deuteron beams from the new ion source.

Two instrumentation projects for CEBAF are underway – one is a contribution to the design and field-mapping of a magnetic spectrometer for Hall A, and the other is a Möller electron polarimeter for Hall B. These two projects are described in section 5.7.

Progress has been made in building, testing, and calibrating several detectors (sections 5.8.1, 5.8.2) and in constructing thermometers, targets, and detectors to be used at very low temperatures (sections 5.8.3 – 5.8.5).

Finally, an up-to-date workstation-based nuclear-physics network for data-acquisition and analysis, and for theoretical calculations, has been completed at TUNL and on each of the three campuses (section 5.9).

5.1 FN Tandem Accelerator Operation and Upgrade

C.R. Westerfeldt, E.P. Carter

5.1.1 Tandem Accelerator Operation

The TUNL FN tandem Van de Graaff accelerator operated a total of 3,400 hours during the period September 1, 1990, through August 31, 1991. The accelerator was shut down in October of 1990 to begin the upgrade and was first used for experiments in January 1991 following the successful upgrade. The upgraded tandem has operated 2,700 hours since the research program was resumed in January. The maximum terminal potential during this period was 9.1 MV, and a new record low terminal potential of 0.65 MV was also utilized on several occasions for new experiments. The upgrade is described in more detail below. Beams accelerated during this period include polarized protons and deuterons at up to 10 μA, and unpolarized protons and deuterons.

5.1.2 Tandem Accelerator Upgrade

The TUNL FN tandem accelerator was shut down to begin installation of the various upgrade components on October 20, 1990. The first step involved the removal of the accelerator tubes after having been in continual operation since 1968 and having accumulated over 132,000 hours of operation during this 22 year period. Following this, the old column resistors were removed and then the belt charging system was removed. We used a high-pressure washer to clean the accumulated belt dust and oil from the column structure and the tank walls. The interior was blown dry with compressed nitrogen, then

the tank was closed and evacuated overnight to speed drying. Because of the removal of the old charging system, resistors and belt guides, the column is now considerably lighter and in fact the terminal rose by 0.570".

Installation of the new accelerator tubes was begun following the cleaning, and each tube was optically aligned using a precision alignment telescope. When installing the new tubes, we allowed for 0.050" drop in the terminal due to the tank pressurization. We determined the stripper to be 0.120" low following pressurization – compared to >0.130" prior to the upgrade. The left-right alignment is better than 0.090". Beam transmission was very good, so we decided to leave the alignment where it is until we install the new terminal stripper. The assistance of Dr. Mark Roberts of LLNL-CAMS with the installation and alignment of these new tubes is much appreciated.

Installation of the Pelletron charging system and new column grading resistors was accomplished in parallel with the tube installation by TUNL graduate students and staff members. The first voltage test was made on December 18, and first beams were accelerated on December 19, 1990. This very successful upgrade could not have been accomplished without the willing assistance of many TUNL graduate students and staff.

More detail on the characteristics of the new accelerator components and their contributions to the improved performance of the FN tandem accelerator will now be described.

New Accelerator Tubes

The new Dowlish/HVEE titanium electrode, spiral inclined-field accelerator tubes are performing superbly. The beam transmission through these tubes is markedly superior to that with our original HVEC aluminum inclined-field tubes. At terminal potentials of several MV the transmission is typically 90% or better. At terminal potentials below about 2 MV, where previously transmission was too low to be useful, we now obtain about 50% transmission at 650 kV terminal voltage.

As important as transmission is the stability of the accelerated beam, which is also greatly improved. Whereas we previously measured ±2mm of vertical motion in the accelerated beam due to the combination of inclined-field tubes and the belt charging system, we now see much less than 1 mm of motion. The vertical beam motion is reduced by at least a factor of 10. Beam current on target is now extremely stable. Whereas we previously always had 10% - 50% bounce in the integrated beam current, we now have a very stable dc current.

Pelletron Charging System

Installation of the National Electrostatics Corporation (NEC) Pelletron charging system was accomplished in four days with the assistance of a field engineer provided by NEC. A few minor changes to the terminal hardware were required but these were made by our instrument shop. Other than this, the installation was very straightforward and the chains ran perfectly on the first test. The chains have been inspected twice since their installation, and only minor adjustments to several pulleys have been required. To compensate for the reduced charging current available for the chains (100 μA/chain guarantee), we installed new column grading resistors using the system employed by McMaster University, the

University of Pennsylvania at Philadelphia, and LLNL-CAMS. We chose to use ±2%-tolerance Caddock-type MX resistors instead of the style MG that the other three laboratories used. During a maintenance in May 1991 we replaced four failed resistors (out of about 400). Two of these failures could be blamed on improper installation.

With this new set of 1000-MΩ resistors, we required only 138 μA of charging current to accelerate 1μA of protons to 18.2 MeV with 40 μA of corona current for the acceptance test. We feel that we have an excess charging capacity of at least 60 μA at 9 MV (30%). For 9-MV operation, approximately 2% of SF_6 was added to the regular 80% nitrogen, 20% CO_2 gas mixture. The moisture content of the gas was about 12 ppmv. The chain-charging system has dramatically improved the basic voltage stability of the accelerator. The terminal voltage ripple — as measured by a two-plate capacitive pickup monitor — is typically <500 V_{pp}.

New Beam Foil Stripper

A new 200-position beam foil stripper mechanism was ordered from NEC and was received in late July 1991. This device will be installed in the terminal of the tandem later in 1991 in order to triple the number of stripper foils available. We expect the 200 foils to last nearly one year under normal usage and therefore essentially eliminate tank openings for foil changes.

Terminal Potential Stabilizer

The stability of the upgraded tandem is now limited by the noise inherent in the feedback system. The present HVEC Voltage Stabilizer was built in 1968 and is becoming very difficult to maintain, since many of its components are now obsolete. We decided that the circuit should be replaced, and we have purchased a new stabilization system from NEC. This system (NEC model TPS-5.5) will be installed in fall 1991. The new system should improve the voltage regulation of the tandem.

Along with the new TPS system, we wanted to replace our logarithmic slit current preamplifiers. The present preamps were designed and built at TUNL in 1975 and are no longer state-of-the-art. The NEC preamplifiers were designed for relatively high beam currents (10 nA to 100 μA). We have on occasion had the need to stabilize the tandem using on the order of 1 nA of beam per slit — and we did not want to lose that capability. At the University of Washington - Seattle, Trainor [Trai81] developed an improved logarithmic slit current preamplifier. At Yale, this preamplifier design was modernized and some improvements were incorporated [Hyd88]. This new design has logarithmic response from 50 pA to 100 μA with very low noise and good bandwidth. With the assistance of Dr. H.R.McK. Hyder of Yale University, TUNL was able to obtain four of these new log slit preamps and we will use them in conjunction with the NEC TPS system.

New Radiation Area Monitors

The TUNL radiation area monitoring system was installed in 1968 when the laboratory was established. This system incorporates one gamma monitor and seven neutron (Rem) monitors interfaced to an interlock system to ensure that personnel are not exposed to radia-

tion in excess of 2.5 mR/hr. In addition, the laboratory has seven modern X/γ survey meters and six older neutron survey instruments. The area monitors and older survey instruments are increasingly difficult to maintain due to the age of many of the components. Since TUNL is a growing laboratory, with the addition of the low-energy beam facility (LEBF), the new few-body-interaction beam leg, and the installation of the Enge split-pole magnetic spectrograph, we now have three additional experimental areas to monitor. The present monitoring system is not expandable as the manufacturer has been out of business for many years. This, coupled with the maintenance problems and the increased concern for radiation safety, has prompted us to begin immediately to replace the present monitoring system.

After reviewing five commercially available area monitoring systems, we chose the Ludlum Measurements Inc. (LMI) model-306 system. An order for four monitors (two for γ rays and two for neutrons) was placed in July 1991. This system will provide new X /γ and neutron monitoring capability for our ion source and LEBF. After the beginning of 1992, a second order will be placed to permit us to replace and augment the remaining neutron monitors. This new system will be tied into our existing safety system.

5.2 KN Accelerator Operation, Maintenance, and Improvements

C.R. Westerfeldt, E.G. Bilpuch, E.P. Carter, J. Drake, R. Bybee, S. Frankle, G.E. Mitchell

The TUNL KN Van de Graaff accelerator was improved in several aspects during 1990 – 91. We now describe operations, maintenance, and improvements for this accelerator.

5.2.1 KN Accelerator Operation and Maintenance

The TUNL KN Van de Graaff was operated for 330 hours this past year. The terminal voltage ranged from 0.9 to 3.4 MV. Operation at high terminal potentials (>3 MV) has been difficult and several openings have been made to try to determine the cause of the instabilities. The stainless-steel electrode accelerator tube now has 11,680 hours of operation at terminal potentials up to 4.1 MV. We have found five insulators which exhibit breakdown damage which could be contributing to the instability. We are investigating the possibility of refurbishing this tube during fall 1991. Our spare tube is an aluminum electrode tube of an older design and has never successfully been operated above 3.5 MV.

If it is necessary to rebuild this tube, we would like to have magnetic suppression of secondary electrons added during the rebuild. This tube is totally unsuppressed and the addition of good magnetic suppression should reduce the bremmstrahlung radiation by at least an order of magnitude. This is important both for radiation-safety implications and for extended life of the tube, as well as for improved stability of the accelerator.

Work in progress includes upgrading of the corona stabilizer system and the fiber-optic feedback system (beam homogenizer), and design studies for the new Compton-Suppressed Spectrometer scattering chamber and required beam optics.

5.2.2 Energy-Resolution Measurements

S. Frankle, C.R. Westerfeldt

Prior to late 1989, typical measured FWHM (energy spread) for the resolution function with solid targets values were Δ=360-400 eV. During late 1989, a new (commercially made) 130 MHz rf exciter was installed in the terminal of the KN Van de Graaff to replace the original 80-100 MHz exciter. Modifications were made to the new exciter which increased the frequency to 155-165 MHz. We noticed an immediate improvement in the overall energy resolution. We theorize that the increase in frequency reduced the time that the protons in the plasma are accelerated in the rf electric field. This reduces the amount of kinetic energy the protons can acquire from the rf field prior to extraction. Recent measurements determined the resolution function parameters to now be Δ=220 eV. Without the high-voltage target-rod correction signal from our beam-homogenizer system, the energy spread Δ=350 eV. In fig. 5.2-1 the data and fit for these recent measurements are shown.

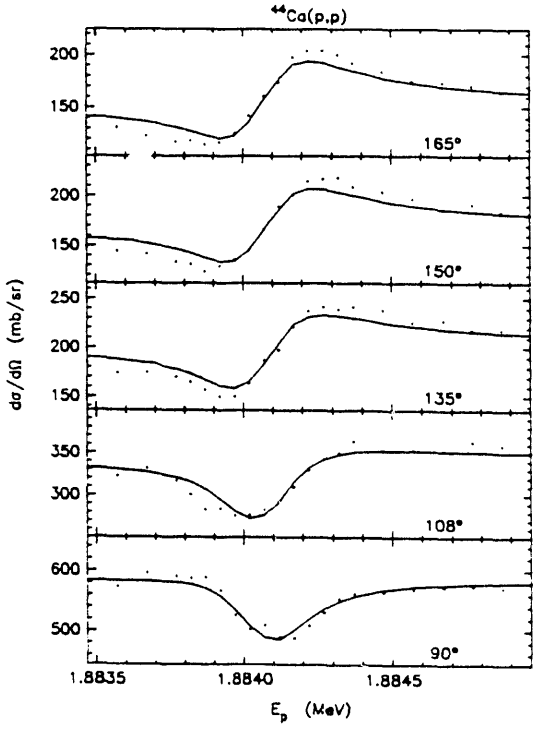

Fig. 5.2-1a Beam energy resolution test utilizing a resonance in ^{44}Ca(p,p) at 1.8841 MeV. The measured value of Δ is 220 eV (FWHM).

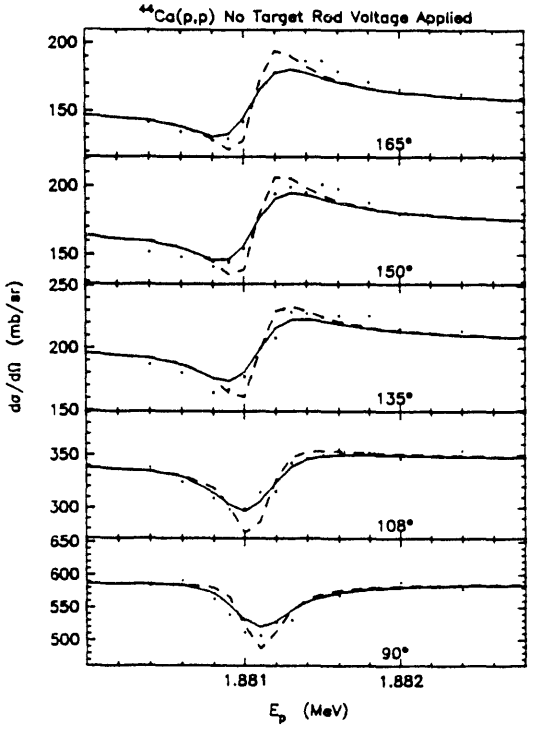

Fig. 5.2-1b Beam energy resolution for the same resonance with no target-rod correction signal applied. The solid line is a fit with Δ=360 eV, while the dashed line indicates the fit using Δ=220 eV.

5.2.3 Compact ECR Ion Source for the KN Accelerator

C.R. Jackson, G.A. Vavrina, G.E. Mitchell, W.M. Hooke, C.R. Westerfeldt, E.G. Bilpuch

Evaluation of the new compact electron cyclotron resonance (ECR) ion source for the KN Van de Graaff accelerator has continued during the past year. This ion source is being developed to decrease the contribution of the ion source to the energy spread in the ion beam. The ion source design utilizes several novel features to achieve miniaturization, including a magnetic-mirror and sextupole system consisting entirely of permanent magnets and a coaxial feedthrough for microwave coupling to heat the plasma, in place of the usual waveguide coupler. The ECR ion source as adapted for bench test operation is shown in fig. 5.2-2.

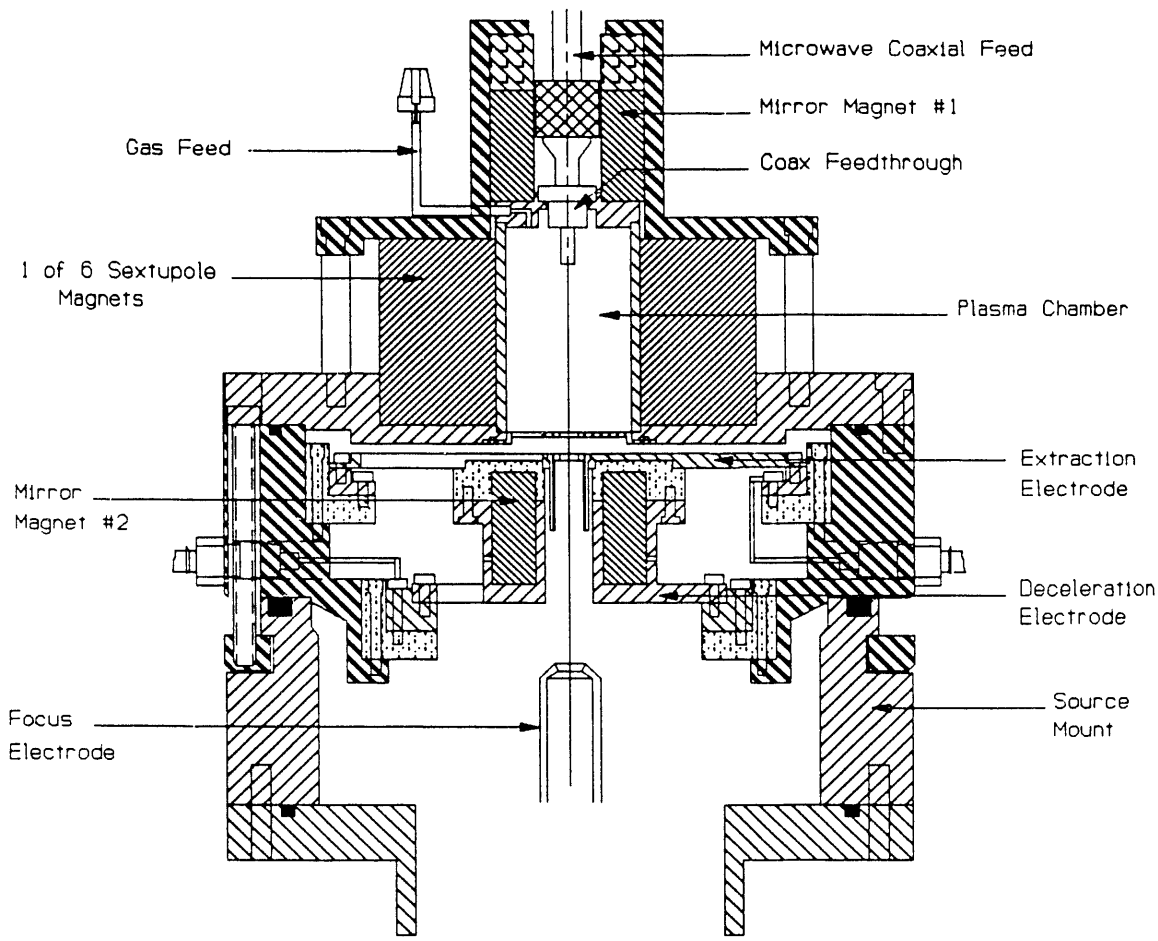

Fig. 5.2-2 Assembly drawing of the ECR ion source adapted for bench test operation.

The mirror and sextupole magnetic system are the same as in the last Progress Report. Further field measurements have been performed on this system in order to obtain a three-dimensional representation of the magnetic-field configuration.

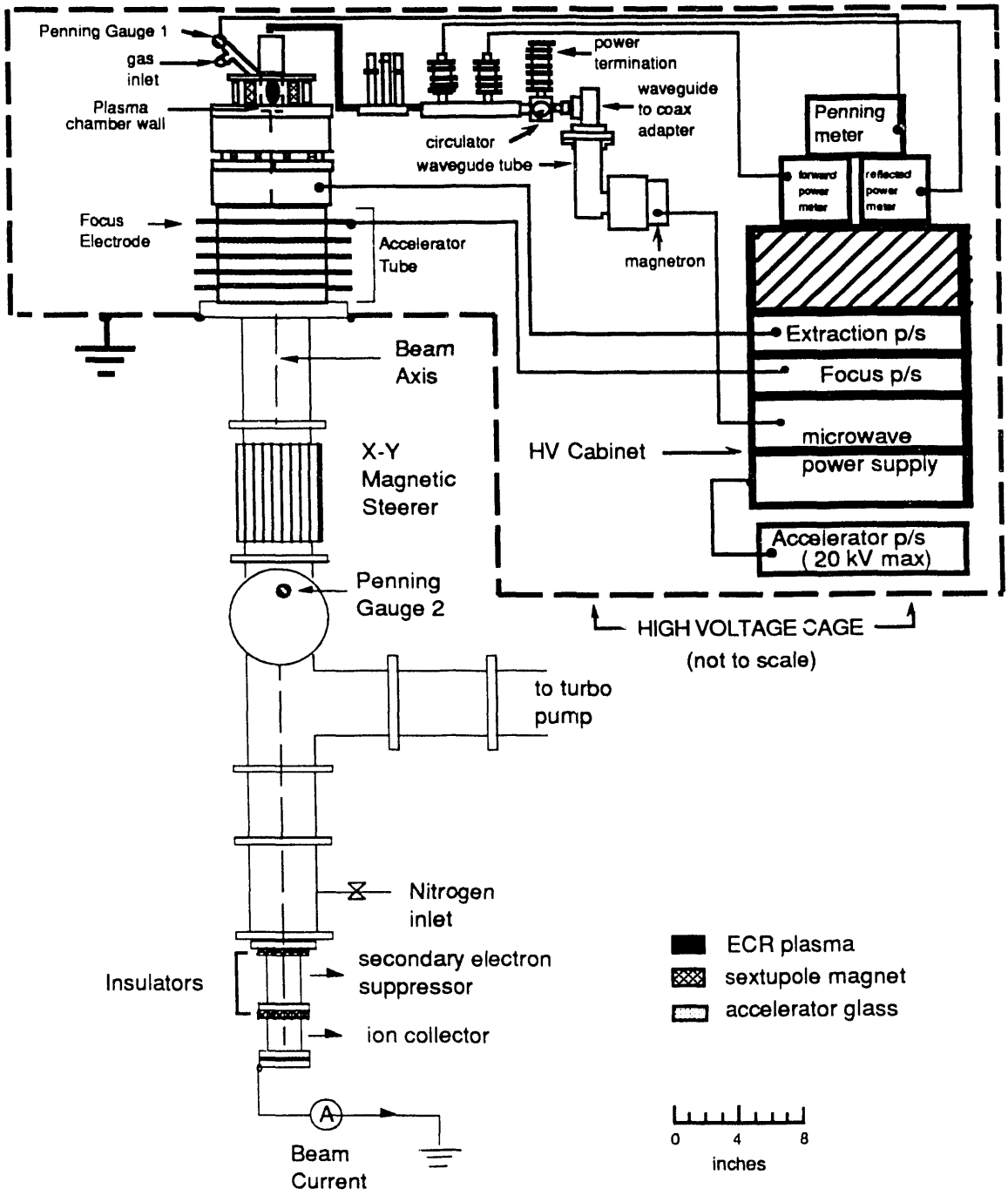

Fig. 5.2-3 ECR ion source bench test facility

An ion-source bench test facility has been constructed to study the new ECR ion source, as illustrated in fig. 5.2-3. This facility provides 20 keV of hydrogen beam acceleration, beam collection, and mass analysis for the extracted beam. The ECR ion source is driven by a 2.45-GHz continuous-wave generator. In the setup in the figure, the microwave generator is designed around a YJ1530S continuous-wave, variable-power magnetron from Richardson Electronics, which provides a 300 W maximum output. This magnetron is energized and controlled by a 3 kV power supply with voltage and current control. The microwave transmission system is coaxial and includes components such as a circulator, a bi-directional coupler, and a stub tuner. These components protect the magnetron, sense the flow of microwave energy, and vary the transmission line impedance respectively. There has been difficulty in maintaining stable injection of microwave energy into the ECR ion source over a wide range of pressure with this system. Study of the microwave injection for this system is continuing.

To evaluate the feasibility of installing this ECR ion source in the KN Van de Graaff accelerator, characterization of this new source relative to the presently installed RF ion source will be performed. A 100-MHz RF ion source was installed in this facility and measurements made using a data-acquisition system developed for use with this test-bench facility. These beam characteristics and mass analysis measurements will serve as a calibration for future testing of the ECR ion source.

[Trai80] T.A. Trainor, Proceedings of the Third International Conference on Electrostatic Accelerator Technology, Oak Ridge, TN, April 1981. Available from IEEE Service Center, Piscataway, NJ 08854, Cat. No. 81CH1639-4

[Hyd88] H.R.McK Hyder, Symposium of Northeastern Accelerator Personnel, Yale University, October 1988. (World Scientific, Singapore)

5.3 TUNL Intense Polarized-Ion Source

E. R. Crosson, J.D Dunham, S. K. Lemieux, T.B. Clegg

The atomic beam polarized ion source has been used for about 70% of the scheduled beam time during 1990 – 91, with substantially improved operational efficiency. As the number of experimental users has increased, our techniques for optimizing the source and maintaining successful operation for long running periods (up to 1 month) have improved. We have completed an operation manual for users, have instituted routine maintenance procedures, and we are now usually able to assure satisfactory performance for most experimental groups.

In the following we describe the ion source operation and improvements during the past year.

5.3.1 Ion-Source Operation

Maximum polarized beam currents over the past year have ranged between 1 and 7 μA of H^- (or D^-) on the low-energy cup of the FN tandem accelerator, or between 25 and 70 μA of D^+ on the first beam stop after the source analyzing magnet. Polarizations as high as 85% (~75%) of the theoretical maximum for deuterium (hydrogen) have been obtained.

Achieving the highest values of current and polarization still depend to a great extent on the care with which routine maintenance is performed and on the skill of the operator. To facilitate maintaining highest beam polarization values and switching between states of different beam polarization quickly, we have purchased and installed new programmable transition magnet power supplies to replace the small bench-top lab supplies used previously.

Three projects in the past year to improve source operation are noteworthy. The most significant has been our learning how to maximize quickly the polarization of the beam as it emerges from the source. This is achieved using a simple lock-in amplifier measurement of the effect of rf transition operation on the emerging polarized beam intensity. Having mastered this, we now believe that the rf transitions used to produce the polarization of the H or D atomic beam often do not operate at 100% efficiency. They are also clearly affected by stray magnetic fields from the electron-cyclotron-resonance (ECR) ionizer. Thus, new magnet systems and substantial magnetic shielding for the rf transitions have been designed and are under construction. Finally, an increasing number of experiments with the source utilize beams with energies below 85 keV. Here there is no convenient polarimeter having sensitivity to proton or deuteron vector polarization. We are developing for this purpose a Lamb-Shift polarimeter. More details on each of these projects follow.

5.3.2 Lock-in Amplifier Measurement to Optimize Beam Polarization

We have utilized the spin-dependence of the cross section for electron impact ionization of H and D atoms in the ECR ionizer to study the performance of the rf transitions [Rob89] that provide the nuclear polarization of the atomic beam. Switching the transitions on and off modulates the output polarized beam current [Jac81]. Maximizing this modulation provides a fast and reliable method for optimizing rf-transition-unit parameters. This procedure is described fully in a forthcoming publication [Cro91].

In the source, beam polarization is produced by a system of sextupole magnets and rf-transition units. Consider, as an example, a beam of deuterium atoms. The atomic beam emerging from the sextupoles is equally distributed in states 1, 2,and 3 and has deuteron tensor polarization $P_{zz} = 0$. If an rf-transition unit is turned on and tuned to select the $3 \rightarrow 5$ transition, then, ideally, the atomic beam emerging consists of equal populations of states 1, 2, and 5 and has deuteron tensor polarization $P_{zz} = -1$. Upon emerging from the rf-transition unit, the neutral beam then drifts into the ECR ionizer where the atoms are stripped by electron impact ionization, and then extracted. In the ECR ionizer, the electron population of the plasma is generated by two sources. The first source is the electrons from previously ionized D atoms. The quantization axis of the spin projection of these electrons is defined in the plasma by the magnetic fields used to contain the plasma. The second source of electrons is the ionization of nitrogen atoms which are introduced into the plasma to maintain its stability. These latter electrons are unpolarized.

A number of experiments have demonstrated the existence of the spin-spin dependence of the cross section for electron impact ionization of light atoms [Alg77, Gay82]. Since turning the rf transitions off (unpolarized) and on (polarized) changes the electron spin-state population of the beam, and thus changes the electron spin state population in the ECR ionizer plasma, and since there is an electron spin-dependent term in the total cross section

for electron impact ionization, turning the rf transition off and on modulates the total beam current extracted from the ionizer. This beam current fluctuation is proportional to the vector and tensor nuclear polarizations, P_z and P_{zz}, of the beam.

In a measurement we demonstrated the proportionality of beam current fluctuation and beam polarization by turning the rf transition unit on and off at a rate of 42 Hz and measuring the output beam current modulation on a Faraday cup at the exit of the source by using a lock-in amplifier. The measured current modulation, I_L, divided by the total beam current, I_T, as a function of the transition unit magnetic field for the $2 \rightarrow 6$ and the $3 \rightarrow 5$ transitions, along with the corresponding vector and tensor beam polarizations, are shown in fig. 5.3-1.

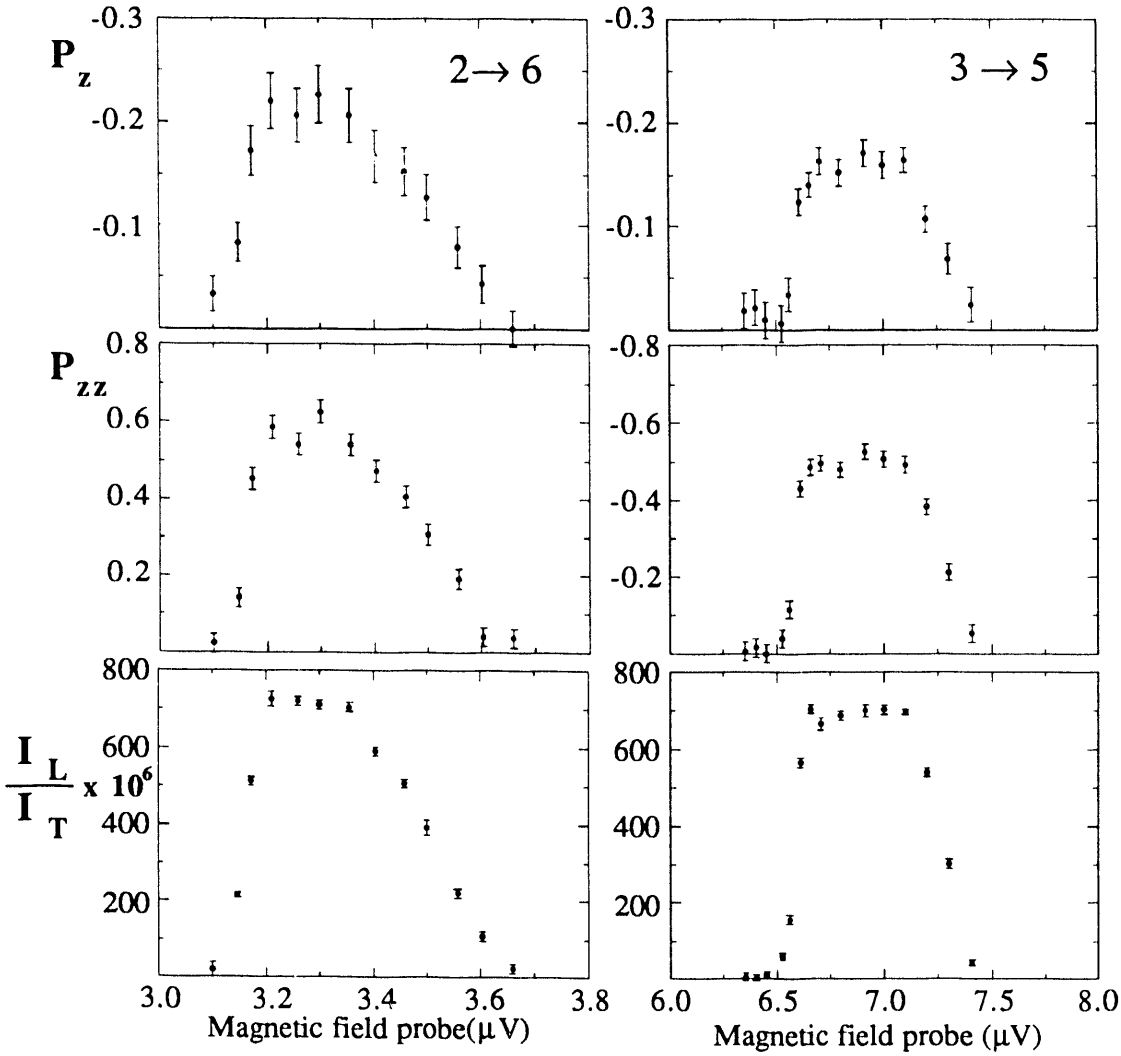

Fig. 5.3-1 Plots of measured deuteron beam vector and tensor polarizations, P_z and P_{zz}, and the normalized lock-in amplifier signal, all plotted versus the Hall probe signal indicating the magnetic field in the rf transition unit. Strong correlation is immediately apparent.

5.3.3 Medium Field Transition Unit Development

One of the most persistent difficulties with atomic-beam-type polarized sources is assuring proper operation of the radio-frequency transitions which induce the nuclear polarization in the atomic beam. In these devices, it is particularly important to maintain the correct spatial configuration of dc electric and magnetic fields and rf electromagnetic fields. The fields desired are dictated by which hyperfine states are involved in the transition to be achieved.

Traditionally, the most common transition used has been the so-called weak-field transition in which the atomic spin is inverted, i.e. $\Delta F=0$; m_F->m_{-F}. This operates at magnetic fields of ~5 to 10 Gauss. It also must operate in close proximity inside the source to spatial regions of very much higher magnetic field. For example, in the TUNL source the electron-cyclotron-resonance ionizer is only ~10 cm away and requires a magnetic field of at least 1200 Gauss. Shielding against this nearby, large field is very difficult.

In addition, greater flexibility of atomic transitions would add to the variety of beam polarizations available from the source. Recently in Heidelberg and Wisconsin,a medium-field transition has been developed which will not only accomplish the traditional weak-field transitions, but will also allow interchange of populations of adjacent hyperfine states (i.e. $\Delta F=0$; $\Delta m_F=\pm 1$). An added advantage is that these latter transitions occur at magnetic fields which are larger than for the weak-field transitions. Thus any stray, unshielded B-field has a smaller influence on the operation of the experimental systems.

We have begun to develop a medium field transition system. A compact tapered coil magnet has been built following generally designs developed at Heidelberrg and Wisconsin [Hae91] (see fig. 5.3-2). Outside the source on a test bench, the axial magnetic field distribution produced by this magnet is suitable for the desired medium field transitions. We plan to insert this into our atomic beam source within the next month for initial magnetic field measurements in the actual source environment. Assuming the proper shielding is then found and the B-field distribution is still good, we will plan experiments soon thereafter to make measurements of the actual polarization of the emerging beam from the source.

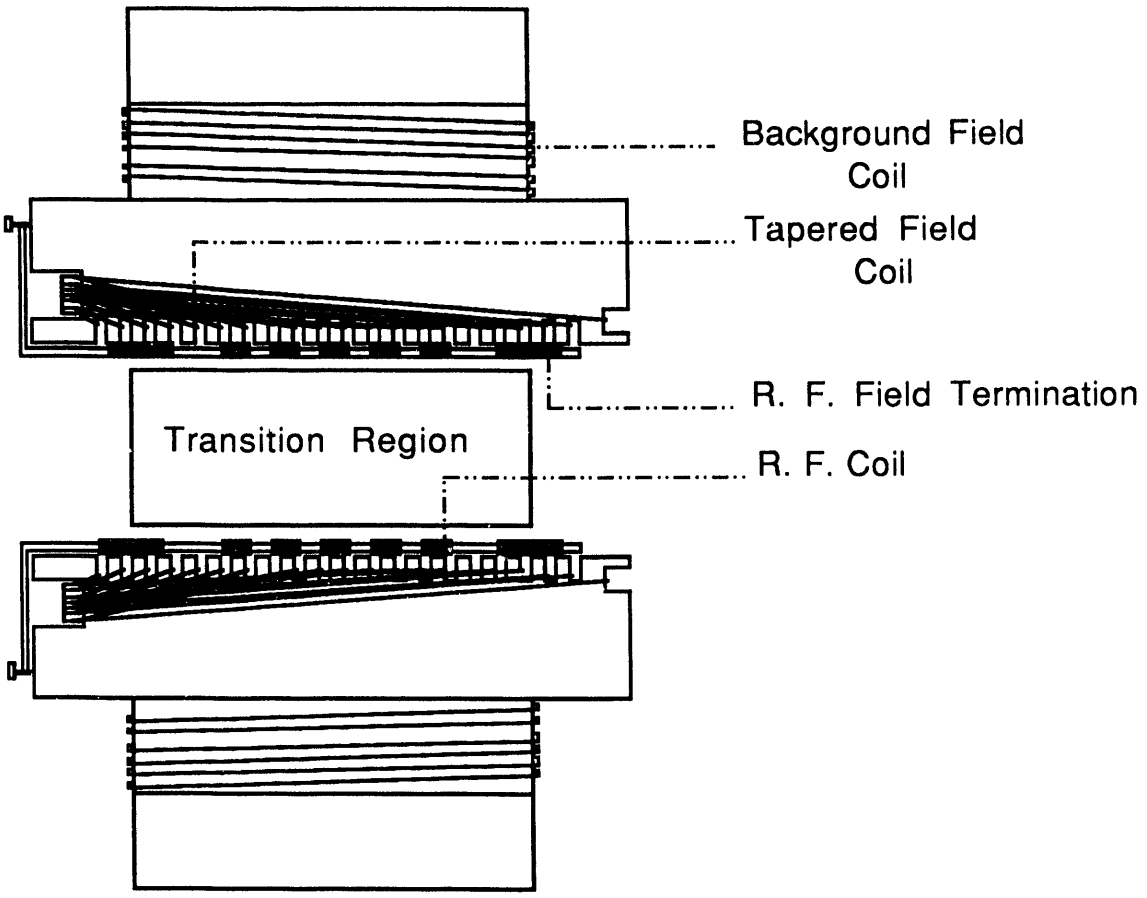

Fig. 5.3-2 Schematic of the new medium-field transition magnet with a coil which produces the required axially tapered magnetic field.

5.3.4 Lamb-Shift Spin Filter Polarimeter Development

T.B.Clegg, S.K.Lemieux

The TUNL Atomic Beam Polarized Ion Source produces proton and deuteron beams of energies from 30-80 keV, which can be used for experiments in the low-energy beam facility. The Spin Filter Polarimeter (SFP) will be used on this source to calibrate polarimeters for low-energy experiments for which no polarization standard exists. The SFP uses an atomic technique to measure nuclear polarization. This device will also facilitate testing new r.f. transition units for the ion source.

The nuclear spin filter, developed first by McKibben *et al.* [McK65] at LANL and used for many years on the Lamb-shift polarized source at TUNL [Cle72], can be used to pass selectively metastable ($2S_{1/2}$) hydrogen (or deuterium) atoms of a given nuclear magnetic spin projection. The metastable atoms are formed by passing H^+ (or D^+) ions through cesium vapor; the cross-section for metastable atom formation peaks at 550 eV for hydrogen and at 1100 eV for deuterium. By applying an rf field at 1.6 GHz, and dc electric and magnetic fields, a three-level resonance in the atomic system causes all the metastable atoms except those of a particular hyperfine state to be quenched to their ground state. The re-

maining metastable atoms are thus nuclear spin polarized. Their polarization can be altered simply by changing slightly the magnetic field of the spin filter.

The spin filter can also be used as a polarimeter, since it simply passes without change atoms in the hyperfine state chosen. If these emerging metastable atoms are subsequently quenched in an electric field when they emerge from the spin filter, they emit Lyman-alpha radiation which can be detected. Measuring the radiation intensity as a function of the spin-filter magnetic field gives a direct measurement of the relative hyperfine-state populations of the entering beam and therefore the beam's nuclar polarization.

The decommissioned TUNL Lamb-Shift source has been used as a test bench to study the feasibility of this technique. We measured the ultra-violet radiation from quenching metastable atoms using a Hamamatsu R1187 phototube. As the spin-filter magnetic field was varied, the two (three) peaks corresponding to the two (three) spin states in hydrogen (deuterium) can be cleanly separated, as shown in fig. 5.3-3. The results have been reliably reproduced. Currently we are testing in the Lamb-shift source a new and more compact configuration of quench plates and detector designed to fit in the limited axial space on the ABPIS high-voltage frame. We are also testing an Ithaco 564 pre-amplifier which converts the picoampere signal from the detector into a millivolt signal for input to an oscilloscope and an ADC.

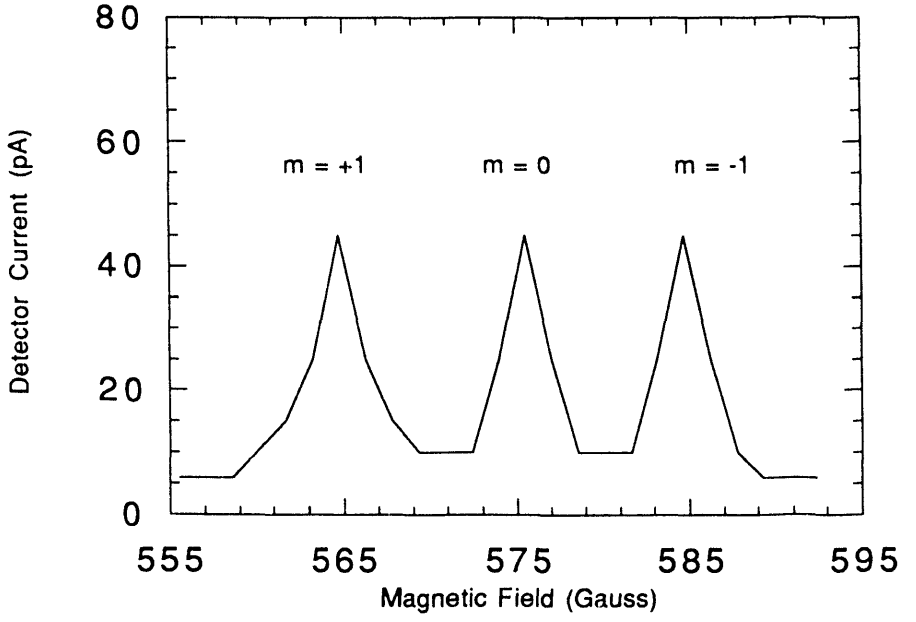

Fig. 5.3-3 A plot of the Hamamatsu phototube output current versus the magnetic field in the spin filter polarimeter when an unpolarized $D_o(2S_{1/2})$ atomic beam of 1100 eV enters the polarimeter.

Initial installation on the polarized ion source frame requires disassembling the portion of the ion-source beamline between the ECR ionizer and the high-voltage protection cage.

The frame will be extended, then the quadrupole doublet after the Wien Filter will be removed so that the Wien filter can be moved downstream leaving room for the spin-filter polarimeter. Since the beam polarization measurements must be made with the frame at ground potential, the power supplies for the polarimeter will be kept outside the cage during this first stage of testing on the ion source.

Plans include later installation of the power supplies on a new rack at Wien filter potential so that the SFP can be operated remotely.

[Alg77] M.J. Alguard *et al.*, Phys. Rev. Lett. **39** (1977) 334

[Cle74] T.B. Clegg, G.A. Bissinger and T.A. Trainor, Nucl. Instrum. Meth. **120** (1974) 445

[Cro] E.R. Crosson *et al.*, Nucl. Instrum. Meth., to be published.

[Gay82] T.J. Gay *et al.*, Phys. Rev. **A26** (1982) 3664

[Hae] W. Haeberli, private communication

[Jac81] S. Jacarrd, Am. Inst. of Phys. Conf. Proc. **80** (1981) 95

[McK68] J.L. McKibben, G.P. Lawrenc and G.G. Ohlsen, Phys. Rev. Lett. **20** (1968) 1180

[Rob89] H.G. Robinson *et al.*, Nucl. Instrum. Meth. **A278** (1989) 655

5.4 Installation of the TUNL Enge Split-Pole Magnetic Spectrometer

A.E. Champagne, L.W. Seagondollar, D. Hennesey, E.E. Gross

The split-pole spectrometer has been installed on the R-15° leg of target room 4 at TUNL. Some of the concrete shielding between this area and the time-of-flight setup was removed in order to permit spectrometer rotation over the range $-30° \leq \theta \leq 160°$. Once the spectrometer was placed on its track, the track was leveled to an accuracy of better than ±0.125 mm over most of its travel. This procedure ensured that localized deflections of the floor could be corrected for with the appropriate shims. In fact, it was found that the floor was quite stable and at no point did it deflect by more than 0.5 mm. The spectrometer was then cleaned and painted, and aligned with respect to the beam axis. Some of the original equipment associated with the spectrometer, notably the detector chamber and detector carriage have been removed, cleaned and replaced. Installation of compressed air, power and cooling water, as well as the beam line, is currently in progress.

Funds from the DOE have been obtained for the first of a planned 2-stage upgrade of the spectrometer and ancillary equipment. The components to be upgraded are the following.

Control systems. An NMR-based magnet control system has been purchased and will be interfaced with the magnet-power supply (obtained as surplus from LLNL). In addition, hard-wired controls for the vacuum system and for motion control of the detector, target, etc. have been built or are under construction.

Vacuum system. Components have been purchased for a new vacuum system featuring a high-capacity cryopump for the target chamber and a large turbopump for the magnet. Installation of the magnet system is underway.

Target chamber. In order to afford the greatest flexibility in mounting experiments with the spectrometer, we have contracted with Mr. Erich Feldl (CEBAF) for the design of a new sliding-seal chamber. The design is nearly complete and the chamber will be fabricated in the Duke shop during early fall 1991. A new entrance-aperture assembly is also being designed.

Focal-plane detector. We have ordered implanted silicon position-sensitive detectors (PSD) which have been designed and are being constructed to our specifications by Micron Semiconductor, Ltd. Each PSD has an active length of 18 cm and is made up of two 9-cm-long sections with an intervening dead space of 1 mm. Thicknesses will be 100, 300 and 500 μm. Particle position is derived from a resistive readout and is expected to be accurate to ≤0.5 mm. Ultra-low-noise preamps have been manufactured for these detectors by eV Products Corp. Both the preamps and a prototype PSD have been delivered for testing.

5.5 Compton-Suppression γ-Ray Spectrometer

J.F. Shriner, Jr.[1], A.A. Adams, E.G. Bilpuch, C.R. Bybee, J.M. Drake, G.E. Mitchell, E.A. Moore[1], S.S. Patterson, C.R. Westerfeldt

We have been funded by DOE to purchase a Compton-suppressed γ-ray spectrometer whose initial use will be to study $^{29}Si(p,\gamma)^{30}P$ with the goal of establishing a complete level scheme of ^{30}P at low excitation energies. The fluctuation properties of the energy levels will then be studied in a manner similar to that for ^{26}Al [Mit88, Shr90] to look for evidence of chaotic behavior and isospin-symmetry breaking.

The core of the system will be two 60% relative efficiency HPGe detectors and a BGO Compton suppressor for one of the two Ge detectors. When used with the suppressor, a Ge detector will be mounted transversely in a configuration similar to that of Aarts *et al.* [Aar80a, Aar80b]. The BGO suppressor, shown in fig. 5.5-1, will be a cylinder of radius 10 cm and length 18 cm; a taper on the front will allow the system to be placed at lab angles ranging from 55° to 125° relative to the beam direction. The suppressor will have a cylindrical opening of radius 2 cm where the γ-rays will enter; we plan to insert heavy metal collimators here to define the region viewed by the Ge detector. The solid angle of the Ge in this configuration is about 80 msr. The dimensions of the BGO suppressor were chosen after extensive simulation with the computer code BOCKVI [Bea89].

We have begun developing software for data acquisition with the new system. We wish to record singles spectra for each of the two Ge detectors, a singles spectrum from a surface-barrier detector which will be used to monitor elastic scattering, and γ–γ coincidences. The singles spectra can be handled with our present electronics, but recording coincidences requires additional ADC's. We have acquired an ORTEC AD413 ADC (purchased by Tennessee Technological University for use in this experiment) for this purpose. XSYS programs are being written for communicating with this module and for sorting the data.

---

[1]Tennessee Technological University, Cookeville, TN

Orders have been placed for the Ge detectors, BGO suppressor, and NIM electronics needed for the system. Design of beamline components and a new target chamber has begun. We are currently running beam-optics calculations to study appropriate placement and design of the new beam line on the KN Van de Graaff accelerator.

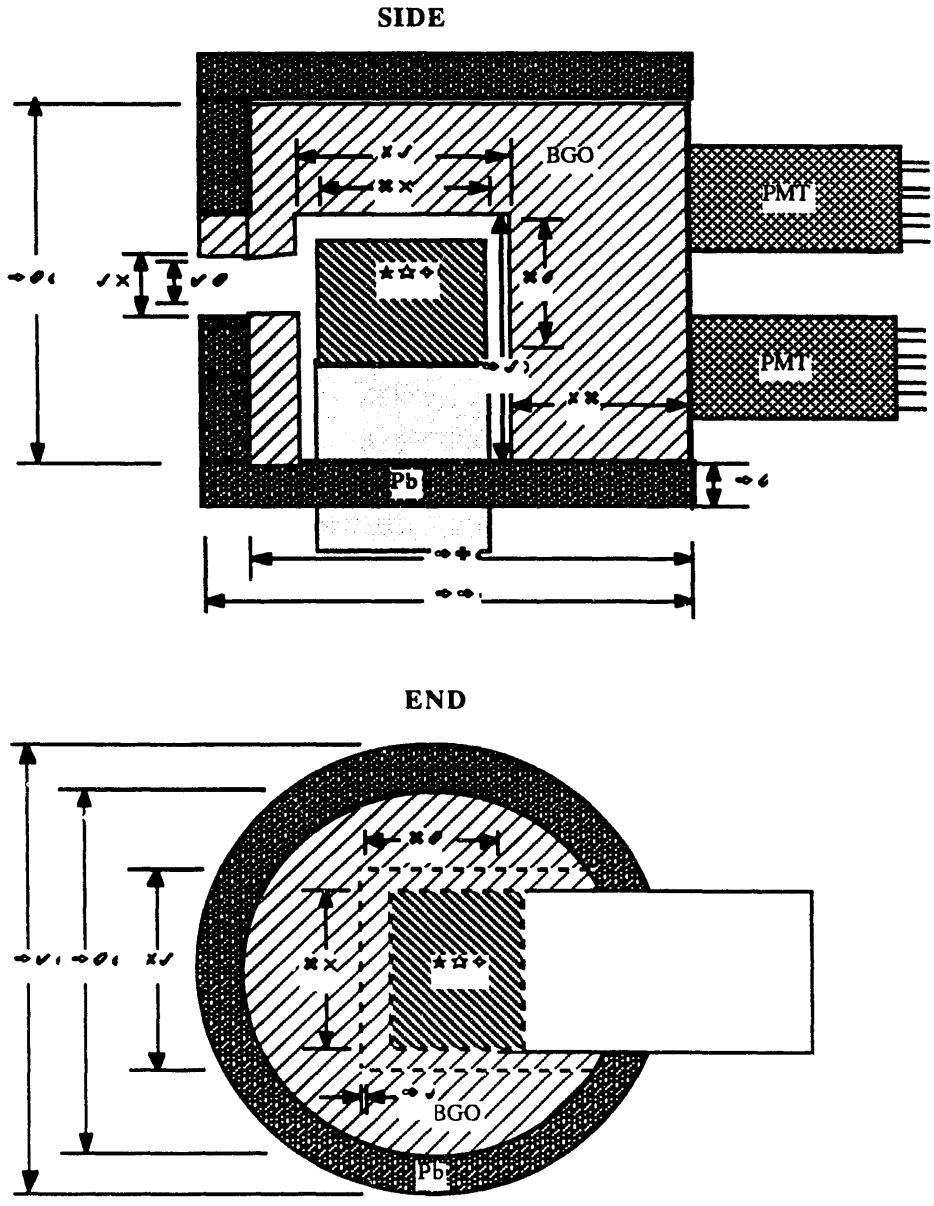

Fig. 5.5-1 Top and side views of the Compton-suppression spectrometer. All dimensions are in millimeters.

[Aar80a] H.J.M. Aarts *et al.*, Nucl. Instr. Meth. **172** (1980) 439
[Aar80b] H.J.M. Aarts *et al.*, Nucl. Instr. Meth. **177** (1980) 417
[Bea89] K. Beard, private communication, 1989
[Mit88] G.E. Mitchell *et al.*, Phys. Rev. Lett. **61** (1988) 1473
[Shr90] J.F. Shriner, Jr. *et al.*, Z. Phys. A **335** (1990) 393

5.6 Development of the Low Energy Beam Facility at TUNL

T.C. Black, B.E. Hendrix, H.J. Karwowski, E.J. Ludwig

Modifications to the new Low Energy Beam Facility (LEBF) are underway which will enable us to perform charged-particle and gamma-ray experimemnts with light-ion beams in the energy range between 10 and 480 keV. The availability of polarized beams in this energy range will permit detailed studies of low-energy scattering and studies of reaction mechanisms in the very low energy regime, such as is of interest for nuclear astrophysics. Although the TUNL Intense Polarized Ion Source can accelerate beams to about 80 keV, there is a very interesting but unexplored energy region from this energy up to about 500 keV that is difficult to reach with existing accelerators that use intense polarized beams. A sketch of the developing facility is shown in fig. 5.6-1.

The centerpiece of the upgraded facility is the Mini-Tandem Accelerator, an "in-air" high-voltage chamber capable of accelerating proton and deuteron beams by up to 200 keV using the tandem principle. The accelerator consists of a squat cylindrical chamber 51-cm in diameter, encapsulated top and bottom by two highly polished hemispherical aluminium domes. Accelerating tubes lead into and out of the chamber, which contains a set of carbon stripping foils mounted on a rod in the center of the chamber. The chamber itself is then biased by up to 100 kV using a high-voltage power supply.

The resulting beam will be momentum-analyzed to remove singly-stripped atoms by using a bending magnet with exit ports at +45°, 0° and -40°. The 0° port leads into the existing LEBF scattering chamber, while the +45° port leads into a dual-purpose Large Volume Scattering Chamber (LVSC). The –40° port exists to accommodate experiments requiring large gamma detectors. The LVSC can be fitted with an entrance acceleration tube, permitting it to be biased to +200 kV, bringing the effective maximum energy of the LEBF to 480 keV. Alternately, the LVSC can be operated at ground potential as a differentially-pumped gas target, capable of sustaining target gas pressures up to 500 mTorr. In this configuration, the entrance accelerating tube is replaced by a three-stage differential-pressure pumping system.

Construction of the Mini-Tandem is nearing completion; It is expected that installation and testing of the first stage of the upgraded LEBF (up to the analyzing magnet exit ports) will begin by September 1991. The LVSC is currently being re-designed to accommodate the differentially-pumped gas target configuration.

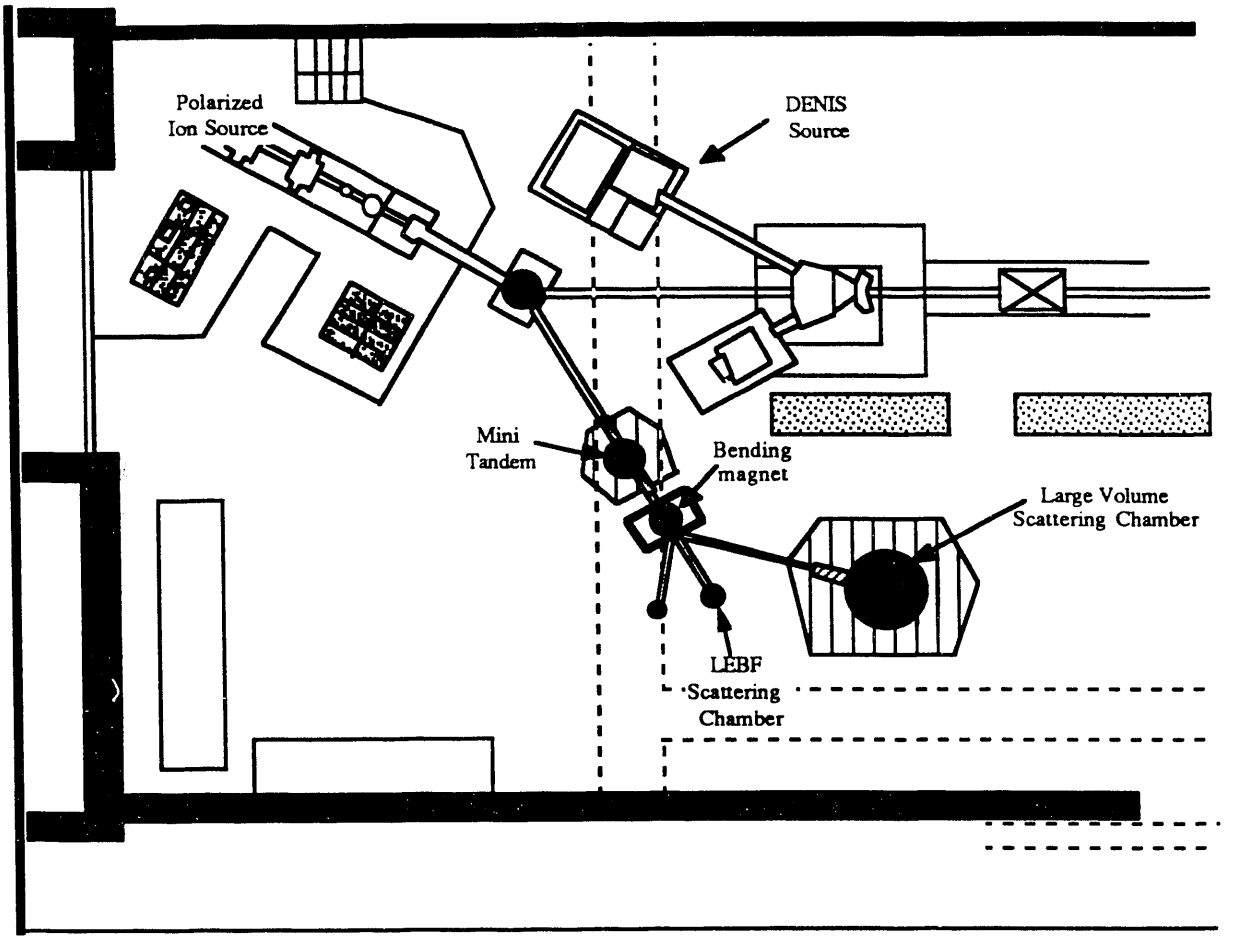

Fig. 5.6-1 Planned modifications to LEBF.

5.7 Instrumentation Development for CEBAF

The TUNL Long-Range Plan (February 1990) includes increasing involvement of our laboratory with CEBAF research activities over the next five years, so that by the time this state-of-the-art electron-scattering facility is in production we will have a strong and continued presence at CEBAF, while continuing at TUNL an active research program in several areas of nuclear physics. This year has seen the development of two research collaborations at CEBAF, whose progress we now describe.

5.7.1 Spectrometer Mapping and Software for Hall A

C.R. Howell, W. Tornow, R.L. Walter

As members of the Hall-A collaboration at CEBAF, we will be involved in the first set (PAC1) of experiments conducted in that experimental hall. Each institute in the collaboration has the responsibility of providing instrumentation for the experimental hall. We have agreed to provide the data-analysis software package and to map the fields in the large dipole and quadrupole magnets of the two spectrometers. Howell is the user coordin-

ator for software developments and Tornow is the user coordinator for magnetic measurements.

A survey of available data-analysis packages was conducted in summer 1991. The results of this survey will be presented at the January 1992 collaboration meeting. Howell will develop the foundation of the software package while on sabbatical leave at CEBAF during spring 1992. Research on techniques to make high precision field maps of the large spectrometer magnets is underway.

5.7.2 Möller Electron Polarimeter for Hall B

R.M. Chasteler, H.R. Weller

CEBAF is a superconducting electron accelerator with a maximum energy of 4 GeV, 100% duty-cycle, and a maximum current of 200 mA. A toroidal multi-gap spectrometer, CLAS (CEBAF Large Acceptance Spectrometer) is being installed in Hall B. Experiments proposed for Hall B and CLAS will require use of CEBAF's high-luminosity polarized electron beam. Part of the TUNL responsibility in the CLAS collaboration is to build an electron polarimeter for Hall-B for the purpose of measuring the beam polarization.

The simplest method of measuring the beam polarization, for the beam energies to be used in Hall-B, is by the scattering asymmetry of electron-electron scattering. The dependence of the cross section on the polarization components of the electron beam, P_i^B, and of the target, P_i^T, can be shown in a first-order QED calculation in the high-energy limit ($\gamma >> 1$) to be:

$$\frac{\partial\sigma}{\partial\Omega} = \frac{e^4(4 - \sin^2\theta)^2}{4m_e^2\gamma^2\sin^4\theta}\left\{1 - \frac{\sin^2\theta}{(4 - \sin^2\theta)^2}\left[(8 - \sin^2\theta)P_z^B P_z^T - \sin^2\theta(P_y^B P_y^T - P_x^B P_x^T)\right]\right\} \quad (1)$$

where θ and γ are c.o.m. parameters [Ols68]. The analyzer strengths exhibit their maxima at $\theta = 90°$ ("symmetric" scattering) where Eq. (1) becomes:

$$\frac{\partial\sigma}{\partial\Omega} = \frac{9e^4}{4m_e^2\gamma^2}\left\{1 - \frac{1}{9}\left[7P_z^B P_z^T - (P_y^B P_y^T - P_x^B P_x^T)\right]\right\} \quad (2)$$

Because of the large background of electron-atom scattering, coincidence detection of both electrons is necessary in order to obtain an unambiguous signature of Möller Scattering.

The design of a Möller Polarimeter at CEBAF energies is not an easy task because of the small scattering angles in the laboratory system for "symmetric" scattering ($\theta_{lab} = 1.83°$ for 1-GeV and $\theta_{lab} = 0.916°$ for 4-GeV). Separation of the Möller electrons from the primary beam plus the possibility of moderate momentum analysis with coincidence detection can be conveniently achieved with a quadrupole magnet arrangement. The quadrupole field is set to be defocussing in the x-plane, which will bend the "symmetric" Möller electrons into a pair of fixed Cerenkov detectors, as shown in fig. 5.7-1. This method of using a quadrupole has worked successfully up to 183 MeV at the Mainz racetrack microtron (MAMI) [Wag90] and at 868 MeV at Bates [Bea91].

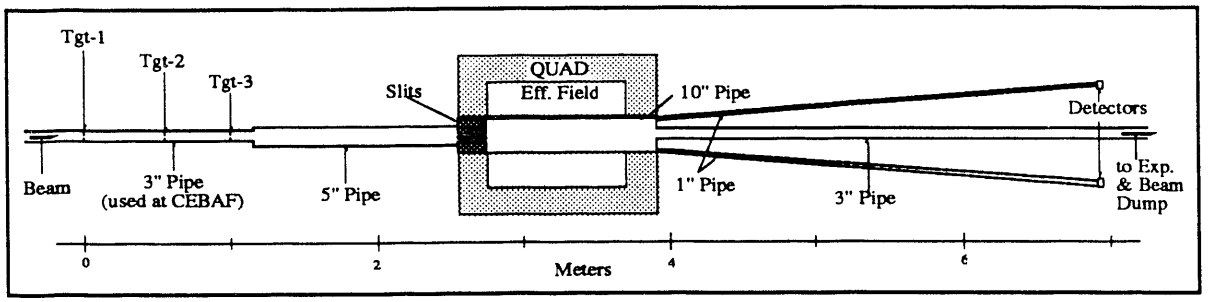

Fig. 5.7-1 Proposed Möller polarimeter for Hall-B at CEBAF.

The magnetic components of the Möller polarimeter are being designed with the aid of TRANSPORT [Bro77], a matrix multiplication and fitting program which optimizes the elements of an electron beam transport line so as to achieve the desired optics. The quadrupole to be used is an Oerlikon 10Q36A quadrupole which has an aperture diameter of 10", an effective length of 38"; a magnetic field gradient of up to 10 T/m can be obtained. A preliminary drawing of the proposed spectrometer is shown in fig. 5.7-1. The target location is selected depending on the polarized electron beam energy. Three target locations are used to achieve adequate momentum analysis at the various beam energies and still have a fixed detector position, which is a requirement for the eventual automation of the spectrometer. The slits before the quadrupole effective field and the long detector arms, which will be shielded with lead exterior to the 1" pipes, are to reduce background electrons from electron-atom and inelastic electron-electron scattering.

The targets will be Vanadium Permendur (49% Fe, 49% Co, 2% Va) foils which will be polarized by using external field coils. Vanadium Permendur is a magnetic alloy which has about 8% polarization of its electrons in an external field of more than 10 Gauss. This polarization shows a preferential alignment to the plane of the foil. Three separate targets will be placed at different orientations at each target location for the purpose of measuring all three of the polarization components of the beam. Two targets (approx. 1" by 5") will be oriented with their planes perpendicular to the beam and their long dimension aligned with the x or y axis. They will measure the transverse polarization components of the beam, P_x^B and P_y^B, respectively.

To obtain the longitudinal component of the beam polarization, P_z^B, the target foil plane will be at 20° to the beam. The polarization of the foils will be monitored after each asymmetry measurement by measuring the induced voltage in small pickup coils wound around the ends of each of the foils while reversing the direction of the external magnetic field applied by the field coils. The induced voltage is measured with an integrating digital voltmeter and the target polarization in the plane of the foil is equal to

$$P_i^T = \frac{(g-1)\text{Å}}{2\pi g N \alpha N_A \mu_B \rho Z}$$

$$x\left[\int E_{IN}\partial t - \int E_{OUT}\partial t\right] \qquad (3)$$

where μ_B is the Bohr magneton, N is the number of turns on the pickup coils, α is the cross-sectional area of the foil, ρ is the density of the foil (8.15 g/cm^3), $\bar{A}$ and $\bar{Z}$ are the average atomic mass and number of the foil (57.261 and 26.43, respectively), N_A is Avogadro's number, and g is the electron g factor. The integral over time of E_{IN} is the integrating voltmeter reading with the foil in, while E_{OUT} is the reading with the foil removed.

Design of the target chamber is under way and the target materials are presently being ordered. The spectrometer design is being finalized and construction will begin soon.

[Bea91] K. Beard, private communication, 1991

[Bro77] K.L. Brown, F. Rothacker, D.C. Carey and Ch. Iselin, SLAC Report SLAC-91, Rev. 2 (1977)

[Ols68] H. Olsen, *Springer Tracts in Mod. Phys.* **44** (1968) 83

[Wag90] B. Wagner *et al.*, Nucl. Instr. and Methods **A294** (1990) 541

5.8 Development of Detectors, Polarimeters, and Targets

We are developing detectors, polarimeters, and targets for a variety of uses in basic nuclear physics research. The following articles summarize our progress during the past year.

5.8.1 Calibration of Efficiencies for an Array of Neutron Detectors

H.R. Setze, C.R. Howell, R.T. Braun, J.M. Lambert[1]*, G. Mertens*[2]*, W. Tornow, B. Vlahovic*[3]*, R.L. Walter*

In preparation for making cross-section measurements of the n+d→n+n+p breakup reaction (see section 2.2.3), the absolute efficiency of each detector in the eleven-detector array had to be measured. The neutron energies relevant to our breakup experiment are in the range from 0.25 MeV to 10 MeV. To cover this neutron energy range completely with one measurement technique, we used the neutrons from the spontaneous fission of a ^{252}Cf radioactive source. The ^{252}Cf source was enclosed in a cylindrical gas scintillator and positioned at the center of the arc containing the 11 neutron detectors as shown in fig. 5.8-1. The walls of the scintillator were made of a 0.79-mm thick brass. The scintillator had a 7.30-cm long x 5-cm diameter cylindrical section followed by a 2.54-cm radius dome. The dome shape made the correction for neutron attenuation through the scintillator wall identical for all detectors. The scintillator was filled to 254 Torr of argon and was viewed through a glass window by a fast 5-cm diameter photomultiplier tube (PMT).

---

[1] Georgetown University, Washington, D.C.

[2] University of Tübingen, Tübingen, Federal Republic of Germany

[3] Ruder Boskovic Institute, Zagreb, Yugoslavia

The ^{252}Cf source consisted of 2 μg of ^{252}Cf electroplated onto the center of a 12.7-mm diameter x 0.127-mm thick platinum foil. The spot size of the active area was 5 mm in diameter. A 50-mg/cm^2 layer of gold was evaporated onto the ^{252}Cf deposit to prevent loss of ^{252}Cf by recoil. The source was purchased from Isotopes Products Laboratories in Burbank, CA. The center of the ^{252}Cf deposit was positioned at the center of curvature of the dome on the gas scintillator with the deposit side of the foil facing the PMT. All measurements were conducted in the neutron time-of-flight target room at TUNL.

To minimize background due to neutrons scattering from the floor, the gas scintillator containing the ^{252}Cf source and the 11 neutron detectors were supported 3.3 m above the floor by wooden scaffolds. This placed the gas scintillator and neutron detectors midway between the floor and ceiling. The total angle spread of the detector array was kept well below 180° to minimize effects due to non-uniformity of the surface of the platinum foil. On the other hand, the detectors had to be placed far enough apart to minimize cross talk between the detectors. The neutron detectors were placed about 13° apart in an arc of radius about 3 m with the gas scintillator at the center of the arc. Background measurements were taken for each detector by blocking the path of the neutrons from the ^{252}Cf source to the detector with a shadow bar as shown in fig. 5.8-1. The shadow bars were designed to attenuate 10 MeV neutrons by a factor of 6000. They were conical in shape with a 25.4-cm-long copper section followed by a 45.7-cm-long polyethelene section. To allow simultaneous background and forward measures, only three background measurements were done concurrently as shown in fig. 5.8-1. Background measurements were also made with an extra 25.4-cm of copper added to each shadow bar to determine the amount of neutron leakage through our standard shadow bars. The shadow bars were placed in front of detectors positioned 52° apart.

To reduce electronics costs, the signals from two neutron detectors were fanned into each set of detector electronics. The gains of the neutron detectors were monitored by pulsing the PMT of each detector with light from a stabilized LED. The energy of the detected neutrons was determined from the time-of-flight (TOF) between the detection of a fission fragment in the gas scintillator and a hit in a neutron detector. For each event (the coincidence within 800 ns between a signal in the gas scintillator and a hit in any of the 11 neutron detectors) the following parameters are stored in the computer: (1) pulse height in fission detector, (2) TOF of each pair of detectors, (3) pulse height in neutron detector for each pair, (4) pulse shape for each detector pair and (5) a hit register, to identify which neutron detector fired to cause the event.

The data taking phase of this project was completed July 1991, and the analysis is underway. Our results for two of the detectors will be compared to a previous calibration of these detectors using the $^2H(d,n)^3He$ reaction as the source of neutrons.

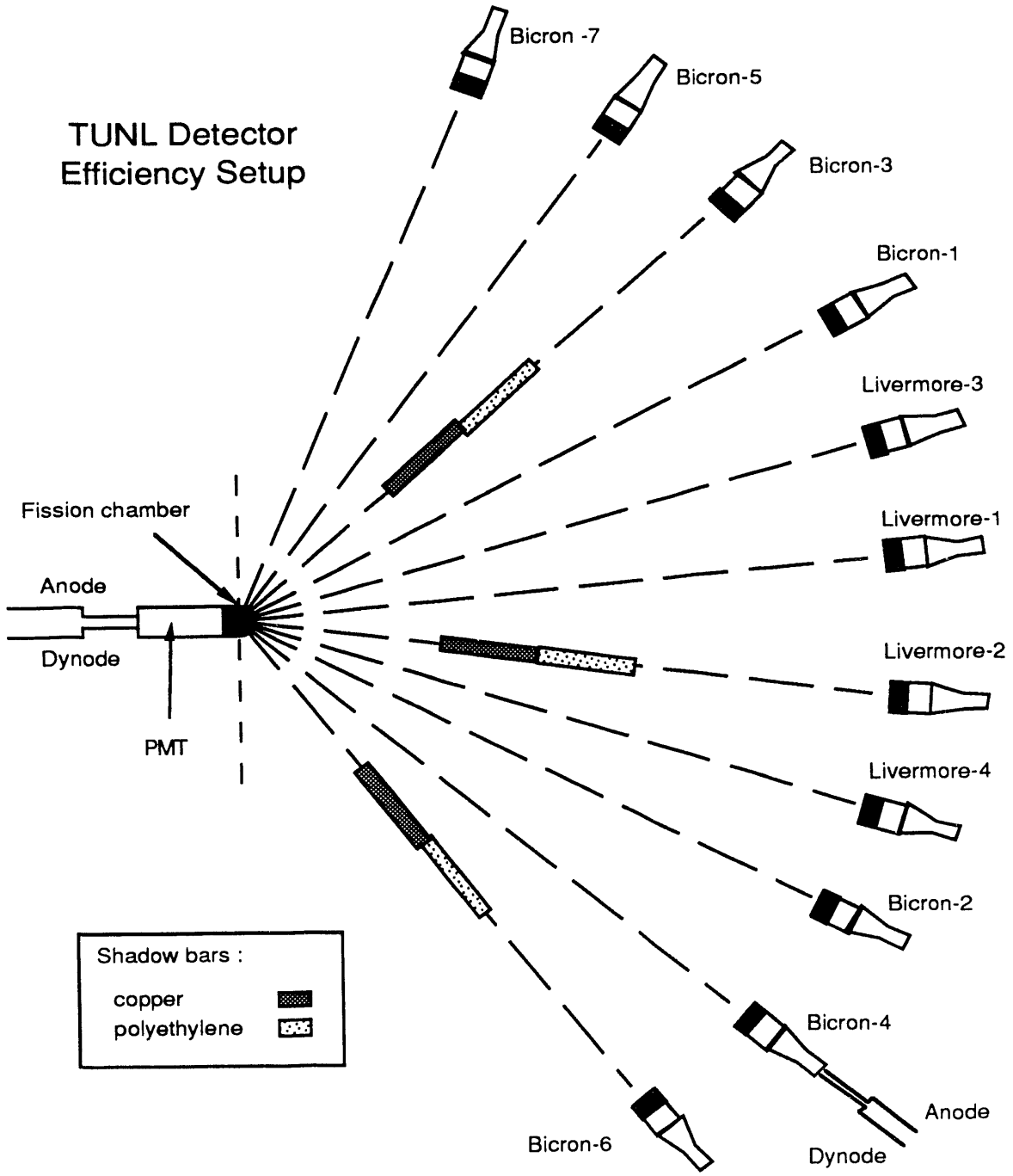

Fig. 5.8-1 Experimental setup figures for neutron detector efficiency measurements using a ^{252}Cf source.

5.8.2 An Improved Deuteron Polarimeter

C. Philp, H. J. Karwowski, E.J. Ludwig, T.B. Clegg

Precise measurements of the polarization of deuteron beams containing vector and tensor components are of great importance in the determination of vector and tensor analyzing powers. The polarization of the deuteron beams used at TUNL on the FN tandem acceler-

ator has been for a number of years determined with a three-detector polarimeter designed by Tonsfeldt *et al.* [Ton80]. To increase the flexibility and accuracy of the determination of polarization components for the beams coming from the new atomic beam polarized ion source and to provide a back-up device, a new deuteron-beam polarimeter was constructed and the calibration process has begun.

The new device, as did the Tonsfeldt polarimeter, uses the ^{3}He(d,p)^{4}He reaction. At energies of interest (4 to 20 MeV) this reaction provides the highest figure of merit and has analyzing powers which are large and vary smoothly with energy in this energy range. The ^{3}He(d,p)^{4}He reaction has an exceptionally large Q-value of 18.4 MeV, which allows easy identification of outgoing protons and gives clean spectra with very small background.

The side view of the device is shown in fig. 5.8-2. The polarimeter has five detectors (left, right, up, down, and center) and all but the center detector are 24.5° off the incoming beam axis. The addition of up and down detectors greatly facilitates the measurement of certain analyzing powers (such as the Cartesian A_{xz}) in the present data-taking scheme. The elastically-scattered deuterons are stopped by a tantalum foil, while allowing the protons to pass through to the CsI scintillation counters coupled to Hamamatsu R1166 phototubes. The body and structure of the polarimeter is made of aluminum, and the gas-cell windows are made of 6.35 mm Havar. A typical proton spectrum is shown in fig. 5.8-3.

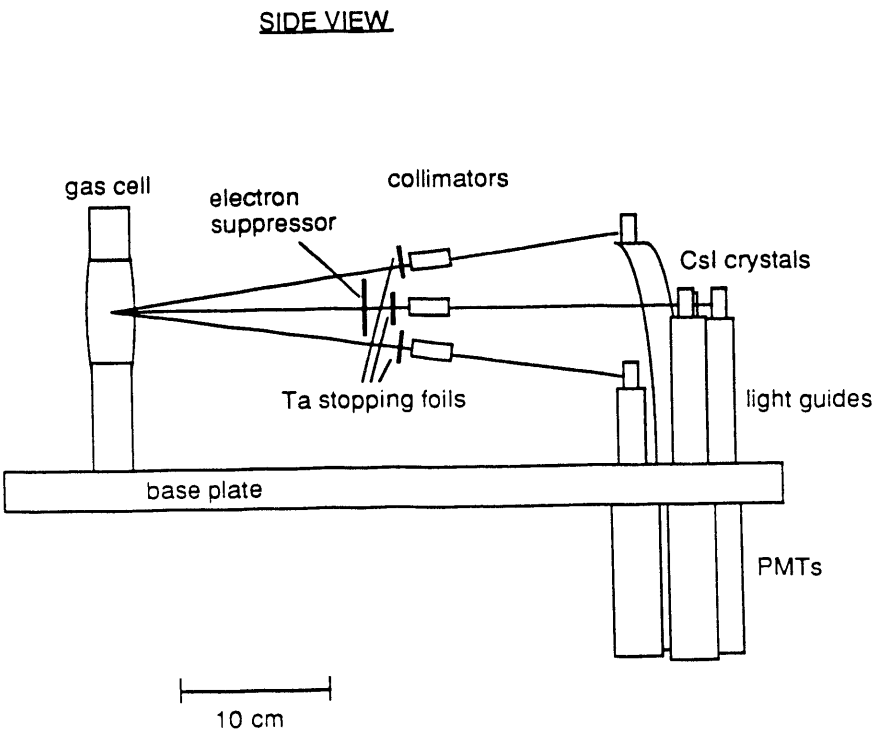

Fig. 5.8-2 Side view of the polarimeter. The aluminum collimator support is not shown.

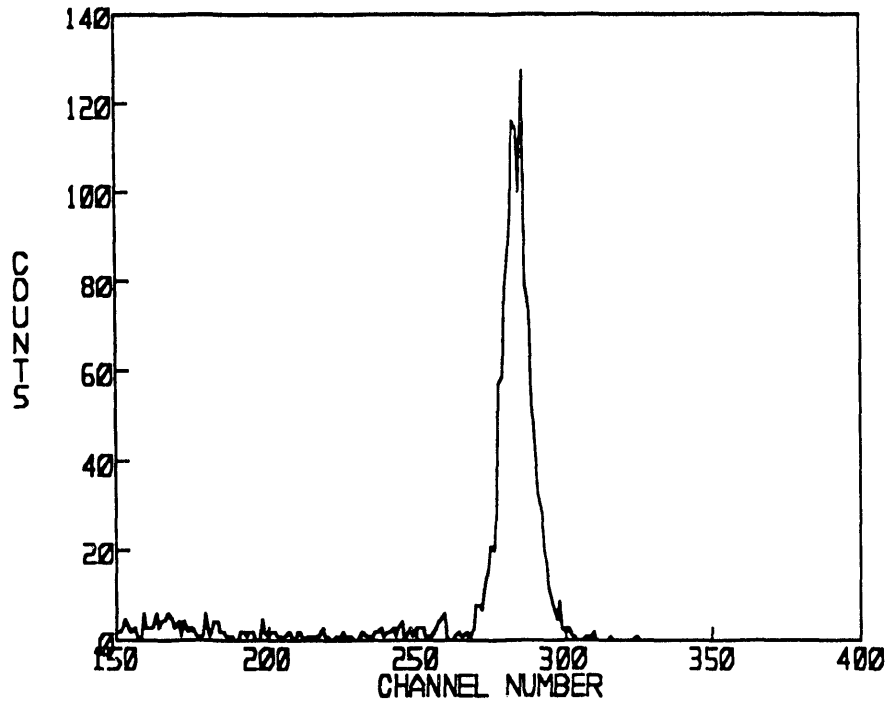

Fig. 5.8-3 Spectrum of charged particles observed in CsI counter. The peak is from protons from the ^{3}He(d,p)^{4}He reaction.

We have started calibration of the polarimeter for 4- to 12-MeV beams by using ^{4}He(d,d)^{4}He elastic scattering as the reference reaction. This selection of calibration reaction was made because there is a large set of high-precision analyzing-power data for this reaction in the energy range of interest [Grü75]. In the calibration process we took a three-run sequence for each of ten deuteron energies (one unpolarized and two polarized states), simultaneously counting elastically-scattered deuterons in a large scattering chamber and ^{3}He(d,p)^{4}He protons in the polarimeter. Then we used sums and differences of ratios of polarized to unpolarized counts from the chamber detectors, along with the known [Grü75] analyzing powers, to calculate the beam polarization [Ton80]. The use of ratios cancels out first-order errors due to detector efficiency, solid angle, and target thickness.

A preliminary data analysis resulted in curves of A_{yy} and A_{zz}, versus energy. These were compared to curves from the previous polarimeter and agreed quite well, alhough the error bars were large. The calibration will be completed in fall of 1991.

[Grü75] W. Grüebler *et al.*, Nucl. Phys. **A242** (1975) 285

[Ton80] S.A. Tonsfeldt, Ph.D. dissertation, University of North Carolina at Chapel Hill, 1980 (unpublished), available from University Microfilms International, 300 N. Zeeb Road, Ann Arbor, Michigan 48106

5.8.3 Polarized Solid ^{3}He and ^{3}He Melting-Curve Thermometers

C.D. Keith, D.G. Haase, C.R. Gould, N.R. Roberson, W.S. Wilburn, J.E. Koster

We are designing a solid ^{3}He polarized target to be mounted on the large dilution refrigerator cryostat for studies of the spin-spin component of the neutron-nucleus interaction. The target will contain 1/2 mole of solid ^{3}He at density of 24 cm^3/mole. The equilibrium nuclear polarization of such a target at 10 mk and 2T would be about 46%. For the new ^{3}He target we have built a room temperature gas handling system and a capacitance pressure measurement system which are currently being used for our ^{3}He melting curve thermometry.

In 1990 two ^{3}He melting curve thermometers (MCT's) [Gre86] were installed in the TUNL brute-force-polarization cryostat being used to polarize the TiH_2 target. Melting-curve thermometers are very sensitive, continuously reading devices with distinct advantages over nuclear orientation thermometers that are often used for such cryostats. The initial use of the MCT's was successful. The thermometers exhibited a sensitivity of ± 1.4 mK and were used to stabilize the dilution refrigerator temperature to within ± 5.5 mK at 16 mK. The MCTs agreed with the ^{60}CoCo nuclear orientation already in use to within 2% at 13 mK.

Subsequent use of the MCTs was hindered by contamination of the ^{3}He, despite attempts to filter out impurities. The ^{3}He gas was replaced in the summer of 1991 with 99.995%-pure ^{3}He. The cryostat has since been cooled once. The MCTs operated as expected, indicating dilution refrigerator and TiH_2 temperatures of 9 mK and 48 mK respectively. The latter temperature in general agreement with the ^{60}CoCo thermometer, although the MCT has much greater precision in that temperature range. The MCTs were used to calibrate a number of resistance thermometers installed in the cryostat, and the melting curve thermometers are ready for routine use.

The MCTs will be used for a close comparison of the ^{3}He melting curve and the ^{60}CoCo temperature scales. Two superconducting fixed-point devices consisting of samples of In, Ir, and Be have been installed in the cryostat. These fixed points may then be used as reproducible reference temperatures to provide run-to-run comparisons of thermometer calibrations.

5.8.4 Rotating Aligned Holmium Target for Neutron Transmission Measurements

J.E. Koster, C.R. Gould, D.G. Haase, N.R. Roberson

The operation of the TUNL rotating target dilution refrigerator cryostat was reported at the International Conference on Low Temperature Physics at Brighton, UK [Kos90] and a more complete report is being prepared for submission to Nuclear Instruments and Methods. The cryostat cooled a single crystal ^{165}Ho target to less than 250 mK for neutron transmission measurements. The target was aligned to about 67% of the maximum possible value. The target did not warm during rotation and could be kept aligned for long periods. Using the nuclear deformation of holmium, we were able to measure the degree of nuclear alignment and to accurately determine the target crystal orientation.

We have previously reported [Ann90] measurements of the nuclear deformation effect in aligned holmium. We measured neutron transmission through a cryogenically aligned single crystal. The target was cylindrical, with its alignment axis oriented radially and its symmetry axis oriented vertically. By rotating the target about the vertical axis, we mapped out for the first time the angular signature $P_2(\cos\theta)$ of the deformation effect, where θ is the angle between the alignment axis and the beam direction. Transmission yields were measured at different θ for various sequences of angles.

Since last year's report, we have used Fourier analysis to exploit the periodicity in angle (run number) of the transmission yields. The raw data are shown in fig. 5.8-3 for 1.8-MeV neutrons. For transmission values that repeat every t runs due to the deformation effect, the largest contiguous set is used having an integer multiple number of runs, n t. A Fourier transform is calculated for the set, in which the deformation effect periodicity should appear as a peak at frequencies $f = \pm nt/p+1$. The Fourier transform of the data in fig. 5.8-3 is shown in fig. 5.8-4. The amplitude of the transform at the frequency representing the deformation effect – where there is clearly a peak – is directly proportional to the deformation cross section σ_2, with the constant of proportionality determined by the target alignment and thickness. Deformation cross sections extracted through Fourier-transform analysis agree well with the values obtained by directly fitting the average transmission data at each angle.

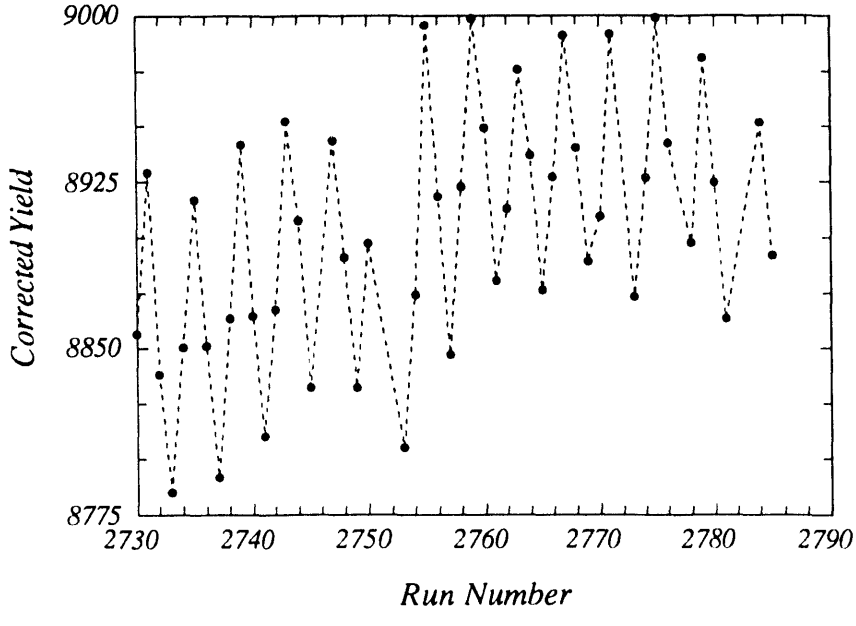

Fig. 5.8-3 Count rate versus run number for transmission of unpolarized neutrons through aligned ^{165}Ho, showing periodic dependence of count rate upon orientation θ of target relative to beam direction. The slowly varying backgroung drift has not been removed.

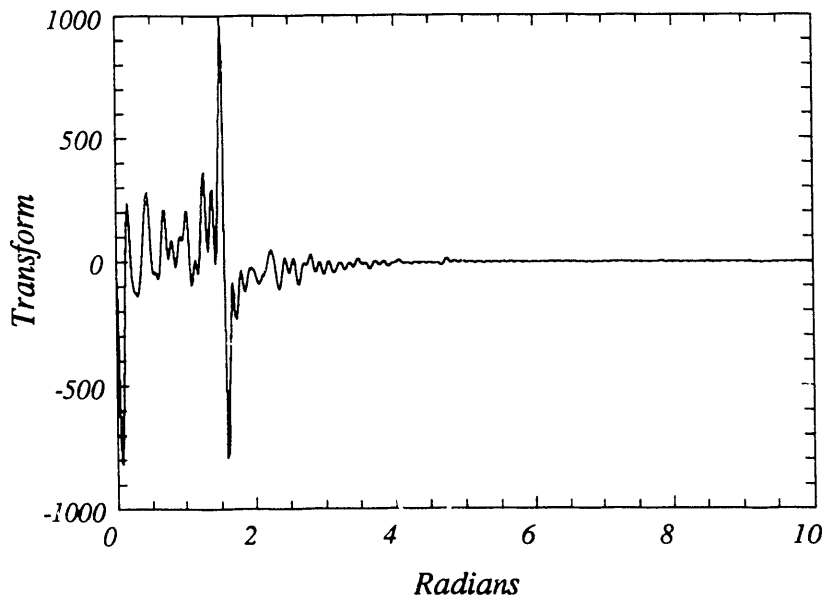

Fig. 5.8-4 Fourier transform of the data in the previous figure. The lower frequency components are primarily due to the background drift.

[Ann 90] TUNL Annual Report 1991

[Kos90] J.E. Koster, C.R. Gould, D.G. Haase, and N.R. Roberson, Physica **B165** (1990) 153

5.8.5 Bolometric Detector Development

C.G. DePree, L.A. Jones, A.E. Champagne, D.G. Haase

We have recently begun development of a microcalorimeter optimized for the detection of x- and β radiation. These devices exploit the low heat capacity of materials at cryogenic temperatures and allow the measurement of energy via temperature rise. In principle, superb energy resolution can be achieved. This is because the total energy of an event can be measured independently of the mode of energy loss and because the thermal noise [proportional to $(CT^2)^{1/2}$ where C is the heat capacity and T is the temperature] can be made arbitrarily small by simply lowering the temperature. These properties have been demonstrated in a number of laboratories, for example by [Mos88], and further development continues. Our work at TUNL is a natural extension of our current applications of low-temperature techniques to nuclear studies.

A typical bolometer design is shown in fig. 5.8-5. It consists of an absorber which is connected by a thermal link to a thermometer (often a thermistor). The electrical leads also provide mechanical support as well as a weak thermal link to the bath. For our absorber,

we have chosen to use a wafer of bismuth, about 1 mm in diameter and 0.5 to 1 mm in thickness. The radioactive source of

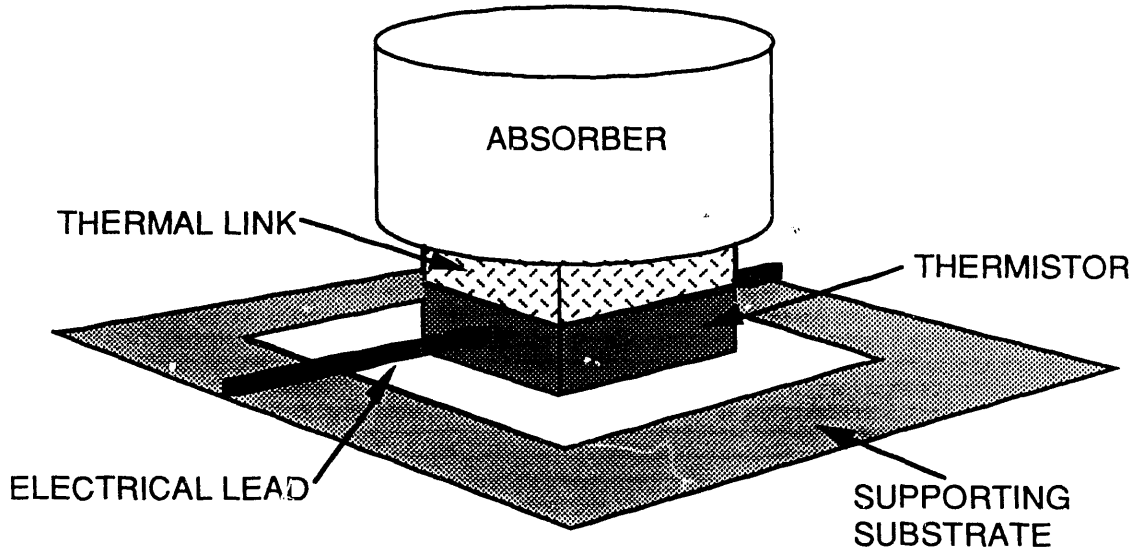

Fig. 5.8-5 Schematic of the bolometer under construction.

interest could either be placed on the surface of the bismuth or can be encapsulated within it. The absorber will be connected to a RuO_2 thermistor with epoxy. For electrical connections, we expect to use aluminum wire.

There are disadvantages as well as advantages associated with the use of RuO_2 as a thermistor: Although it is commercially available, and exhibits good stability and reproducibility, it has a fairly high heat capacity . Hence our thermal noise will be relatively high (on the order of 100 eV) at our expected operating temperature of 40-60 mK. However, this detector could be ideal for applications where low background and spectral fidelity are more important than energy resolution.

We have completed extensive numerical simulations of the response of this bolometer and are now in the process of fabricating a prototype. Front-end electronics have been built and they appear to be adequate for our needs. When finished, the prototype will be mounted inside a dilution-refrigerator cryostat for source tests.

[Mos88] S.H. Moseley *et al.*, IEEE Trans., **NS35** (1988) 59 and references therein

5.9 The TUNL Computing Network

N.R. Roberson, S. Edwards, C.R. Gould, C.R. Howell, C.R. Westerfeldt

The upgraded TUNL data-acquisition and analysis facility was planned and funded in 1988 by the US DOE and by the University. A block diagram of the system as currently configured is shown in fig. 5.9-1. The local network consists of nine VS3200 work-

stations and one μVAX 3500. In addition, VS 3200 workstations are located in the physics departments at North Carolina State University in Raleigh and at the University of North Carolina at Chapel Hill.

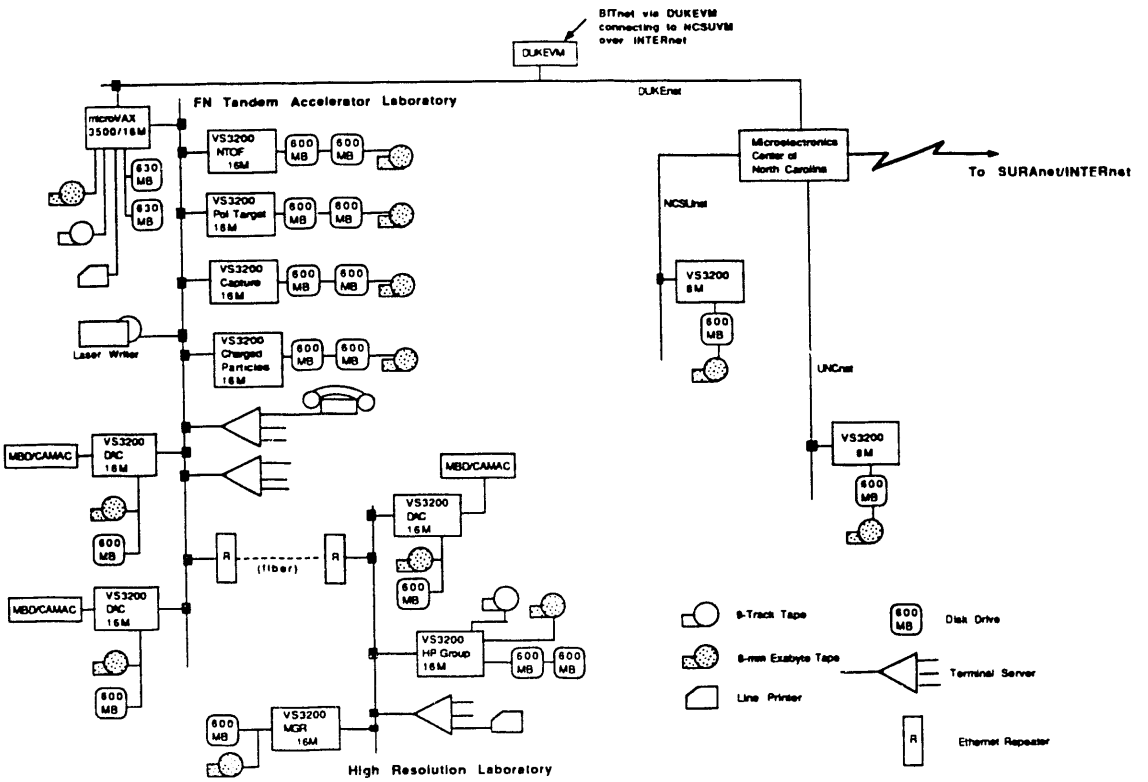

Fig. 5.9-1 Block diagram of the TUNL computer system.

The μVAX 3500 is the boot-node machine and is equipped with 16 MB of memory, a TR70 magnetic tape, a 6250-bpi 9-track magnetic tape, an Exabyte 8-mm tape system, two 630-MB disk drives and a 300-lpm line printer. The data-acquisition (DAC) machines for the tandem and the high-resolution laboratories are operated as stand-alone systems. Each has 16 MB of memory, a 600-MB disk, a 8-mm Exabyte tape system and a Q-bus to Unibus converter to permit the connection of a MBD-11 CAMAC branch driver to the VS 3200 Q-bus. The DAC machines utilize the fully-mature and TUNL-developed XSYS data-acquisition software package. Six of the VS 3200 machines are booted from the μVAX 3500: four are used for data analysis and general computing by the four major experimental groups operating in the tandem laboratory, one is used by the high-resolution experimental group, and one is for the system manager. These machines have 16 MB of memory, two 600-MB disk drives and one 8-mm Exabyte tape drive. Terminal servers are

located in both laboratories and have a total of 72 ports. A laser printer is also connected to the network.

A separate Ethernet card in the μVAX 3500 connects TUNL to the campus networks (DUKEnet, NCSUnet and UNCnet) and to the Microelectronics Center of North Carolina. The connection to the Microelectronics Center also provides access to INTERnet via SURAnet. The μVAX 3500 and the two workstations at NCSU and UNC/CH are using the MultiNet software package from TGV Inc., which allows network communication using the TCP/IP protocol.

We had planned to also connect to the DOE Energy Sciences Network (ESnet) by establishing a DECnet-over-IP link to a computer at CEBAF. However, the ESnet Coordinating Committee has discouraged us from making this link because of problems with DECnet-over-IP in the next version of DECnet. We are currently investigating connecting to ESnet by sharing, with the Duke University high energy physics group, a leased 56K communications line to FNAL.

APPENDICES

I. Ph. D. Dissertations

1. David Abbott, "An Investigation of the Deuteron-Nucleus Tensor Interaction in $^{90}Zr(\vec{d},\vec{d})^{90}Zr$ Elastic Scattering," Ph.D. degree, UNC. *Supervisor*--H.J. Karwowski
2. Paul D. Felsher, "Vector and Tensor Polarization Measurements for d-p and d-n Quasifree Scattering Using the $\vec{d}$+d→d+p+n Breakup Reaction at 12 MeV," Ph.D. degree, Duke. *Supervisor*--R.L. Walter
3. Christen M. Frankle, "Parity Nonconservation for Neutron Resonances in ^{81}Br and ^{232}Th," Ph.D. degree, NCSU. *Supervisor* -- G.E. Mitchell
4. Stephanie C. Frankle, "Nuclear Resonances Spectroscopy in ^{30}P," Ph.D. degree, NCSU. *Supervisors* -- G.E. Mitchell and J.F. Shriner, Jr.
5. James E. Koster, "A Test of Time Reversal Invariance with Polarized Neutrons and Aligned ^{165}Holmium," Ph.D. degree, NCSU. *Supervisor*--C.R. Gould
6. Xianzhou Zhu, "Measurement of the RMS Parity Violating Matrix Element in ^{239}U," Ph.D. Degree, Duke. *Supervisor*--N.R. Roberson

II. Journal Articles

Published articles

1. Parity Nonconservation for Neutron Resonances in ^{238}U, J.D. Bowman, C.D. Bowman, J.E. Bush, P.P.J. Delheij, C.M. Frankle, C.R. Gould, D.G. Haase, J. Knudson, G.E. Mitchell, S. Penttila, H. Postma, N.R. Roberson, S.J. Seestrom, J.J. Szymanski, V.W. Yuan and X. Zhu, Phys. Rev. Lett. **65** (1990) 1192
2. Proton Mean Field in ^{40}Ca between -60 MeV and +200 MeV Deduced from a Dispersive Optical-Model Analysis, W. Tornow, Z.P. Chen and J.P. Delaroche, Phys. Rev. **C42** (1990) 693
3. Two-Deuteron Radiative Capture: Polarization Observables at $E_d \leq 15$ MeV, J. L. Langenbrunner, H.R. Weller and D.R. Tilley, Phys. Rev. **C42** (1990) 1214
4. $^3H(p,\gamma)^4He$ Reaction and the $(\gamma,p)/(\gamma,n)$ Ratio in ^4He, G. Feldman, M.J. Balbes, L.H. Kramer, J.Z. Williams, H.R. Weller and D.R. Tilley, Phys. Rev. **C42** (1990) R1167
5. Parity Violation in ^{239}U Neutron Resonances, S. Penttila, C.D. Bowman, J.D. Bowman, J.E. Bush, P.P.J. Delheij, C.M. Frankle, C.R. Gould, D.G. Haase, J.N. Knudson, G.E. Mitchell, H. Postma, N.R. Roberson, S.J. Seestrom, J.J. Szymanski, B. Tippens, V.W. Yuan and X. Zhu, 7th International Conference on Polarization Phenomena in Nuclear Physics, eds. A. Boulard and Y. Terrien (Les Editions de Physique, Les Ulis, 1990) Colloque de Physique C6, Tome **51**, 523
6. Isovector Giant Quadrupole Resonance Observed in $^{30}Si(\vec{p},\gamma)^{31}P$, G. Feldman, L.H. Kramer, H.R. Weller, E. Hayward and W.R. Dodge, Phys. Rev. **C43** (1991) 223

7. Ground-State Widths of ^{5}He and ^{5}Li Determined in the ^{3}H(d,γ)^{5}He and the ^{3}He(d,γ)^{5}Li Reactions, M.J. Balbes, G. Feldman, L.H. Kramer, H.R. Weller and D.R. Tilley, Phys. Rev. **C43** (1991) 343
8. Neutron-Proton Analyzing Power Data at 7.6, 12.0, 14.1, 16.0, 18.5 MeV, G.J. Weisel, W. Tornow, C.R. Howell, P.D. Felsher, M. Alohali, Z.P. Chen, R.L. Walter, J.M. Lambert and P.A. Treado, Colloque de Physique **C6** (1990) 515
9. Resolution of the Twofold Ambiguity in the $E1$ Capture Amplitudes for the ^{13}C(p,γ)^{14}N Reaction, V. Wijekumar, J.Z. Williams, G. Feldman, H.R. Weller and D.R. Tilley, Phys. Rev. **C43** (1991) 1363
10. Scattering of Polarized and Unpolarized Neutrons from ^{93}Nb from 8 to 17 MeV and Optical Model Descriptions, R.S. Pedroni, R.C. Byrd, G.M. Honoré, C.R. Howell and R.L. Walter, Phys. Rev. **C43** (1991) 2336
11. A Determination of the Asymptotic D- to S-State Ratio for ^{3}He, C.M. Bhat, E.J. Ludwig, T.B. Clegg and H.J. Karwowski, Nucl. Phys. **A526** (1991) 36
12. Neutron-Deuteron Elastic Scattering and Breakup Reactions below 20 MeV, C.R. Howell, W. Tornow, H.G. Pfützner, M.L. Roberts, K. Murphy, P.D. Felsher, G.J. Weisel, G. Mertens, R.L. Walter, J.M. Lambert, P.A. Treado and I. Slaus, Nucl. Phys. **B56/57** (1991) 459
13. Fluctuation Properties of Spacings of Low-Lying Nuclear Levels, J.F. Shriner, Jr., G.E. Mitchell and T. von Egidy, Z. Phys. **A338** (1991) 309
14. Novel Applications of Narrow Nuclear Resonances, G.E. Mitchell and C. Rolfs, Nucl. Instr. Methods **B56/57** (1991) 473
15. Chaotic Behavior of Nuclear Spectra, G.E. Mitchell, E.G. Bilpuch, P.M. Endt, J.F. Shriner, Jr. and T. von Egidy, Nucl. Instr. Methods **B56/57** (1991) 446
16. Parity and Time-Reversal Symmetry Violation in Neutron-Nucleus Interactions," J.D. Bowman, C.D. Bowman, J. Knudson, S. Penttila, S.J. Seestrom, J.J. Szymanski, V.W. Yuan, J.E. Bush, C.M. Frankle, C.R. Gould, D.G. Haase, G.E. Mitchell, P.P.J. Delheij, H. Postma, N.R. Roberson and X. Zhu, Progress in High Energy Physics, eds. W.Y.P. Hwang, S.C. Lee, C.E. Lee and D.J. Ernst (North Holland, New York, 1991) p.81
17. Test of Level Densities with Proton Resonances, J. Li, E.G. Bilpuch, C.R. Westerfeldt, G.E. Mitchell and F. Yang, Phys. Rev. **C44** (1991) 345
18. Sign Correlations and Parity Nonconservation for Neutron Resonances in ^{232}Th, C.M. Frankle, J.D. Bowman, J.E. Bush, P.P.J. Delheij, C.R. Gould, D.G. Haase, J.N. Knudson, G.E. Mitchell, S. Penttila, H. Postma, N.R. Roberson, S.J. Seestrom, J.J. Szymanski, S.H. Yoo, V.W. Yuan and X. Zhu, Phys. Rev. Lett. **67** (1991) 564
19. Three-Nucleon Physics: Paradigm and Pitfalls, I. Slaus, R. Machleidt, W. Tornow, W. Glöckle, H. Witała, Comments Nucl. Part. Phys. **20** (1991) 85
20. The Low-Energy Neutron-Deuteron Analyzing Power and the $^{3}P_{0,1,2}$ Interactions of Nucleon-Nucleon Potentials, W. Tornow, C.R. Howell, M. Alohali, Z.P. Chen, P.D. Felsher, J.M. Hanly, R.L. Walter, G. Weisel, G. Mertens, I. Slaus, H. Witala and W. Glöckle, Phys. Lett. B **257** (1991) 273

21. D-State Parameter Determinations for ^{3}He and ^{4}He, E.J. Ludwig, C.M. Bhat, T.B. Clegg, E.R. Crosson,H.J. Karwowski, G. Graw, P. Schiemenz, R. Hertenberger, H. Kader, D. Hofer, A.M. Eiro and F.D. Santos, 7th International Conference on Polarization Phenomena in Nuclear Physics, Paris 1990, C6-439
22. A Global Nucleon Optical Model Potential, R.L. Varner, W.J. Thompson, E.J. Ludwig and T.B. Clegg, Phys. Rep. **201** (1991) 58
23. Correcting Parameter Bias Caused by Taking Logs of Exponential Data, W.J. Thompson and J.R. Macdonald, Am. J. Phys. **59** (1991) 854
24. Sources of Spin-Polarized Beams, T.B. Clegg, in Proc. of Intern. Conf. on Ion Sources, Berkeley, July 10-14, 1989, ed. I. Brown, Rev. Sci. Instrum. **61** No. 1 Part III (1990) 385
25. Recent Technical Advances for Polarization Studies, T.B. Clegg, 7th Intern. Conference on Polarization Phenomena in Nuclear Physics, Paris, July 9-13, 1990, ed. A. Boudard (Colloque de Physique, Paris, 15 November 1990) **C6** 533
26. A Mechanism for Precise Proton Rotation of Nuclear Targets at Low Temperatures, J.E. Koster, C.R. Gould, D.G. Haase, N.R. Roberson, Physica **B165&166** (1990) 153

Articles accepted

1. Recent Developments in Low-Energy Nucleon-Nucleon Interaction Studies, W. Tornow (Adv. in Nucl. Phys.)
2. Strongly Heteroscedastic Nonlinear Regression, J.R. Macdonald and W.J. Thompson (Comm. in Statistics: Simulation and Computation)
3. A Concise Derivation of the Plane-Wave Partial-Wave Expansion, W.J. Thompson (Am. J. Phys.)
4. Least Squares Fitting When Both Variables Contain Errors: Pitfalls and Possibilities, J.R. Macdonald and W.J. Thompson (Am. J. Phys.)
5. Fourier Series and the Gibbs Phenomenon, W.J. Thompson (Am. J. Phys.)
6. Optimization of the Performance of R. F. Transitions for TUNL Atomic Beam Polarized Source, E.R. Crosson, T.B. Clegg, H.J. Karwowski and S.K. Lemieux (Nucl. Instrum. Meth.)
7. Recent Developments in Intense Polarized Hydrogen and Deuterium Ion Sources, T.B. Clegg, Proc. IEEE Particle Accelerator Conference, San Francisco, May 6-9, 1991 (IEEE Conference Record)

Submitted articles

1. Recent Advances in Low-Energy Few-Nucleon Physics, R. Machleidt, I. Slaus, W. Tornow, W. Glöckle and H. Witała, (Few-Body Systems)
2. Coulomb Effects in Three-Nucleon Scattering versus Charge-Symmetry Breaking in the ^3P_J Nucleon-Nucleon Interactions, W. Tornow, C.R. Howell, R.L. Walter and I. Slaus, (Phys. Rev. C)

3. Neutron-Proton Analyzing Power Data Between 7.6 and 18.5 MeV G.J. Weisel, W. Tornow, C.R. Howell, P.D. Felsher, M. AlOhali, Z.P. Chen, R.L. Walter, J.M. Lambert, P.A. Treado and I. Slaus, (Phys. Rev. C)
4 Energy Dependence of Nucleon-Deuteron Elastic Scattering Observables and Its Bearing on the ^3P_J NN Interactions, W. Tornow, H. Witała and W. Glöckle, (Few-Body Systems)
5. Isospin-Nonconserving Particle Decays in Light Nuclei, J.F. Wilkerson, T.M. Mooney, R.E. Fauber, T.B. Clegg, E.J. Ludwig and W.J. Thompson, (Nucl. Phys.)
6. Probing α-Particle Wave Functions by (d,α) Tensor Analyzing Powers, E.R. Crosson, R.K. Das, E.J. Ludwig, W.J. Thompson, M. Bisenberger, R. Hertenberger, D. Hofer, H. Kader, P. Schiemenz, G. Graw, A.M. Eiro and F.D. Santos, (Phys. Rev. Letters)
7. An Energy-Resolution-Function Measurement System for Charged-Particle Beams, T.M. Mooney, T.B. Clegg, R.E, Fauber and E.J. Ludwig, (Nucl. Inst. and Methods)
8. Algorithms for Normalizing by Least Squares, W.J. Thompson (Computers in Physics)
9. Ground State Gamow-Teller Strength in ^{64}Ni(n,p)^{64}Co Cross Sections at 90-240 MeV, A. Ling, X. Aslanoglou, F.P. Brady, R.W. Finlay, R.C. Haight, C.R. Howell, N.S.P. King, P.W. Lisowski, B.K. Park, J. Rapaport, J.L. Romero, D.S. Sorenson, W. Tornow, J.L. Ullmann (Phys. Rev. C)
10. The Energy Dependence of the Gamow-Teller Strength in p-shell Nuclei Observed in the (n,p) Reaction, D.S. Sorenson, J.L. Ullmann, A. Ling, P.W. Lisowski, N.S.P. King, R.C. Haight, F.P. Brady, J.L. Romero, J.R. Drummond, C.R. Howell, W. Tornow, J. Rapaport, B.K. Park, X. Aslanoglou (Phys. Rev. Lett.)
11. Search for Charge Symmetry Breaking in the Deuteron-Induced Deuteron Breakup, P.D. Felsher, C.R. Howell, I. Slaus, W. Tornow, M.L. Roberts, J.M. Hanly, G.J. Weisel, M. AlOhali, R.L. Walter, J.M. Lambert, P.A. Treado, G. Mertens, Y. Koike (Phys. Rev. Lett.)
12. Angular Distribution Coefficients for (γ,χ) Reactions with Linearly Polarized Photons, H.R. Weller *et al.*(Atomic Data and Nuclear Data Tables)
13. The ^{6}Li($\vec{d}$,γ)^{8}Be Reaction at E_d=9.0 MeV and the D-State of ^{8}Be, J.Z. Williams, G. Feldman, H.R. Weller, D.R. Tilley (Phys. Lett.)
14. Energy Levels of Light Nuclei A=4, D.R. Tilley, H.R. Weller, G.M. Hale (Nucl. Phys.)

III. Invited Talks

1. Chaotic Behavior of Nuclear Levels, G.E. Mitchell, VI International School on Neutron Physics, Alushta, USSR (1990)
2. Chaos in Nuclei?, G.E. Mitchell, Bull. Am. Phys. Soc. **35** (1990) 1662 – DNP meeting

3. Chaotic Behavior of Nuclear Spectra, G.E. Mitchell, Bull. Am. Phys. Soc. **35** (1990) 1736 -- Deuteron Accelerator Conference
4. Recent Developments in Low-Energy Nucleon-Nucleon Interaction Studies, W. Tornow, Int. Conf. on Spin and Isospin in Nucl. Int., Telluride, Colorado, 1991, to be published in Adv. in Nucl. Phys.
5. Advances in Few-Body Physics, W. Tornow, Centre d'Etudes de Brujeres-le-Châtel, France
6. Wenig-Nucleonen Systeme, W. Tornow, University of Erlangen, Germany
7. Fortschritte in Zwei und Drei-Teilchen System, W. Tornow, University of Tübingen, Germany
8. Low-Energy Few-Nucleon Physics: A Testing Ground of the Nucleon-Nucleon Interaction, W. Tornow, Ohio University, Athens, Ohio
9. Beta-neutrino Correlations in the Decay of ^{33}Ar, H.J. Karwowski, Warsaw University, Warsaw, Poland
10. Review of Capture Program at Lawrence Berkeley Laboratory, H.R. Weller, NSAC Review Board at 88" Cyclotron Laboratory, Berkeley, California (1990)
11. Studies of Few Body Nuclear Systems Using Radiative Capture Reactions, H.R. Weller, Gordon Research Conference on Simple Systems in Physics and Chemistry (1990)
12. Isovector Giant Quadrupole Resonances in $(\vec{p},\gamma)$ Reactions, H.R. Weller, Seventh International Symposium on Capture Gamma-Ray Spectroscopy, Asilomar, California (1990)
13. Few Body Capture Reactions at Very Low Energies, H.R. Weller, Fast Nucleon Radiative Capture Workshop, Berkeley, California (1990)
14. Resolution of the $(\gamma,p)/(\gamma,n)$ Ratio Problem in ^{4}He, H.R. Weller, Nuclear Division Meeting of the American Physical Society, Urbana, Illinois (1990)
15. Radiative Capture of Deuterons in Light Nuclei, H.R. Weller, Few Body Topical Group Meeting of the American Physical Society, Washington, D.C. (1991)

IV. Conference Reports

1. A Dispersion-Relation Optical Model for n + ^{28}Si, M.A. Alohali, J.P. Delaroche C. R. Howell, W. Tornow and R.L. Walter, Bull. Am. Phys. Soc. **36** (1990) 1650
2. The (n,p) Reaction on Sulfur for Incident Neutron Energies of 50 MeV - 250 MeV, B.K. Park, X. Aslanglou, F.P. Brady, G. Fink, R.W. Finlay, C.R. Howell, A. Ling, P.W. Lisowski, J. Rapaport, J.L. Romero, D. Sorenson, W. Tornow and J.L. Ullmann, Bull. Am. Phys. Soc. **36** (1990) 1650
3. The D-State of ^{3}H Determined from the Sub-Coulomb ^{95}Mo(d,t) ^{94}Mo Reaction, R.K. Das, D.J. Abbott, T.B. Clegg, E.R. Crosson, K.A. Fletcher, H.J. Karwowski, S. Lemieux and E.J. Ludwig, Bull. Am. Phys. Soc. **36** (1990) 1659
4. Ground-State Widths of ^{5}He and ^{5}Li, M.J. Balbes, L.H. Kramer, G. Feldman, H.R. Weller and D.R. Tilley, Bull. Am. Phys. Soc. **36** (1990) 1660
5. Chaos in Nuclei?, G.E. Mitchell, Bull. Am. Phys. Soc. **36** (1990) 1662

6. Resolution of the (γ,p)/(γ,n) Ratio Problem in ^{4}He, H.R. Weller, Bull. Am. Phys. Soc. **36** (1990) 1662
7. Microscopic Optical Model Calculations for Nucleon-Nucleus Scattering in Light Nuclei ($6 \leq A \leq 11$), L.F. Hansen, F.S. Dietrich and R.L. Walter, Bull. Am. Phys. Soc. **36** (1990) 1668
8. Neutron-Diffraction Elastic Scattering and Breakup Reactions Below 20 MeV, C.R. Howell, Bull. Am. Phys. Soc. **36** (1990) 1696
9. Prospects for Single State High Charge State ECR Ion Sources, T. Clegg, Bull. Am. Phys. Soc. **36** (1990) 1704
10. Chaotic Behavior of Nuclear Spectra, G.E. Mitchell, Bull. Am. Phys. Soc. **36** (1990) 1736
11. Radiative Capture of Deuterons on Light Nuclei, H.R. Weller, Bull. Am. Phys. Soc. **36** (1991) 1238
12. Test of a Prototype 275 MHz Epithermal Neutron Detector, Sung Hoon Yoo, J.D. Bowman, J. Knudson, S. Penttïla, S.J. Seestrom, J.J. Szymanski, V.W. Yuan, C.R. Gould, J.E. Bush, C.M. Frankle, D.G. Haase, G.E. Mitchell, P.P.J. Delheij, N.R. Roberson, X. Zhu, H. Postma, H.M. Shimizu and Y. Masuda, Bull. Am. Phys. Soc. **36** (1991) 1301
13. A Lamb-Shift Polarimeter for Low-Energy Beam Polarization Measurements, S.K. Lemieux and T.B. Clegg, Bull. Am. Phys. Soc. **36** (1991) 1302
14. Acquired Polarization Effects in Parity Violation Experiments with Neutron Beams, P.A. Larson, J.R. Vanhoy and G.E. Mitchell, Bull. Am. Phys. Soc. **36** (1991) 1350
15. Spin and Non-Spin Resonances from the (n,p) Reaction on ^{40}Ca for Incident Neutron Energies of 50 MeV - 250 MeV, B.K. Park, F.P. Brady, G. Fink, C.R. Howell, A. Ling, J. Rapaport, J.L. Romero, D. Sorenson, T.C. Ronnqvist, W. Tornow, J.L. Ullmann and X. Yang, Bull. Am. Phys. Soc. **36** (1991) 1350
16. The Gamow-Teller Transition for ^{64}Ni(n,p) ^{64}Co at Neutron Energies from 60 to 260 MeV, A. Ling, R.C. Haight, N.S.P. King, P.W. Lisowski, J.L. Ullmann, X. Aslanoglou, R.W. Finlay, B. Park, J. Rapaport, F.P. Brady, J.L. Romero, D.S. Sorenson, C.R. Howell and W. Tornow, Bull. Am. Phys. Soc. **36** (1991) 1350
17. The Energy Dependence of the Gamow-Teller Transition for ^{6}Li(n,p), ^{12}C(n,p) and ^{13}C(n,p) from Bombarding Energies of 65 to 250 MeV, D.S. Sorenson, X. Aslanoglou, F.P. Brady, J.R. Drummond, R.C. Haight, C.R. Howell, N.S.P. King, A. Ling, P.W. Lisowski, C.L. Morris, B.K. Park, J. Rapaport, J.L. Romero, W. Tornow and J.L. Ullmann, Bull. Am. Phys. Soc. **36** (1991) 1350
18. Optimization of the Performance of R. F. Transitions for TUNL Polarized Ion Source, E.R. Crosson, H.J. Karwowski, S.K. Lemieux and T.B. Clegg, Bull. Am. Phys. Soc **36** (1991) 1393
19. Coulomb Effects in Three-Nucleon Scattering Versus Charge-Symmetry Breaking in the ^{3}P Nucleon-Nucleon Interactions, W. Tornow and R.L. Walter, Bull. Am. Phys. Soc. **36** (1991) 1400
20. A Measurement of D-state Parameters for the Triton Using ^{149}Sm(d,t)^{148}Sm Reaction at Sub-Coulomb Energies, R.K. Das, T.C. Black, T.B. Clegg, E.R. Crosson, D.C.

Dinge, K.A. Fletcher, H.J. Karwowski, S.K. Lemieux and E.J. Ludwig, Bull. Am. Phys. Soc. **36** (1991) 1401

21. The ^{6}Li $(\vec{d},\gamma)^{8}$Be Reaction and the D-State of ^{8}Be, J.Z. Williams, G. Feldman, H.R. Weller and D.R. Tilley, Bull. Am. Phys. Soc. **36** (1991) 2152
22. Analyzing Powers in the Radiative Capture of Polarized Deuterons on Deuterons at 80 keV and the D-State of ^{4}He, L.H. Kramer, R.M. Chasteler, E. Hayward, H.R. Weller and R.M. Prior, Bull. Am. Phys. Soc. **36** (1991) 2121
23. Deuteron Capture in ^{3}He and the Role of the Tensor Force, M.J. Balbes, G. Feldman, H.R. Weller and D.R. Tilley, Bull. Am. Phys. Soc. **36** (1991) 2122

V. Seminars at TUNL

1. Bernhard Mecking, CEBAF (8/30/90)
   Physics Program and Instrumentation of CEBAF's Hall B
2. B. Sur, Lawrence Berkeley Laboratory (9/6/90)
   Search for Massive Neutrinos and Their Astrophysical Implications
3. R. Bruce Vogelaar, Princeton University (9/18/90)
   The Destruction of ^{26}Al at Low Stellar Temperature
4. Larry Lamm, University of Wisconsin (9/20/90)
   The Influence of the Level Structure of ^{20}Na Upon the Stellar Reaction Rate for ^{19}Ne(p,γ)^{20}Na
5. Wolfgang Kretschmer, University of Erlangen, Germany (9/27/90)
   Investigation of the Nucleon-Nucleon Interaction from Proton-Proton and Proton-Deuteron Experiments with Polarized Protons
6. Hiroyuki Okamura, University of Tokyo, Japan (10/2/90)
   Spin- and Isospin-Flip Excitation via the Deuteron Breakup Reaction with Strong Final State Interaction
7. Joe McDermott, NIKHEF, The Netherlands (10/4/90)
   Photo-Nuclear Knockout Beyond PWIA
8. Stefan Schramm, California Institute of Technology (11/6/90)
   Cold Fusion in Stars
9. Karl Pitts, University of Wisconsin (11/8/90)
   Spin-Triplet Strength in the ^{3}H(p,γ)^{4} He Reaction with Polarized Protons
10. Evans Hayward, Duke University (11/13/90)
    Absorption and Scattering of Photons by Nuclei
11. Mark Roberts, Lawrence Livermore National Laboratory (11/15/90)
    The Computer Control System and AMS at LLNL
12. Michael J. Finn, College of William and Mary (11/16/90)
    The Electromagnetic Structure of the Nucleon
13. Makoto Tanifuji, Hosei University, Japan (11/20/90)
    Tensor Interactions in Deuteron Scattering

14. Evans Hayward, Duke University (11/29/90)
    The Threshold π^o Production Cross Section and the Low-Energy Theorem
15. Evans Hayward, Duke University (12/6/90)
    The Drell-Hearn-Gerasimov Sum Rule
16. Frank Moore, Argonne National Laboratory (1/29/91)
    Nuclei Near Mass 190: A New Region of Superdeformation
17. Craig Ogilvie, GSI, Germany (2/5/91)
    The Disappearance of Flow and its Relevance to Nuclear Matter Physics
18. Jerry Garrett, Oak Ridge National Laboratory (2/7/91)
    Plans for Radioactive Ion Beams from the Holifield Facility at Oak Ridge
19. S. F. Pate, Indiana University Cyclotron Facility (2/19/91)
    Spin Correlations in Neutron-Proton Radiative Capture
20. Richard A. Arndt, Virginia Polytechnic Institute and State University (2/21/91)
    Partial Wave Analyses at VPI & SU; The π-NN Coupling Constant
21. W. K. Pitts, University of Wisconsin (2/26/91)
    Progress Towards Spin-Correlation Measurements at the IUCF Cooler
22. V. V. Flambaum, Institute of Nuclear Physics Novosibirsk (3/26/91)
    P- and T-Odd Nuclear Moments and P- and T-Nonconservation in Atoms and Molecules
23. James Pantaleone, University of California (3/28/91)
    The Solar Neutrino Problem: Possible Solutions and Future Experimental Tests
24. John Behr, University of Washington (4/30/91)
    Giant Dipole Radiation and Isospin Purity in Highly Excited Compound Nuclei
25. Chris Lyndon, College of William and Mary (5/21/91)
    Coincidence Analyzing Powers for the Reaction $^{12}C(p,p'\gamma)^{12}C$ Through the 15.11-MeV State
26. Joachim Görres, University of Notre Dame (5/23/91)
    Capture Reactions on ^{14}C and Nonstandard Big-Bang Nucleosynthesis
27. M. Khandakar, University of Maryland (5/30/91)
    Pion Absorption on Quasi-Deuterons in ^4He
28. Zeid Ayer, University of Notre Dame (6/4/91)
    Study of the $^3He(d,^3He\ p)n$ and $^3He(d,t\ p)p$ Reactions Using Polarized Deuterons
29. Conrad Knight, Duke University (6/10/91)
    Radiation Safety-Biological Effects
30. David Jorgensen, Duke University (6/10/91)
    Radiation Safety-Instrumentation
31. Paul Carter, Duke University (6/11/91)
    Radiation Safety & Emergency Procedures at TUNL
32. Alton Lovette, Duke University (6/17/91)
    The Instrumentation Shop for Nuclear Physics

33. Thomas Clegg, UNC-Chapel Hill (6/18/91)
    The Physics of the TUNL Polarized Ion Source
34. Eric Crosson, UNC-Chapel Hill and John Dunham, Duke University (6/18/91)
    The Operation and Maintenance of the TUNL Polarized Ion Source
35. Sidney Edwards, Duke University (6/19/91)
    An Overview of the TUNL Electronic Shop and Computer System
36. Calvin Howell, Duke University (6/19/91)
    The Data Acquisition System at TUNL
37. Ross Setze and Robert Chastler, Duke University, and Tim Black, UNC-Chapel Hill (6/20/91)
    Experimental Techniques for Low-Energy Neutron, Gamma-Ray, and Charged-Particle Detection
38. Paul Carter and Chris Westerfeldt, Duke University (6/21/91)
    Vacuum Systems in an Accelerator Laboratory and The Upgraded TUNL Tandem Accelerator and Details of the Accelerator Control Circuits
39. Dufei Fang, Fudan University (8/6/91)
    An Overview of the Current Research Program at the Fudan University Accelerator Laboratory
40. Yasuro Koike, Hosei University, Japan (8/8/91)
    A New Method for Solving the Lippmann-Schwinger Equation, and Its Relation to the Three-Body Problem
41. Henryk Witała, Jagellonian University, Cracow, Poland (8/22/91)
    Recent Advances in Three-Nucleon Continuum Studies
42. Richard Prior, West Georgia College (8/29/91)
    $^{24}Mg + p$: From Compound Nucleus to Direct Processes

END

DATE
FILMED
12/11/91